

Amazonia under mid-Holocene drought

Doctor of Philosophy

School of Archaeology, Geography and Environmental Science

Richard J. Smith

September 2018

Declaration

I confirm that this is my own work and the use of all material from other sources has been properly and fully acknowledged

Signed

Richard J. Smith

Thesis Abstract

Improving understanding of the long-term impacts of climate change on Amazonian ecosystems remains an important scientific challenge. Of particular concern is the impact of a drier climate, given that many climate models simulate decreased precipitation for Amazonia over the coming century. However, the impacts of such climate change on Amazonia are uncertain, with scenarios ranging from widespread rainforest dieback, to overall forest resilience. This thesis uses the middle Holocene (ca. 6,000 years ago) as an approximate analogue for future climate change, given the evidence that this period was significantly drier than present across much of Amazonia. The overall aim is to improve our understanding of the impact of long-term mid-Holocene drought on Amazonia using a multi-disciplinary approach, integrating both palaeoecology and Earth system modelling. Results are presented over three chapters in the form of academic papers. Chapter 2 presents a new multi-proxy synthesis of mid-Holocene palaeoecological records from across tropical South America, demonstrating concurrent mid-Holocene expansion of savannah in southern and eastern Amazonia and south-east Brazil, with resilience of rainforest in central Amazonia. Chapter 3 presents a new fossil-pollen record from a small palm swamp (Cuatro Vientos) in south-west Amazonia, which is compared with a previously published pollen record of a nearby large lake (Laguna Chaplin), demonstrating that palm swamps can yield useful Quaternary pollen archives recording the history of terrestrial vegetation beyond the swamp, rather than merely a history of localised swamp vegetation dynamics. Chapter 4 presents an ensemble of 21 mid-Holocene vegetation model simulations in one of the first palaeo-vegetation modelling-data comparison projects of mid-Holocene Amazonia, demonstrating that the models can replicate mid-Holocene rainforest resilience in the core of the Amazon basin, with savannah expansion restricted to the ecotonal regions of eastern and southern Amazonia. However, uncertainty exists between the models regarding the spatial position and extent of this savannah expansion.

Acknowledgements

Firstly, I wish to thank my main supervisor, Frank Mayle, for his continued support and guidance throughout my PhD research. His expertise, patience and motivation have been invaluable. I am very grateful for the opportunities he has made possible, most notably the amazing field season spent in Bolivia. Thanks also go to my second supervisor, Joy Singarayer, who provided great assistance in overcoming the various challenges faced in setting up multiple model simulations, as well providing insightful comments and suggestions that helped the project grow.

I am thankful for the help and support of John Carson and Macarena Cárdenas during their time as PDRAs at the University of Reading. They both provided excellent training and support in the laboratory, but perhaps more importantly were great mentors and friends. Thanks must also go to Heather Plumpton – we shared this journey through our PhDs together, with all the associated ups and downs. I have always been very grateful for her friendship and positivity.

Financial support for this PhD was provided through the NERC SCENARIO Doctoral Training Partnership scheme (NE/L002566/1). The SCENARIO scheme has been very supportive and has provided opportunities for me to undertake the field work in Bolivia, attend various training courses, and participate in national and international academic conferences.

Special thanks go to my wonderful family, who have provided unlimited support and encouragement throughout the last four years. Finally, my greatest thanks must go to Lucy Barker for all her love and support, without which I would never have gotten to this point.

Contents

Thesis Abstract	3
Acknowledgements	4
Contents	5
List of figures	9
List of tables	10
Chapter 1. General introduction	11
1.1 Amazonia's vulnerability to drought	11
1.2 Concern for the future	12
1.2.1 Future precipitation changes.....	12
1.2.2 Future vegetation changes.....	15
1.2.3 Direct human impacts.....	17
1.3 Looking into the past	18
1.3.1 Palaeoclimate of mid-Holocene Amazonia.....	19
1.3.2 Palaeoecology of mid-Holocene Amazonia.....	20
1.3.3 Past human land use.....	22
1.4 Thesis aims and objectives	23
Chapter 2. Impact of mid-to-late Holocene precipitation changes on vegetation across lowland tropical South America: a paleo-data synthesis....	25
2.1 Preface	25
2.2 Abstract	26
2.3 Introduction	27
2.3.1 Modern environmental setting.....	28
2.4 Methods	34
2.4.1 Proxy types.....	36
2.4.2 Archive types and spatial scale of reconstructions.....	37
2.4.3 Paleoclimate records.....	37
2.5 Synthesis and discussion	51
2.5.1 Central and western lowland Amazonia (CW).....	51

2.5.2	South-Western Amazonia (SW)	52
2.5.3	South-Eastern Brazil (SB)	54
2.5.4	Eastern Amazonia (EA).....	56
2.5.5	North-Eastern Brazil (NE)	57
2.6	Conclusions.....	59
2.7	Acknowledgements	60
2.8	Supporting information	61
Chapter 3. How does basin type and size influence late Quaternary vegetation reconstructions in south-west Amazonia?		65
3.1	Preface	65
3.2	Abstract.....	66
3.3	Introduction	67
3.3.1	Study area.....	70
3.4	Methods	74
3.4.1	Sediment core	74
3.4.2	Chronology.....	74
3.4.3	Pollen analysis	74
3.4.4	Laguna Chaplin core	75
3.5	Results	78
3.5.1	Cuatro Vientos - core stratigraphy and chronology.....	78
3.5.2	Cuatro Vientos pollen data.....	79
3.6	Interpretation and discussion.....	85
3.6.1	Comparison between pollen records of Cuatro Vientos palm swamp and Laguna Chaplin	85
3.6.2	Implications of the paleoecological history of CV.....	91
3.7	Conclusions.....	93
3.8	Acknowledgements	93
Chapter 4. Response of Amazonian forests to mid-Holocene drought: a model-data comparison		95
4.1	Preface	95
4.2	Abstract.....	96

4.3	Introduction	97
4.4	Materials and methods	99
4.4.1	Geographic Setting	99
4.4.2	Dynamic Global Vegetation Models (DGVMs)	99
4.4.3	Experimental design.....	100
4.4.4	Climate data	101
4.4.5	Soil data	103
4.4.6	Palaeo-data reconstructions	103
4.4.7	Classification method.....	108
4.5	Results	109
4.5.1	Modern vegetation simulations	109
4.5.2	MH climate anomalies.....	111
4.5.3	Simulated MH PFT anomalies	114
4.5.4	LDA Classification maps and comparison with palaeoecological reconstructions.....	117
4.6	Discussion	124
4.6.1	Assessment of the overall resilience of Amazonian HETF to MH precipitation changes 124	
4.6.2	Sources of simulation uncertainty	128
4.6.3	The need for increased palaeo-data in Amazonia	128
4.6.4	Implications for understanding the future resilience of Amazonian HETF	129
4.7	Acknowledgements	130
4.8	Supporting information	131
Chapter 5.	<i>General discussion.....</i>	135
5.1	Importance of palaeo-data syntheses in tropical South America	135
5.2	Relationship between tropical basin characteristics and their fossil pollen archive	137
5.2.1	Implications for the rainforest refugia hypothesis.....	138
5.3	Integration of palaeo-data and palaeo-modelling in Amazonia	139
5.4	Implications for combining information on landscape and cultural changes 141	
5.5	Implications for the future of Amazonia	142
5.6	Potential for future work.....	143
References	145

<i>Appendix A. Out of Amazonia: Late-Holocene climate change and the Tupi–Guarani trans-continental expansion</i>	175
Preface	175
<i>Appendix B. Unknown pollen grains of Cuatro Vientos</i>	185
Preface	185

List of figures

Figure 2.1 - Observed long-term mean precipitation and wind fields for tropical South America	30
Figure 2.2 - Overview maps of tropical South America study area.....	33
Figure 2.3 - Selected paleoclimate records representing proxy records for precipitation changes through the last 6 ka	38
Figure 2.4 - Paleoecological reconstructions at 0.5 ka time slices from 6 ka to present	49
SI Figure 2-A - Summary of vegetation changes at each palaeoecological site, alongside regional maps of the location of each site	61
Figure 3.1 - Overview Map of Noel Kempff Mercado National Park (NKMNP).....	73
Figure 3.2 - Radiocarbon dates, age-depth model and lithological description for Cuatro Vientos.....	79
Figure 3.3 - Pollen percentage diagram of taxa from Cuatro Vientos, plotted against calibrated years BP	81
Figure 3.4 - Pollen percentage diagram of taxa from Laguna Chaplin, plotted against calibrated years BP	82
Figure 3.5 - Summary percentage diagram for (a) Cuatro Vientos, (b) Laguna Chaplin.....	83
Figure 4.1 - Overview maps of study area for model-data Intercomparison.....	100
Figure 4.2 - Modern distribution of simulated PFT distributions	110
Figure 4.3 - Mid-Holocene annual mean precipitation anomalies.....	113
Figure 4.4 - Average annual cycle of mid-Holocene precipitation anomalies.....	114
Figure 4.5 - Mid-Holocene anomalies of simulated PFT fractions for each model combination	116
Figure 4.6 - Results of LDA vegetation classification for each model combination	121
Figure 4.7 - Percentage change in the proportion of savannah cells (based on the LDA classification) relative to total cells between MH and modern control for each of the areas of Amazonia.....	123

List of tables

Table 2.1 - List of paleoecological sites included in mid- to late Holocene synthesis	40
Table 2.2 - Description of the broad vegetation classifications used in palaeosynthesis.....	47
Table 2.3 - Size categories representing the different catchment areas of the paleoecological sites	48
Table 3.1 - List of the accelerator mass spectrometry radiocarbon dates from the Cuatro Vientos sediment core	76
Table 3.2 - List of the accelerator mass spectrometry radiocarbon dates from the Laguna Chaplin sediment core.....	77
Table 4.1 - PMIP3 climate models used in this study.	102
Table 4.2 - List of palaeoecological sites used for model-data comparison.....	104
Table 4.3 - List of palaeoclimate sites.....	107
SI Table 4-A - List of plant functional types (PFTs) used by the DGVMs in this mid-Holocene vegetation simulations	131
SI Table 4-B - Required climate variables and units for each DGVM.....	132
SI Table 4-C - Climate variable codes and descriptions	132
SI Table 4-D - Required soil variables for each DGVM.....	134
SI Table 4-E - Soil variable codes and descriptions.....	134

Chapter 1. General introduction

The Amazonian region of tropical South America contains the world's largest tropical rainforest that accounts for ~40% of global tropical forest area (Malhi *et al.* 2008; Aragão *et al.* 2014). This rainforest is incredibly biodiverse, hosting ~20-25% of all global terrestrial species (Dirzo & Raven 2003; May *et al.* 2013). This region provides globally important ecosystem services, including carbon sequestration (Phillips *et al.* 2009; Pan *et al.* 2011; Aragão *et al.* 2014; 2018), and impacts regional and global climate through hydrological cycling (Werth & Avissar 2002; Harper *et al.* 2014). The forests provide a wide variety of ecosystem services, including food, shelter, medicine, flood protection and soil stabilisation, as well as their importance for cultural and religious purposes. Therefore, the potential impacts of future climate change on this region are a cause of major concern.

1.1 Amazonia's vulnerability to drought

Moisture availability, particularly during the dry season, is one of the key limiting factors controlling Amazonia's forest productivity (Meir & Woodward 2010), raising concerns about the impact of severe droughts on plant growth, mortality and biomass carbon dynamics. However, much of the early research into ecosystem responses to drier conditions relied on remotely sensed data, as direct field-based monitoring was in its infancy. Huete *et al.* (2006) showed that areas of Amazonia that experience longer dry seasons would "green up" during dry conditions, suggesting that greater sunlight availability would enhance photosynthesis; this phenomenon was observed in remote sensing data during the 2005 Amazon drought (Saleska *et al.* 2007). Early forest plot data from tropical forests in Panama appeared to record increased productivity and sapling growth during drier periods, potentially in response to greater sunlight and insolation (e.g. Graham *et al.* 2003; Condit *et al.* 2004), though these studies only had data collection at a limited number (1-3) of sites and were outside of Amazonia.

To help improve understanding of Amazonian ecosystem dynamics, the Amazon Forest Inventory Network project was set up to gather direct, field-based data across the whole of Amazonia (RAINFOR; Malhi *et al.* 2002). RAINFOR is an extensive network of 1-hectare plots located across Amazonia that record detailed annual inventories of soil and plant biogeochemical data, as well as providing detailed monitoring of carbon cycle processes. Field-based ecological impact analyses from RAINFOR before, during and after two major droughts in 2005 and 2010 demonstrated the sensitivity of Amazonian forests to severe short-

term drought events. These droughts were associated with increased tree mortality and substantial loss of biomass carbon at plots located in all areas of the Amazon basin (Phillips *et al.* 2009; Doughty *et al.* 2015; Feldpausch *et al.* 2016). Of most concern is the evidence that during these drought events, Amazonia switched from a net carbon sink to a net carbon source of up to 1.6 Pg C (Phillips *et al.* 2009; Gatti *et al.* 2014; Doughty *et al.* 2015). Detailed analyses of the carbon cycle processes in thirteen forest plots have shown that trees invest more carbon into growth as a very short-term survival strategy during drought events, with less carbon invested in tissue maintenance and defence, thus increasing vulnerability to mortality (Doughty *et al.* 2015). This may help to explain the apparent 'greening' seen in the earlier remote sensing studies. Further evidence that Amazonian forests are finely balanced between being a net carbon sink or source comes from a study analysing 30 years of data collection, which has identified a gradual decline in the Amazonian carbon sink, potentially as a result of greater climate variability, increased temperatures and the periodic drought events (Brienen *et al.* 2015).

1.2 Concern for the future

1.2.1 Future precipitation changes

The demonstration of the vulnerability of Amazonia's forests to short-term drought events has raised concerns over the impacts of potential changes to the long-term precipitation regime of Amazonia under future climate change. The primary method of studying potential future climate change is by using computer models. General Circulation Models (GCMs) are considered the most fundamental way of representing the global climate system. GCMs vary in their scope, but their primary purpose is to numerically represent the physical components of Earth's climate system (e.g. the atmosphere, ocean, sea ice and land surface) and allow us to make climate projections based on different levels of external forcings (e.g. greenhouse gas concentrations, solar forcing, volcanic forcing) (Randall *et al.* 2007; Flato 2011).

In the early 2000s, modelling studies into future climate change across Amazonia first proposed that a combination of increasing global temperatures, El Niño like sea surface temperature increases, and internal vegetation feedbacks could cause a decrease in precipitation rates across the region (Cox *et al.* 2000; Betts *et al.* 2004; Cox *et al.* 2004). This generated considerable interest in the community, especially as other studies suggested that rising CO₂ could cause an increase in precipitation (Costa & Foley 2000; Giorgi & Francisco 2000), and suggested that increased warming could intensify the effects of the South

American Summer Monsoon (SASM) thus increasing precipitation during the rainy season. It was clear that a greater investigation into the mechanisms and uncertainties surrounding these future simulations was needed.

The 2007 Intergovernmental Panel on Climate Change (IPCC) Fourth Assessment Report (AR4) compiled a suite of Atmosphere-Ocean GCMs (AOGCMs) to simulate future climate under a series of emissions scenarios (Nakicenovic & Swart 2000). This was coordinated through the Coupled Model Intercomparison Project phase three (CMIP3), which outlined a set of experiments each modelling group had to perform with their GCM (Meehl *et al.* 2007; Randall *et al.* 2007). This enabled a multi-model, multi-scenario assessment of the projected changes in future precipitation over Amazonia. Validation exercises show that these CMIP3 models were able to reproduce large scale planetary features of precipitation with reasonable accuracy (Randall *et al.* 2007). Across Amazonia, basic characteristics such as the seasonal cycle of northwestward to southeastward migration of precipitation are reproduced relatively well. However, most of the CMIP3 climate models show a pronounced underestimation of precipitation across Amazonia, are inconsistent in their spatial distribution of precipitation over the region and have difficulty reproducing features of the SASM (Vera *et al.* 2006; Malhi *et al.* 2009; Joetzjer *et al.* 2013).

Despite some of the difficulties in reproducing modern Amazonian precipitation, intercomparison studies of future CMIP3 model simulations were undertaken to determine levels of model agreement and potential sources of uncertainty between models. Whilst some studies showed broad levels of model agreement with regards to trends such as less dry season precipitation and later onset of the wet season (e.g. Vera *et al.* 2006; Seth *et al.* 2010), overall the results from the CMIP3 models show high levels of uncertainty between the models. Li *et al.* (2006) investigated 11 CMIP3 models, finding no agreement in trends in future annual rainfall across Amazonia, with 5 simulations producing a wetter climate, 3 a drier climate, and 3 no change. Malhi *et al.* (2009) showed similar levels of disagreement when investigating relationships between annual precipitation and Maximum Climatological Water Deficit (MCWD - a measure of dry season intensity).

As advances in modelling continued, the IPCC Fifth Assessment Report (AR5 - released in 2013) used an updated suite of models under the Coupled Model Intercomparison Project phase five (CMIP5) (Stocker *et al.* 2013). A new 'state-of-the-art' in modelling was established at this time. Earth System Models (ESMs) expand upon GCMs by including modules that

represent biogeochemical cycles, such as the carbon cycle and its associated interactions (Flato 2011; Flato *et al.* 2013). The models in CMIP5 also benefitted from increased spatial resolution and general development of the model dynamics and parameterization schemes. The AR5 report also updated future scenarios by introducing Representative Concentration Pathways (RCPs), which move away from the socioeconomic scenarios of SRES. RCPs are pathways of greenhouse gas concentrations, reflecting the fact that the same concentrations could occur given more than one socioeconomic scenario (van Vuuren *et al.* 2011; Cubasch *et al.* 2013). Relative to the multi-model mean of the CMIP3 models, the CMIP5 multi-model mean of precipitation shows a reduction in the dry bias across Amazonia. However, improvements are generally limited to the rainy season, with the dry season precipitation still underestimated (Flato *et al.* 2013; Joetzjer *et al.* 2013; Yin *et al.* 2013). Where there is a marked improvement from CMIP3 is the CMIP5 multi-model mean's ability to represent the relationship and lagged correlations between sea surface temperatures (linked with ENSO variability and the tropical Atlantic) and precipitation (Joetzjer *et al.* 2013; Duffy *et al.* 2015). However, the skill of individual models still varies greatly, suggesting that the multi-model mean may mask the uncertainties inherent in each model.

Joetzjer *et al.* (2013) investigated the differences between future simulations of two sets of 13 models – one set from the CMIP3 and another set from their upgraded counterparts from CMIP5. They found that CMIP5 shows a weaker increase in wet season precipitation, but a drier and longer dry season – perhaps linked to enhanced ocean warming in CMIP5 compared to CMIP3 and the improved model responses to sea surface temperatures. However, it is noted that RCP8.5 is a slightly more severe scenario than that of SRES A2 which could explain some of this difference. Boisier *et al.* (2015) take a more detailed look at the full suite of 36 models from CMIP5. The multi-model ensemble trend is for a gradual decrease in precipitation through the coming century, although large uncertainties are immediately obvious when the ensemble of model outputs are viewed together, with a roughly even split between models simulating an increase or decrease in precipitation. To try and account for inherent bias in individual models, the authors build an empirical relationship between model output and observed precipitation. When these constrained simulations are investigated, there is considerably higher model agreement for a much drier dry season and an increase in the areas affected by dry season water deficits (> 90% agreement in some areas such as Southern Amazonia). The authors conclude that there is an important underestimation of decreased precipitation in the model outputs, and therefore an underestimation of the impacts that decreased precipitation may bring (i.e. rainforest decline).

Overall, the results from the IPCC AR5, like AR4, show high levels of uncertainty, with simulation results largely model and scenario dependent. However, there is mounting evidence that the detectable climate trends of increased seasonality of rainfall are likely, with a general consensus between studies that there is likely to be wetter, but shorter wet seasons, and drier, longer dry seasons by the end of the century (Joetzjer *et al.* 2013; Llopart *et al.* 2014; Boisier *et al.* 2015). Additionally, extreme events on meteorological time-scales (such as severe droughts and extreme wet events) are expected to increase (Duffy *et al.* 2015). The biggest impacts are likely to occur in the east and south of Amazonia due to their vulnerable locations at climatic and ecotonal boundaries

1.2.2 Future vegetation changes

Investigating the impacts of a potentially drier future climate on Amazonian vegetation has become a major research focus. Dynamic Global Vegetation Models (DGVMs) are the primary way to investigate the large-scale, long-term responses of vegetation to future climate change scenarios. DGVMs aim to model biogeochemical and hydrological exchanges (e.g. carbon, water and energy exchanges between the vegetation, soil and atmosphere), as well as vegetation dynamics (e.g. growth, competition, mortality), in response to given climate forcings.

One of the first studies to investigate the potential impacts of future climate change on global vegetation was Cox *et al.* (2000). Using a GCM (HadCM3) coupled with a dynamic vegetation model (TRIFFID) they found the global terrestrial biosphere would switch from a net carbon sink to a net carbon source by the end of the 21st century, largely driven by the widespread loss of Amazonian forests and associated loss of vegetation and soil carbon. Building on this work, further studies looked specifically at the potential for major loss of Amazonian vegetation from this model (Betts *et al.* 2004; Cox *et al.* 2004; Huntingford *et al.* 2008). They suggested that decreases in precipitation simulated by HadCM3 could cause a catastrophic loss of Amazonian forest by the end of the 21st century; broadleaf tree cover could reduce from 80% to <10%, being replaced with C4 grass savannah or even desert like conditions. This basin-wide dieback could then exacerbate the reduction in precipitation in two main ways by reducing regional evapotranspiration and accelerating global climate change by releasing stores of carbon previously held in the biomass. To explore uncertainties in these predictions, Huntingford *et al.* (2004) carried out multiple simulations of HadCM3/TRIFFID using a variety of different vegetation parameterisations and initial conditions; such as different

photosynthesis equations, different stomatal response parameter values, and using observed climatology as the initial conditions. They found that Amazonian forest dieback was a feature in most scenarios, though with differences in the timing and magnitude of forest loss and biomass carbon loss.

More recently, the robustness of the original HadCM3/TRIFFID-simulated widespread dieback has been brought into question. Studies comparing future simulations of forest cover from HadCM3/TRIFFID with the updated version of the GCM, HadGEM2-ES have shown that HadGEM2 simulates very little Amazon dieback under a scenario of 140 years of 1% CO₂ increase (Good *et al.* 2013; Huntingford *et al.* 2013). These differences have been attributed to the difference in the climate projections of the two GCMs, with HadGEM2 simulating a much less severe decrease in precipitation, linked with differences in the changes of Atlantic sea-surface temperatures (Good *et al.* 2013). Other studies have demonstrated that the choice of climate model is a major source of uncertainty in future vegetation simulations. For example, Schaphoff *et al.* (2006) investigated the effect of using different GCMs to drive the LPJ-DGVM vegetation model. They show that, by the end of the 21st century, there is no model consensus on whether the terrestrial biosphere is a net sink or source of carbon. Across Amazonia, some models produce near-neutral carbon changes, whilst the CSIRO GCM produced a net carbon sink and the HadCM3 GCM produced a strong net carbon source. Whilst not comprehensive in terms of the number of models employed and the broad geographic focus, this study showed the importance of a multi-model approach to looking at the fate of the Amazon.

In addition to climate models introducing uncertainty into vegetation simulations, the choice of the vegetation model itself contributes substantial uncertainties, linked to difficulties in representing fine-scale biogeochemical processes in parameterisation schemes (Fisher *et al.* 2010; Quillet *et al.* 2010). Sitch *et al.* (2008) ran five different DGVMs with a modified 'climate analogue model' version of HadCM3 and found large model variation with respect to Amazonian vegetation changes. There was most disagreement in changes in soil carbon storage, with the DGVMs of Hyland, LPJ and TRIFFID simulating decreases in soil carbon stocks, whereas Orchidee and SDGVM simulated an increase. As expected, TRIFFID simulates a severe Amazon dieback, as does Hyland, whereas LPJ and Orchidee simulate relatively little dieback. Zhang *et al.* (2015) show similar levels of disagreement between three DGVMs driven by three different climate models. The JULES vegetation model was consistent in simulating extensive biomass carbon loss in response to precipitation changes in all three

climates, IBIS simulated moderate loss, and ED2 only simulated biomass loss under the driest climate model.

Overall, there remains considerable uncertainty in future modelling simulations as to the response of Amazonian vegetation to future precipitation changes. Further adding to this uncertainty is how other environmental drivers may contribute to a changing ecosystem – in particular the relative contributions of temperature and atmospheric CO₂ concentrations. Increased future temperatures could exacerbate dieback as it enhances evapotranspiration and reduces photosynthetic rates (Schaphoff *et al.* 2006; Galbraith *et al.* 2010; Zhang *et al.* 2015). However, a CO₂ rise in the future has the potential to stimulate photosynthesis and increase water use efficiency, thus counteracting dieback (the so called ‘CO₂ fertilisation effect’), but there is uncertainty as to how significant this process will be (Lapola *et al.* 2009; Galbraith *et al.* 2010; Rammig *et al.* 2010).

1.2.3 Direct human impacts

As well as the potential impacts of anthropogenically-induced climate change on Amazonia, as discussed in section 1.2.1 and 1.2.2, humans are having a more direct effect on Amazonian vegetation through practices such as intense deforestation and uncontrolled burning. Deforestation rates in the Brazilian Amazon reached record highs between 2000 and 2005, reaching a high of 27,400km² year⁻¹ in 2004. This was driven by the expansion in cattle ranching and soybean production, primarily in the eastern and southern ecotonal regions of Amazonia (Malhi *et al.* 2008). Since then, deforestation rates have considerably reduced, driven by a number of environmental, economic and political policies (Soares-Filho *et al.* 2010; Nolte *et al.* 2013; Nogueira *et al.* 2018). However, there is concern that forest protection could be cut and deforestation rates could rise again (Tollefson 2012; Watson *et al.* 2018). If the trend of reducing deforestation reverses and rates return to the levels of the early 21st century, policy-sensitive simulations of future deforestation show the potential for the loss of ~40% of Amazon forests (Soares-Filho *et al.* 2006).

Therefore, in considering the future of Amazonia, two potential sources of environmental change are identified: 1. Climate change induced vegetation shifts, and 2. Direct human induced forest loss. This project aims to reduce the uncertainties surrounding the first source; however, it is beyond the scope of this project to directly account for the second source.

1.3 Looking into the past

Reducing the uncertainty surrounding future model projections of environmental change in Amazonia remains a key scientific challenge. Model skill is often only demonstrated through the ability to simulate the observation period of the last century. However, during this time, the Earth's climate system has been relatively stable and so model-data comparisons do not provide a robust test of a model's ability to simulate the large and long-term changes expected in the future. Improving our knowledge of the impact of long-term climate change on Amazonian ecosystems requires the study of interactions between vegetation and climate on timescales longer than those offered by modern ecology and modern model-data comparisons.

As a result, the modelling community recognised relatively early on the potential for using a 'palaeo-modelling' approach. Models are run for some known period in the far past (e.g. 6,000 years ago) when the climate system experienced large-scale change due to long-term changes in external forcings, thus giving the models a more robust test of their ability to simulate long-term future climate change (Kohfeld & Harrison 2000; Schmidt 2010). The palaeo-model simulations can be benchmarked against observational palaeo-data, thus providing important information about where we can have most confidence in environmental changes simulated by the models. In 1991, the Paleoclimate Modelling Intercomparison Project (PMIP) was set up in order to coordinate palaeo-modelling experiments between different modelling groups around the world (Joussaume & Taylor 1995). The PMIP initiative was a formal attempt to get modelling communities to engage with the palaeo-data community by running prescribed palaeo-simulations and comparing the model output to palaeo-observations (Harrison *et al.* 2002; Braconnot *et al.* 2011). The idea of such a collaborative initiative is that the modelling community benefits from the supply of palaeo-data to test their models, and the palaeo community benefit from more robust palaeo model outputs that can help them to better understand their data (Gallimore *et al.* 2005). The importance of this approach has been recognised through the formal inclusion of palaeoclimate modelling in the IPCC AR4 report (Jansen *et al.* 2007) and strengthened through the inclusion of PMIP (phase 3 – PMIP3) in the CMIP5 initiative in the IPCC AR5 report (Masson-Delmotte *et al.* 2013). This latest development meant that the same models were to be used for past and future simulations, allowing a direct quantitative link between model performance in the past and the future (Schmidt 2010; Braconnot *et al.* 2011; 2012; Schmidt *et al.* 2014a).

However, throughout the history of PMIP, there have been very few studies that focus on past Amazonian climate and vegetation changes. Many of the PMIP studies, especially from the early PMIP phases, focused on large scale or global processes in order to gain better understanding of the fundamental workings of the models (e.g. Harrison *et al.* 1998; Kohfeld & Harrison 2000; Braconnot *et al.* 2007). Model-data comparisons have, understandably, focused on regions for which abundant palaeo-data exists; e.g. Europe, North America and Asia (e.g. Kohfeld & Harrison 2000; Harrison & Prentice 2003; Braconnot *et al.* 2012). This thesis attempts to address this issue by providing one of the first palaeo model-data comparison studies of Amazonia, focusing on the middle Holocene (ca. 6,000 years before present, 6 ka BP).

1.3.1 Palaeoclimate of mid-Holocene Amazonia

The middle Holocene is one of the key time periods that the PMIP initiative organises model simulations for, as this is a period when the global climate system experienced large changes in external forcings leading to large-scale, long-term climate change. Variations in summer insolation levels were a primary source of external forcing changes, predominantly driven by the precessional cycle of Earth's orbit (Berger 1978; Berger & Loutre 1991). Southern hemispheric tropical South America would have experienced a decrease in austral summer insolation, restricting the southerly migration of the Inter-tropical Convergence Zone (ITCZ; Haug *et al.* 2001; Singarayer *et al.* 2017) and decreasing the strength of the SASM, reducing precipitation across much of the region (Cruz *et al.* 2009; Baker & Fritz 2015). One of the first studies to demonstrate this mechanism of precipitation change was the lake-level reconstruction at Lake Titicaca on the Peruvian/Bolivian altiplano in the central Andes. Chemical, isotopic and biotic (diatom) analyses of lake sediments have shown that lake levels at Lake Titicaca were as much as 100 m below present levels between ca. 6 ka BP and 5 ka BP (thousand years before present), the lowest level found in the past 25,000 years. Lake levels didn't begin to rise again until ca. 4.5 ka BP and didn't reach modern levels until ca. 2 ka BP (Cross *et al.* 2000; Baker *et al.* 2001). Although located in the high Andes, this site was deemed representative of lowland Amazonia because the annual precipitation cycle on the Peruvian/Bolivian altiplano is highly correlated with that of lowland Amazonia. This argument is strengthened when other sources of evidence across tropical South America are considered. For example, speleothem records from the Peruvian Andes (Kanner *et al.* 2013) and the western Peruvian Amazon (van Breukelen *et al.* 2008; Cheng *et al.* 2013) also record lower precipitation levels during the middle Holocene. Laguna La Gaiba, located in the Pantanal wetlands of eastern Bolivia/western Brazil, has shown increases in shallow water

species of *Pediastrum* algae (Whitney & Mayle 2012) and peaks in aerophilous diatom taxa (Metcalf *et al.* 2014). Speleothem records from southeast Brazil, such as those from Botuverá cave and Santana cave, show high values of $\delta^{18}\text{O}$, indicating weakened SASM activity (Cruz *et al.* 2005; 2006a; 2006b; Wang *et al.* 2007; Bernal *et al.* 2016).

The middle Holocene therefore represents a time period for which we can investigate the long-term response of Amazonian ecosystems to long-term climate change, particularly with respect to decreased levels of precipitation. However, it must be noted that the middle Holocene still remains an imperfect analogue for other important aspects of future climate change; especially with respect to atmospheric CO_2 concentrations and temperature. Mid-Holocene atmospheric CO_2 concentration has been reconstructed to around 265-285 ppm from the Antarctic EPICA Dome C ice core (Monnin *et al.* 2001), whereas global atmospheric CO_2 concentrations at 2100 AD under the IPCC AR5 RCP scenarios range from 421ppm (RCP 2.6) to 936ppm (RCP 8.5) (Meinshausen *et al.* 2011). Reconstructions of mid-Holocene temperatures for tropical South America are more sparse, though it is likely that they have remained fairly stable from the middle Holocene to the present (van Breukelen *et al.* 2008; Whitney *et al.* 2011). Future simulations suggest that temperatures across tropical South America could increase between 1°C and 7°C by 2100 AD, depending on the RCP scenario employed (Collins *et al.* 2013). However, despite the imperfect nature of the mid-Holocene analogue, it remains the best 'natural experiment' available for us to determine how Amazonian vegetation responds to a long-term drier climate.

1.3.2 Palaeoecology of mid-Holocene Amazonia

Fundamental for a palaeo model-data comparison of mid-Holocene vegetation simulations is a suitable database of palaeoecological records that reconstruct mid-Holocene vegetation across Amazonia. Although tropical palaeoecology is a nascent field in comparison with temperate regions, there are a growing number of records reconstructing late-Quaternary vegetation changes across tropical South America. For example, in southern Amazonia, a number of records provide evidence for forest-savannah ecotonal shifts related to the changing climate over the Holocene. Pollen data from two large lakes (Laguna Bella Vista and Laguna Chaplin) in eastern lowland Bolivia show that the southern Amazonian rainforest-savannah ecotone was at least 130 km farther north during the middle Holocene (Mayle *et al.* 2000; Burbridge *et al.* 2004). This ecotonal movement is corroborated by evidence from pollen analyses from other lakes in this area (Taylor *et al.* 2010; Carson *et al.* 2014) and stable carbon isotope records from nearby soil pits (Pessenda *et al.* 1998). In eastern Amazonia,

evidence of similar fluctuations between rainforest and savannah comes from several studies of lakes on the Serra dos Carajás plateau, with palynological evidence that savannah was likely dominant during the middle Holocene (e.g. Absy *et al.* 1991; Sifeddine *et al.* 2001; Hermanowski *et al.* 2012a; 2014). However, because these lakes are small and isolated on top of a 700m high plateau, it is questionable whether these changes reflect regional changes in the surrounding rainforest.

In central and western Amazonia, some studies have shown that the humid rainforest biome was potentially resilient to mid-Holocene climate change (e.g. Colinvaux *et al.* 1996; Behling *et al.* 1999; 2001c; Bush *et al.* 2004b; Horbe *et al.* 2011), though there is also some evidence of localised reduction in flooded forests and expansion of open ground near to rivers in the mid-Holocene, reflecting lower river levels linked to the decreased precipitation (Behling *et al.* 2001c; Horbe *et al.* 2011). Whilst not in the Amazonian region itself, there is evidence for vegetation changes in southeast, subtropical Brazil, which is linked climatically to Amazonia through the SASM. Several studies have demonstrated the dominance of grassland (Campos) vegetation on the southern Brazilian highlands during the middle Holocene, with expansion of moist *Araucaria* forests occurring from ca. 3 ka BP, with a marked increase at ca. 1.5 ka BP (Behling 1997b; 1998; Behling *et al.* 2001a; Behling & Pillar 2007).

However, these sites are often considered in isolation, precluding the ability to consider the full spatial variability of changes occurring across Amazonia as a whole. Synthesis projects are crucial for bringing these data together. Early syntheses only considered a handful of Amazonian sites (e.g. Mayle & Power 2008), whereas other syntheses focused predominantly on using palaeoecological data to reconstruct past climate (e.g. Prado *et al.* 2013b; Flantua *et al.* 2016). Perhaps the most extensive recent synthesis of South American mid-Holocene palaeoecological records is the pollen-based biome reconstructions of Marchant *et al.* (2009). Here, they applied a 'biomisation' method (Prentice *et al.* 1996; Prentice & Webb 1998) to reconstruct broad biome classifications from fossil-pollen records that were available at that time. Although this allows a standardised method to be applied to each record in the synthesis, information is potentially lost from the in-depth knowledge that the author(s) will have about their site; for example, regarding pollen taphonomy, catchment type/size and local hydrological dynamics. In addition, sole reliance upon lake/bog pollen records precludes the ability to consider sites that apply other palaeoecological proxies, such as stable carbon isotopes and phytoliths from soil profiles, which can be especially informative for those regions where suitable lakes/bogs (required for pollen analysis) are absent or rare. Finally, existing

palaeo-data syntheses are now considerably out of date, due to the publication of new palaeoecological records over the past decade. There is therefore a clear need for an up-to-date synthesis of multi-proxy palaeoecological sites to be able to conduct a robust palaeo model-data comparison of mid-Holocene Amazonia.

1.3.3 Past human land use

Although the central aim of this project is to consider the effect of mid-Holocene climate change upon Amazonian vegetation, the importance of past human cultures in shaping landscapes and ecosystems should not be forgotten. For a long time, the native cultures of Amazonia (i.e. before the arrival of Europeans in the Americas in AD 1492, or 'pre-Colombian') were considered to have had a very limited impacts on the environment. Instead, Amazonia was considered to be a 'pristine' natural wilderness, with sparse human settlements existing using only subsistence practices (Meggers 1992; 2003), with arguments that low nutrient status of tropical soils and physical barriers of dense rainforest largely prohibited sedentism (Meggers 1954). More recent archaeological discoveries have been dismissed as 'the exception' rather than 'the rule' (Barlow *et al.* 2012). However, in the past couple of decades, the rapidly increasing discoveries of extensive Amazonian settlements (Heckenberger & Neves 2009), numerous earthworks (e.g. Pärssinen *et al.* 2009; Walker 2013), and vast coverage of nutrient rich 'terra preta' soils (e.g. Glaser & Woods 2004) make it difficult to argue that pre-Colombian humans had only negligible effects on the environment.

There are a number of reasons that pre-Colombian land use is not being explored in this thesis. Most of the major human impacts, associated with major earthworks and landscape management, occurred within the last few millennia, well after the primary period of focus of the middle Holocene (ca. 6,000 years ago). Additionally, the impacts of humans before these major artificial earthworks, raised fields, sedentism, cultural forests (etc.) were most likely on small, local scales (e.g. Bush *et al.* 2007; Carson *et al.* 2014; Bush *et al.* 2016), whereas this thesis aims to look at potential for climate-driven regional scale biome stability. More practically, there are many sources of uncertainties that already exist in investigations using climate models and dynamic vegetation models (see sections 1.2.1 and 1.2.2). Including human impacts into these modelling investigations would add even more uncertainties that would not be easy to disentangle, thus compromising the overall focus of this thesis. Overall, given that climate change and human impacts are the two major causes of environmental change, it is this thesis' aim to isolate climate change-induced impacts to help others put human-induced impacts into context.

1.4 Thesis aims and objectives

The overall aim of this thesis is to improve our understanding of the impact of long-term mid-Holocene drought upon Amazonian ecosystems. This will be achieved using a novel, multi-disciplinary approach, integrating knowledge from both palaeoecology and Earth system modelling. A new, up-to-date mid- to late Holocene synthesis of existing palaeoecological records helps to put the vegetation changes seen during the middle Holocene into context and will provide a dataset for model-data comparisons. A new fossil-pollen record was created from a palm swamp (Cuatro Vientos) located in the Bolivian Amazon to provide new insights into (a) the mid-Holocene vegetation history of this ecotonal region of Amazonia and (b) the suitability of palm swamps as repositories of palaeoecological data. Finally, an ensemble of 21 mid-Holocene (6 ka BP) Amazonian vegetation simulations was created, using three different DGVMs and seven different climate models, in one of the first palaeo modelling-data comparison projects for mid-Holocene Amazonia.

The results are presented as stand-alone papers in three chapters, formatted in the style of the journal to which they have been submitted for publication. The topic of this thesis is unique, in that the scope of the aims provides a rare opportunity to gain a broad range of complementary skills relevant to studying past environments. Chapter 2 provides skills in synthesising large amounts of relevant data, Chapter 3 provides skills in fossil-pollen analysis, and Chapter 4 provides experience running computer models and analysing their output. The specific research aims and objectives of each chapter are given below.

Chapter 2 was published in *Quaternary Research* (Smith & Mayle 2018). It aims to provide new insights into the spatio-temporal dynamics of biome-scale vegetation changes across tropical South America over the past 6,000 years. The following objectives are addressed:

- Create a new, up-to-date multi-proxy synthesis of existing mid- to late Holocene palaeoecological records from across tropical South America, providing a baseline for the current extent of our knowledge of Amazonian palaeoecology
- Consider the spatial scale of each record's vegetation reconstruction to help differentiate between local- and regional-scale changes
- Use independent palaeoclimate records to assess the relationship between vegetation change and long-term climate change

Chapter 3 was submitted to *Quaternary Research* in September 2018 and is currently in review (Smith et al.). It aims to improve our knowledge of the relationship between basin

characteristics and their fossil pollen archives in tropical regions. The following objectives are addressed:

- Produce a new fossil-pollen record from the Cuatro Vientos palm swamp, located in north-eastern Bolivia near the southern Amazonian rainforest-savannah ecotone
- Compare the Cuatro Vientos pollen record with that of Laguna Chaplin, a nearby large lake, to examine the effect of basin type (swamp versus lake) and size (small versus large) upon tropical palaeoecological archives
- Demonstrate that palm swamps can yield useful pollen archives recording the history of terrestrial vegetation beyond the basin margin, rather than merely a history of localised swamp vegetation dynamics
- Use the local-scale catchment of Cuatro Vientos to assess the extent to which riverine/gallery forests were present in southern Amazonia during the drier climatic conditions of the middle Holocene and Last Glacial Maximum.

Chapter 4 was submitted to *Global Change Biology* in September 2018 and is currently in review (Smith et al.). It aims to investigate how resilient Amazonian forests were to the drier climate of the middle Holocene using an ensemble of vegetation simulations, benchmarked against the palaeoecological knowledge gained from previous chapters. The following objectives are addressed:

- Produce an ensemble of mid-Holocene vegetation simulations using three different DGVMs (JULES, IBIS, SDGVM) driven with the mid-Holocene climate simulations from seven climate models, thus allowing consideration of the uncertainty surrounding the choice of DGVM and/or climate model in vegetation simulations
- Compare these simulations with the palaeoecological dataset created in Chapter 2 in order to assess the relative skill of each model combination
- Determine those regions of Amazonia for which we have the most/least confidence in the mid-Holocene vegetation simulations
- Consider the implications for the future of Amazonia

Appendix. A The data syntheses from Chapter 2 was also used in a paper examining the relationship between expansion of the Tupi-Guarani pre-Columbian culture, climate change, and vegetation change (Iriarte *et al.* 2017). A copy of this paper is provided here.

Chapter 2. Impact of mid-to-late Holocene precipitation changes on vegetation across lowland tropical South America: a paleo-data synthesis

Authors: **Richard J. Smith**, Francis E. Mayle

2.1 Preface

The following chapter is taken from a paper published in the journal *Quaternary Research* (Smith & Mayle 2018). The chapter is therefore written in the style of a journal article, conforming to the regulations of the journal. **RS** led the data collection, interpretation and writing of the paper, with comments and edits by **FM**.

The work presented in this chapter also provided the palaeoecological dataset used in another paper examining the relationship between expansion of the Tupi-Guarani pre-Columbian culture, climate change, and vegetation change (Iriarte *et al.* 2017). A copy of this paper is provided in Appendix A.

Reference

Smith RJ, Mayle FE (2018) Impact of mid- to late Holocene precipitation changes on vegetation across lowland tropical South America: a paleo-data synthesis. *Quaternary Research*, **89**, 134–155. DOI: 10.1017/qua.2017.89

2.2 Abstract

A multi-proxy paleo-data synthesis of 110 sites is presented, exploring the impact of mid-to-late Holocene precipitation changes upon vegetation across Southern Hemisphere tropical South America. We show that the most significant vegetation changes occurred in south-west Amazonia and south-east Brazil, regions reliant on precipitation derived from the South American summer monsoon (SASM). A drier mid Holocene in these regions, linked to a weaker SASM, favoured more open vegetation (savannah/grasslands) than present, while increased late-Holocene precipitation drove expansion of humid forests (e.g. evergreen tropical forest in south-west Amazonia, *Araucaria* forests in south-east Brazil). The tropical forests of central, western and eastern Amazonia remained largely intact throughout this 6000-year period. North-eastern Brazil's climate is 'anti-phased' with the rest of tropical South America, but a lack of paleo data limits our understanding of how vegetation responded to a wetter(drier) mid(late) Holocene. From this paleo-data perspective, we conclude that ecotonal forests already close to their climatic thresholds are most vulnerable to predicted future drought, but the forest biome in the core of Amazonia is likely to be more resilient. Of greater concern is widespread deforestation and uncontrolled anthropogenic burning, which will decrease ecosystem resilience, making them more vulnerable than they might be without current anthropogenic pressures.

2.3 Introduction

The response of the vegetation across tropical South America to long-term climate change is of great concern, given the importance of the ecosystem services this region provides. Of particular concern is how vegetation will respond to a drier climate, given the future projections of more intense dry seasons and increased frequency of severe drought events (Joetzjer *et al.* 2013; Boisier *et al.* 2015; Duffy *et al.* 2015). The extensive work carried out by the RAINFOR ecological monitoring project (Malhi *et al.* 2002) has demonstrated the short-term vulnerability of Amazonian forests to severe drought events (Phillips *et al.* 2009; Doughty *et al.* 2015; Feldpausch *et al.* 2016). However, whilst the effects of these short-term severe drought events are relatively well understood (e.g. Rowland *et al.* 2015), considerable uncertainty exists as to how long-term climate change will affect the vegetation of tropical South America. Results of future model simulations using process-based dynamic global vegetation models (DGVMs) range from catastrophic large-scale Amazonian forest die-back as a result of positive feedbacks between the biosphere and atmosphere (Cox *et al.* 2000; 2004), to other studies suggesting that the forests will be resilient to climate change (Cowling & Shin 2006; Huntingford *et al.* 2013). One problem in predicting future vegetation dynamics is the lack of direct long-term observational data of vegetation responses to long-term climate change in the past. However, the use of proxy-based vegetation reconstructions allows us to extend our observational period back millennia through times of significant, long-term climate change. The role of paleoecology in increasing our understanding of long-term vegetation dynamics is well established within the paleo-data community, and is playing an increasingly important role in helping to understand mechanisms and uncertainties within model simulations through initiatives such as PMIP (Paleoclimate Modelling Intercomparison Project) (Joussaume & Taylor 1995; Braconnot *et al.* 2011).

Several mid-late Holocene paleoecological syntheses have been undertaken in the past, but these are now relatively outdated (e.g. Mayle & Power 2008; Marchant *et al.* 2009) due to the publication of both new paleoecological and paleoclimate records over the past decade. Furthermore, more recent syntheses (e.g. Prado *et al.* 2013b; Flantua *et al.* 2016) have used paleoecological data (predominantly pollen) to reconstruct past climate, which precludes examination of vegetation-climate relationships. We therefore present an updated multi-proxy synthesis of published paleoecological records from across lowland tropical South America from the mid Holocene (ca. 6000 years ago, 6 ka) to the present. This time period is important both paleoecologically and paleoclimatologically, as there is widespread evidence that millennial-scale changes in insolation (driven by the precessional cycle of Earth's orbit) caused

long-term precipitation changes, and associated vegetation changes, across the region (Mayle & Power 2008; Prado *et al.* 2013a; Baker & Fritz 2015). Therefore, we will consider the paleoecological records alongside key paleoclimate records from across the study region in order to assess any vegetation changes in the context of long-term climate change.

This synthesis will provide new insights into the spatio-temporal dynamics of biome-scale vegetation changes on a sub-continental scale over the past 6000 years, in the context of climate change inferred from independent paleoclimate data. Although there is increasing evidence that pre-Columbian (pre-AD1492) peoples managed the floristic composition of their forest resources (especially by promoting palms, e.g. Watling *et al.* 2017), there is little evidence, to date, that they practiced large-scale deforestation. We therefore expect natural drivers (i.e. climate change) to be the most likely explanation for any biome-scale vegetation shifts over the broad, regional scales that we consider in this synthesis – an assumption borne out by a recent study of local-scale human land use nested within regional-scale, climate-driven, forest-savannah biome turnover (Carson *et al.* 2014). However, if the vegetation history of a given site(s) is inconsistent with independent paleoclimate data from the area, we will consider whether human land use can reconcile this apparent vegetation-climate mismatch.

2.3.1 Modern environmental setting

Modern climatic setting

Figure 2.1 shows long-term mean precipitation over South America for austral winter (June, July, August, Fig. 2.1a) and austral summer (December, January, February, Fig. 2.1b), along with mean wind speed and direction at 850 mb. The relatively narrow, longitudinally orientated belt of precipitation over the tropical oceans marks the location of the Intertropical Convergence Zone (ITCZ). The ITCZ refers to a band of low pressure and convergence of the moist trade winds over the equatorial oceans and is associated with rising air and intense convective precipitation. The rising air at the ITCZ diverges polewards when it nears the tropopause, and descends when over the subtropics, causing semi-permanent high pressure cells over the subtropical oceans such as the South Atlantic subtropical high (SASH – Fig. 2.1); this loop of air movement is known as the Hadley cell circulation (Garreaud *et al.* 2009). The different thermal properties of the continental land mass of South America and the surrounding oceans gives rise to a distinct seasonal cycle of precipitation over most of the tropical South American continent. During austral winter, when the thermal equator and ITCZ

are located further north, maximum precipitation over the continent is located in northern South America, whereas central South America experiences its dry season (Fig. 2.1a). Southern Brazil maintains an important source of moisture from both moist winds fed into the region by the circulation of the SASH and extra-tropical frontal systems (Cruz *et al.* 2006b; Garreaud *et al.* 2009). During austral spring/summer the thermal equator moves south and heats the central South American land mass up relative to the surrounding oceans. This continental heating causes areas of intense convection to form over central Brazil and southern Amazonia, which are fed with moist easterly trade winds blowing in from the Atlantic Ocean, helped by an intensified SASH. This marks the onset of a system commonly referred to as the South American Summer Monsoon (SASM) (Fig. 2.1b - Zhou & Lau 1998; Raia & Cavalcanti 2008; Silva & Kousky 2012). As the moist easterly trade winds reach the Andean mountain range, they are diverted southward and are intensified by an area of deep low pressure that forms over the Gran Chaco region (the 'Chaco Low'). This flow creates a feature known as the South American Low Level Jet (SALLJ), associated with very strong low-level winds that are channelled southwards by the eastern Andes and the Brazilian planalto highlands (Marengo *et al.* 2002). The SALLJ helps to transport moisture from Amazonia into subtropical south-east Brazil where the South Atlantic Convergence Zone (SACZ) is intensified (Carvalho *et al.* 2004).

In contrast to the central and southern areas of tropical South America, the north-east of Brazil is conspicuously dry throughout most of the year (Garreaud *et al.* 2009). The intense updrafts in the central part of the continent (in particular the Chaco Low) during the mature phase of the SASM requires compensating subsidence in surrounding regions. This subsidence manifests as an upper tropospheric low pressure feature called the 'Nordeste Low', which suppresses rainfall over the region of north-east Brazil (Chen *et al.* 1999; Cruz *et al.* 2009). This east-west difference in precipitation caused by zonal overturning circulations has been referred to as the east-west South American precipitation dipole (Cheng *et al.* 2013). Interannual variability in precipitation over tropical South America is linked to the El Niño Southern Oscillation (ENSO); during El Niño episodes, precipitation rates are below average across eastern Amazonia and north-eastern Brazil (Garreaud *et al.* 2009).

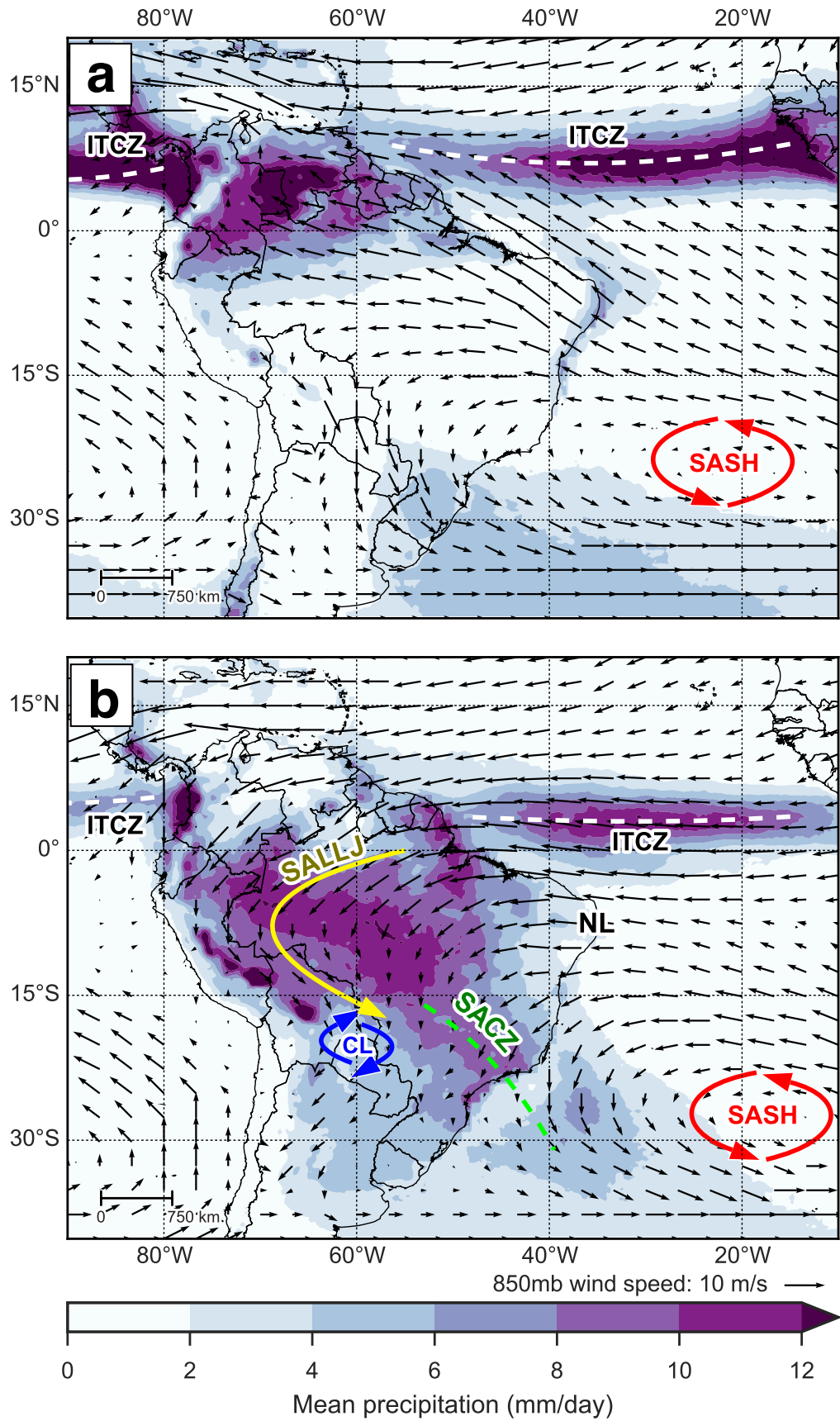


Figure 2.1 - (Caption overleaf)

Figure 2.1 - Observed long-term mean precipitation (mm/day), 850 mb wind speed and wind direction for (a) June, July and August (JJA), and (b) December, January, February (DJF). Labels indicate key climate features: Intertropical Convergence Zone (ITCZ), South American Low Level Jet (SALLJ), Chaco Low (CL), South Atlantic Convergence Zone (SACZ), South Atlantic Subtropical High (SASH), and Nordeste Low (NL) - see text for details. Precipitation data taken from Tropical Rainfall Measuring Mission v7 (TRMM) 3B43 dataset (1998-2014) (Huffman *et al.* 2007). Wind data taken from NCEP Climate Forecast System Reanalysis (CFSR) dataset (1979-2010) (Saha *et al.* 2010a; 2010b).

Modern vegetation setting

The lowlands of tropical South America support a wide variety of ecoregions, ranging from humid rainforests to xeric scrublands (Fig. 2.2a). The ecoregions described here refer to the *potential* ecoregions, as the *actual* vegetation cover has been highly affected by modern deforestation, agriculture and industrialisation. The Amazon humid evergreen tropical forest (HETF) is the largest biome of tropical South America, covering most of northern and western Brazil and extending into neighbouring countries to the west and north where annual precipitation is high (>1600 mm). The southern and eastern ecotonal margins of the Amazon HETF exist in a much more seasonal climate with longer dry seasons. Small patches of savannah can occur within the Amazon HETF where edaphic conditions are favourable (Adeney *et al.* 2016). Along the foothills of the Andes lies a band of Yungas forest, a transitional area ranging from moist evergreen lowland forest to montane forests. The Atlantic forest biome, supporting a mix of lowland and montane evergreen forests, exists on the east coast of Brazil where coastal and orographic rainfall maintain a moist climate (Fig. 2.2c). The *Araucaria* moist forest biome (characterised by the high abundance of the evergreen tree *Araucaria angustifolia*) exists on the highlands of southern Brazil where annual precipitation is high (~2000 mm) and there is a short dry season (< 2 months) (Hueck 1953; Behling & Pillar 2007).

In between the Amazon and Atlantic rainforests exists the 'dry diagonal' (Prado & Gibbs 1993). This is a large area, characterised by highly seasonal rainfall, that contains a mixture of deciduous and semi-deciduous trees, shrubland and savannah. Most of this area is covered by the Cerrado savannah biome. Due to the variety of climatic, edaphic and topographic features in the region, the savannah types range from open grassland to more dense shrub and savannah tree cover (Silva & Bates 2002). Gallery forests can occur along the streams

that flow through the Cerrado, as well as small patches of closed canopy deciduous and semi-deciduous trees where edaphic conditions are favourable (Silva & Bates 2002; Werneck 2011). Larger areas of semi-deciduous tropical dry forests (SDF) exhibit a fragmentary distribution. 'Nuclei' of SDF exist across: the Chiquitano region of eastern lowland Bolivia; across southern Brazil along the Paraná and Paraguay rivers and into the Misiones province of northern Argentina; and inland areas of the Atlantic forest biome. SDF exist in highly seasonal climates, with annual precipitation <1600 mm and a dry season length of ~5 – 6 months (Gentry 1995; Werneck 2011). These SDF areas exist under similar climatic conditions to the Cerrado savannah, but are restricted to soils with higher nutrient content and high pH (Pennington *et al.* 2000; Werneck 2011). The Caatinga region of north-eastern Brazil supports a complex mosaic of xerophytic vegetation types that range from dense SDF cover, more open tree cover with a shrubby sub-canopy, to open thorn scrubland and savannah. The semi-arid climate is the main control upon this Caatinga vegetation; precipitation rates are low and erratic meaning that long periods of drought are common (Sampaio 1995). However, small 'islands' of humid evergreen rainforest and semi-deciduous tropical dry forests do exist on isolated plateaus inland and near the coast where orographic and coastal rainfall can maintain a humid microclimate (Sampaio 1995; Montade *et al.* 2014).

Figure 2.2 - (Caption overleaf)

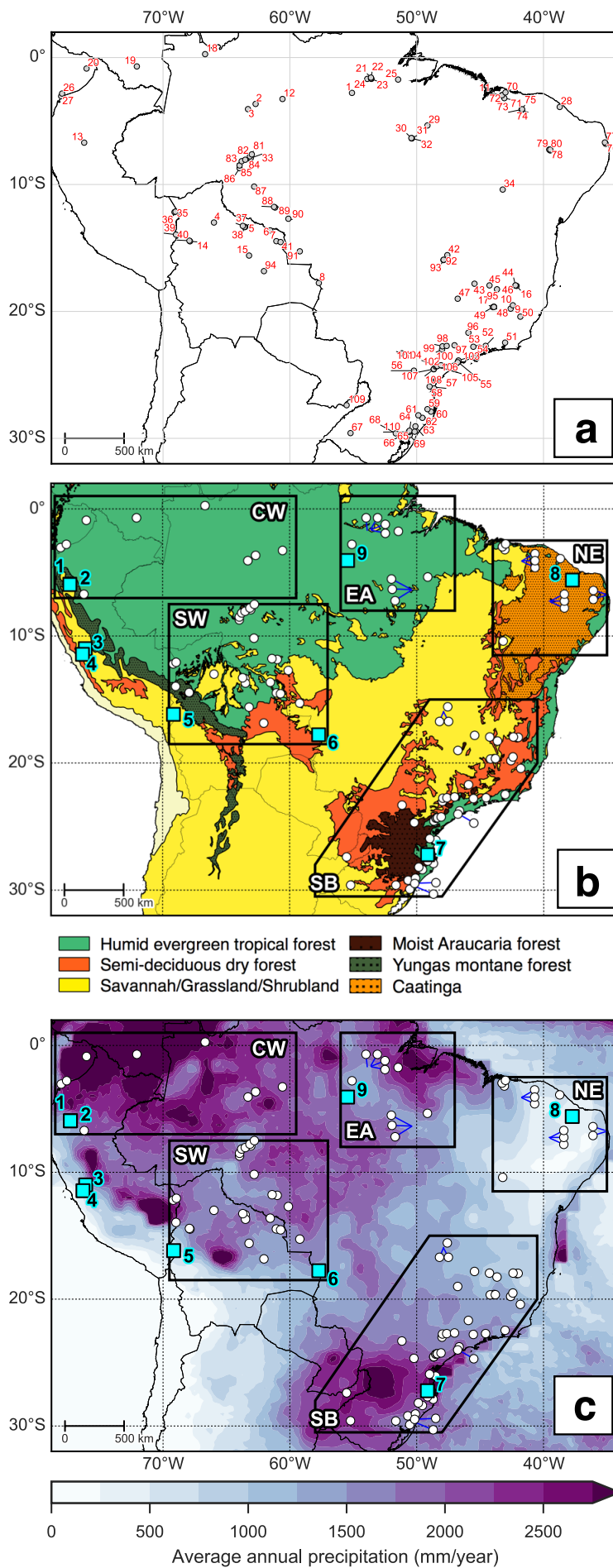


Figure 2.2 - Overview maps of study area, (a) location and numeric ID of each site corresponding to Table 2.1, (b) broad modern vegetation biomes, modified from Olson et al. (2001), (c) long term average annual precipitation based on Tropical Rainfall Measuring Mission v7 (TRMM) 3B43 dataset (1998-2014) (Huffman *et al.* 2007). The polygons shown in (b) and (c) represent the regions discussed in text: CW = Central and western lowland Amazonia, EA = Eastern Amazonia, SW = South-Western Amazonia, SB = South-eastern Brazil, NE = North-eastern Brazil. The blue squares in (b) and (c) show locations of the paleoclimate sites discussed in text: 1 = El Condor, 2 = Cueva del Tigre Perdido, 3 = Lake Junin, 4 = Huaguapo, 5 = Lake Titicaca, 6 = Laguna La Gaiba, 7 = Botuvera Cave, 8 = Rio Grande do Norte, 9 = Paraíso Cave

2.4 Methods

A database of 110 paleoecological sites from 87 previously published papers was created through literature searches and interrogation of repositories such as the Latin American Pollen Database (LAPD - Flantua *et al.* 2015) and Neotoma (<http://www.neotomadb.org>) (Table 2.1). This synthesis considers sites from the Southern Hemisphere tropical lowlands, extending into the subtropics of south-east Brazil (a latitudinal range extending from the equator to 30°S) (Fig. 2). We do not include coastal mangrove sites, as vegetation changes at these sites are predominantly driven by sea level change (e.g. Behling *et al.* 2001b; Guimarães *et al.* 2012; 2013b; Lorente *et al.* 2014). For each paleoecological site, we assign a vegetation classification at 500-year time slices from the mid Holocene (6 ka) to the present, based on a critical evaluation of the authors' interpretations of the proxy data. The broad scale vegetation classifications we use are outlined in Table 2.2. A 'mosaic' classification (a combination of any two vegetation types) was used when interpretation suggests that the vegetation cover at a site was most likely a mixture of vegetation types. Ideally, a site will cover the whole period from 6 ka to the present, although there are a number of sites that cover a shorter period. It does not seem appropriate to ignore sites that do not quite cover the whole period as they may still provide valuable information about vegetation trends in a particular area. Therefore, the sites included in our synthesis must have a vegetation reconstruction spanning from earlier than 4 ka, up to at least 2 ka; this ensures that the sites cover a period where there is strong evidence that the region underwent long-term climate change.

Imposing strict criteria on the chronological quality of each site is problematic in this research area. Sedimentation rates are highly variable between samples; sites with low sedimentation

rates are particularly problematic as a relatively short core could encompass many millennia. Sub-sampling resolution also varies between sites depending on the length of the record and the specific research questions of the authors. The paucity of sites across tropical South America means that rejecting sites based on low chronological resolution would result in only a handful of sites being considered. Therefore, we have been relatively flexible in our consideration of sites with lower chronological resolution; this means that this synthesis can only provide an overview of the broad scale vegetation trends in the region over the last 6000 years, rather than exact timings of any changes. Where possible, calibrated radiocarbon dates and age-depth models that are presented in the original paper(s) of each site are used to inform the timings of any changes at that site. If a site records key vegetation changes through its record but does not present calibrated dates or an age-depth model, we use the Bacon age-depth model v2.2 in R (Blaauw & Christen 2011) to produce an independent age-depth model for that site using the raw chronological data from the paper. This is the case with 26 of the sites, indicated in Table 2.1. The IntCal13 calibration curve (Reimer *et al.* 2013) was chosen over SHCal13 (Hogg *et al.* 2013), given the hydrological links of the study area with the northern hemisphere (through the SASM and ITCZ).

We acknowledge that other more quantitative methods of classifying vegetation from paleoecological data are available, such as Biomisation (Prentice *et al.* 1996; Prentice & Webb 1998) and the REVEALS/LOVE Landscape Reconstruction Algorithm (Sugita 2007a; 2007b). However, these methods are based predominantly on pollen data from lakes, require access to the raw data of each site, and, in the case of REVEALS, require a high density of sites of multiple sizes in a given area. Furthermore, the REVEALS model has yet to be proven in a Neotropical setting where important assumptions about anemophily are violated by most taxa. The paucity of pollen sites that extend back to the mid-Holocene in our research area limits the usefulness of these quantitative methods (which focus solely on pollen data) in producing a thorough synthesis. For example, in the most recent application of the Biomisation method across Latin America (Marchant *et al.* 2009), there are only around 24 pollen records in our research area that date back to the mid Holocene. Our method allows us to consider other vegetation proxies in addition to pollen (e.g. phytoliths, stable carbon isotopes) and other paleoecological archives in addition to lakes (e.g. soil pits), thus increasing the number of sites we can include in our synthesis by utilising the full suite of paleovegetation data available. In addition, our method allows us to take advantage of the in-depth knowledge that the author(s) will have about their site (e.g. pollen taphonomy, catchment), which is lost when using a standardised objective method.

2.4.1 Proxy types

This synthesis includes a variety of paleoecological proxy types, all of which have strengths and limitations that must be considered. The two most common proxy types in this synthesis are fossil pollen and stable carbon isotopes ($\delta^{13}\text{C}$). Fossil pollen analysis is the most widely used paleovegetation proxy as it gives a direct indication of what vegetation was growing in an area at a given time. However, care must be taken in interpreting a fossil pollen record as pollen loading into a basin does not necessarily reflect the true vegetation assemblage in the catchment area due to previously mentioned taxonomic-differences in pollen productivities and dispersal characteristics. Additionally, the taxonomic resolution of pollen is highly variable; very few are identifiable to species level, some are identifiable to genus level, and many are only identifiable to family level. These issues mean that reliable interpretation of fossil pollen records is dependent upon modern 'pollen rain' studies whereby pollen traps are left in an area for a set time, after which the pollen assemblages are compared with floristic inventories to determine pollen-vegetation relationships (e.g. Behling *et al.* 1997; Bush & Rivera 2001; Gosling *et al.* 2005; 2009; Jeske-Pieruschka *et al.* 2010; Guimarães *et al.* 2014). Stable carbon isotope fractionation ($\delta^{13}\text{C}$) utilises the fact that C_3 vegetation (woody plants) and C_4 vegetation (savannah grasses and sedges) have distinct $\delta^{13}\text{C}$ carbon isotope signatures (Boutton 1996; Pessenda 2004). Whilst this differentiation between C_3 and C_4 vegetation is quite broad, it does reveal whether the landscape was closed-canopy forest or open savannah, especially if bolstered by knowledge of the modern isotopic-vegetation relationships in a given area. We also include a small number of sites with phytolith (plant silica bodies)-based vegetation reconstructions (Piperno 2006). Unlike pollen, phytoliths preserve well in oxidised environments (e.g. soils) and are particularly useful in increasing the taxonomic resolution of grass. Although few phytolith-based paleoecological studies have yet been undertaken, recent studies have shown the effectiveness of phytoliths in distinguishing between modern tropical ecosystems in the Amazon (Dickau *et al.* 2013; Watling *et al.* 2016).

Several other proxies can provide important complementary information for pollen, $\delta^{13}\text{C}$, and/or phytolith studies. Charcoal analysis is commonly used to reconstruct past fire activity, which can be an indication of past changes in climate and vegetation characteristics (Power *et al.* 2008). Isotopic analysis of nitrogen ($\delta^{15}\text{N}$) and chemical analyses of carbon/nitrogen (C/N) ratios can indicate whether the organic matter in a sediment record originates from an aquatic source (elevated levels of ^{15}N , low C/N ratios) or a terrestrial source (low levels of ^{15}N , high C/N ratios) (Meyers 1994; Horák *et al.* 2011). Measurements of chemical element

concentrations, using methods such as X-ray fluorescence (XRF), can reveal catchment erosion which in turn may be linked to local/regional environmental change.

2.4.2 Archive types and spatial scale of reconstructions

When drawing paleoecological inferences from vegetation proxy data, it is important to consider the spatial scale that the latter represents. This spatial scale is influenced by both the type of proxy, as well as the size and type of deposit that the proxy came from. It is widely accepted in the field of palynology that the spatial scale represented by pollen assemblages in lake sediments is related to the size of that lake; small lakes (and bogs) represent local-scale vegetation, whereas large lakes represent regional-scale vegetation (Davis 2000). This relationship has been shown through practical experiments that correlate pollen signals from lake surface-sediment samples to vegetation inventories at increasing distances from the lake, as well as being formerly quantified in a pollen deposition/dispersal model (Prentice 1985; Sugita 1993; 1994). Whilst most of this research has been done for mid to high latitudes, the pattern is expected to be valid for the tropics. Soil pits are a common archive type that usually use $\delta^{13}\text{C}$ isotope as a paleoecological proxy (and in some cases phytoliths). These records essentially represent a 'point' scale (i.e. a record of the vegetation that grew directly in that soil) and as such transects/networks of soil pits are often taken to help represent a larger spatial area. For this synthesis, we categorise each site into one of 4 archive types: lakes, peat bogs, terrestrial (e.g. unspecified sediment hollows or swamps) and soil pits. In an attempt to visually represent the spatial scale that each record represents, we display different sized circles in Figure 2.4 based on the rules defined in Table 2.3. In some cases, the display of soil profiles that are very close together have been combined; this has been indicated in Table 2.1 whenever this is the case.

2.4.3 Paleoclimate records

To assess the relationship between vegetation change and long-term climate change, we have selected 8 key paleoclimate records from across the region (Figs. 2.2 and 2.3). Five of these sites (El Condor, Tigre Perdido, Huaguapo, Botuvera Cave and Rio Grande do Norte) have precipitation reconstructions based on speleothem stable oxygen isotope ($\delta^{18}\text{O}$) records, while precipitation records of the other sites are based upon lake-level reconstructions (Lake Titicaca and Laguna La Gaiba) or $\delta^{18}\text{O}$ analyses of lake calcite deposits (Lake Junin). As with the paleoecological records, we rely upon the authors' expert knowledge of these sites to inform our interpretations. This is particularly important for the speleothem records, as

changes in isotopic composition can be influenced by a number of factors, including changes in moisture source, temperature, and/or rainfall amount (Lachniet 2009).

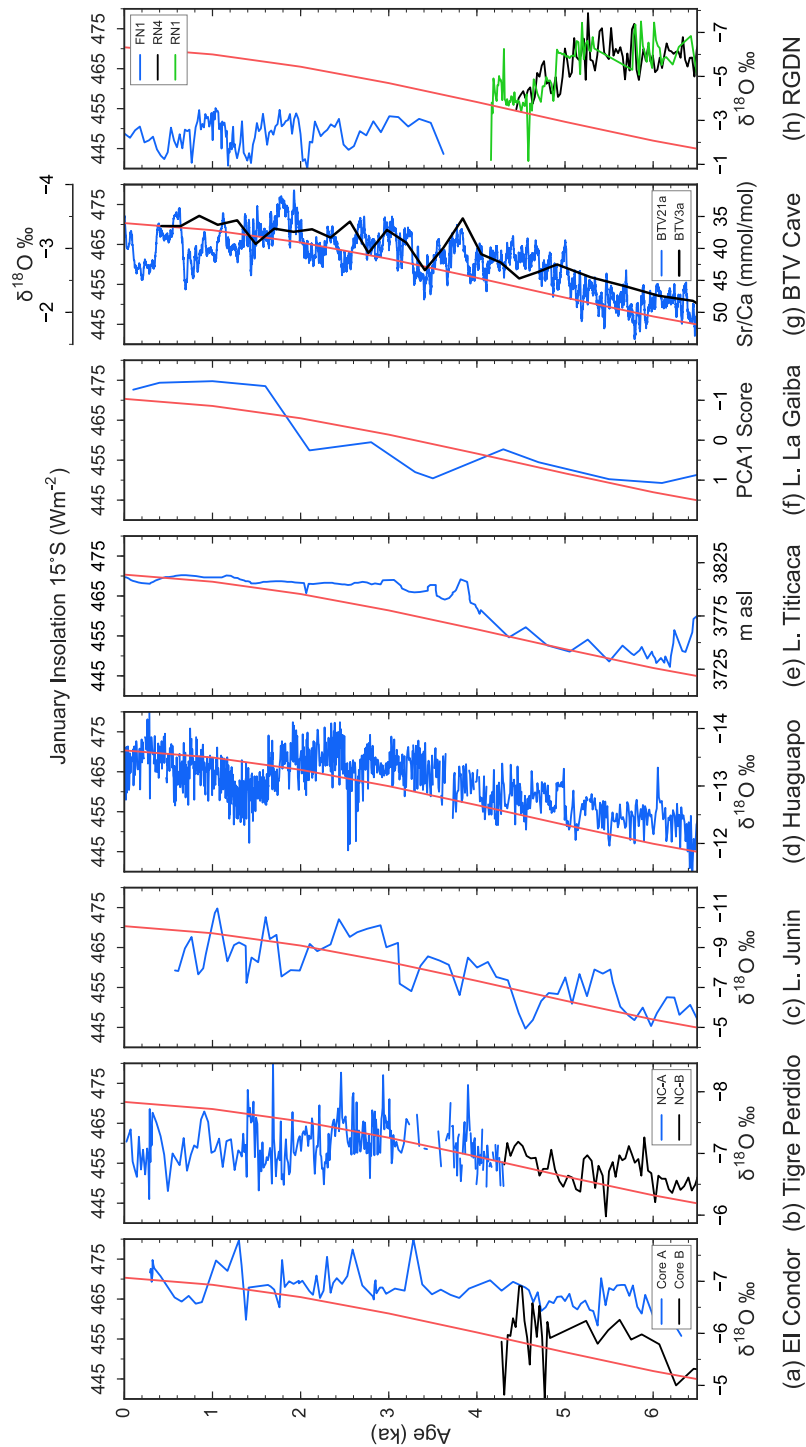


Figure 2.3 - (Caption overleaf)

Figure 2.3 - Selected paleoclimate records representing proxy records for precipitation changes through the last 6 ka, shown alongside calculated January insolation at 15°S (Berger & Loutre 1991; Berger 1992) (a) $\delta^{18}\text{O}$ of stalagmite Core A and Core B from El Condor Cave (Cheng *et al.* 2013), (b) $\delta^{18}\text{O}$ of stalagmite records NC-A and NC-B from Cueva del Tigre Perdido (van Breukelen *et al.* 2008), (c) $\delta^{18}\text{O}$ of calcite from Lake Junin (Seltzer *et al.* 2000), (d) $\delta^{18}\text{O}$ of speleothem record Huaguapo (Kanner *et al.* 2013), (e) lake-level changes as measured by $\delta^{13}\text{C}$ at Lake Titicaca (Rowe *et al.* 2002), (f) *Pediastrum*-inferred lake-level change at Laguna La Gaiba (Whitney & Mayle 2012), (g) $\delta^{18}\text{O}$ of speleothem record BTV3a, Sr/Ca of speleothem BTV21a from Botuvera Cave (BTV) site (Wang *et al.* 2007; Bernal *et al.* 2016), (h) $\delta^{18}\text{O}$ of speleothem records FN1, RN1 and RN4 from the Rio Grande do Norte (RGDN) record (Cruz *et al.* 2009).

Table 2.1 - List of paleoecological sites. 'ID' number refers to location number in Fig. 2.2a. Size categories refer to those outlined in Table 2.3. Subscript numbers next to site names refer to the proxy types used in that study: 1 = pollen analysis; 2 = charcoal analysis; 3 = isotopic analysis; 4 = physio-chemical analysis. Asterisk next to site ID indicates a site where an independent age-depth model was created (see methods).

ID	Site Name	Latitude	Longitude	Reference(s)
Size category: Large (L)				
1	Lago Tapajós TAP02 _{1,2,3,4}	2°47.14'S	55°6.13'W	(Irion <i>et al.</i> 2006)
2*	Acará lake _{1,3,4}	3°39.32'S	62°42.07'W	(Horbe <i>et al.</i> 2011)
3*	Coari Lake _{1,3,4}	4°3.85'S	63°18.11'W	(Horbe <i>et al.</i> 2011)
4	Lago Rogaguado _{1,2}	12°59.84'S	65°59.16'W	(Brugger <i>et al.</i> 2016)
5	Laguna Orícore _{1,2}	13°20.74'S	63°31.53'W	(Carson <i>et al.</i> 2014)
6	Laguna Bella Vista _{1,2}	13°37.00'S	61°33.00'W	(Mayle <i>et al.</i> 2000; Burbridge <i>et al.</i> 2004)
7	Laguna Chaplin _{1,2}	14°28.00'S	61°4.00'W	(Mayle <i>et al.</i> 2000; Burbridge <i>et al.</i> 2004)
8	Laguna La Gaiba _{1,3,4}	17°45.69'S	57°42.95'W	(Whitney <i>et al.</i> 2011; Metcalfe <i>et al.</i> 2014)
9*	Lagoa Silvana _{1,4}	19°31.00'S	42°25.00'W	(Rodrigues-Filho <i>et al.</i> 2002)
10*	Lake Dom Helvécio _{1,2,3,4}	19°46.94'S	42°35.48'W	(Ybert <i>et al.</i> 2000; Turcq <i>et al.</i> 2002; Sifeddine <i>et al.</i> 2004)
Size category: Medium (M)				
11	Lagoa do Caçó _{1,2,3}	2°57.64'S	43°15.20'W	(Sifeddine <i>et al.</i> 2003; Pessenda <i>et al.</i> 2005; Ledru <i>et al.</i> 2006)
12*	Lago Calado _{1,4}	3°16.00'S	60°35.00'W	(Behling <i>et al.</i> 2001c)
13	Lake Sauce _{1,2}	6°42.28'S	76°13.07'W	(Bush <i>et al.</i> 2016)

ID	Site Name	Latitude	Longitude	Reference(s)
14	Lake Santa Rosa _{1,2}	14°28.61'S	67°52.48'W	(Urrego <i>et al.</i> 2013)
15	Laguna Yaguarú _{1,2,3}	15°36.00'S	63°13.00'W	(Taylor <i>et al.</i> 2010)
16	Lago Aleixo _{1,3,4}	17°59.27'S	42°7.13'W	(Enters <i>et al.</i> 2010)
17*	Lagoa Santa ₁	19°38.00'S	43°54.00'W	(Parizzi <i>et al.</i> 1998)
Size category: Small (S)				
18	Lake Pata ₁	0°16.00'S	66°41.00'W	(Colinvaux <i>et al.</i> 1996; Bush <i>et al.</i> 2004a)
19*	Pantano de Monica ₁	0°42.00'S	72°4.00'W	(Behling <i>et al.</i> 1999)
20	Maxus 4 _{1,2}	0°52.00'S	76°2.00'W	(Weng <i>et al.</i> 2002)
21	Lake Santa Maria _{1,2}	1°34.76'S	53°36.41'W	(Bush <i>et al.</i> 2007b)
22	Lake Geral _{1,2,4}	1°38.75'S	53°35.95'W	(Bush <i>et al.</i> 2000; 2007b)
23	Lake Saracuri _{1,2}	1°40.82'S	53°34.21'W	(Bush <i>et al.</i> 2007b)
24*	Lake Comprida _{1,2,4}	1°40.93'S	53°53.83'W	(Bush <i>et al.</i> 2000)
25*	Rio Curuá _{1,2,4}	1°44.12'S	51°27.79'W	(Behling & da Costa 2000)
26*	Lake Kumpaka ₁	2°50.20'S	77°57.68'W	(Liu & Colinvaux 1988)
27	Lake Ayauchi _{1,2}	3°2.72'S	78°2.07'W	(Bush & Colinvaux 1988; McMichael <i>et al.</i> 2012)
28	Maranguape ₁	3°53.67'S	38°43.22'W	(Montade <i>et al.</i> 2014)
29*	Lake Marabá _{1,2,3,4}	5°21.00'S	49°9.00'W	(Guimarães <i>et al.</i> 2013a)
30*	Carajás CSS2 _{1,3,4}	6°20.51'S	50°25.16'W	(Absy <i>et al.</i> 1991; Sifeddine <i>et al.</i> 1994; 2001)
31	Lagoa da Cachoeira _{1,2}	6°21.30'S	50°23.59'W	(Hermanowski <i>et al.</i> 2014)
32	Pântano da Maurítia _{1,2,4}	6°22.55'S	50°23.16'W	(Hermanowski <i>et al.</i> 2012a; 2012b)
33	Humaitá HU01 _{1,3,4}	7°55.43'S	63°4.99'W	(Cohen <i>et al.</i> 2014b)

ID	Site Name	Latitude	Longitude	Reference(s)
34*	Saquinho _{1,2}	10°24.00'S	43°13.00'W	(De Oliveira <i>et al.</i> 1999)
35	Lake Parker _{1,2}	12°8.47'S	69°1.30'W	(Bush <i>et al.</i> 2007a; 2007b)
36	Lake Gentry _{1,2}	12°10.64'S	69°5.86'W	(Bush <i>et al.</i> 2007a; 2007b)
37	Laguna Granja _{1,2,5}	13°15.73'S	63°42.62'W	(Carson <i>et al.</i> 2014; 2015)
38	La Luna _{1,2}	13°21.33'S	63°35.03'W	(Carson <i>et al.</i> 2016)
39	Lago Consuelo ₁	13°57.00'S	68°59.00'W	(Bush <i>et al.</i> 2004b)
40	Lake Chalalán _{1,2}	14°25.67'S	67°55.25'W	(Urrego <i>et al.</i> 2013)
41	Huanchaca _{2,3,5}	14°32.18'S	60°43.93'W	(Maezumi <i>et al.</i> 2015)
42*	Vereda de Águas Emendadas VAE _{2,1,2}	15°34.00'S	47°35.00'W	(Barberi <i>et al.</i> 2000)
43	Vereda Laçador ₁	17°49.06'S	45°26.47'W	(Cassino & Meyer 2013)
44*	Lago do Pires ₁	17°56.85'S	42°12.62'W	(Behling 1995a; 1998)
45	Vereda Juquinha ₁	17°56.96'S	44°15.51'W	(Pires <i>et al.</i> 2016)
46*	Lagoa Nova _{1,2}	17°58.00'S	42°12.00'W	(Behling 2003)
47*	Salitre de Minas _{1,2,3,5}	19°0.00'S	46°46.00'W	(Ledru 1993; Alexandre <i>et al.</i> 1999; Pessenda 2004)
48	Lagoa Olhos D'Água ₁	19°38.92'S	43°54.59'W	(Raczka <i>et al.</i> 2013)
49	Lagoa dos Mares ₁	19°39.79'S	43°59.26'W	(Raczka <i>et al.</i> 2013)
50	Primeiro Rancho _{1,2}	20°24.83'S	41°49.57'W	(Nuno Veríssimo <i>et al.</i> 2012)
51	Serra dos Órgãos _{1,2}	22°27.50'S	43°1.69'W	(Behling & Safford 2010)
52	Serra da Bocaina 2 ₁	22°42.83'S	44°34.00'W	(Behling <i>et al.</i> 2007)
53*	Morro de Itapeva _{1,2}	22°47.00'S	45°32.00'W	(Behling 1997a; 1998)
54	Colônia Crater ₁	23°52.00'S	46°42.34'W	(Ledru <i>et al.</i> 2005; 2009)
55*	TU Peat Bog ₁	23°59.00'S	46°44.75'W	(Pessenda <i>et al.</i> 2009)
56*	Serra Campos Gerais _{1,2}	24°40.00'S	50°13.00'W	(Behling 1997a; 1998)

ID	Site Name	Latitude	Longitude	Reference(s)
57*	Serra do Araçatuba _{1,2}	25°55.00'S	48°59.00'W	(Behling 2007)
58	Volta Velha ₁	26°4.00'S	48°37.98'W	(Behling & Negrelle 2001)
59*	Serra da Boa Vista ₁	27°42.00'S	49°9.00'W	(Behling 1995b; 1998)
60	Serra do Tabuleiro _{1,2}	27°53.81'S	48°52.09'W	(Jeske-Pieruschka <i>et al.</i> 2012)
61*	Morro da Igreja ₁	28°11.00'S	49°52.00'W	(Behling 1995b; 1998)
62*	Serra do Rio Rostro ₁	28°23.00'S	49°33.00'W	(Behling 1995b; 1998)
63	Cambará do Sul _{1,2}	29°3.15'S	50°6.07'W	(Behling <i>et al.</i> 2004; Behling & Pillar 2007)
64*	Fazenda do Pinto ₁	29°24.00'S	50°34.00'W	(Behling <i>et al.</i> 2001a)
65	Rincão das Cabritas _{1,2}	29°28.58'S	50°34.37'W	(Jeske-Pieruschka & Behling 2011)
66	Alpes de São Francisco ₁	29°29.59'S	50°37.30'W	(Leonhardt & Lorscheitter 2010)
67	Itajuru Farm _{1,2}	29°35.20'S	55°13.03'W	(Behling <i>et al.</i> 2005)
68*	Serra Velha ₁	29°36.37'S	51°38.92'W	(Leal & Lorscheitter 2007)
69	Santo Antônio da Patrulha _{1,2}	29°44.75'S	50°32.93'W	(Macedo <i>et al.</i> 2010)
Size category: Extra small (XS)				
70	Combination of soil profiles: C17, C20, C25, C54, F15 _{2,3}	2°45.00'S	43°0.00'W	(Pessenda <i>et al.</i> 2004; 2005)
71	Combination of soil profiles: F46, C78 _{2,3}	3°12.00'S	43°5.33'W	(Pessenda <i>et al.</i> 2004)
72	Combination of soil profiles: LCF50, LCF150, LCF200 ₃	2°57.98'S	43°16.03'W	(Pessenda <i>et al.</i> 2004; 2005)
73	Combination of soil profiles: Parna I, Parna IV _{2,3}	4°5.69'S	41°43.71'W	(Pessenda <i>et al.</i> 2010)

ID	Site Name	Latitude	Longitude	Reference(s)
74	Combination of soil profiles: Parna II, Parna VII _{2,3}	4°7.81'S	41°42.65'W	(Pessenda <i>et al.</i> 2010)
75	Combination of soil profiles: Parna III, Parna V, Parna VI, Parna VIII _{2,3}	4°4.45'S	41°41.17'W	(Pessenda <i>et al.</i> 2010)
76	Combination of soil profiles: Rebio I, Rebio II, Rebio III, Rebio IV _{2,3}	6°47.79'S	35°5.98'W	(Pessenda <i>et al.</i> 2010)
77	Combination of soil profiles: Rebio V, Rebio VI, Rebio VII, Rebio VIII _{2,3}	6°41.42'S	35°9.67'W	(Pessenda <i>et al.</i> 2010)
78	Combination of soil profiles: Flona km4, Flona km8 _{2,3}	7°19.20'S	39°28.20'W	(Pessenda <i>et al.</i> 2010)
79	Combination of soil profiles: Flona km6', Flona km12' _{2,3}	7°15.00'S	39°33.00'W	(Pessenda <i>et al.</i> 2010)
80	Combination of soil profiles: Flona km0, Flona km0' _{2,3}	7°15.00'S	39°28.20'W	(Pessenda <i>et al.</i> 2010)
81	Combination of soil profiles: BR319 km178.5, BR319 km179 ₃	7°37.80'S	63°0.00'W	(de Freitas <i>et al.</i> 2001)
82	Combination of soil profiles: BR319 km154, BR319 km188 ₃	7°47.00'S	63°9.00'W	(de Freitas <i>et al.</i> 2001)
83	Combination of soil profiles: BR319 km80, BR319 km82, Humaitá C, Humaitá D ₃	8°10.00'S	63°48.00'W	(de Freitas <i>et al.</i> 2001)
84	Combination of soil profiles: BR319 km100, BR319	8°3.00'S	63°31.00'W	(de Freitas <i>et al.</i> 2001)

ID	Site Name	Latitude	Longitude	Reference(s)
	km111, BR319 km142, BR319 km161 ₃			
85	Combination of soil profiles: BR319 km46, BR319 km68, Humaitá A, Humaitá B, Humaitá E ₃	8°30.00'S	63°58.00'W	(de Freitas <i>et al.</i> 2001)
86	BR319 km5 ₃	8°43.00'S	63°58.00'W	(de Freitas <i>et al.</i> 2001)
87	Ariquemes ₃	10°10.00'S	62°49.00'W	(Pessenda <i>et al.</i> 1998)
88	Pimenta Bueno - forest ₃	11°46.00'S	61°15.00'W	(Pessenda <i>et al.</i> 1998)
89	Pimenta Bueno - cerradão ₃	11°49.00'S	61°10.00'W	(Pessenda <i>et al.</i> 1998)
90	Vilhena ₃	12°42.00'S	60°7.00'W	(Pessenda <i>et al.</i> 1998)
91	Pontes e Lacerda _{2,3}	15°16.00'S	59°13.00'W	(Gouveia <i>et al.</i> 2002)
92	Pitoco ₃	15°55.87'S	47°52.61'W	(Silva <i>et al.</i> 2008)
93	Taquara ₃	15°57.22'S	47°53.32'W	(Silva <i>et al.</i> 2008)
94	Laguna Sucuara _{3,4}	16°49.60'S	62°2.60'W	(Zech <i>et al.</i> 2009)
95	Pau-de-Fruta _{3,4}	18°15.45'S	43°40.06'W	(Horák <i>et al.</i> 2011)
96	Machado soil core _{3,5}	21°40.70'S	45°55.45'W	(Calegari <i>et al.</i> 2013)
97	Jaguaríuna _{2,3}	22°40.00'S	47°1.00'W	(Gouveia <i>et al.</i> 2002; Pessenda 2004)
98	Piracicaba _{2,3}	22°43.00'S	47°38.00'W	(Pessenda 2004)
99	Anhembi _{2,3}	22°45.00'S	47°58.00'W	(Gouveia <i>et al.</i> 2002; Pessenda 2004)
100	Botucatu _{2,3}	23°0.00'S	48°0.00'W	(Gouveia <i>et al.</i> 2002; Pessenda 2004)
101	Londrina _{2,3}	23°18.00'S	51°10.00'W	(Pessenda 2004)

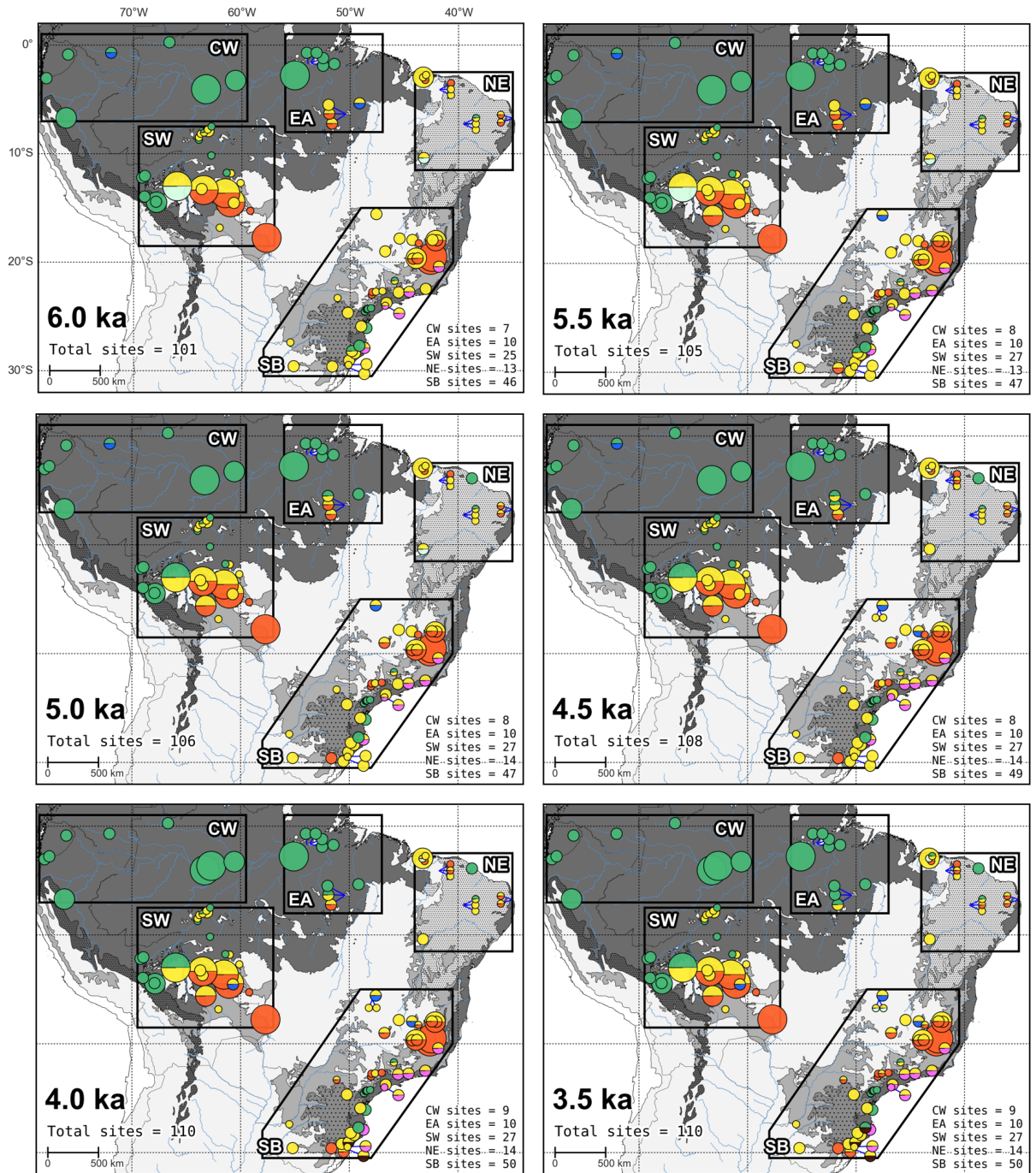
ID	Site Name	Latitude	Longitude	Reference(s)
102	Combination of soil profiles: CER1, CER2, PCN, LN, AC, AF, FSM, EG, EG ₃	24°0.15'S	46°45.97'W	(Pessenda <i>et al.</i> 2009)
103	Saibadela ₃	24°14.42'S	48°4.87'W	(Saia <i>et al.</i> 2008)
104	Bairro Lajeado ₃	24°18.31'S	48°21.91'W	(Saia <i>et al.</i> 2008)
105	Base do Carmo ₃	24°18.41'S	48°24.86'W	(Saia <i>et al.</i> 2008)
106	Bulha D'Água ₃	24°20.25'S	48°30.15'W	(Saia <i>et al.</i> 2008)
107	Bairro Camargo Baixo ₃	24°32.53'S	48°39.19'W	(Saia <i>et al.</i> 2008)
108	Iporanga ₃	24°33.32'S	48°39.45'W	(Saia <i>et al.</i> 2008)
109	Misiones _{3,4}	27°23.40'S	55°31.50'W	(Morrás <i>et al.</i> 2009; Zech <i>et al.</i> 2009)
110	Centro de Pesquisas e Conservação da Natureza ₃	29°28.48'S	50°9.79'W	(Dümig <i>et al.</i> 2008)

Table 2.2 - Description of the broad vegetation classifications used in this study.

Code	Vegetation classification	Description
HETF	Humid evergreen tropical forest	Tall, closed canopy evergreen forest occurring in climates of > ~1600 mm annual precipitation. Can occur in seasonal conditions with dry season length < ~ 4 months.
SDF	Semi-deciduous tropical forest	Shorter trees, varying canopy cover, deciduous/semi-deciduous drought adapted taxa common, < ~1600 mm annual precipitation, marked dry season of 5 – 6 months
GAL	Gallery forest	Occur along streams and rivers where moisture levels can be maintained
ARF	Araucaria forest	Exist on high elevations (500 – 1800 m) under moist conditions, annual precipitation ~2000 mm and a short or no marked dry season
CLF	Cloud/montane forest	Mostly evergreen, closed forests with medium sized trees and shrubs, existing at high elevations (> ~ 1000 m), where orographic rain and persistent low-level clouds can maintain moisture levels
SAV	Savannah/ Grassland/ Scrubland	Generally, refers to open savannahs with few arboreal elements indicative of low annual precipitation (< ~1500 mm) and a long dry season (> 5 – 6 months). We also include sub-tropical campos grassland in this classification to represent open vegetation on the south Brazilian highlands that can exist in climates with dry season lengths ~ 3 months.
PSW	Palm swamp	Flooded, wetland areas (often due to poor soil drainage), often dominated by the palm <i>Mauritia flexuosa</i>

Table 2.3 - Size categories representing the different catchment areas of the paleoecological sites.

Category	Definition
Large (L)	Lakes larger than ~5 km ² , vegetation reconstructions representative of regional scale
Medium (M)	Lakes between ~800 m ² and 5 km ² , vegetation reconstructions representative of local to regional scale
Small (S)	Peat bogs, terrestrial swamps, lakes less than 800 m ² , vegetation reconstructions representative of local scale
Extra-small (XS)	Soil pits, representative of point-scale (i.e. wherever the pit was taken)



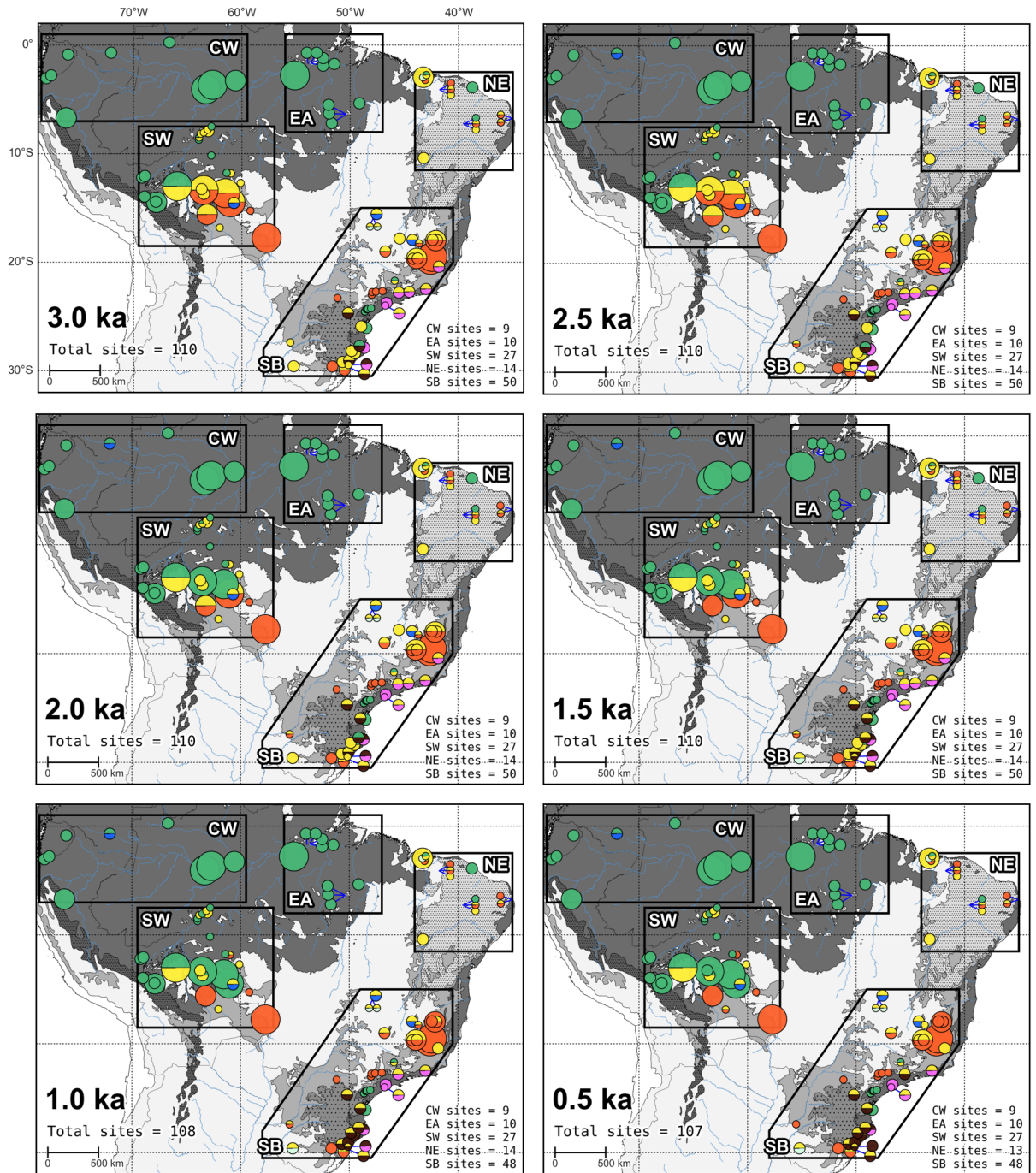
Modern ecoregions

- Humid Evergreen Tropical Forest
- Savannah/Grassland/Scrubland
- Semi-deciduous tropical dry forest
- Caatinga
- Araucaria forest
- Yungas forest

Palaeoecological classifications

- Humid Evergreen Tropical Forest
- Savannah/Grassland/Scrubland
- Gallery Forest
- Semi-deciduous tropical forest
- Cloud/Montane Forest
- Araucaria forest
- Palm Swamp

Figure 2.4 - (Continued overleaf)



Modern ecoregions

- Humid Evergreen Tropical Forest
- Savannah/Grassland/Scrubland
- Semi-deciduous tropical dry forest
- Caatinga
- Araucaria forest
- Yungas forest

Palaeoecological classifications

- Humid Evergreen Tropical Forest
- Savannah/Grassland/Scrubland
- Gallery Forest
- Semi-deciduous tropical forest
- Cloud/Montane Forest
- Araucaria forest
- Palm Swamp

Figure 2.4 - (Caption overleaf)

Figure 2.4 - Paleoeological reconstructions at 0.5 ka time slices from 6 ka to present. Background of modern vegetation biomes, modified from Olson *et al.* (2001). Vegetation classifications outlined in Table 2.2. Size of circles represents catchment area of that site, outlined in Table 2.3.

2.5 Synthesis and discussion

Figure 2.4 shows the paleovegetation reconstruction for each site at 500-year time slices from 6 ka to present. SI Figure 2-A in the supplementary information provides a summary of the changes at each site for each area defined in Figure 2.2. Our discussion of these paleovegetation records is divided into the areas defined in Figure 2.2, within the context of precipitation changes inferred from key paleoclimate records from across the study area (Figure 2.3). The main mechanism for these millennial scale precipitation changes has been attributed to changes in austral summer insolation driven by the precessional cycle of Earth's orbit. During the middle Holocene, lower austral summer insolation levels caused a northward shift in the mean position of the ITCZ (Haug *et al.* 2001) and a decrease in intensity of the SASM (Cruz *et al.* 2005; Wang *et al.* 2007; Vuille *et al.* 2012). In addition, lower austral summer insolation during the mid-Holocene dampened ENSO activity and reduced associated interannual variability of rainfall associated with El Niño/La Niña events (Moy *et al.* 2002; Koutavas & Joanides 2012). Individual interpretations of the paleoclimate records will be drawn upon in the sections below.

2.5.1 Central and western lowland Amazonia (CW)

Speleothem records from the western Peruvian Amazon show slightly elevated $\delta^{18}\text{O}$ values at the mid-Holocene (Fig. 2.3 a-b). This finding suggests that convective precipitation may have been slightly reduced at this time, consistent with a weakened SASM linked to lower summer insolation (Haug *et al.* 2001; van Breukelen *et al.* 2008). However, an overall reduction in total rainfall amount across western lowland Amazonia was probably relatively small due to mechanisms such as the important source of moisture from transpiration processes across central and eastern Amazonia (Eltahir & Bras 1994; Spracklen *et al.* 2012; Cheng *et al.* 2013). The paleovegetation records support the idea that moisture levels have been relatively stable in this region from 6 ka to present. The sites from across central and western lowland Amazonia show that the HETF biome stayed largely intact in this region throughout the mid-to-late Holocene. Evidence of this biome stability comes from consistent

HETF pollen signals from large lake sites (reflecting regional scale vegetation signals - e.g. Behling *et al.* 2001c; Horbe *et al.* 2011) and small sites (reflecting local vegetation signals - e.g. Liu & Colinvaux 1988; Behling *et al.* 1999; Bush *et al.* 2004b). Even if moisture levels were slightly lower during the mid-Holocene, it is clear this was not enough to cause biome turnover. This is currently one of the wettest parts of tropical South America (annual precipitation >3000 mm Fig. 2.2c) with little or no dry season, therefore precipitation levels would have to reduce drastically to cause widespread forest die-back or biome turnover.

2.5.2 South-Western Amazonia (SW)

The area of south-western Amazonia contains the modern ecotonal boundary between the southern Amazonian HETF, the Chiquitano SDF and the Cerrado savannah (Fig. 2.2a). Precipitation levels in this region are highly dependent on the strength of the SASM, especially with regards to the development of the Chaco low and the SALLJ that help to divert precipitation from central Amazonia along the Andes and southwards into eastern Bolivia. As a result, this area has a modern precipitation regime that is much more seasonal than that of the central Amazon basin, with longer dry seasons and lower total annual precipitation of ~1500-1600 mm (Fig. 2.2c). Therefore, the HETF that grows here is much closer to its climatic limit and is more likely to be sensitive to even small changes in precipitation. During the middle Holocene, paleoclimate records from the high Andes suggest this region was drier than present (Fig. 2.3 c-e). Although these records come from the high Andes, they can be considered as representative of lowland south-west Amazonia, at least in regard to the direction of precipitation changes, as they too are dependent on the components of the SASM to divert moisture from central Amazonia. Lake levels at Lake Titicaca on the Bolivian altiplano were ~100m lower than modern at 6 ka (Baker *et al.* 2001), and enriched $\delta^{18}\text{O}$ values from the Huaguapo speleothem and Lake Junin suggest reduced convective activity and lower moisture levels (Seltzer *et al.* 2000; Kanner *et al.* 2013). These Andean records show that modern levels of precipitation were not reached until ca. 4 – 3 ka. A similar pattern of increasing precipitation through the mid-to-late Holocene is found in the paleoclimate record from the lowland site of Laguna La Gaiba (LLG, Fig. 2.3f), although this record suggests that modern moisture levels perhaps were not reached here until ca. 2.5 – 2 ka. Overall, the signals from these sites are consistent with the explanation of a gradual increase in SASM strength in response to increased insolation through the mid-to-late Holocene (Burbridge *et al.* 2004; Kanner *et al.* 2013; Baker & Fritz 2015). The time delay between the Andean records and LLG reaching modern levels could suggest a lag between precipitation increasing in the Andean highlands and in the south-west Amazonian lowlands.

Two key lake sites, Laguna Bella Vista (LBV, id = 6) and Laguna Chaplin (LCH, id = 7), provide strong evidence of vegetation shifts through the mid-to-late Holocene in response to the changes in precipitation (Mayle *et al.* 2000; Burbridge *et al.* 2004). These are very large lakes (> 3 km diameter) and so their pollen assemblages are assumed to represent regional scale vegetation signals. They currently lie in HETF, 130 km (LBV) and 30 km (LCH) north of the modern HETF/SDF/savannah ecotone. However, during much of the mid-to-late Holocene (ca. 6 ka to 2 ka) a mosaic of SDF/savannah vegetation dominates the catchment of these lakes, providing evidence that the HETF/SDF/savannah ecotone was at least 130 km further north than at present. This SDF/savannah mosaic is persistent in the area until ca. 2 ka, when HETF expanded southward into the catchment of LBV; it is not until ca. 1 ka when HETF reached the catchment of LCH. Another large lake record (Laguna Oricore, id = 5), located 200 km to the west of LBV, shows a consistent pattern of a SDF/SAV dominated landscape changing to HETF at ca. 2 ka (Carson *et al.* 2014). The two small sites near to Oricore record a later expansion of HETF at ca. 0.5 ka, but this delay has been attributed to pre-Columbian human land management by the authors (Carson *et al.* 2014; 2016). To the east of these records on the eastern edge of the Chiquitano SDF, the regional pollen record from Laguna La Gaiba (id = 8) suggests that there was no significant contraction of the SDF biome associated with mid-Holocene drought (Whitney *et al.* 2011). Around 600 km north of LBV lies a series of natural savannah 'islands' located within the dense Amazon rainforest. Evidence that these savannah islands expanded by ~60 km at the expense of HETF during the middle Holocene comes from $\delta^{13}\text{C}$ data from a 200 km transect of soil pits between Porto Velho and Humaitá (de Freitas *et al.* 2001; Pessenda *et al.* 2001), spanning the savannah islands. A contemporaneous drying out of a nearby bog (Cohen *et al.* 2014b), together with the 100 m lowstand in Lake Titicaca in the high Andes (Baker *et al.* 2001) suggests that a drier climate likely drove these savannah island expansions. The subsequent contraction of these savannah islands began between ca. 2.5 and 2 ka, with modern $\delta^{13}\text{C}$ values reached by ca. 1.5 ka, concurrent with the forest expansion seen in north-eastern Bolivia (Mayle *et al.* 2000).

A weaker SASM in the mid Holocene is likely to have increased the length and severity of the dry season and decreased annual precipitation below the ~1500 mm climatic threshold between HETF and SDF/SAV, thus driving the northward ecotonal movement. The resilience of the SDF in the eastern Chiquitano region suggests that climate was not sufficiently dry to cause a drastic vegetation shift to dry savannah/scrubland or Caatinga-type vegetation such as that seen in the modern nordeste region of Brazil. Severe drought events were likely more

common, which would have favoured the opportunistic expansion of the savannah vegetation into the vulnerable areas of HETF in the savannah island region, perhaps aided by more frequent fire events. The ca. 1000-year time lag between HETF expansion at LCH versus LBV could reflect the latitudinal time-transgressive nature of precipitation increase, and/or a degree of hysteresis in vegetation response (Burbridge *et al.* 2004). It is important to note that sites from the western Bolivian/south-eastern Peruvian Amazon show stability of HETF through the last 6000 years (Bush *et al.* 2004b; 2007a; Urrego *et al.* 2013). This area receives more precipitation than eastern Bolivia, partly due to its location on the Andean flank and the associated orographic rainfall (Killeen *et al.* 2007). Even if moist winds associated with the SASM and SALLJ were reduced in the mid Holocene, the orographic processes are still likely to have maintained a moist windward Andean flank (Killeen *et al.* 2007; Urrego *et al.* 2013).

2.5.3 South-Eastern Brazil (SB)

South-eastern Brazil marks the 'exit region' of the SASM; during the mature phase of the SASM moisture is transported from central Amazonia to this region via the SALLJ – helped by the Chaco Low and the channelling of the Andes and south Brazilian highlands (Fig. 2.1b). The speleothem records from Botuvera Cave (Wang *et al.* 2007; Bernal *et al.* 2016) provide evidence that this region was drier during the mid-Holocene as less moisture was being received from the Amazon Basin (Fig. 2.3g), consistent with the paleoclimate records from the Andes (Baker *et al.* 2001) and the interpretation of a weaker SASM in response to lower austral summer insolation. The enhancement of moisture transport from the Amazon Basin into south-east Brazil is recorded from ca. 4 ka, around the same time that precipitation levels are shown to increase in the Andean speleothem records. Modern moisture levels were not reached until ca. 2 to 1.5 ka. Bernal *et al.* (2016) note that even though the region receives moisture from extratropical sources, the changes in total rainfall for south-eastern Brazil during the mid-to-late Holocene were predominantly driven by insolation changes and associated SASM intensity.

The paleovegetation records from south-eastern Brazil suggest that open vegetation was more widespread at 6 ka, with increases in arboreal vegetation types through to the present. However, given the diverse range of landscapes in this region, it is unsurprising to find that the timing, magnitude and type of forest expansion is highly variable between different areas. The sites located in the SDF region in the SE Brazilian state of Minas Gerais suggest that this area of SDF remained largely intact through the mid-to-late Holocene. This pattern is exemplified by the reconstructions from two large lakes in the core of this area of SDF, Lago

Silvana (id = 9, Rodrigues-Filho *et al.* 2002) and Dom Helvecio (id = 10, Ybert *et al.* 2000; Turcq *et al.* 2002), that show consistent SDF pollen signals, depleted $\delta^{13}\text{C}$ and low erosional rates throughout the last 6 ka. However, records from smaller sites do reveal more localised vegetation changes from increased SAV in the mid-Holocene (6 ka) to an increase in SDF cover between ca. 5 – 4 ka and again in the last ca. 1 ka. These timings are roughly consistent with the precipitation pattern interpreted from the Botuvera Cave speleothem. Development of dry forest occurred near the borders of the Misiones SDF region from ca. 2 – 1 ka (Pessenda 2004; Zech *et al.* 2009). This SDF expansion suggests that whilst the mid-Holocene climate was not dry enough to cause biome turnover from SDF to savannah, there was sufficient drying, due to an increase in dry season length, to cause an opening of more marginal areas of SDF. The limited records from within the central Brazilian Cerrado show the expansion of gallery forests from ca. 3.5 – 3 ka (Silva *et al.* 2008), and in the southernmost Brazilian Cerrado at ca. 1.5 ka (Behling *et al.* 2005). However, the paucity of these sites means that it is uncertain whether this gallery forest expansion happened across the Cerrado biome.

Across the southern Brazilian highlands, there is clear evidence of extensive areas of SAV type vegetation (most likely campos grassland) from ca. 6 – 4 ka. An expansion of montane forests along the coastal mountains of São Paulo and Rio de Janeiro states occurred from ca. 5 – 4 ka, and expansion of *Araucaria* forest on the southern Brazilian highlands occurred from ca. 4 – 3.5 ka. Further expansion of *Araucaria* forests occurred within the last ca. 1.5 – 1 ka. The *Araucaria* forests were likely to have been particularly sensitive to even small changes in the precipitation regime, as they currently grow where there is high annual precipitation and a short, or ill-defined, dry season. The drier mid-Holocene climate and associated expansion of campos grassland was probably linked with an increased dry season length of around 3 months (Behling 1997b; 1998; Behling & Pillar 2007). The initial phase of *Araucaria* expansion from ca. 4 – 3.5 ka was likely in the form of gallery forests where moisture levels could be maintained more easily (Behling 1997b; Behling *et al.* 2004). The second phase of expansion from ca. 1.5 ka marks a more regional expanse of *Araucaria* forest, suggesting that the precipitation regime was back to near-modern levels, with high annual precipitation and a short, or ill-defined, dry season (Behling & Pillar 2007). Again, these timings seem to match well with the Botuvera Cave paleoclimate records, which record increased tropical moisture source from ca. 4 ka, and a return to modern moisture levels from ca. 2 – 1.5 ka. The timings of *Araucaria* expansion also coincide with increasing human activity in the region, raising the possibility that humans could have taken advantage of a wetter climate and influenced the

expansion of this economically useful taxon (Bitencourt & Krauspenhar 2006; Iriarte & Behling 2007; Iriarte *et al.* 2017).

2.5.4 Eastern Amazonia (EA)

A recently published speleothem record from Paraíso cave in eastern Amazonia suggests that this region may have been wetter than present at the mid Holocene (Wang *et al.* 2017), in contrast to other areas of the Amazon basin that record a drier mid-Holocene. The explanation for this pattern is still unclear; early-mid Holocene warming could have increased moisture supply, while weaker ENSO activity during the mid-Holocene may have reduced drought events in the eastern Amazon (Koutavas & Joanides 2012; Wang *et al.* 2017), but these explanations do not necessarily account for the apparent wetter-than-present mid Holocene. Clearly, the robustness of, and potential mechanisms for, such a pattern requires more investigation. Vegetation reconstructions from most sites near to this speleothem record (e.g. site id's 1, 21-25) show stable HETF cover at the mid-Holocene (Behling & da Costa 2001; Iriarte *et al.* 2006; Bush *et al.* 2007b), which is unsurprising if climate was wetter at this time.

This story is clearly a more complicated one if we consider the evidence of mid-to-late Holocene vegetation changes near to the south-eastern Amazonian ecotone, which appear to contradict Paraíso cave's mid-to-late Holocene precipitation history. A number of sites located on the Serra Sul dos Carajás plateau (ids = 30 – 32) indicate dominance of savannah and dry-adapted SDF arboreal taxa during the mid-Holocene (6 – 5 ka), suggesting drier conditions, after which humid evergreen forest elements gradually increase up to ca. 4 – 3 ka, suggesting increasing moisture (Absy *et al.* 1991; Sifeddine *et al.* 2001; Hermanowski *et al.* 2014). Even though human occupation has been recorded in this region for at least the last 10 ka (Kipnis *et al.* 2005), the decrease in fire occurrences on the Carajás plateau that are recorded during the mid-Holocene at Lagoa de Cachoeira (id = 31) would suggest that the more open vegetation at this time was not initiated by human land management. In fact, a more likely scenario is the abandonment of the plateau by humans at this time (so fewer anthropogenic fires) due to a reduction in both water sources and forest resources (Hermanowski *et al.* 2014). Therefore, the apparent mismatch between these vegetation changes and the climate change at Paraíso Cave is unlikely to be due to human impacts. Around 175 km north-east of the Carajás plateau, the Lake Marabá record (id = 29) indicates a switch to a HETF dominated signal at ca. 5 ka (Guimarães *et al.* 2013a).

Some important considerations must be noted with regards to these records that seem to contradict the regional paleoclimate history. There is clearly a paucity of paleoecological sites across this south-eastern Amazonian ecotonal area, so it is difficult to infer any regional scale vegetation changes. Furthermore, the sites we do have are predominantly located on the Serra Sul dos Carajás plateau. It has long been debated as to how well the HETF surrounding the plateau is represented in the plateau based pollen records (Absy *et al.* 1991; 2014; Guimarães *et al.* 2014). The consensus at this time is that the plateau vegetation, along with some input from the forests growing on the slopes, dominates the pollen assemblages of the lake and bog records from the plateau, suggesting that the mid-to-late Holocene Carajás records only reflect local changes on the plateau itself (Hermanowski *et al.* 2012a; 2012b; 2014). At the nearby Lake Marabá record, the vegetation changes could be due to successional vegetation changes after the formation of the lake (Guimarães *et al.* 2013a). Even given these caveats, there is still a mismatch between vegetation reconstructions apparently indicating a drier mid-Holocene (at a local scale) and the Paraíso cave record indicating a wetter regional climate. Clearly more work needs to be done to reconcile these differences.

2.5.5 North-Eastern Brazil (NE)

As the modern east-west precipitation dipole between north-eastern Brazil (dry climate) and the central South American tropics (wet climate) is largely controlled by the strength of the SASM and associated features, it is not unexpected to find that the paleoprecipitation history of the Rio Grande do Norte speleothem shows a distinct ‘anti-phased’ relationship to the rest of tropical South America (Cruz *et al.* 2009; Cheng *et al.* 2013). During the mid-Holocene, when insolation levels were low and the south and west SASM region was drier, the nordeste was wetter than at present (Fig 3h). Mechanistically, this is most likely due to a weaker SASH and weaker convective activity in the core of the SASM region reducing the strength of the nordeste low and subsidence over the region (Cruz *et al.* 2009; Cheng *et al.* 2013). Weaker ENSO activity during the mid-Holocene may also have reduced severe drought events in this region (Koutavas & Joanides 2012; Wang *et al.* 2017). As insolation levels increase through the Holocene, the region becomes gradually drier, reaching approximately modern levels at ca. 4 ka. Reconstructing the paleovegetation history of this region in response to this sort of long-term precipitation change is of great interest, for example in terms of revealing important information about the potential connectivity between the Amazon and Atlantic rainforests (De Oliveira *et al.* 1999; Behling *et al.* 2000; Costa 2003; Batalha-Filho *et al.* 2013). However, a fundamental issue in this semi-arid region is the difficulty in finding permanent lake basins,

bogs, or undisturbed locations for taking soil profiles, that would provide suitable records for paleoecological study (De Oliveira *et al.* 1999; Pessenda *et al.* 2010).

The pollen record from the site Saquinho (id = 34), taken in the Caatinga region in the Rio Icatu river valley, suggests that a more humid mid-Holocene may have promoted the expansion of palms and gallery forests at the expense of Caatinga/savannah vegetation. Between ca. 5 and 4.5 ka, the trend of increasing aridity in the region is marked by an increase in Caatinga and Cerrado taxa as well as a reactivation of dune activity shown by thermoluminescence data (De Oliveira *et al.* 1999). The Maranguape bog core taken from the Serra de Maranguape mountains on the north coast (id = 28) records continuous forest cover through the mid-to-late Holocene, though compositional changes in the pollen record suggest increased disturbance at ca. 4.5 ka, contemporaneous with the start of drier conditions in the nordeste (Montade *et al.* 2014). However, other records in this region do not seem to reflect the more humid mid-Holocene in their paleovegetation reconstructions, though this is most likely due to the unique characteristics of their site locations. A transect of soil profiles on the Araripe Plateau in the central Caatinga region (ids = 78 – 80) records gradual depletion of $\delta^{13}\text{C}$ from the mid-Holocene to present, suggesting greater savannah extent before ca. 3.5 – 3 ka, after which forested areas increase. A transect of soil profiles on the east coast of Paraíba state (ids = 76 – 77) also show some indications of more open vegetation in the mid-Holocene, with an increase in forest cover after ca. 3 ka. The modern rainforest enclaves on plateaus such as Araripe and on higher elevations near the coast are maintained by significant orographic rainfall derived from easterly winds that help to mitigate against the arid conditions caused by the persistent subsidence (Andrade-Lima 1982; Sampaio 1995). Even though this subsidence was likely reduced during the mid-Holocene causing the region in general to become less arid, changes to low-level divergent circulation patterns and Walker cell dynamics may also have reduced the moist easterlies (Cruz *et al.* 2009) that helps maintain these plateau-based forests. Whilst these small plateaus and coastal areas can yield suitable sites, clearly they may not be representative of vegetation changes across the Caatinga on a regional scale. The site of Lagoa do Caçó (id = 11) is located on the northernmost reach of the Cerrado savannah biome and records no major changes in the Cerrado vegetation through the mid-to-late Holocene (Ledru *et al.* 2006). The increase in gallery forests around the lake shown in the nearby soil pits may indicate increased moisture after ca. 4 ka, though it is difficult to say whether this is due to climate, natural vegetation succession or sea level dynamics. The authors suggest that the location of this lake lies in a transitional area between the east-

west climate zones and as such, precipitation changes may be fairly stable in contrast to the surrounding areas (Pessenda *et al.* 2005; Ledru *et al.* 2006).

2.6 Conclusions

Our multi-proxy paleoecological data synthesis shows how the vegetation from different regions of tropical South America responded to orbitally forced long-term precipitation changes through the mid-to-late Holocene (Cheng *et al.* 2013; Baker & Fritz 2015). The HETF biome of central and western Amazonia remained intact, even though paleoclimate records suggest that this region may have been slightly drier than present during the mid-Holocene. In eastern Amazonia, similar HETF stability is recorded, however the apparent mid-Holocene savannah expansion at the eastern Amazonian ecotone (from the Serra Sul dos Carajás plateau) is difficult to reconcile with new paleoclimate data from Paraíso cave that suggests this region was wetter than present at this time (Wang *et al.* 2017). The Paraíso cave record perhaps only reflects precipitation conditions from far north-east Amazonia and is not representative of Carajás' location in south-east Amazonia. Nearer to the south-eastern Amazonian ecotone and the Carajás plateau, local lake level records appear to indicate lower lake productivity and water levels during the mid-Holocene, indicative of a drier climate (Cordeiro *et al.* 2008). Clearly more investigation is needed in this area to reconcile local and regional paleoclimate and paleoecological records. The north-east of Brazil was wetter than present during the middle Holocene, due to a suppression of the subsidence across the region resulting from a weaker SASM and SASH (Cruz *et al.* 2009). However, the lack of paleovegetation records means a regional interpretation of vegetation response is problematic.

Significant vegetation changes are recorded in south-west Amazonia and south-east Brazil. These regions are more reliant on SASM-derived precipitation and so vegetation here is likely to be especially susceptible to long-term changes in SASM strength. The vegetation reconstructions during a drier mid-Holocene show: a more northerly location of the HETF/SDF/SAV ecotone in north-eastern Bolivia; greater expanse of campos grassland across the south Brazilian highlands; and decreased expanse of montane forests and HETF across the southern Atlantic forest region. As precipitation levels gradually rose through the mid-to-late Holocene, vegetation responded as follows: progressive southward expansion of the HETF in north-east Bolivia from ca. 2 ka; expansion of *Araucaria* on the south Brazilian highlands from ca. 4 ka, with enhanced expansion from ca. 1.5 – 1 ka; expansion, or greater canopy density, of SDF in the Misiones and interior Atlantic forest regions; increase of gallery

forests in the south-east Brazilian Cerrado. The difference in the timing of forest expansion between these two regions is probably due to the important extra-tropical source of precipitation that mitigates somewhat against a weaker SASM in south-east Brazil.

Whilst this synthesis includes more sites than previous studies, in part due to inclusion of non-pollen proxy reconstructions, it is clear that more sites are needed to help increase our understanding of long-term vegetation dynamics across the region. In south-west Amazonia, more sites could help to quantify the maximum extent of the HETF/SDF/savannah mid-to-late Holocene ecotonal shift. We particularly highlight eastern Amazonia, north-east Brazil and the cerrado region of central Brazil as key areas that need more paleoecological data. We recognise that the paucity of suitable lake sites in these areas is a big hindrance to improving the regional coverage of pollen-based vegetation reconstructions. However, in such regions, where suitable lakes/bogs are scarce, soil-based proxies – such as $\delta^{13}\text{C}$ isotopes and, in particular, phytoliths – which have hitherto been underutilised by the paleoecological community, show considerable potential for paleovegetation reconstruction (Dickau *et al.* 2013; Watling *et al.* 2016; 2017).

With regards to possible implications for future climate change, this study highlights that the ecosystems most vulnerable to long-term climate change are those that are already close to their climatic limits. However, given the resilience of the central Amazonian HETF biome to past climate change, future projections of widespread forest dieback across Amazonia (Cox *et al.* 2000; 2004) seem unlikely. It is important to point out that we have used the mid-to-late Holocene as a period in which we can assess regional vulnerability to long-term climate changes, not as a direct analogue for a future drier climate. Factors such as temperature and CO_2 levels will be significantly different between the future and the mid-Holocene, which will undoubtedly have an impact on vegetation responses (Rammig *et al.* 2010; Huntingford *et al.* 2013). In addition, huge anthropogenic pressures, such as widespread deforestation and uncontrolled burning, will only act to reduce the ability of vegetation to maintain local feedbacks and thus reduce overall ecosystem resilience (Laurance *et al.* 2000; Malhi *et al.* 2008; Levine *et al.* 2016).

2.7 Acknowledgements

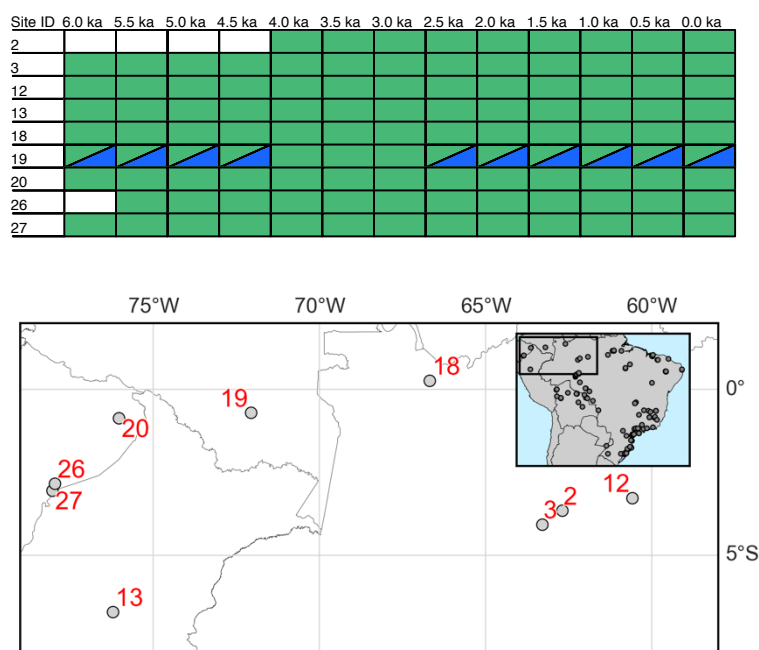
We thank Francisco Cruz and Bronwen Whitney, who provided paleoclimate data for Rio Grande do Norte and Laguna La Gaiba, respectively. Other speleothem data and insolation data were accessed online via the National Oceanic and Atmospheric Administration (NOAA)

website: <https://www.ncdc.noaa.gov/paleo>. Tropical Rainfall Measuring Mission (TRMM) data (<https://trmm.gsfc.nasa.gov>) were processed by the TRMM Science Data and Information System (TSDIS) and the TRMM office and are archived and distributed by the Goddard Distributed Active Archive Center. RS was funded by a NERC 'SCENARIO' DTP PhD award. We thank Mark Bush for the invitation to submit a paper to this special issue of QR and are grateful for his comments, and those of two referees, which improved the manuscript.

2.8 Supporting information

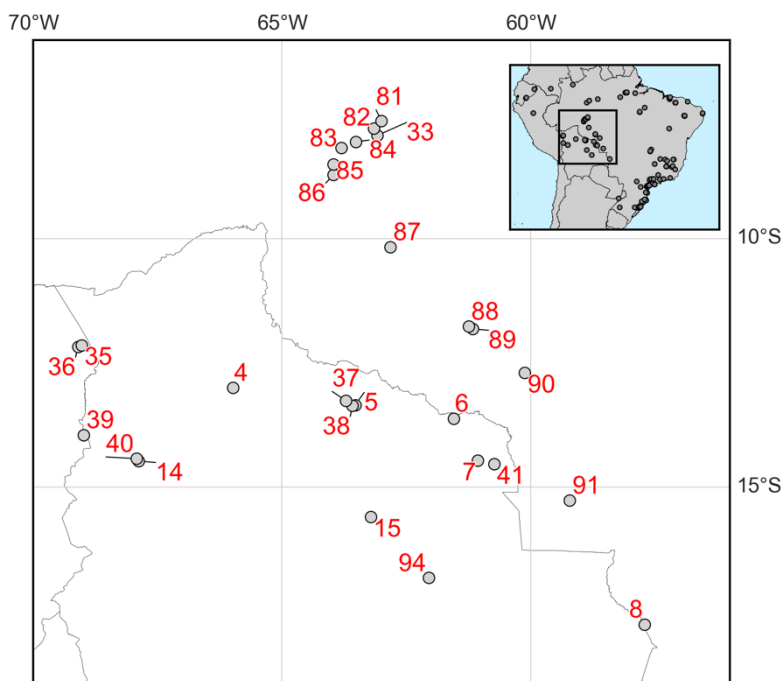
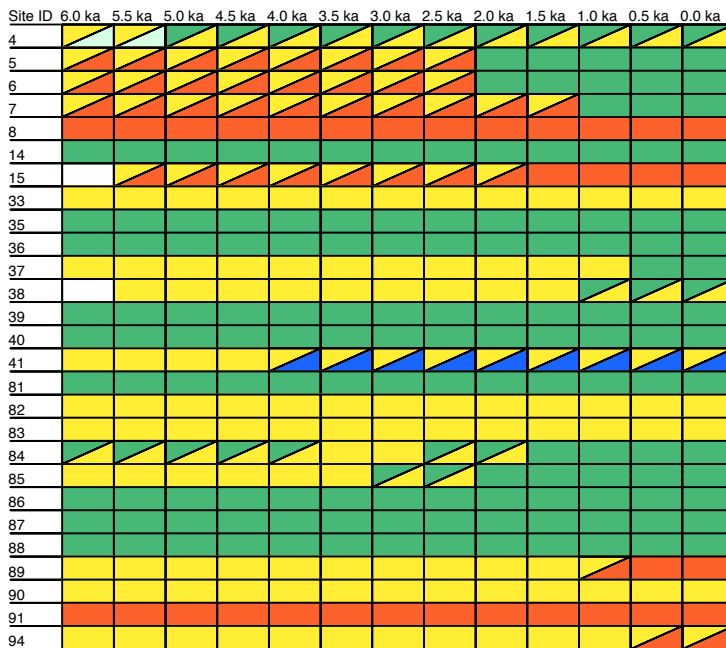
The following was provided as supporting information for the paper submitted to *Quaternary Research* (Smith & Mayle 2018).

(a) Central and western lowland Amazonia



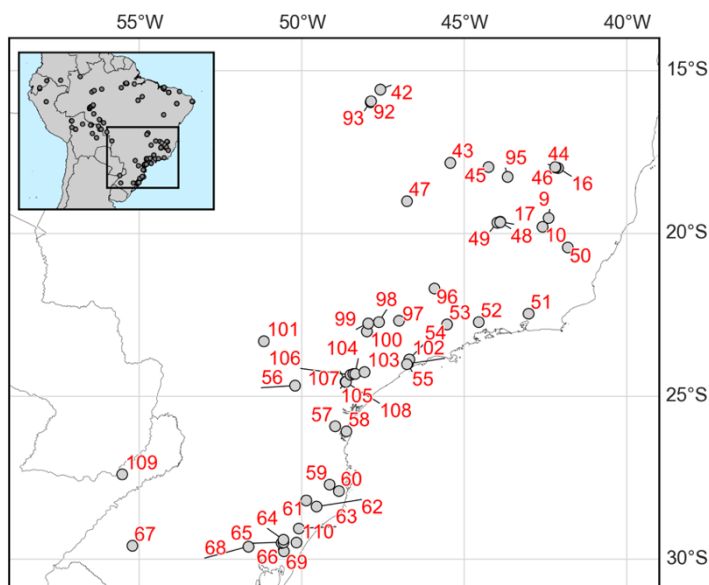
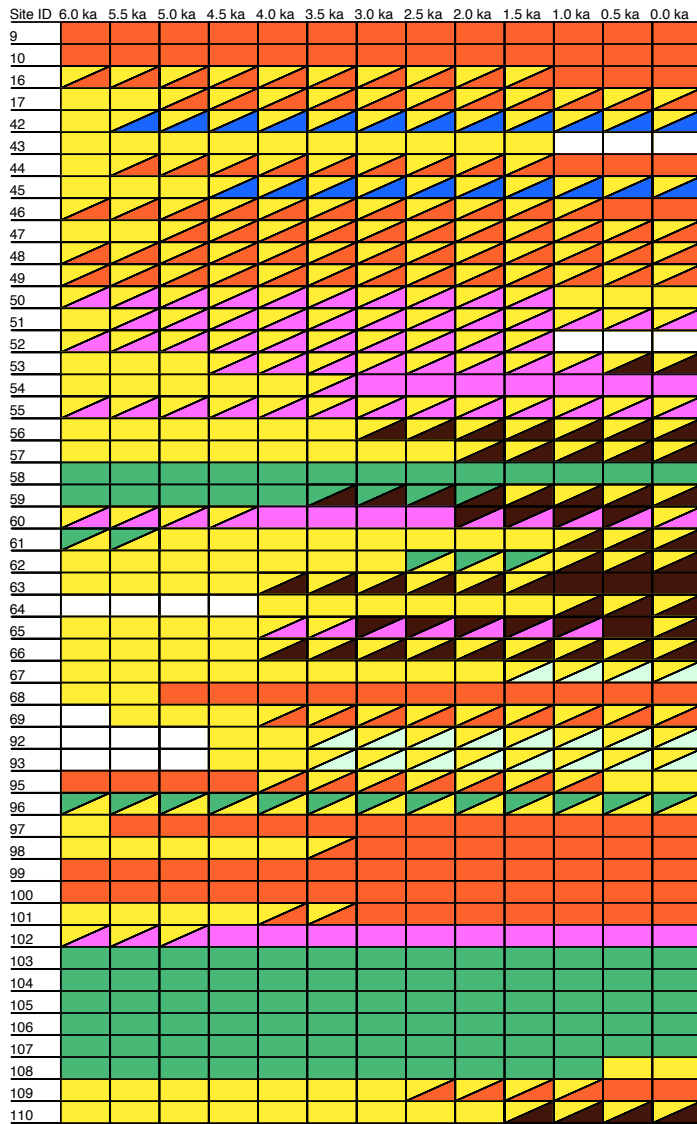
SI Figure 2-A - Summary of vegetation changes at each palaeoecological site, alongside regional maps of the location of each site. Site IDs correspond to those in Table 2.1.

(b) South-Western Amazonia



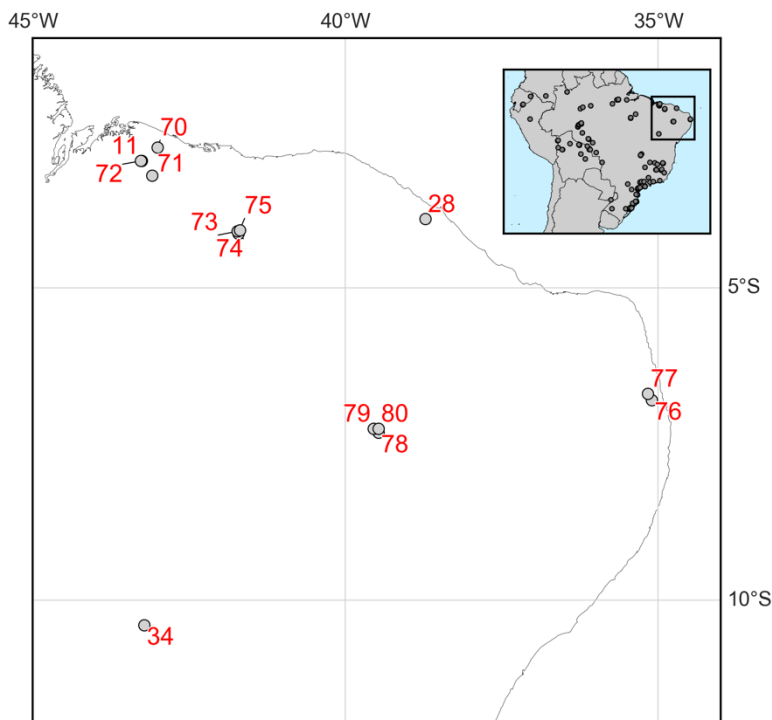
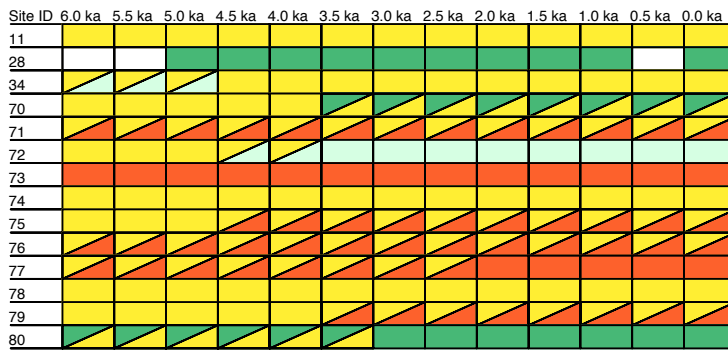
SI Figure 2-A (continued)

(c) South-eastern Brazil



SI Figure 2-A (continued)

(e) North-eastern Brazil



Palaeoecological classifications



SI Figure 2-A (continued)

Chapter 3. How does basin type and size influence late Quaternary vegetation reconstructions in south-west Amazonia?

Authors: **Richard J. Smith**, Francis E. Mayle, S. Yoshi Maezumi, Mitchell J. Power

3.1 Preface

The following chapter is taken from a paper submitted for publication to the journal *Quaternary Research*. The chapter is therefore written in the style of a journal article, conforming to the regulations of the journal. **RS** led the writing of the paper. **RS** and **FM** designed the research project. **RS** carried out pollen analysis of Cuatro Vientos. **YM** provided loss-on-ignition data. **RS** and **FM** interpreted the data. All authors contributed to writing the paper.

3.2 Abstract

In contrast to temperate regions, relationships between basin characteristics (e.g. type/size) and fossil pollen archives have received little attention in Amazonia. Here, we compare fossil pollen records of a small palm swamp (Cuatro Vientos; CV) and a nearby large lake (Laguna Chaplin; LCH) in Bolivian Amazonia, demonstrating that palm swamps can yield Quaternary pollen archives recording the history of terrestrial vegetation beyond the basin margin, rather than merely a history of localised swamp vegetation dynamics. The pollen assemblages from these two contrasting basins display remarkable agreement throughout their late Quaternary history, indicating past drier climates supported savanna landscape during the Last Glacial Maximum (LGM; 24,000-18,000 cal. yr BP) and savanna/semi-deciduous forest mosaic during the middle Holocene (7,000-4,750 cal. yr BP) at both regional (inferred from LCH) and local (inferred from CV) spatial scales. Additionally, the local-scale catchment of CV and the basin's proximity to the riverine forests of the Río Paraguá enables exploration of the extent of gallery/riverine forests during the LGM and middle Holocene. We show that, between 24,000-4,000 cal. yr BP, riverine/gallery rainforests were substantially reduced compared to present, challenging hypotheses that gallery rainforests were important refugia for rainforest species during the drier LGM and mid-Holocene.

3.3 Introduction

The role of paleoecology in determining how Amazonian ecosystems responded to long-term past climate change is of paramount importance, given its relevance for understanding the fate of Amazonia under future climate change. Particular focus should be given to ecotonal regions of Amazonia, where humid evergreen forests form boundaries with savannas and/or semi-deciduous tropical dry forests; rainforest taxa in these regions exist near to their climatic limits and should therefore be highly sensitive to climate change. Existing paleoecological records have demonstrated this vulnerability, with evidence for climate-induced expansion of savanna and/or dry forests during the Last Glacial Maximum (LGM) and the middle Holocene in ecotonal eastern Amazonia (e.g. Absy *et al.* 1991; Hermanowski *et al.* 2012a; Fontes *et al.* 2017; Reis *et al.* 2017) and southern Amazonia (e.g. Mayle *et al.* 2000; Burbridge *et al.* 2004; Carson *et al.* 2014). However, the paucity of these paleo-records means that considerable uncertainty exists as to the full nature and extent of these biome shifts. Unfortunately, finding suitable palaeoecological sites is often a challenge in this region. The dynamic hydrology of Amazonia means that long-lived, permanent lake basins are uncommon (Colinvaux *et al.* 1985; Latrubesse 2012). Small oxbow lakes are widespread, but they rarely have sediment records that span the multi-millennial timescales needed to capture long-term climate change (Toivonen *et al.* 2007; Latrubesse 2012; Rodríguez-Zorro *et al.* 2015).

In the absence of suitable lake sediment records, bogs and palm swamps are often targeted for paleoecological analysis. However, their value is often called into question due to uncertainty over whether their sedimentary-based pollen reconstruction reliably capture the history of local terrestrial vegetation beyond the bog/swamp, or instead merely reveal the history of swamp/bog vegetation growing within the basin itself. In the latter case, they are of little use for paleoecologists seeking to understand Holocene/Quaternary forest dynamics. Such concerns are borne out by pollen records from sites such as the Pantano de Monica palm swamp in the central Colombian Amazon (Behling *et al.* 1999) and the Vereda de Águas Emendadas palm swamp in central Brazil (Barberi *et al.* 2000), both of which are dominated by swamp taxa (e.g. palms and sedges) through much of the Holocene. Furthermore, because key pollen taxa such as grass and sedge can only be identified to family level (Poaceae and Cyperaceae, respectively), it is often unclear whether their presence signifies semi-aquatic species growing within the swamp (e.g. floating sedge mat) or instead open, seasonally-flooded savanna beyond the swamp.

Here, we present the results of a natural experiment, whereby analysis of fossil pollen records from a small palm swamp and an adjacent large lake provides a rare opportunity to determine the potential for palm swamps to reliably record glacial-Holocene terrestrial vegetation histories, or merely a history of swamp vegetation. We present a 24,000-yr fossil pollen record from Cuatro Vientos palm swamp located in Noel Kempff Mercado National Park (NKMNP), north-eastern Bolivia (southern Amazonian forest-savanna ecotone). The current state of knowledge of the late Quaternary paleoecology of this region is predominantly based on the pollen records from two large lakes: Lagunas Bella Vista and Chaplin (Mayle *et al.* 2000; Burbridge *et al.* 2004). These records demonstrate that most of the regional catchments of these two lakes, which are today dominated by humid evergreen rainforest, were previously characterized by a mosaic of savanna and semi-deciduous dry forest communities during the LGM and early/middle Holocene under drier-than-present climatic conditions. The regional climate became gradually wetter through the late Holocene, causing the progressive replacement of savanna and dry forest by humid evergreen rainforest, which expanded in the northern part of NKMNP ~3,000 yr BP (around Laguna Bella Vista) and attained current levels in the south of the park (around Laguna Chaplin) by ~750 yr BP (Mayle *et al.* 2000; Burbridge *et al.* 2004).

Cuatro Vientos (CV) palm swamp is located only 6.5 km from Laguna Chaplin, and thus presents a unique opportunity to directly compare the paleoecological record of a palm swamp with that of a neighbouring large lake (~20 km²). Given the close proximity of these two sites, located within the same vegetation type (humid evergreen rainforest), we expect that they will have undergone the same climatic and regional vegetation changes in the past. Therefore, our assumption is that any differences between the paleoecological records can be attributed to the effects of basin type and/or basin size, thus enabling a robust assessment of the potential value of palm swamps as repositories of paleoecological data in southern Amazonia; e.g. whether they reflect a history of *terra firme*, climate-driven vegetation change beyond the swamp, or merely a history of a palm swamp community controlled by local hydrological conditions within the basin. The findings of our study may have implications for the interpretation of other palm swamp records elsewhere in the Neotropics, as well as criteria for the selection of appropriate sites for paleoecological analyses and palaeo-data syntheses.

If it is found that the Cuatro Vientos record does provide a long-term (multi-millennial) record of vegetation changes beyond the swamp itself, the pairing of Cuatro Vientos and Laguna Chaplin also provides an opportunity to explore the dynamics of local versus regional-scale

vegetation changes in the park. This strategy of pairing small and large neighbouring sedimentary basins has long been advocated as a sound approach for differentiating local versus regional pollen catchments in mid to high latitude North America and Europe (Jacobson & Bradshaw 1981). In these temperate ecosystems, where most tree taxa are wind-pollinated, modelling approaches based upon pollen productivity and dispersal data have led to quantitative estimates of pollen catchment area, whereby large lakes ($>5 \text{ km}^2$) have regional-scale pollen catchment areas ($> \sim 50 \times 50$ – $100 \times 100 \text{ km}$) and are relatively insensitive to localised or patch-size vegetation changes (Sugita 1994; Sugita *et al.* 1999; Davis 2000; Sugita 2007a), whereas small lakes ($< \sim 0.1$ – 1 km^2) instead have local-scale pollen catchment areas ($< \sim 10 \times 10 \text{ km}$) (Sugita 2007b). These temperate ecosystem pollen catchment estimates are unlikely to hold true for humid tropical rainforests due to the different constituent taxa and far greater complexity of pollination syndromes (wind, insects, bats, birds) associated with these more biodiverse ecosystems. However, in our study area at least, modern pollen rain studies (Gosling *et al.* 2005; 2009; Burn *et al.* 2010) show that wind-pollinated Moraceae pollen dominates rainforest pollen assemblages in NKMNP. The general premise that large lakes and small lakes capture regional- and local-scale pollen rain, respectively, therefore likely holds true, corroborated by Carson *et al.* (2014). The area of the Cuatro Vientos swamp basin is $\sim 5 \text{ km}^2$, compared with $\sim 20 \text{ km}^2$ for neighbouring Laguna Chaplin, thus enabling local-scale vegetation dynamics (Cuatro Vientos) to be differentiated from regional-scale vegetation dynamics (Laguna Chaplin).

The local-scale catchment of Cuatro Vientos is particularly pertinent given the location of this site at the margin of the riverine forests of the Río Paraguá (Fig. 3.1), as this provides a unique opportunity to investigate the Quaternary history of riverine/gallery rainforest. During drier periods of the Pleistocene when humid evergreen rainforest cover was reduced, it has previously been proposed that rainforest taxa may have survived within refugia provided by riverine gallery rainforest, due to the more continuous water supply from the river (Meave *et al.* 1991; Meave & Kellman 1994; Pennington *et al.* 2000). These gallery rainforest refugia may have provided important routes and source areas for the spread of plant and animal species (Redford & da Fonseca 1986; Meave *et al.* 1991; Costa 2003), as well as providing routes for human population expansion (Iriarte *et al.* 2017). Investigating the extent of gallery rainforests in NKMNP through the late Quaternary may also help to explain the mechanism of rainforest expansion in the late Holocene, e.g. whether the gallery rainforests served to expedite the spread of rainforest taxa in response to climate change (e.g. Mayle *et al.* 2007). However, the extent to which these gallery rainforests survived through the drier climatic

periods of the LGM and middle Holocene in NKMNP is uncertain, given that, until now, only regional-scale vegetation records are available from pollen data from the two large lakes in this area (i.e. Lagunas Chaplin and Bella Vista), which lack the spatial resolution to capture changes in the extent of riverine vegetation.

This paper addresses the following questions:

1. How do Amazonian Quaternary paleoecological records from palm swamps (< 5 km²) compare with those of large lakes (>20 km²)?
2. Was there significant gallery rainforest lining the rivers of Noel Kempff Mercado National Park (ecotonal southern Amazonia) during the drier climatic conditions of the LGM and middle Holocene when the interfluves were dominated by savanna and/or semi-deciduous tropical dry forest?

3.3.1 Study area

Noel Kempff Mercado National Park (NKMNP) is a 15,230 km² protected reserve located near the southern margin of the Amazon basin in north-eastern Bolivia (Fig. 3.1) (Killeen & Schulenberg 1998). The park has been designated a UNESCO world heritage site due to its exceptionally high beta (habitat) diversity and is considered to be largely undisturbed by modern anthropogenic land use (Killeen *et al.* 2003; Heyer *et al.* 2018).

Geomorphology and regional vegetation

NKMNP is located on the western reach of the Precambrian Brazilian shield, the geomorphology of which splits the park into two distinct landscapes (Fig. 3.1). To the east, the park is dominated by the Huanchaca Plateau, a table-mountain ~600–900 m above sea level (a.s.l) comprised of Precambrian sandstone and quartzite. The plateau is predominantly covered in upland cerrado savanna vegetation that has been present since at least the end of the last glacial (Maezumi *et al.* 2015). To the west lies a lowland peneplain, where the Precambrian bedrock is blanketed by Tertiary and Quaternary alluvial sediments and is covered predominantly in *terra firme* humid evergreen tropical forest (HETF). The black-water rivers of the Río Iténez and Río Paraguá form the north/eastern and western boundaries of NKMNP, respectively. These rivers and other smaller streams in the park are lined by evergreen riverine forests, usually on the natural levees that form from deposition events during seasonal flooding. Patches of seasonally-inundated savanna occur near the rivers where soil drainage is poor. The southern border of NKMNP defines the modern ecotone

between the HETF of southern Amazonia and the Chiquitano semi-deciduous tropical dry forest (SDTF) of eastern lowland Bolivia. The term ‘semi-deciduous’ is used here to describe the flexible phenologic response (deciduousness) of the constituent trees, depending on the degree and duration of the dry season (Killeen & Schulenberg 1998; Killeen *et al.* 1998). In contrast to the HETF, the SDTF supports a denser understorey vegetation as more light can penetrate the canopy.

Climate

The precipitation regime of the region is distinctly seasonal, predominantly controlled by the South American Summer Monsoon (SASM; Zhou & Lau 1998; Raia & Cavalcanti 2008; Silva & Kousky 2012). The majority of the ~1400–1600 mm mean annual precipitation falls during the wet season during austral summer, with a dry season lasting for ~4–6 months during austral winter. Mean annual temperatures are ~25–26°C, with little monthly variation. However, during austral winter, cold fronts (‘surs’ or ‘surazos’) originating in Patagonia can reach the area and cause temperatures to drop below 10°C for several days (Killeen *et al.* 2003).

Site descriptions

Cuatro Vientos (CV, 14°31'18.5"S, 61°7'11.3"W; elevation ~170 m a.s.l.) is a palm swamp, ~5 km² in area, located in western NKMNP, ~5 km from the Río Paraguá (Fig. 3.1). The surrounding vegetation (beyond the palm swamp) consists of *terra firme* HETF to the east and riverine (riparian) forest of the Río Paraguá to the west. The riverine forests in NKMNP vary in their structure, from young pioneer communities, with trees such as *Cecropia*, *Sapium* and *Acacia*, through to older communities with later successional tree taxa, particularly from the Moraceae family (e.g. *Brosimum lactescens*, *Pseudolmedia* spp., *Ficus* spp.). Most of these species are dioecious and wind-pollinated (anemophilous), and are therefore over-represented in the pollen record due to their prolific pollen production (Bush & Rivera 2001; Burn *et al.* 2010). Although similar to communities of *terra firme* evergreen forests, the riverine forests can be distinguished by their sparse understoreys (due to seasonal flooding), smaller stature, flood-tolerant species and lower overall species diversity (Killeen & Schulenberg 1998; Burn *et al.* 2010). Growing within the CV basin itself is a floating mat of sedge/grass swamp vegetation, interspersed with small pools of open water and scattered clumps of *Mauritiella* palm trees.

Laguna Chaplin (LCH, 14°28'12"S, 61°2'60"W; elevation ~170 m a.s.l.) is a large (~12 km²), shallow (2–2.5 m in the dry season), flat-bottomed lake (within a ~20 km² basin), located ~6.5 km north-east of CV (Mayle *et al.* 2000; Burbridge *et al.* 2004). The LCH basin is surrounded by HETF, with a mix of seasonally-inundated riverine forest (around much of the lake margin and along the small, ephemeral streams that flow in and out of LCH) and *terra firme* (upland) HETF. Adjacent to the lake, in the southern half of the basin, lies a patch of savanna wetland. Comparison of the modern pollen spectra of the surface sediments of the lake (Burbridge *et al.* 2004) with pollen trap data from all the constituent plant communities in NKMNP (Gosling *et al.* 2005; Burn *et al.* 2010; Jones *et al.* 2011) reveals that the modern pollen assemblage of this lake originates from both the riverine and *terra firme* HETF ecosystems in the lake catchment. Crucially, however, the regional-scale pollen source area of this large lake means that differentiation of the relative extent of riverine versus *terra firme* ecosystems is not possible. Both LCH and CV are located ~30 km from the modern HETF/SDTF ecotone at the southern limit of NKMNP (Fig. 3.1).

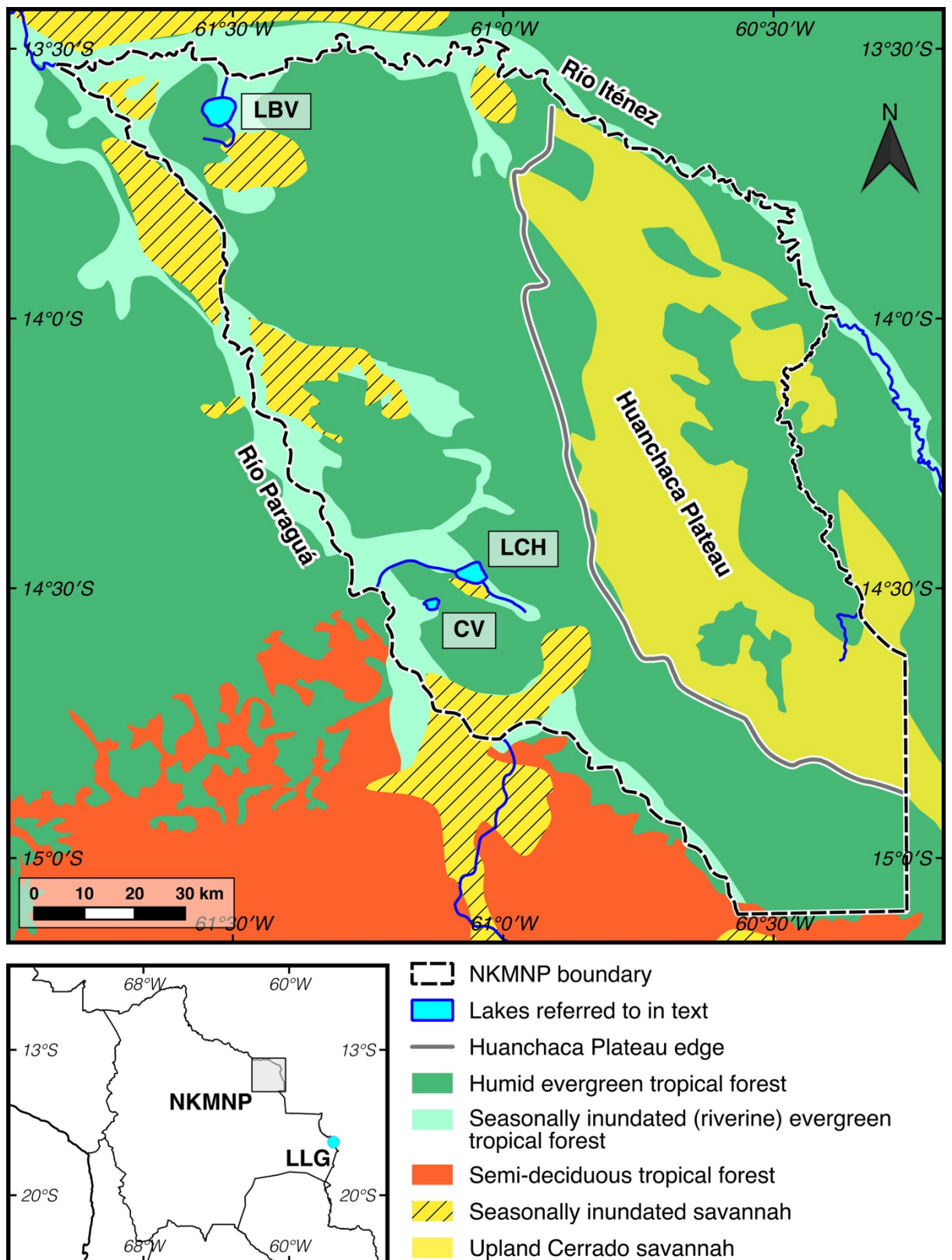


Figure 3.1 - Map of Noel Kempff Mercado National Park (NKMNP), showing modern day vegetation distribution (modified from Olson *et al.* 2001) and the location of sites referred to in text: Cuatro Vientos (CV), Laguna Chaplin (LCH), Laguna Bella Vista (LBV) and Laguna La Gaiba (LLG).

3.4 Methods

3.4.1 Sediment core

Cuatro Vientos (CV) was cored in August 1995 with a modified square-rod Livingstone piston corer (Wright 1967; Colinvaux *et al.* 1999). The core location was ~300 m in from the eastern edge of the palm swamp, with the inherent difficulty in traversing swamp environments making it impossible to penetrate further into the basin. The top 20 cm of the core site comprised a floating mat of grasses and sedges. Below this was a ~1 m water column, the bottom of which was well mixed with the top layers of sediment making it difficult to determine the depth of the sediment-water interface. Therefore, core depths were recorded by reference to the top of the floating mat vegetation (FMV). A 154 cm core was recovered, between 155 and 309 cm below the FMV. Unfortunately, the sediment above 155 cm was too soft to be recovered. Lithological descriptions are based on the colour (using a Munsell soil colour chart) and texture of the sediment core. Loss-on-ignition (LOI) analysis was carried out at 4 cm intervals through the CV core. After drying at 100°C for 24 hours, each 1 cm³ sample was combusted at 550°C for 2 hours (LOI₅₅₀). The relative loss of weight before and after combustion determines the percentage organic carbon content that was present in that sample (Dean 1974; Heiri *et al.* 2001).

3.4.2 Chronology

The chronological framework for CV is based on 9 Accelerator Mass Spectrometry (AMS) radiocarbon (¹⁴C) dates (Table 3.1). Due to the absence of sufficient plant macrofossils, the majority of the dates were obtained from non-calcareous bulk sediment. However, two of the samples (Beta-467884 and Beta-467885) contained enough decayed plant remains during pre-treatment to be dated. All samples selected for dating were treated to remove carbonates, and the plant remains were treated to remove mobile humic acids. Radiocarbon ages were calibrated using the IntCal13 calibration curve (Reimer *et al.* 2013), and a chronology was constructed using the Bayesian age modelling software Bacon v2.3.4 (Blaauw & Christen 2011). The IntCal13 calibration curve was chosen over SHCal13 because of the hydrological connection of the study area to the northern hemisphere, via the SASM (McCormac *et al.* 2004; Hogg *et al.* 2013).

3.4.3 Pollen analysis

The CV core was sub-sampled for pollen analysis at 4 cm intervals, apart from between 220–252 cm where sub-samples were taken at 2 cm intervals. The last 29 cm of the core (280–

309 cm) was unsuitable for pollen analysis as the sediment had oxidized, preventing pollen preservation. For each horizon, 1 cm³ of sediment was prepared for pollen analysis using standard protocols (Faegri & Iversen 1989), including hot treatments of 40% HF and 10% NaOH. Samples particularly rich in clay were given pre-treatments of hot 5% sodium pyrophosphate to help disperse the clays, but were not subjected to a fine-sieving stage to ensure small grains (<5 µm) were retained. A known concentration of the exotic marker spore *Lycopodium clavatum* was added to each sample so that absolute pollen concentrations could be calculated (Stockmarr 1971). Prepped samples were mounted in silicone oil and were counted to the standard 300 Terrestrial Land Pollen (TLP) sum. Cyperaceae pollen was included in the TLP sum (as per Laguna Chaplin, Burbridge et al. 2004) as this taxon is important in the seasonally flooded savannas of the study region. Pollen identifications were made with reference to published tropical pollen atlases (Roubik & Moreno Patiño 1991; Colinvaux et al. 1999; Lorente et al. 2017), a freeware digital database of neotropical pollen (Bush & Weng 2007), and an extensive modern tropical pollen reference collection of >1,000 specimens housed at the laboratory of the Tropical Palaeoecological Research Group, University of Reading. Pollen of the Moraceae/Urticaceae families were grouped into a single 'Moraceae' category (with the exception of *Cecropia*). It is notoriously difficult to distinguish between these families and their genera, and given the grains from CV were often obscured or damaged there was little confidence in genus-level identification, even with the help of published morphological descriptions (Burn & Mayle 2008). Zones for the pollen data were drawn based on a stratigraphically constrained cluster analysis by incremental sum of squares (CONISS; Grimm 1987), with the number of statistically significant zones evaluated using the broken-stick model (Bennett 1996). All analyses and plotting of the pollen data were performed in R (v.3.4.4), using the rioja (v.0.9-15.1) and vegan (v.2.4-6) packages (Juggins 2017; Oksanen et al. 2018).

3.4.4 Laguna Chaplin core

Laguna Chaplin (LCH) was cored in 1998, with the methodology and results of the paleoecological analyses presented in subsequent publications (Mayle et al. 2000; Burbridge et al. 2004; Maezumi et al. 2018b). The pollen data from the analyses of LCH are presented here and compared with those of CV to provide the necessary regional-scale, late Quaternary vegetation and climate context for determination of the paleoecological significance of the CV palm swamp fossil pollen record. We replot the LCH data with an updated age-depth model because the original age-depth model was based on simple linear interpolation between consecutive radiocarbon dates (Burbridge et al. 2004) – a method no longer favoured in the

paleoenvironmental community (Blaauw *et al.* 2018). The chronological framework for LCH presented here is based on 14 Accelerator Mass Spectrometry (AMS) radiocarbon (^{14}C) dates (Table 3.2) and, as with CV, uses the Bacon Bayesian age modelling software package (Blaauw & Christen 2011). Note that only the 0-24,000-year portion of the 40,000-year LCH pollen record is plotted here, to allow direct comparison with the 24,000-year CV pollen record.

Table 3.1 - List of the accelerator mass spectrometry radiocarbon dates from the Cuatro Vientos sediment core.

Laboratory code	Sample depth (cm below FMV)	Dated material	AMS ^{14}C age (yr BP $\pm 1\sigma$)	Calibrated age range (cal. yr BP) $\pm 2\sigma$
UGAMS 13197	161.5	Bulk sediment	3760 \pm 25	4231 – 3990
Beta-467884	195	Plant remains	4400 \pm 30	5211 – 4866
UGAMS 11809	229	Bulk sediment	5750 \pm 30	6639 – 6468
A20294	231.5	Bulk sediment	6800 \pm 26	7678 – 7593
Beta-467885*	240	Plant remains	4640 \pm 30	5465 – 5307
Beta-467886	250	Bulk sediment	9180 \pm 30	10477 – 10245
UGAMS 15265	260	Bulk sediment	16140 \pm 40	19637 – 19295
Beta-467887*	276	Bulk sediment	25700 \pm 90	30276 – 29502
UGAMS 15157	292	Bulk sediment	21070 \pm 50	25607 – 25216

*dates not included in age-depth model

Table 3.2 - List of the accelerator mass spectrometry radiocarbon dates from the Laguna Chaplin sediment core, taken from Burbridge et al. (2004).

Laboratory code	Sample depth (cm)	Dated material	AMS ¹⁴C age (yr BP ± 1σ)	Calibrated age range (cal. yr BP) ± 2 σ
Beta-137570	36.5	Bulk sediment	710 ± 50	732 – 558
AA39700	51.5	Bulk sediment	2240 ± 40	2342 – 2153
AA39701	69.5	Bulk sediment	2740 ± 40	2925 – 2760
AA39702	85	Bulk sediment	3870 ± 50	4421 – 4151
AA39703	100	Bulk sediment	4330 ± 80	5284 – 4648
AA39704	125	Bulk sediment	6040 ± 50	7143 – 6745
AA39705	135	Bulk sediment	9000 ± 100	10404 – 9770
AA39706	155	Bulk sediment	17820 ± 140	21945 – 21135
AA39707	175	Bulk sediment	31060 ± 440	35941 – 34190
AA39708	195	Bulk sediment	34820 ± 700	41160 – 37945
AA39709	213	Bulk sediment	37750 ± 970	43801 – 40455
AA39710*	250	Bulk sediment	43400 ± 1900	-
AA39711*	285	Bulk sediment	41200 ± 1400	-
AA39712*	296	Bulk sediment	38100 ± 1000	-

*dates not included in age-depth model

3.5 Results

3.5.1 Cuatro Vientos - core stratigraphy and chronology

Figure 3.2 shows the age-depth model derived from Bacon. The model used seven of the nine ^{14}C AMS dates, with the dates at 240 cm and 276 cm rejected based on Bacon's outlier identification. The date at 240 cm was based on a particularly small sample size of extracted decayed plant remains, raising the possibility that the younger-than-expected age could be due to down-core movement of the sample. The date at 276 cm is consistently rejected by multiple Bacon runs, as well as through an exploratory run of OxCal's statistical outlier model (Bronk Ramsey 1995; 2009), and may be anomalously old due to incorporation of older, reworked sediment, for example by bioturbation. The dates for the top (155 cm) and bottom (309 cm) of the core are based on extrapolation, and so must be interpreted with care.

The sediments from CV can be split into three main stratigraphic sections (Fig. 3.2).

- (1) 309–255 cm: comprised of inorganic greyish-brown silty clay, with a sedimentation rate of ca. 0.05 mm/yr. The age range of this section is ca. 33,000–28,000 to 19,000–16,000 cal. years BP, corresponding to the late Pleistocene and including the Last Glacial Maximum (LGM). The upper boundary of 255 cm likely marks hiatus in the core lasting from ca. 19,000–16,000 to 12,000–10,500 cal. years BP.
- (2) 255–230 cm: comprised of grey, silty clays, with some organic inclusions. This section corresponds to the early Holocene, between ca. 12,000–10,500 and 8,000–7,500 cal. years BP. A particularly sandy layer of sediment is present within this section, between ca. 238–232 cm where pollen preservation is very poor. Sedimentation rates increase to ca. 0.07–0.1 mm/yr.
- (3) 230–155 cm: comprised of poorly humified black detrital peat with an increased sedimentation rate of ca. 0.2–0.3 mm/yr. The age range of this section is ca. 8,000–7,500 to 4,000–3,000 cal. years BP, spanning the middle Holocene and part of the late Holocene.

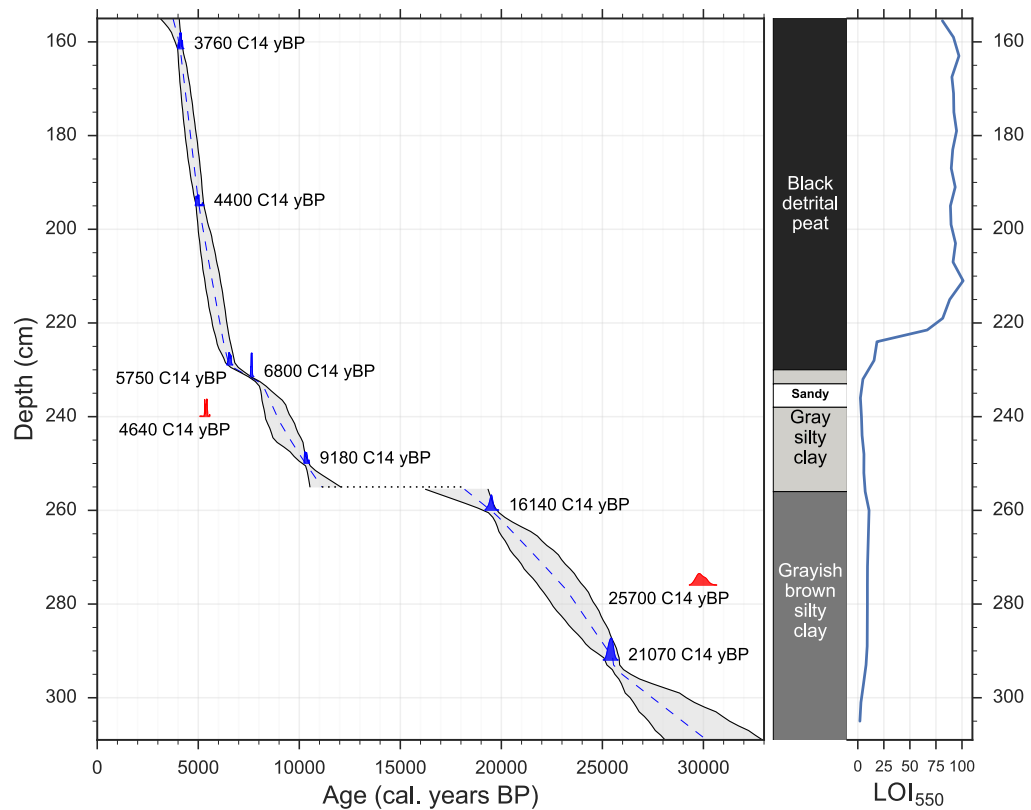


Figure 3.2 - Radiocarbon dates, age-depth model and lithological description for Cuatro Vientos.

3.5.2 Cuatro Vientos pollen data

Figure 3.3 shows the fossil pollen data for the CV core between 155 and 280 cm (below FMV). Three statistically significant zones were identified in the cluster analysis, but to aid in interpretation, zone 1 was split into two sub-zones (before and after the hiatus) and an additional zone was added to mark the period of poor pollen preservation between 239 and 230 cm (zone 2), thus giving a total of four pollen assemblage zones. The results of CV will be discussed alongside the updated pollen diagram from LCH (Figs. 3.4 and 3.5). Appendix B. provides details and images of unknown pollen grains found in the Cuatro Vientos core.

Zone 1a and Zone 1b: 280–240 cm, ca. 24,000–8,750 cal. yr BP (LGM to Early Holocene); includes sediment hiatus ca. 18,000–11,000 cal. yr BP

This pollen assemblage has abundant grass (Poaceae; 40–60%) and sedge (Cyperaceae; 5–10%) pollen, and the highest abundance of the herb taxa Asteraceae (5–10%), *Borreria* (~2%) and Amaranthaceae (~1%). Levels of ‘cold-adapted’ taxa such as *Podocarpus*, *Alnus*, and *Ilex* peak in this zone, though at low levels of up to 1%. This is the only zone to contain any significant amounts of *Paullinia/Roupala*; levels of this pollen type are consistent at 3–5% for

most of the zone, rising to ~10% near the top of the zone. The savanna indicator *Curatella americana* is present, but in low amounts (<1%). Other arboreal taxa are limited, with low quantities (<3%) of Moraceae, *Celtis*, Arecaceae (palms), and *Alchornea* – though *Alchornea* reaches its highest abundance in this zone. Few grains were recovered of the aquatic/semi-aquatic taxa of *Sagittaria* and *Isoetes*. In general, the pollen grains recovered in these zones were often degraded. LOI₅₅₀ values are consistently low (~5–10%) throughout these zones, reflective of the inorganic, silty clay sediment.

Zone 2: 239–230cm, ca. 8,750–7,000 cal. yr BP (early-middle Holocene)

Pollen preservation in this zone was very poor, most likely a result of the coarse sandy sediment damaging the grains.

Zone 3: 230–206cm, ca. 7,000–5,500 cal. yr BP (middle Holocene)

During this mid-Holocene section of the core, pollen characteristic of SDTF become established, including *Anadenanthera* (2–4%), *Astronium* (5–7%) and the understory taxon *Clavija* (3–5%). At the same time, *Curatella americana* becomes more abundant (2–4%) and Poaceae levels remain consistent at 50–60%. Other arboreal taxa remain at low levels, though Moraceae does increase slightly from 4% to 10%. Palm taxa are uncommon in this zone. Levels of weed and herb taxa (e.g. *Asteraceae*, *Borreria*) as well as the ‘cold-adapted’ taxa found in Zone 1, decrease to negligible amounts. The aquatic/semi-aquatic taxa *Sagittaria* and *Isoetes* increase throughout this zone, with *Sagittaria* in particular becoming a large proportion of the total pollen sum (~20%) between ca. 6,000–5,500 cal. yr BP. A sudden increase in LOI₅₅₀ occurs at ca. 6,000 cal. yr BP (from <20 to ~80%), reflecting the switch from clay to organic, peaty sediment (Fig. 3.2).

Zone 4: 206–155cm, ca. 5,500–3,750 cal. yr BP (middle to late Holocene)

This zone is similar to zone 3, with only subtle differences in the abundances in some of the taxa. Moraceae percentages stabilise at ~10%, with other HETF arboreal taxa remaining at low/negligible levels. Palm (Arecaceae spp., *Mauritia/Mauritiella*) pollen grains have a more consistent presence in the assemblage, being present in most samples within this zone, but only at very low levels (<1%). *Curatella americana* decreases slightly towards the top of this zone. *Sagittaria* becomes established at 20–30% of the total pollen sum, with *Isoetes* decreasing slightly from Zone 3a to values of 0–5%. LOI₅₅₀ values remain consistent at ~90% through this zone.

Figure 3.3 -
(Caption
overleaf)

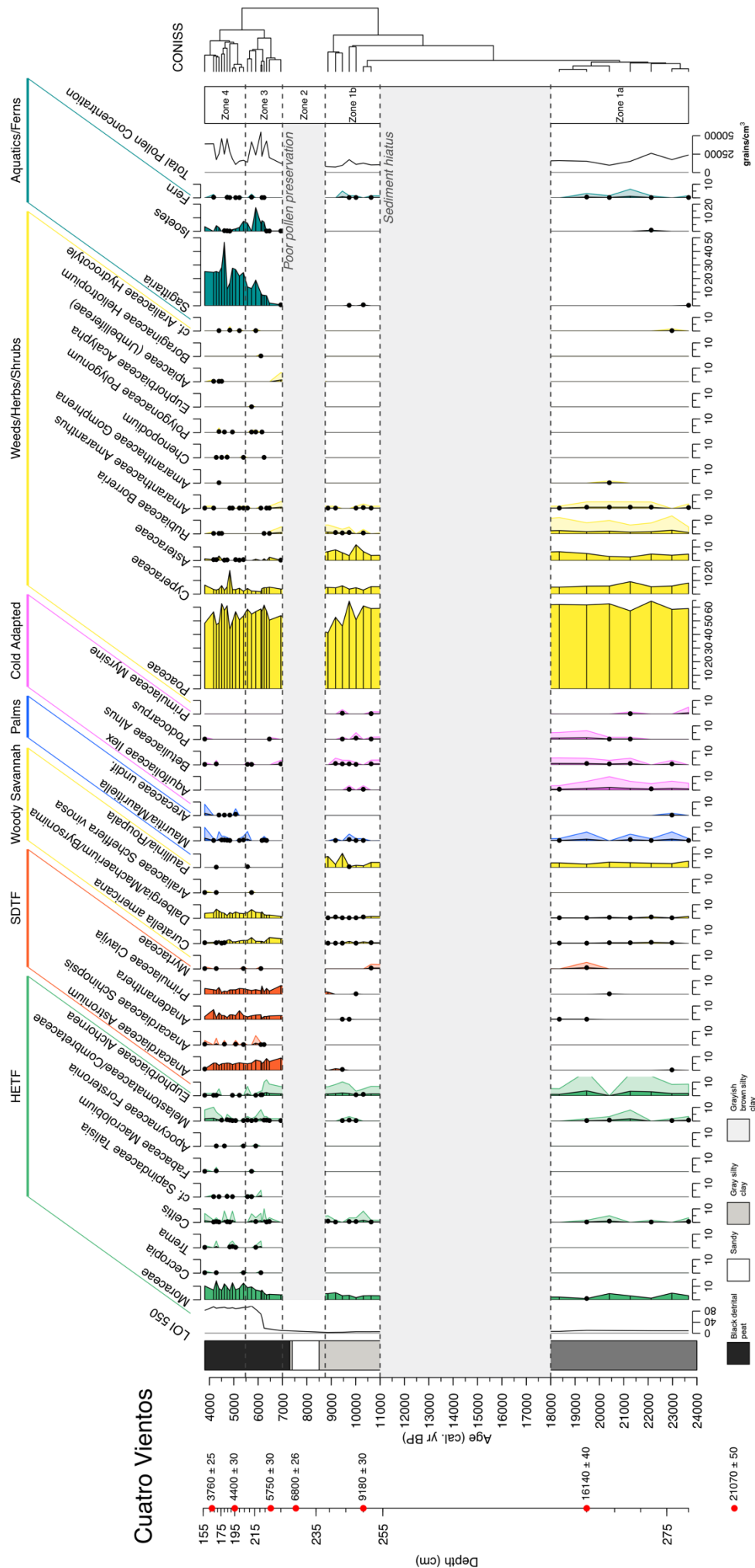


Figure 3.4 -
(Caption
overleaf)

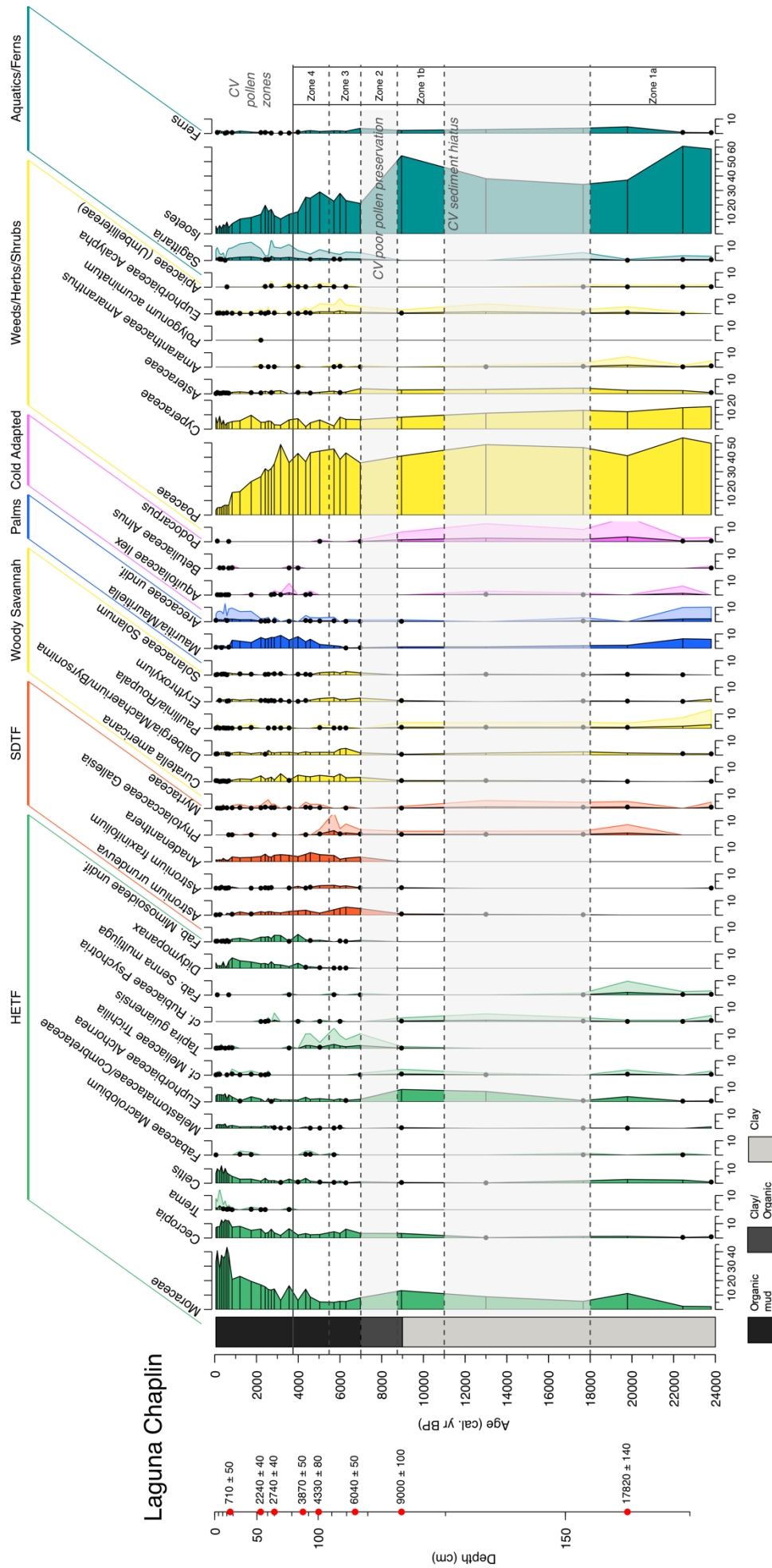


Figure 3.5 - (Caption overleaf)

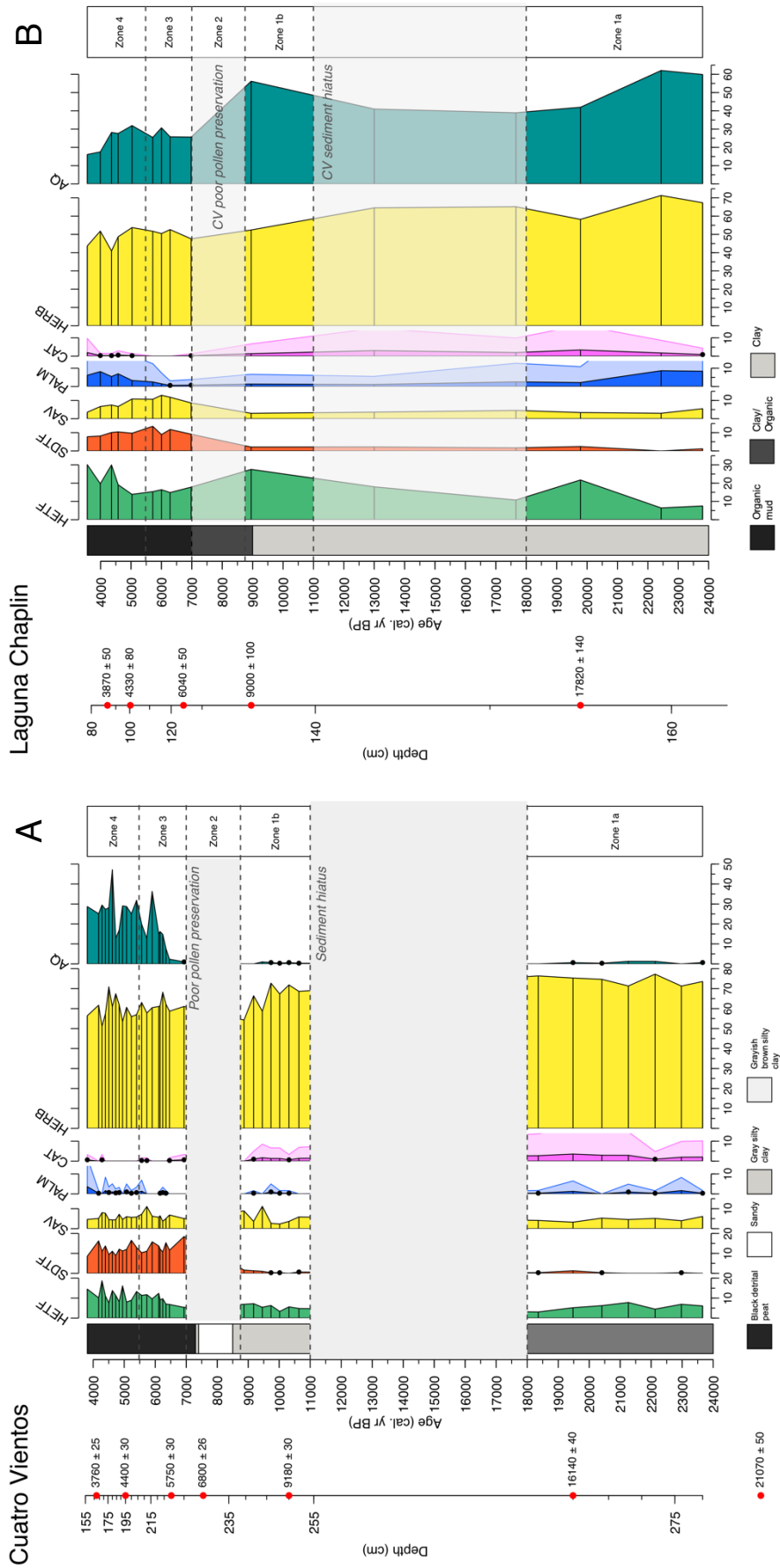


Figure 3.3 - Pollen percentage diagram of taxa from Cuatro Vientos, plotted against calibrated years BP. Dots signify <1% abundance.

Figure 3.4 - Pollen percentage diagram of taxa from Laguna Chaplin, plotted against calibrated years BP. Dots signify <1% abundance. Zonations are based on the pollen zones of Cuatro Vientos to aid in comparison. Lithological descriptions taken from Burbridge et al. (2004)

Figure 3.5 - Summary percentage diagram for (a) Cuatro Vientos, (b) Laguna Chaplin, for the time period covered by the Cuatro Vientos record (ca. 24,000–3,750 cal. yr BP). Groupings as in Figs. 3.3 and 3.4: Humid Evergreen Tropical Forest (HETF), Semi-deciduous Tropical Forest (SDTF), Savanna (SAV), Palm trees (PALM), Cold Adapted Taxa (CAT), Herbs, weeds and shrubs (HERB), Aquatic/Semi-Aquatic (AQ).

3.6 Interpretation and discussion

3.6.1 Comparison between pollen records of Cuatro Vientos palm swamp and Laguna Chaplin

Last Glacial Maximum (ca. 24,000–18,000 cal. yr BP)

The paleoecological data indicate that the Cuatro Vientos (CV) basin type was very different during the LGM compared with today. The scarcity of palm pollen (*Arecaceae* undiff. and *Mauritia/Mauritiella*) in the pollen record is a clear indication that, unlike today, there were no substantial stands of palm trees growing on or near the basin during this time. Additionally, *Mauritiella* palm swamps, such as CV, are characterised by highly organic, peaty sediment. However, this LGM section of the core is characterized by fine-grained inorganic clay sediment (<10% LOI₅₅₀), suggestive of a low-productivity, low-energy lake rather than a peat swamp. The absence of emergent macrophytes (e.g. *Sagittaria*, *Isoetes*) suggests that CV was unsuitable for supporting aquatic/semi-aquatic vegetation, possibly indicating very low water levels and the basin perhaps drying out seasonally. Low water levels would be consistent with the regional paleoclimate reconstructions of a drier LGM in this region, not only from neighbouring LCH (Burbridge *et al.* 2004), but also Laguna La Gaiba ~500 km to the south (Whitney *et al.* 2011; Metcalfe *et al.* 2014). An intermittently dry basin may also account for the generally degraded nature of the pollen grains in this section of the core, whereby the grains are exposed to short-term oxidation.

If our interpretation that CV was an open lake at this time (rather than a palm swamp) is correct, the LGM pollen assemblage would reflect the local vegetation growing *outside* the basin, rather than *within* the basin. This gives us confidence that CV is a useful repository of paleoecological data during the LGM, reflecting the history of *terra firme* vegetation changes beyond the basin. Therefore, any significant differences between the pollen records of LCH and CV will most likely be a result of basin size (i.e. regional *versus* local pollen catchments, respectively), rather than basin type (i.e. lake *versus* palm swamp).

The LGM pollen records from CV and LCH are remarkably similar (Figs. 3.4 and 3.5), both indicating an open landscape covered with grasses, herbs and sparse tree cover typical of an open savanna. There is abundant Poaceae alongside relatively high percentages of other terrestrial herbs (*Borreria*, Asteraceae) and Cyperaceae. The modern pollen rain study of Jones *et al.* (2011), based on pollen trap samples from 1 ha ecological plots within NKMNP, suggests that this type of assemblage may be characteristic of an open seasonally-flooded

savanna, favoring herbaceous plants that cope better with contrasting seasonal water stresses. Although they are negligible in the CV record, *Mauritia/Mauritiella* palms are slightly more abundant in LCH, which Burbridge et al. (2004) and Jones et al. (2011) use as further evidence of a seasonally-flooded savanna. Nevertheless, Jones et al. (2011) notes that the differences between seasonally-flooded and *terra-firme* cerrado savanna are subtle, and the LGM landscape was most likely a mix of these two savanna types. The presence of the woody savanna tree *Curatella americana* is noteworthy as this is a key indicator of savanna environments. Within a seasonally-flooded environment, this species typically grows on top of termite mounds to avoid waterlogging (Killeen & Schulenberg 1998; Jones et al. 2011); this limited growing area may explain the small quantities of *Curatella americana* in this section of the core, though the fact this species is hermaphroditic and entomophilous (insect-pollinated) will also be a key factor in it being under-represented in the pollen record. Overall, the similarities in the pollen records of CV and LCH show that the local-scale vegetation (CV) was similar to the regional-scale vegetation (LCH), corroborating the interpretations from Burbridge et al. (2004) that much of southern NKMNP was covered in an open savanna during the LGM in response to glacial aridity, lower atmospheric CO₂ levels (Monnin et al. 2001) and cooler temperatures (Stute et al. 1995; Thompson et al. 1998; Whitney et al. 2011).

Burbridge et al. (2004) infer that the low levels of arboreal rainforest taxa at LCH most likely indicate scarce communities of HETF regionally, most likely existing as gallery rainforests bordering the Río Paraguá. However, the extent of these gallery rainforests is impossible to determine with the regional-scale pollen catchment of LCH. Given that we have established that the LGM pollen record from CV is representative of vegetation growing beyond its basin, the smaller catchment size of CV and the basin's closer proximity to the Río Paraguá allows us to gain more information about the gallery rainforests at this time. Modern pollen rain studies suggest that a closed-canopy gallery rainforest would be expected to contain Moraceae levels of ~40%, alongside pioneer species such as *Cecropia* and potentially small abundances of taxa such as *Pouteria*, *Sapium* and *Symmeria* (Gosling et al. 2005; Burn et al. 2010). However, the LGM pollen assemblage of CV are not indicative of this kind of gallery rainforest. In particular, Moraceae and *Cecropia* percentages never exceed ~5%, which, given that these taxa are prolific pollen producers and are over-represented in pollen assemblages (Gosling et al. 2005; Burn et al. 2010), is strong evidence against a substantial gallery rainforest lining the nearby Río Paraguá.

Following Zone 1a, the sediment hiatus at CV from ca. 18,000–11,000 cal. yr BP suggests a period of very dry conditions, perhaps causing the basin to dry out completely. Similar hiatuses or periods of low sedimentation have been identified in other basins across lowland Amazonia during the last glacial period, for example: in NKMNP, Laguna Bella Vista (LBV; ca. 110km north of CV) records a hiatus between ca. 42,500–13,000 cal. yr BP and LCH records very low sedimentation rates during this period (Burbridge *et al.* 2004); in south-eastern Amazonia, hiatuses are recorded on the Serra dos Carajás plateau between ca. 22,000–13,000 cal. yr BP (Sifeddine *et al.* 2001) and at Lago do Saci between ca. 18,200–9,200 cal. yr BP (Fontes *et al.* 2017); several basins outlined in Ledru *et al.* (1998) from across Amazonia and southern Brazil record low sedimentation or hiatuses spanning the LGM.

Early to middle Holocene (ca. 11,000–7,000 cal. yr BP)

The end of the sediment hiatus at CV occurred at ca. 11,000 cal. yr BP and is concurrent with the change in the lithology of the sediment, with grayer clays and some organic inclusions. Nevertheless, there is no evidence that the basin changed significantly from the shallow open lake of the LGM; the LOI₅₅₀ values remain low and there is no change in the levels of sedge, aquatic or palm taxa. The hiatus termination may indicate slightly wetter conditions in the region, allowing water levels in the basin to rise and for local runoff to increase, inputting more sediment to the basin. This is consistent with the paleoclimatic interpretation of increased precipitation levels from ca. 12,200 cal. yr BP at Laguna La Gaiba (Whitney *et al.* 2011) and with the hiatus termination at LBV in the north of NKMNP (Burbridge *et al.* 2004). Holocene temperatures were ca. 5°C higher than the LGM, with deglacial warming of tropical South America occurring from ca. 19,500 cal. yr BP (Seltzer *et al.* 2002; Whitney *et al.* 2011). Atmospheric CO₂ levels in the Holocene were ca. 76 ppm higher than the LGM (Monnin *et al.* 2001). Both temperature and CO₂ levels remained relatively stable throughout the Holocene, prior to the industrial period (Indermühle *et al.* 1999; van Breukelen *et al.* 2008; Whitney *et al.* 2011).

The CV pollen assemblage in Zone 1b (ca. 11,000–8,750 cal. yr BP) does not differ significantly from that of the LGM Zone 1a, which suggests that the open savanna persisted in the area into the early Holocene. This is consistent with the pollen assemblage from LCH, which is relatively stable from the LGM through most of the Holocene (including through the hiatus phase from CV). Therefore, even with the increase in precipitation at this time (restarting sedimentation at CV), it clearly wasn't enough to support a humid arboreal landscape. The period of poor pollen preservation in the CV core from ca. 8,750 to 7,000 cal. yr BP (Zone 2)

is associated with a layer of sandy sediment. This may reflect a period where fluvial dynamics caused a change in river course so that it flowed near, or even into, CV, therefore creating a higher-energy deposition environment. A higher-energy environment would inhibit deposition of pollen-size particles, instead favoring the deposition of the larger, heavier sand particles, thus potentially explaining the lack of pollen in this section of the core. Additionally, agitation of the pollen grains against the large sandy grains could have caused mechanical damage and poor pollen preservation (Twiddle & Bunting 2010).

Middle Holocene (ca. 7,000–5,500 cal. yr BP)

It has been well established that the middle Holocene was associated with a significantly drier-than-present climate across much of southern hemispheric tropical South America, with peak dryness occurring at ca. 6,000 cal. yr BP (Baker *et al.* 2001; Wang *et al.* 2007; Whitney & Mayle 2012; Cheng *et al.* 2013; Kanner *et al.* 2013; Bernal *et al.* 2016). The drier climate has been attributed to lower southern-hemispheric summer insolation levels at this time, driven by the precessional cycle of Earth's orbit (Berger & Loutre 1991), which would have acted to restrict the southerly migration of the Inter-tropical Convergence Zone (Haug *et al.* 2001) and decrease the strength of the South American summer monsoon (Cruz *et al.* 2009; Baker & Fritz 2015).

The mid-Holocene section of the CV core is marked by significant changes to the CV basin, in particular, a switch to highly organic (LOI₅₅₀ values > ~80%), peaty sediment ca. 6,000 cal. yr BP (Fig. 3.2). Concurrent with this dramatic lithological change is increased abundance of the aquatic/semi-aquatic macrophytes *Sagittaria* and *Isoetes*. These changes suggest a change from a clear, shallow, open lake to a more eutrophic environment with high levels of deposition of organics. We infer that this is the start of the transition of CV from a lake to a palm swamp. The timing of this switch is interesting, given that it occurs at the peak of the mid-Holocene drought at ca. 6,000 cal. yr BP and previous dry conditions during the LGM were associated with low sedimentation rates and a sediment hiatus at CV. A drier mid-Holocene climate would most likely cause a decrease in water levels at CV, but unlike in the LGM, the closer river course (as argued for in the early-Holocene Zone 2) would cause intermittent flooding at CV inundating the basin with organic matter and maintaining an anaerobic environment. Nevertheless, it is important to note that there are a great diversity of successional pathways in swamp environments that can be caused by a variety of different factors (Behling & Hooghiemstra 1999; Kelley *et al.* 2013; Roucoux *et al.* 2013) which may or may not be related to changes in precipitation.

Despite the change of CV to a swamp basin at this time, we can remain reasonably confident that vegetation growing in the swamp is not masking the influx of pollen from vegetation beyond the swamp. Other than the increase in emergent aquatics (*Sagittaria*, *Isoetes*), there are no increases in other taxa that would be expected to grow in a swamp environment and dominate the pollen rain (e.g. Cyperaceae, *Mauritia/Mauritiella*). Increases in pollen percentages of arboreal taxa that do not grow in a swamp environment (e.g. *Astronium*, *Anadenanthera*) are especially significant, as these pollen must have come from the surrounding *terra firme* area beyond the perimeter of the basin. Therefore, as with the LGM, this gives us confidence that CV is a useful repository of mid-Holocene paleoecological data, reflecting the history of *terra firme* vegetation changes beyond the basin.

Considering the clear contrast in the type (palm swamp *versus* lake) and size (5 *versus* 20 km²) of the CV basin compared to the neighbouring LCH basin, it is perhaps surprising that the pollen records of these two sites are so similar. Both records are indicative of a savanna-SDTF mosaic landscape during this mid-Holocene pollen assemblage. The increased levels of the savanna tree *Curatella americana*, decreased levels of herbs (e.g. Asteraceae) and negligible amount of palm taxa at both sites may suggest that the savanna component was more indicative of a woody cerrado (non-flooded) savanna, rather than the more open seasonally-inundated savanna of the LGM (Jones *et al.* 2011). This is plausible given that a weaker mid-Holocene summer monsoon would likely mean less flooding (from the neighboring Río Paraguá) in the rainy season and longer dry seasons. The establishment of *Anadenanthera* and *Astronium* is good evidence of SDTF being present around the basins at this time, both locally (CV) and regionally (LCH), as these are key components of modern SDTF. The *Anadenanthera* pollen type is most likely *Anadenanthera colubrina*, a key drought-tolerant species that is dominant in the modern Chiquitano SDTF region (Killeen & Schulenberg 1998; Gosling *et al.* 2009) and a key dry forest indicator, given its absence from both rainforest and savanna ecosystems (Gosling *et al.* 2009). Both *Anadenanthera* and *Astronium* are often under-represented in pollen assemblages (Gosling *et al.* 2009); therefore, the relatively high percentages of these taxa (5–7%) suggests they would have been abundant in the area. The similarity between the CV and LCH pollen records provides good evidence that the drier climate of the middle Holocene caused a widespread savanna-SDTF mosaic landscape in the area, at both local (evidenced from CV) and regional (evidenced from LCH) spatial scales.

The shifting river course into and out of CV that we infer from Zones 2 and 3 suggests that the Río Paraguá ran just as close, if not closer, to CV during the middle Holocene compared to present. Therefore, we may expect that CV would capture a strong gallery rainforest signal in the pollen record. However, as with the previous pollen zones, there are only low levels of arboreal rainforest pollen taxa at CV (10% Moraceae), certainly not at the levels (> 40% Moraceae) expected from a significant gallery rainforest (Burn *et al.* 2010). We therefore infer that there was insufficient gallery rainforest in NKMNP to provide significant refugia for rainforest species during the drier climate of the middle Holocene. This is somewhat corroborated by other records in the southern Amazonian region; for example, Laguna Granja, a small oxbow lake ca. 300 km northwest of NKMNP, also shows reduced extent of gallery rainforests during the middle Holocene (Carson *et al.* 2014).

Middle to late Holocene (ca. 5,500–3,750 cal. yr BP)

Following the peak of the mid-Holocene dry period at ca. 6,000 cal. yr BP, the climate in the region gradually became wetter through the middle to late Holocene (especially after ca. 4,000 cal. yr BP) (Baker *et al.* 2001; Wang *et al.* 2007; Whitney & Mayle 2012; Cheng *et al.* 2013; Kanner *et al.* 2013; Bernal *et al.* 2016) in response to progressive strengthening of the SASM driven by gradually increasing insolation levels (Berger & Loutre 1991; Cruz *et al.* 2005; Baker & Fritz 2015). In CV Zone 4, the organic, peaty sediment with consistently high LOI₅₅₀ values is now well established, indicating that the basin has remained a swamp throughout this zone. Aquatic vegetation is well represented, with consistently high levels of *Sagittaria*, possibly outcompeting *Isoetes* for space and indicating a continued eutrophic status. However, given that the levels of Cyperaceae and palm taxa remain mostly unchanged, it is unlikely that the basin has yet become a palm swamp analogous to that of today (with the floating mats of grass/sedges and clumps of palms growing throughout the basin). The small increase in percentages of *Mauritia/Mauritiella* pollen is noted, though if these palms were growing abundantly across the CV basin we would expect much higher levels than the 1–3% seen here. For example, *Mauritia/Mauritiella* pollen percentages of between 10–40% are common for other palm swamps across Amazonia (Behling *et al.* 1999; Meneses *et al.* 2015; Rodríguez-Zorro 2017; Maezumi *et al.* 2018a).

At both CV and LCH, only small changes occur in the pollen assemblages between Zone 3 and 4, with no changes to the overall interpretation of a savanna-SDTF mosaic vegetation cover both locally (around CV) and regionally (inferred from LCH). There are some subtle differences, however, that may indicate some minor changes to the vegetation cover. The

small increase in Moraceae in Zone 4 may signify a greater proportion of SDTF relative to savanna in the region, given that: (a) an increase to ~40% Moraceae would be expected from significant expansion of HETF or gallery rainforest (Burn *et al.* 2010), and (b) the presence of Moraceae in the modern pollen rain of savanna ecosystems is predominantly due to long-distance wind-blown transport from the nearby HETF that was absent in the middle Holocene (Gosling *et al.* 2009; Jones *et al.* 2011). The slight increase in *Mauritia/Mauritiella* at CV is concurrent with larger increases seen at LCH, which may suggest the resumption of seasonal flooding at some low-lying areas around the basins. Unfortunately, the CV record terminates at ca. 3,750 cal. yr BP due to the difficulty in acquisition of uppermost sediments beneath a floating mat of sedge/grass. This means that we cannot corroborate the timing of the increase in HETF at LCH from ca. 2,500 to 750 cal. yr BP (Burbridge *et al.* 2004) or determine when the current hydrology and floristic composition of the palm swamp developed.

3.6.2 Implications of the paleoecological history of CV

Although great strides have been taken in recent years, the number of paleoecological sites that provide information about the Quaternary vegetation history of tropical South America is well below that of the temperate regions of North America and Europe. A recent mid- to late Holocene multi-proxy vegetation reconstruction synthesis by Smith and Mayle (2018) reports 110 sites across southern hemispheric tropical South America, though many of these sites were non-pollen based and were clustered in south-east Brazil, with significant gaps across eastern and central Amazonia. Far fewer sites extend to glacial times, with Marchant *et al.* (2009) reporting only 34 sites for the whole of Latin America in a pollen-based biome reconstruction of the LGM. In contrast, there is good spatial coverage of several hundred mid-Holocene sites across North America (e.g. Prentice *et al.* 1993; Sawada *et al.* 2004; Viau *et al.* 2006) and Europe (e.g. Davis *et al.* 2003; Wu *et al.* 2007; Roberts *et al.* 2018), with growing numbers in east Asia (e.g. Ni *et al.* 2010; Tian *et al.* 2017). As a result, tropical South America is poorly represented in global syntheses (e.g. Gajewski 2008; Bartlein *et al.* 2011) and paleodata–model intercomparison projects (e.g. Kohfeld & Harrison 2000; Harrison & Prentice 2003; Braconnot *et al.* 2012), despite the important role the Amazon rainforest plays in global carbon sequestration (Phillips *et al.* 2009; Pan *et al.* 2011; Aragão *et al.* 2014; 2018).

However, increasing the number of sites in tropical regions such as Amazonia is a complicated task and selecting new target sites for paleoecological analysis is limited by site availability. The challenging logistics of field work in Amazonia means that field seasons are often months long and may only yield data from one or two sites. Therefore, researchers may be reluctant

in spending their resources to investigate palm swamps for paleoecological study, given the aforementioned concerns over their suitability for recording terrestrial vegetation history from beyond their basin. Consequently, palm swamps are often viewed as ‘sub-optimal’ compared to lakes as targets for paleoecological study. However, the CV record reveals the importance of considering the potentially dynamic limnological histories of such basins and shows that their present-day characteristics may not be representative of the entire Quaternary sedimentological or catchment history. Within the context of the regional-scale Quaternary vegetation history from neighbouring LCH, we have shown that the CV palm swamp contains a fossil pollen archive of local-scale, terrestrial vegetation history beyond the swamp extending to the LGM, rather than a localised record of palm swamp vegetation dynamics. Given the scarcity of Amazonian sedimentary records that extend to the LGM, palm swamps may therefore hold considerably greater value for reconstructing Amazonian Quaternary vegetation change than commonly assumed.

With regards to the history of riverine/gallery rainforests in NKMNP, at the CV pollen record suggests gallery (riverine) rainforest were absent from the site during the LGM and middle Holocene. Instead, our pollen data reveal that during the LGM and middle Holocene, both the interfluves (presently covered by humid rainforest) and riverine areas were covered by a mosaic of savanna and dry forest. Therefore, our findings do not support the hypothesis, at least in our ecotonal area of Amazonia, that during the LGM and middle Holocene wide ribbons of gallery rainforest lined the rivers, providing important refugia for rainforest species. Narrower gallery forests during the middle Holocene may have implications for the migration routes of pre-Colombian humans. For example, forest dwelling cultures such as the Tupi-Guarani likely used gallery forests as routes for expansion through non-forested landscapes. If the reduced extent of riverine gallery forests in NKMNP is representative of rivers across ecotonal southern Amazonia, as well as the Cerrado savanna biome to the southeast, it would support the hypothesis that the late Holocene expansion of gallery rainforest (e.g. Silva *et al.* 2008) linking the Amazonian and Atlantic forest biomes facilitated the trans-continental migration of the forest-dependent Tupi-Guarani culture from southern Amazonia to southern Brazil ca. 2,000–3,000 cal. yr BP (Iriarte *et al.* 2017).

The vulnerability of the gallery rainforests in NKMNP to drier mid-Holocene climatic conditions raises concern over the fate of ecotonal areas of Amazonia under drier climate scenarios predicted for the mid-to-late 21st century (Christensen *et al.* 2007; Joetzjer *et al.* 2013; Boisier *et al.* 2015). Modern field-based ecological impact analyses have shown that tree mortality

increases significantly in Amazonian forests in response to severe drought events, though regrowth occurs in subsequent wet years (Phillips *et al.* 2009; Doughty *et al.* 2015; Feldpausch *et al.* 2016). However, these drought events are likely to become more frequent under a future drier climate and if gallery rainforests are not likely to provide refugia for rainforest species, then the resilience of ecotonal, southern Amazonian rainforest would likely be reduced.

3.7 Conclusions

The fossil pollen data from the Cuatro Vientos (CV) palm swamp provide a local-scale, late Quaternary vegetation history for southern Noel Kempff Mercado National Park (NKMNP), Amazonian Bolivia, spanning the Last Glacial Maximum (LGM) to the middle Holocene. This local-scale vegetation history complements the previously published, regional-scale vegetation history obtained from the adjacent large lake, Laguna Chaplin (LCH; Mayle *et al.* 2000; Burbridge *et al.* 2004). Our results from CV demonstrate that palm swamps in southern Amazonia have the potential to yield Pleistocene-age paleoecological records that provide information about vegetation on *terra firme* landscapes beyond the basin itself, rather than simply recording a history of localised swamp vegetation dynamics. Comparison between the CV and LCH pollen records reveals both local- and regional-scale evidence for savannas during the LGM, and a savanna/SDTF mosaic during the middle Holocene. These results demonstrate that the paleoecological value of tropical palm swamps, such as CV, is considerably greater than often assumed – with the potential to yield local-scale, glacial-interglacial histories of climate-driven, terrestrial vegetation dynamics.

Due to its local-scale pollen catchment, and close proximity to the Río Paraguá, the CV pollen record also reveals the history of riverine vegetation in ecotonal, southern Amazonia. We find that drier climatic conditions of the LGM and middle Holocene supported expansion of open savanna, not only in the interfluves, but in riverine areas too, challenging the common assumption that rainforest persisted in ribbons of gallery rainforest lining the rivers, which served as important refugia. The absence of significant gallery rainforest during past drier climatic conditions raises concerns that gallery rainforest may not be resilient to projected future increased drought and may therefore not be relied upon to serve as rainforest migration corridors, as has previously been proposed.

3.8 Acknowledgements

Macarena Cárdenas and John Carson provided assistance with pollen sample processing and pollen identification. RS was funded by a NERC ‘SCENARIO’ DTP PhD award (2014-18).

Funding for LOI analysis and 5 radiocarbon dates was provided by to S.Y.M. from the Global Change and Sustainability Center, the Graduate Research Fellowship, and the Don Currey Graduate Research Fellowship at the University of Utah. The further four dates were funded by the School of Archaeology, Geography and Environment Science, University of Reading. We thank Mary McIntyre and Daniel Harris for their help in sample preparation and analysis. Tim Killeen, Juan Surubi, Pastor Sollis, Rene Guillen, and the 'Museo de Historia Natural Noel Kempff Mercado' provided logistical support to access and core the CV site. The University of Leicester provided a start-up grant to FM (1995) to support the fieldwork.

Chapter 4. Response of Amazonian forests to mid-Holocene drought: a model-data comparison

Authors: **Richard J. Smith**, Joy S. Singarayer, Francis E. Mayle

4.1 Preface

The following chapter is taken from a paper submitted for publication to the journal *Global Change Biology*. The chapter is therefore written in the style of a journal article, conforming to the regulations of the journal. **RS** designed the project, undertook the analyses and led the writing of the paper. **JS** provided expertise on the model simulations. **FM** provided expertise on the palaeo-data. All authors contributed to interpretation and writing the paper.

4.2 Abstract

The fate of Amazonia over the coming century, in the face of anthropogenic climate change, is of major concern. A key area of uncertainty is the scale of rainforest die-back to be expected under a future, drier climate. In this study, we use the middle Holocene (MH, ca. 6,000 years before present) as an approximate analogue for a drier future, given that palaeoclimate data show much of Amazonia was significantly drier than present. We explore the uncertainty in model simulations of the degree of resilience of Amazonian biomes under MH climate change by using three dynamic global vegetation models (JULES, IBIS and SDGVM) forced by the bias-corrected MH climate simulations from seven climate models that participated in the Paleoclimate Modelling Intercomparison Project 3 (PMIP3). These model outputs are compared to a multi-proxy palaeoecological dataset to gain a better understanding of where in Amazonia we have most confidence in the MH vegetation simulations. A robust feature across all model combinations is the resilience of the central Amazonian rainforest biome to MH drought – a finding consistent with the palaeo-data and a cause for optimism for the future of this area. Greater divergence in MH simulations exists in ecotonal eastern and southern Amazonia, where the degree of uncertainty is dependent upon the choice of vegetation and climate models. Vegetation models driven with climate models that simulate a drier MH better capture the observed (palaeo-data) savannah expansion in these areas, though the magnitude of savannah expansion varies between model combinations. We highlight the need for the continuation of multi-model ensemble experiments (both past and future), to help capture the range of uncertainty across different vegetation and climate models, and we demonstrate the need for more palaeoecological and palaeoclimate data across lowland Amazonia, particularly in eastern and southern ecotonal regions of the basin.

4.3 Introduction

The fate of Amazonian forests is of great scientific concern, given their global importance in terms of the ecosystem services they provide. The tropical biomes of Amazonia host ~20–25% of global terrestrial species (Dirzo & Raven 2003; May *et al.* 2013). They play an important role in the global carbon budget, constituting a large carbon reserve and a net sink for atmospheric CO₂ (Phillips *et al.* 2009; Pan *et al.* 2011; Aragão *et al.* 2014), and, through moisture recycling, influence regional and global climate patterns (Werth & Avissar 2002; Gash *et al.* 2004; Harper *et al.* 2014). Although Amazonia contains one of the largest remaining areas of intact forest in the world (Potapov *et al.* 2017), decades of deforestation and forest fragmentation has left the ecosystems vulnerable (Skole & Tucker 1993; Soares-Filho *et al.* 2006; Malhi *et al.* 2008). However, direct anthropogenic land use is not the only problem facing Amazonia over the coming century. As moisture availability is considered one of the most important limiting factors controlling Amazonia's forest productivity (Meir & Woodward 2010), the potential for a drier future regional climate is particularly concerning (Malhi *et al.* 2008).

Simulations of future climate change vary between models, but overall they suggest that Amazonia will be subject to a decrease in precipitation, with particular concern for a significant intensification of the dry season (e.g. Joetzjer *et al.* 2013; Boisier *et al.* 2015; Duffy *et al.* 2015). Detailed field-based ecological impact analyses have demonstrated the sensitivity of Amazonian forests to severe short-term drought events. For example, the Amazon Forest Inventory Network (RAINFOR; Malhi *et al.* 2002) project has provided evidence for increased tree mortality and substantial loss of biomass carbon in response to the 2005 and 2010 drought events (Phillips *et al.* 2009; Doughty *et al.* 2015; Feldpausch *et al.* 2016), raising concerns that Amazonian forests are finely balanced between being a carbon sink or source (Aragão *et al.* 2014; Gatti *et al.* 2014; Brienen *et al.* 2015; Cavaleri *et al.* 2017). However, the sensitivity of Amazonia to long-term climate change over the coming centuries is much more uncertain. Dynamic Global Vegetation Models (DGVMs) have become the primary way to investigate the large-scale, long-term responses of Amazonian vegetation to future climate change scenarios. However, projections from these DGVM studies vary considerably; outcomes include widespread replacement of rainforest with savannah (e.g. Cox *et al.* 2000; Betts *et al.* 2004; Huntingford *et al.* 2008), transition of humid to dry forests (e.g. Levine *et al.* 2016), and rainforest resilience (e.g. Cowling & Shin 2006; Good *et al.* 2013; Huntingford *et al.* 2013). Reducing this uncertainty remains a key area of scientific focus.

In this study, we take a palaeo-modelling approach in an attempt to better understand the uncertainties surrounding vegetation simulations of Amazonia. The premise, pioneered by the Paleoclimate Modelling Intercomparison Project (Joussaume & Taylor 1995; Harrison *et al.* 2002; Braconnot *et al.* 2011), is to run model simulations for a period in the past which had a climate-state significantly different to that of the modern day, and for which there is sufficient palaeo-observational data to evaluate the model outputs. This allows an assessment of model performance outside the range of modern forcings, providing potentially useful information about the credibility of future model projections (Schmidt 2010; Braconnot *et al.* 2012; Harrison *et al.* 2015).

One of the key time periods that PMIP focuses on is the mid-Holocene (MH), ca. 6,000 years before present (6ka BP), when levels of incoming solar radiation (insolation) differed from today due to changes in orbital forcing (Berger 1978). Southern-hemispheric tropical South America experienced a decrease in austral summer insolation levels at this time (Berger & Loutre 1991), which restricted the southerly migration of the Inter-tropical Convergence Zone (ITCZ; Haug *et al.* 2001; Singarayer *et al.* 2017) and decreased the strength of the South American summer monsoon (Cruz *et al.* 2009; Baker & Fritz 2015), which is one of the major sources of precipitation for Amazonia (Raia & Cavalcanti 2008; Silva & Kousky 2012). Various palaeoclimate records have shown that this caused much of this region to experience a considerably drier MH climate than present (Fig. 4.1b), e.g. significant lake-level reductions at Lake Titicaca on the Bolivian/Peruvian Altiplano (Baker *et al.* 2001), at Laguna La Gaiba in eastern lowland Bolivia (Whitney *et al.* 2011; Whitney & Mayle 2012), and enriched stable oxygen isotope ($\delta^{18}\text{O}$) values from speleothems in southern Brazil (Wang *et al.* 2007; Bernal *et al.* 2016), the Peruvian Andes (Kanner *et al.* 2013) and the western Peruvian Amazon (van Breukelen *et al.* 2008; Cheng *et al.* 2013). The MH also represents a time period for which there is a growing number of palaeoenvironmental data records for tropical South America (e.g. see Marchant *et al.* 2009; Prado *et al.* 2013b; Smith & Mayle 2018).

Here, we aim to investigate how resilient Amazonian forests were to the drier climate of the MH by producing an ensemble of vegetation simulations for MH Amazonia. Previous studies have shown that two important sources of uncertainty in vegetation model simulations derive from: (1) which DGVM is used (e.g. Sitch *et al.* 2008; Galbraith *et al.* 2010), and (2) the climate data used to drive the DGVM (e.g. Schaphoff *et al.* 2006; Good *et al.* 2013; Zhang *et al.* 2015). Therefore, to incorporate these sources of uncertainty into our analysis, our ensemble consists of simulations using three different DGVMs driven with the MH climate simulations from seven

of the climate models that participated in PMIP phase 3 (PMIP3; Braconnot *et al.* 2011). The simulations will be compared with a multiproxy paleovegetation dataset – a subset of those presented in Smith and Mayle (2018). This will allow us to assess the relative skill of each model combination and help determine those regions of Amazonia for which we have the most/least confidence in the MH vegetation simulations. Although the MH climate is by no means a perfect analogue for potential future climate change (most notably with respect to atmospheric CO₂ levels and temperature), it does provide a means for examining how the models predict vegetation response to large-scale, long-term, precipitation changes in Amazonia, thus providing insights into those regions one can expect to be most vulnerable to a prolonged drier climate in the future.

4.4 Materials and methods

4.4.1 Geographic Setting

The area we define as 'Amazonia' in this study is shown in Figure 4.1. This is predominantly based on the broad *sensu latu* definition of Amazonia, which contains most of the lowland humid evergreen forest biome, including the 'Guyanas' of northern South America (Eva *et al.* 2005). We extend the eastern edge of the defined area into the cerrado savannah/evergreen forest ecotone and extend the southern edge to incorporate the Chiquitano dry forest of eastern Bolivia (Fig. 4.1a), as we are interested in potential ecotonal shifts in these bordering regions.

4.4.2 Dynamic Global Vegetation Models (DGVMs)

Three DGVMs were used in this study: the Joint UK Land Environment Simulator (JULES) version 4.9 (Best *et al.* 2011; Clark *et al.* 2011), the University of Sheffield Dynamic Global Vegetation Model (SDGVM) (Woodward *et al.* 1995; Woodward & Lomas 2004) and the Integrated Biosphere Simulator (IBIS) version 2.6b4 (Foley *et al.* 1996; Kucharik *et al.* 2000). This study focuses predominantly on the simulation of vegetation dynamics within these models, although they have been developed to include water and energy exchange between vegetation, soil and atmosphere. All three of these vegetation models split each grid cell into fractions of different plant functional types (PFTs; see SI Table 4-A), simulating vegetation dynamics and competition between these PFTs using a "big-leaf" approach. More detailed information about each DGVM can be found in the original model description papers.

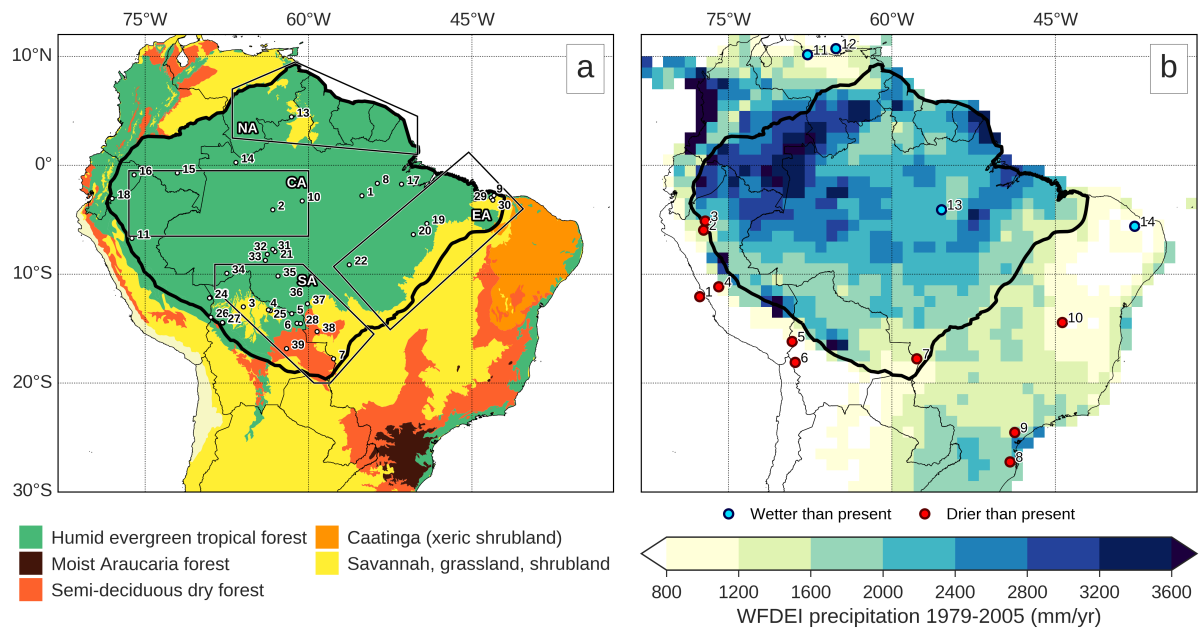


Figure 4.1 - Overview maps of study area. (a) Map of potential broad scale modern ecoregions modified from Olson *et al.* (2001), numbered points show locations of palaeoecological sites use in model-data comparison, see Table 4.2 for list. (b) Annual mean precipitation from the WFDEI dataset 1979-2005 (Weedon *et al.* 2014), numbered points show locations of key paleo-climate sites that provide a qualitative estimate of relative dryness of the MH (blue = MH wetter than present, red = MH drier than present), see Table 4.3 for list. The solid black outline in (a) and (b) marks the delineation of our definition of 'Amazonia'. Polygons in (a) outline key areas referenced throughout this study: Northern Amazonia (NA), Central Amazonia (CA), Eastern Amazonia (EA), Southern Amazonia (SA).

4.4.3 Experimental design

For each DGVM, a control 'pre-industrial' (PI) simulation was conducted using historical climate data and PI levels of CO₂ of 285 ppm, as defined in the PMIP3 pre-industrial experiment (Meinshausen *et al.* 2011; Taylor *et al.* 2012). Land use change was omitted for the control runs, so can be thought of as *potential* modern vegetation simulations. The MH simulations were forced with climate data from the PMIP3 climate model simulations and CO₂ concentration of 280 ppm, as defined in the PMIP3 MH experiment (Braconnot *et al.* 2011). An initial spin-up phase was conducted in all simulations to allow carbon and vegetation fields to equilibrate before the transient runs. Each DGVM required a slightly different spin-up procedure. JULES is the most computationally expensive model to run, so an accelerated spin-up procedure was used that ran for ~400 years rather than the >1,000 years using a

'standard' procedure (Harper *et al.* 2014). For IBIS, a modified spin-up procedure was used, increasing the spin-up length from the default 150 years to 400 years. As SDGVM is the most computationally inexpensive model to run, a long spin-up of 1,500 years was used.

4.4.4 Climate data

The three DGVMs each require different driving climate fields (SI Table 4-B). For the control PI simulation, the climate data come predominantly from the WATCH Forcing Data ERA-Interim (WFDEI) dataset, which contains climate data in 3-hourly time steps created specifically for use in hydrological and land surface models (Weedon *et al.* 2014). WFDEI has data for most of the required climate variables except for cloud cover (for which we use data from the Climatic Research Unit (CRU) TS v4.01 dataset (Harris *et al.* 2014; Harris & Jones 2017)), and relative humidity (for which we used a conversion equation using specific humidity, temperature and surface pressure - see Supporting Information for full details). All the WFDEI climate data were re-gridded to a spatial resolution of $1.0^{\circ} \times 1.0^{\circ}$ for the period 1979-2005.

The climate fields used for the MH runs were processed using the simulations from seven of the CMIP5 GCMs that ran the MH PMIP3 experiment (Table 4.1). These climate models span a range of potential climates for the MH, allowing us to explore the response of vegetation to different MH climate scenarios. As the climate models exhibit considerable biases for Amazonia (Malhi *et al.* 2009), we applied an anomaly approach to produce more realistic (spatially and temporally) climate fields for the MH. For each climate variable (except wet days, temperature delta and temperature range), after re-gridding to the $1.0^{\circ} \times 1.0^{\circ}$ spatial resolution, monthly anomalies were calculated between the MH and PI PMIP3 experiments. These monthly anomalies were then added to the WFDEI 3-hourly climate data to create a 3-hourly MH dataset. The variables of wet days, temperature delta and temperature range were then calculated from the resultant precipitation and temperature fields. IBIS and SDGVM required monthly averages to be calculated from the 3-hourly MH data.

Table 4.1 - PMIP3 climate models used in this study.

Model name	Modelling centre	Original atmospheric grid resolution	Reference(s)
CNRM-CM5	Centre National de Recherches Météorologiques/Centre European de Recherche et Formation Avancees en Calcul Scientifique (CNRM-CERFACS)	T127 (~1.4° x 1.4°) L31	Voltaire <i>et al.</i> (2013)
CSIRO-Mk3-6-0	Commonwealth Scientific and Industrial Research Organisation / Queensland Climate Change Centre of Excellence (CSIRO-QCCCE)	T63 (~1.875° x 1.875°) L18	Gordon <i>et al.</i> (2002; 2010), Jeffrey <i>et al.</i> (2013)
FGOALS-s2	Laboratory of Atmospheric Sciences and Geophysical Fluid Dynamics / Institute of Atmospheric Physics, Chinese Academy of Sciences (LASG-IAP)	R42 (~1.66° x 2.81°) L26	Bao <i>et al.</i> (2013)
GISS-E2-R	National Aeronautics and Space Administration (NASA) Goddard Institute for Space Studies (GISS)	2° x 2.5° L40	Schmidt <i>et al.</i> (2014b)
HadGEM2-CC	Met Office Hadley Centre (MOHC)	1.875° x 1.25° L38	Collins <i>et al.</i> (2011), Martin <i>et al.</i> (2011)
IPSL-CM5A-LR	Institut Pierre Simon Laplace (IPSL)	1.875° x 3.75° L39	Marti <i>et al.</i> (2010), Kageyama <i>et al.</i> (2013b; 2013a)

Model name	Modelling centre	Original atmospheric grid resolution	Reference(s)
MIROC-ESM	Model for Interdisciplinary Research on Climate, University of Tokyo (MIROC)	T42 (~2.8125° x 2.8125°) L80	Watanabe <i>et al.</i> (2011), Sueyoshi <i>et al.</i> (2013)

4.4.5 Soil data

As with the climate data, each DGVM requires different soil parameters to be specified (SI Table 4-D). Both IBIS and SDGVM simply require percentages of sand, silt and clay to be specified for each grid cell; these inputs are then used by internal look-up tables and pedo-transfer functions (PTFs) within the models to generate any additional soil parameters necessary. JULES, however, allows the user to explicitly specify many of the additional soil parameters as gridded input files, giving the opportunity to tailor the soil conditions for specific regions. Following recommendations from Marthews *et al.* (2014), we use PTFs from Hodnett and Tomasella (2002) specifically developed for tropical soils (Tomasella & Hodnett 2004) to create the gridded soil parameter files. Inputs to the PTFs (including the sand, silt and clay percentages required for IBIS and SDVM) were taken from the Global Soil Dataset (GSDE), a comprehensive gridded dataset derived from a methodology that incorporates data from a wide variety of regional, national and global sources (Shangguan *et al.* 2014).

4.4.6 Palaeo-data reconstructions

The palaeoecological vegetation reconstructions used in this study are a subset of the multi-proxy data synthesis of tropical South America from Smith and Mayle (2018), see Table 4.2. These vegetation reconstructions are based primarily on fossil-pollen assemblages, with complementary information derived from stable carbon isotopes, phytoliths and charcoal analyses. This dataset qualitatively assigns a vegetation classification to each palaeoecological record based on a critical evaluation of the original authors' interpretations of their proxy data. In some cases, a combination of two classifications was assigned, when it was deemed that the vegetation cover was a mixture of vegetation types. Additionally, this dataset considers the spatial scale of vegetation cover recorded at each site. For example, in palynology, it is widely accepted that basin area is roughly proportional to the spatial scale that the pollen assemblage from that basin represents, e.g. large (small) lakes collect pollen from regional (local) source areas (Sugita 1994; Sugita *et al.* 1999; Davis 2000; Sugita 2007a).

This is important to consider, as the relatively coarse grid-resolution of the model output (1.0° x 1.0°) will clearly be more comparable with reconstructions from larger basins. However, we do not dismiss the smaller-scale reconstructions as: (1) the already small number of sites across Amazonia would be reduced even further; (2) clusters of smaller sites can help us infer the degree of fine-grain heterogeneity/homogeneity in vegetation cover that cannot be captured by coarse-grain, regional reconstructions from larger basins; and (3) changes occurring at smaller sites may still reflect regional-scale climate change (e.g. Carson *et al.* 2014, Smith *et al.* 2018 (submitted)). The palaeoclimate records shown in Figure 4.1b were chosen for their ability to give qualitative estimates of the relative changes in precipitation between MH and present, which, like the palaeoecological records, were based on the original authors' interpretation of the data. These records provide direct evidence of MH precipitation changes, for example through the changes of stable oxygen isotope ($\delta^{18}\text{O}$) values in speleothems or lake-level reconstructions (see Table 4.3 for full list).

Table 4.2 - List of palaeoecological sites. ID refers to location number in Figure 4.1a. Size refers to basin size, an indication of the spatial scale each site's vegetation reconstruction represents: L=Large, M=Medium, S=Small, XS=Extra-small, see Smith and Mayle (2018) for more information.

ID	Site name	Size	Lon. (°E)	Lat. (°N)	Reference(s)
1	Lago Tapajós	L	-55.1	-2.79	Irion <i>et al.</i> (2006)
2	Coari Lake	L	-63.3	-4.06	Horbe <i>et al.</i> (2011)
3	Lago Rogaguado	L	-65.99	-13.0	Brugger <i>et al.</i> (2016)
4	Laguna Orícore	L	-63.53	-13.35	Carson <i>et al.</i> (2014)
5	Laguna Bella Vista	L	-61.55	-13.62	Mayle <i>et al.</i> (2000), Burbridge <i>et al.</i> (2004)
6	Laguna Chaplin	L	-61.08	-14.5	Mayle <i>et al.</i> (2000), Burbridge <i>et al.</i> (2004)
7	Laguna La Gaiba	L	-57.72	-17.76	Whitney <i>et al.</i> (2011)

ID	Site name	Size	Lon. (°E)	Lat. (°N)	Reference(s)
8	Prainha lake cluster: Lake Santa Maria / Lake Geral / Lake Saracuri / Lake Comprida	M	-53.7	-1.64	Bush <i>et al.</i> (2000; 2007b)
9	Lagoa do Caçó	M	-43.25	-2.96	Sifeddine <i>et al.</i> (2003), Pessenda <i>et al.</i> (2004; 2005), Ledru <i>et al.</i> (2006)
10	Lago Calado	M	-60.58	-3.27	Behling <i>et al.</i> (2001c)
11	Lake Sauce	M	-76.22	-6.71	Bush <i>et al.</i> (2016)
12	Lake Santa Rosa	M	-67.87	-14.48	Urrego <i>et al.</i> (2013)
13	El Paují	S	-61.58	4.47	Montoya <i>et al.</i> (2011a)
14	Lake Pata	S	-66.68	0.27	Colinvaux <i>et al.</i> (1996), Bush <i>et al.</i> (2004a)
15	Pantano de Monica	S	-72.07	-0.7	Behling <i>et al.</i> (1999)
16	Maxus 4	S	-76.03	-0.87	Weng <i>et al.</i> (2002)
17	Rio Curuá	S	-51.46	-1.74	Behling & da Costa (2000)
18	Lake Ayauchi	S	-78.03	-3.05	Liu & Colinvaux (1988), McMichael <i>et al.</i> (2012)
19	Lake Marabá	S	-49.15	-5.35	Guimarães <i>et al.</i> (2013a)
20	Carajás / Pântano da Maurítia / Lagoa da Cachoeira	S	-50.39	-6.36	Absy <i>et al.</i> (1991), Sifeddine <i>et al.</i> (1994; 2001) / Hermanowski <i>et al.</i> (2012a; 2012b)/ Hermanowski <i>et al.</i> (2014)
21	Humaitá HU01	S	-63.08	-7.92	Cohen <i>et al.</i> (2014a)
22	Lago do Saci	S	-56.27	-9.12	Fontes <i>et al.</i> (2017)
23	Lake Parker	S	-69.02	-12.14	Bush <i>et al.</i> (2007a; 2007b)

ID	Site name	Size	Lon. (°E)	Lat. (°N)	Reference(s)
24	Lake Gentry	S	-69.1	-12.18	Bush <i>et al.</i> (2007a; 2007b)
25	Laguna Granja	S	-63.71	-13.26	Carson <i>et al.</i> (2014)
26	Lago Consuelo	S	-68.98	-13.95	Bush <i>et al.</i> (2004b)
27	Lake Chalalán	S	-67.92	-14.43	Urrego <i>et al.</i> (2013)
28	Huanchaca	S	-60.73	-14.54	Maezumi <i>et al.</i> (2015)
29	Barreirinhas soil profile collection 1	XS	-43	-2.75	Pessenda <i>et al.</i> (2004)
30	Barreirinhas soil profile collection 2	XS	-43.09	-3.2	Pessenda <i>et al.</i> (2004)
31	Humaita soil profiles collection 1	XS	-63.3	-7.7	Pessenda <i>et al.</i> (2001), de Freitas <i>et al.</i> (2001)
32	Humaita soil profiles collection 2	XS	-63.8	-8.17	Pessenda <i>et al.</i> (2001), de Freitas <i>et al.</i> (2001)
33	Humaita soil profiles collection 3	XS	-63.97	-8.72	de Freitas <i>et al.</i> (2001)
34	Jaco Sá soil profiles	XS	-67.52	-9.92	Watling <i>et al.</i> (2017)
35	Ariquemes	XS	-62.82	-10.17	Pessenda <i>et al.</i> (1998)
36	Pimenta Bueno	XS	-61.2	-11.79	Pessenda <i>et al.</i> (1998)
37	Vilhena	XS	-60.12	-12.7	Pessenda <i>et al.</i> (1998)
38	Pontes e Lacerda	XS	-59.23	-15.27	Gouveia <i>et al.</i> (2002)
39	Laguna Sucuara	XS	-62.04	-16.83	Zech <i>et al.</i> (2009)

Table 4.3 - List of palaeoclimate sites. ID refers to location number in Figure 4.1b.

ID	Site name	Lon. (°E)	Lat. (°N)	Proxy type	Reference(s)
1	SO147- 106KL	-77.65	-12.05	Marine core erosion indicators (soil lithics)	Rein <i>et al.</i> (2005)
2	Cueva del Tigre / El Condor	-77.3	-5.94	Speleothem ($\delta^{18}\text{O}$ composition)	van Breukelen <i>et al.</i> (2008) / Cheng <i>et al.</i> (2013)
3	Shutuca Cave	-77.15	-5.12	Speleothem ($\delta^{18}\text{O}$ composition)	Bustamante <i>et al.</i> (2016)
4	Lake Junin / Huaguapo Cave	-75.9	-11.15	Lake calcite ($\delta^{18}\text{O}$ composition) / Speleothem ($\delta^{18}\text{O}$ composition)	Seltzer <i>et al.</i> (2000) / Kanner <i>et al.</i> (2013)
5	Lake Titicaca	-69.17	-16.17	Lake level reconstruction (chemical and isotopic composition)	Baker <i>et al.</i> (2001), Rowe <i>et al.</i> (2002)
6	Sajama	-68.88	-18.1	Ice core (dust and snow accumulation)	Thompson <i>et al.</i> (1998)
7	Laguna La Gaiba	-57.72	-17.76	Lake level reconstruction (<i>Pediastrum</i>)	Whitney <i>et al.</i> (2011) Whitney & Mayle (2012)
8	Botuverá Cave	-49.16	-27.22	Speleothem ($\delta^{18}\text{O}$ composition, geochemical analysis)	Cruz <i>et al.</i> (2005), Wang <i>et al.</i> (2007), Bernal <i>et al.</i> (2016)
9	Santana Cave	-48.73	-24.53	Speleothem ($\delta^{18}\text{O}$ composition)	Cruz <i>et al.</i> (2006a)

ID	Site name	Lon. (°E)	Lat. (°N)	Proxy type	Reference(s)
10	Lapa Grande	-44.37	-14.42	Speleothem ($\delta^{18}\text{O}$ composition)	Strikis <i>et al.</i> (2011)
11	Lake Valencia	-67.75	10.17	Geochemistry and isotopic analysis	Bradbury <i>et al.</i> (1981), Curtis <i>et al.</i> (1999)
12	Cariaco Basin	-65.16	10.72	Marine core (Titanium and iron concentrations)	Haug <i>et al.</i> (2001)
13	Paraíso Cave	-55.45	-4.07	Speleothem ($\delta^{18}\text{O}$ composition)	Wang <i>et al.</i> (2017)
14	Rio Grande do Norte	-37.73	-5.6	Speleothem ($\delta^{18}\text{O}$ composition)	Cruz <i>et al.</i> (2009)

4.4.7 Classification method

The palaeo-data that we use for comparison with the MH model outputs are given as qualitative classifications (see Smith and Mayle (2018) for justification), whereas the model outputs are continuous quantitative data. Therefore, qualitative classification of the model output is necessary in order to facilitate direct comparisons between the simulations and observations. A simple approach would be to use the most dominant PFT (in terms of percentage cover) in a grid cell as the classification, but this may not be suitable in this study for several reasons, including: (1) the different DGVMs differ in their representation of PFT coverage making inter-model comparisons difficult, for example JULES typically simulates much more of a mixture of PFTs, whereas IBIS generally simulates a single PFT that dominates a grid cell (e.g. see Figure 2c); (2) in some cases the dominant PFT may be only marginally dominant over other PFTs and may not reflect the actual overall biome, especially in ecotonal areas where a mixture of vegetation types may occur; (3) all the DGVMs perform poorly in differentiating between tree cover and grass cover in savannah ecosystems such as the Cerrado biome (Fig. 4.2), a difficult area to model as important, yet relatively poorly understood, controls on tree density here include edaphic factors and fire frequency (Murphy & Bowman 2012; Baudena *et al.* 2015; Langan *et al.* 2017). Instead, we use a statistical approach to classification, allowing us to utilise a variety of model output variables that, in combination, may provide a more accurate estimation of the overall biome of a given grid cell.

A linear discriminant analysis (LDA) approach was chosen, a popular method in machine-learning classification problems and modern ecological classification using physical attributes of vegetation (e.g. Cutler *et al.* 2007; Gond *et al.* 2011; Zizka *et al.* 2014). LDA is a supervised dimensionality reduction technique which searches for the linear combination of features (i.e. model output variables) that best discriminate between multiple classes (i.e. vegetation classification). In practice, this means that, for each DGVM, an LDA algorithm is trained using a set of the output variables from the modern control simulations and the vegetation classifications based on those shown in Fig. 4.1a. This allows the algorithm to 'learn' what combination of the simulated output variables would be expected for each vegetation class. Then, for a given DGVM, the LDA can be fed with the MH simulated output variables for each grid cell, which allows the algorithm to predict which vegetation class the grid cell most likely belongs to. For this study, the model output variables used in each LDA include: the fraction of three PFTs (evergreen broadleaf, deciduous broadleaf, C4 grass), vegetation biomass, soil carbon, soil moisture content, leaf area index (LAI) and net primary productivity (NPP). To simplify the classification problem, we only considered three vegetation classes: humid evergreen tropical forests (HETF), semi-deciduous tropical dry forest (SDTF), and savannah (SAV).

4.5 Results

4.5.1 Modern vegetation simulations

The results of each DGVM PI control simulation, driven with modern observational climate data, are shown in Figure 4.2 as PFT percentage covers of evergreen broadleaf (EvBL), deciduous broadleaf (DecBL) and C4 grass (C4). We compare these to the modern potential ecoregions (Fig. 4.2a,e,i) rather than satellite observational data as much of the Brazilian Cerrado, eastern Amazonia and the dry forest regions have undergone extensive anthropogenic land use in the last few decades (Soares-Filho *et al.* 2006; Malhi *et al.* 2008), which was not included in these simulations.

All DGVMs reproduce the core of the Amazonian humid evergreen forest reasonably well. Both JULES and SDGVM show denser EvBL cover in the central and western parts than other parts of Amazonia (Fig. 4.2b,d), whereas IBIS shows less spatial variation, essentially simulating 100% EvBL cover across the entire region (Fig. 4.2c). In southern Amazonia, JULES captures the southern Amazonian ecotone in north-east Bolivia reasonably well,

including peaks in DecBL where the Chiquitano dry forest (eastern Bolivia) is located (Fig. 4.2e,f). SDGVM also shows a slight decrease in EvBL (and corresponding increase in DecBL) in this region, though not as pronounced as with JULES (Fig. 4.2d,h). Conversely, IBIS simulates extensive EvBL in north-east Bolivia, with no indication of a mix with semi-deciduous forest (Fig. 4.2c). In eastern Amazonia, IBIS reproduces the location of the eastern ecotone of the Amazonian HETF reasonably well (Fig. 4.2c), although simulates a transition to DecBL rather than the expected C4 grass of the cerrado savannah biome. Similar results are seen in SDGVM, though the ecotone boundary is slightly further east than in IBIS (Fig. 4.2d). JULES simulates EvBL well into the cerrado savannah (Fig. 4.2b). In general, all models have difficulty reproducing the C4 grass dominated landscape of the cerrado savannah, probably due to the complex mix of edaphic and fire-related processes that influence vegetation cover here and which are not well represented in the DGVMs (Castanho *et al.* 2013; Marthews *et al.* 2014; Baudena *et al.* 2015).

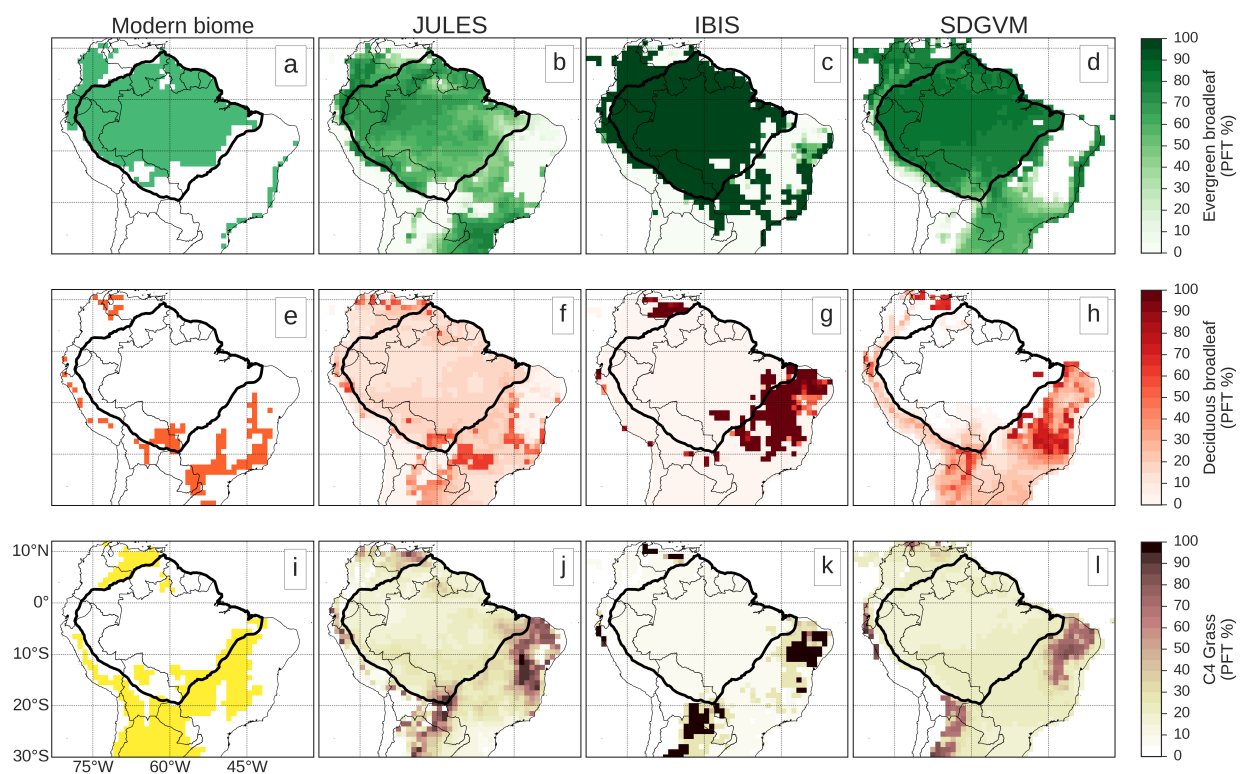


Figure 4.2 - Modern distribution of potential broad ecoregions for (a) humid evergreen tropical forest, (e) Semi-deciduous dry forest and (i) savannah/grassland (as in Figure 4.1), alongside simulated PFT distributions of evergreen broadleaf trees (b-d), deciduous broadleaf trees (f-h) and C4 grass (j-l) from the modern control runs of each vegetation model; JULES (b, f, j), IBIS (c, g, k) and SDGVM (d, h, l).

4.5.2 MH climate anomalies

Overall, the DGVMs simulate the extent of Amazonia EvBL reasonably well when forced with the same observational modern climate data. In order to assess their efficacy at simulating MH vegetation, we first examine inter-model variation in simulated MH climate. Figure 4.3 shows the annual precipitation anomalies between MH and present for each climate model. With the exception of CSIRO-Mk3-6-0 (Fig. 4.3h), all models simulate an overall negative anomaly averaged for the whole of Amazonia. However, the spatial distribution of the direction and magnitude of changes varies quite considerably between the models. GISS-E2-R, HadGEM2-CC and FGOALS-s2 all simulate a drier MH across most of Amazonia. However, GISS-E2-R has much stronger drying in the north (Fig. 4.3b); HadGEM2-CC has small areas of increased MH precipitation in central Amazonia, but with negative anomalies to the north and south (Fig. 4.3c); FGOALS-s2 has fairly consistent but weak drying across the whole region (Fig. 4.3d). CNRM-CM5 simulates most drying in the east and south, with little change in the west of Amazonia (Fig. 4.3e). MIROC-ESM has weak negative anomalies across much of Amazonia, but with increases in MH precipitation along the northeast coastline (Fig. 4.3f). IPSL-CM5A-LR (Fig. 4.3g) has a north-to-south split in the anomalies, with a wetter north and a drier south; however, these anomalies are relatively small. Finally, CSIRO-Mk3-6-0 is the model with the most widespread positive anomalies, particularly in the north and east (Fig. 4.3h).

To explore the changes to the seasonality of simulated MH precipitation, Figure 4.4 presents the annual precipitation cycle anomalies of each climate model for four key areas of Amazonia. In northern Amazonia, most of the climate models simulate a precipitation decrease during the late wet season and into the early dry season (July–October), but a slight increase during the late dry season and into the early wet season (January–April) (Fig. 4.4a). The exceptions are GISS-E2-R and CSIRO-Mk3-6-0, which simulate decreases/increases throughout the year, respectively. In central Amazonia, most climate models simulate precipitation decreases during the wet season (February–May) and increases during the dry season (July–September), thus slightly reducing the seasonality of precipitation in this area (Fig. 4.4b). CNRM-CM5 is an exception, showing the opposite trend (wetter wet season, drier dry season). In eastern Amazonia, most climate models simulate precipitation decreases through the wet season (December–March), with the exception of CSIRO-Mk3-6-0 (Fig. 4.4c). Changes are negligible during the early dry season, then during the late dry season (August–October) there is a general agreement of a decrease in precipitation. Finally, southern Amazonia shows similar patterns to eastern Amazonia, with all climate models simulating a

drier wet season (December–March) and only small changes during the early dry season (Fig. 4.4d). However, there is disagreement amongst models during the late dry season with a roughly equal split in models simulating an increase/decrease in precipitation from August–October.

Unfortunately, there is a lack of independent palaeoclimate data across the Amazonian lowlands, with the majority of speleothem and lake level records coming from the Andean mountain range or southern/eastern Brazil (Fig. 4.1b). Additionally, it is difficult to make quantitative estimates of precipitation changes from the available palaeoclimate records. These factors make it difficult to fully benchmark the simulated MH precipitation across Amazonia from the different climate models. Nevertheless, some important qualitative comparisons can be made and will be discussed in the relevant sections of the discussion section below.

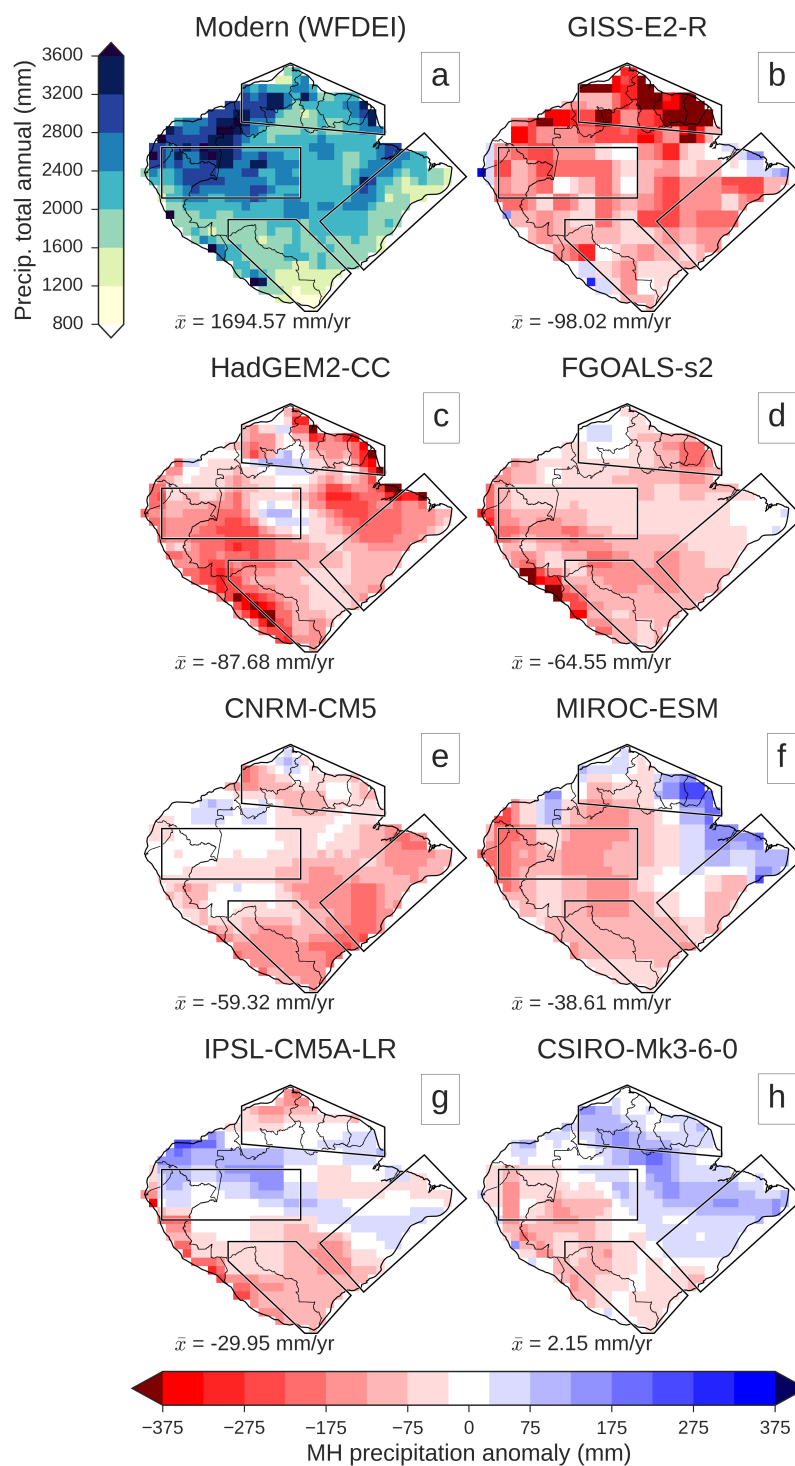


Figure 4.3 - Mid-Holocene annual mean precipitation anomalies (mm/yr) from the CMIP5/PMIP3 climate models used in this study. Blue (red) corresponds to a wetter (drier) mid-Holocene compared to present day. Panel (a) presents the average annual precipitation from the WFDEI dataset to help put the changes in (b) - (h) into context. The value of \bar{x} is the regional spatial mean. Polygons outline main areas of Amazonia, defined in Fig. 4.1a.

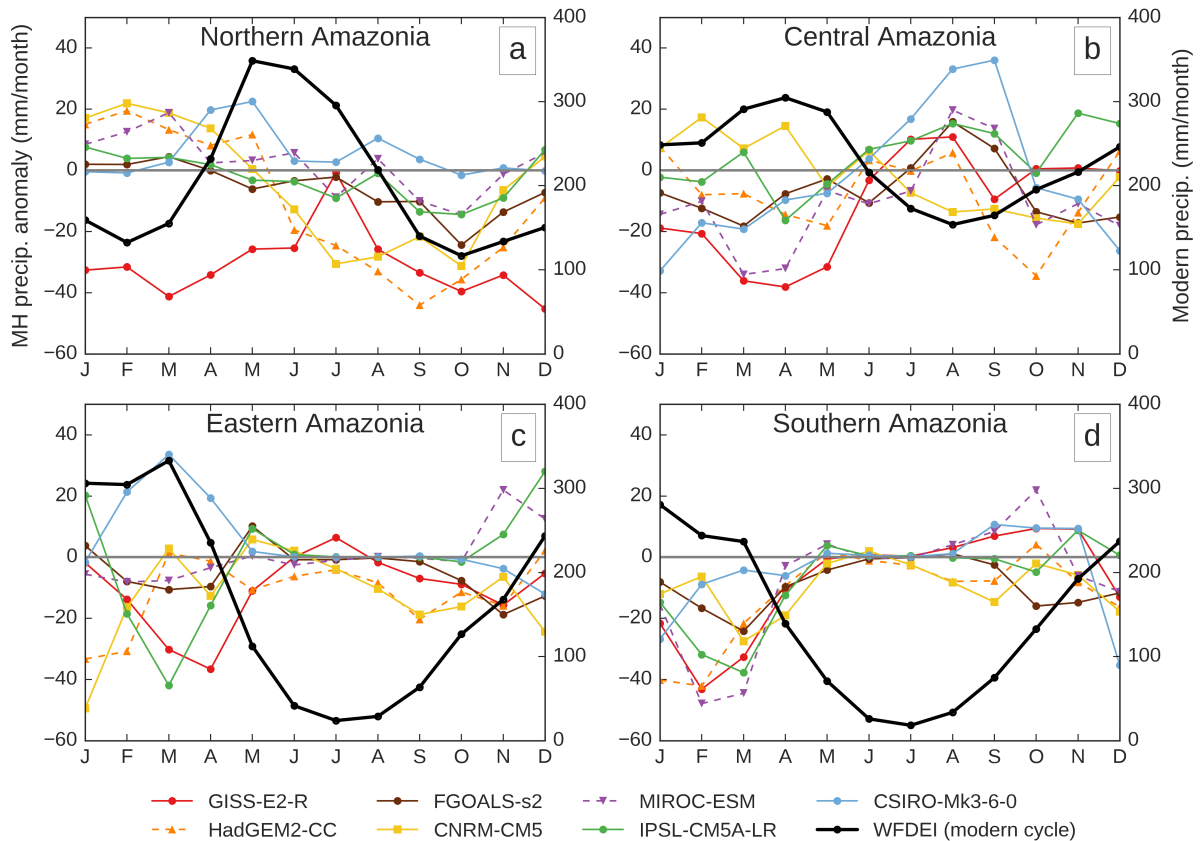


Figure 4.4 - Average annual cycle of MH precipitation anomalies (left hand y-axis) for each PMIP3 climate model used in this study for the four areas of Amazonia: (a) northern, (b) central, (c) eastern, and (d) southern (as defined in Fig. 4.1a). The black dotted line with open circles presents the average WFDEI modern precipitation annual cycle to help put the changes into context (right hand y-axis).

4.5.3 Simulated MH PFT anomalies

For each area of Amazonia, the average MH vs. control anomalies for the EvBL, DecBL and C4 grass PFTs are shown in Figure 4.5, in relation to the anomalies in annual precipitation. In the areas of northern, eastern and southern Amazonia, similar overall trends are shown with respect to the PFTs' changes versus precipitation change. Generally, EvBL anomalies exhibit a positive correlation with precipitation anomalies (i.e. precipitation decrease associated with EvBL decrease), whereas both DecBL and C4 anomalies exhibit a negative correlation with precipitation anomalies (i.e. precipitation decrease associated with increase in DecBL/C4). In central Amazonia, there is very little change in any of the PFTs to any amount of precipitation change in all three DGVMs (Fig. 4.5d-f). Despite the overall trends being similar in northern,

eastern and southern Amazonia, some key differences between the regions and/or DGVMs are evident.

Northern Amazonia

In northern Amazonia (Fig. 4.5a-c), SDGVM simulates very little change to any of the PFTs under any of the climate regimes from the different climate models. The extreme dry climate of GISS-E2-R does appear to elicit a decrease in EvBL and increases in DecBL and C4 in SDGVM, though not at the same magnitude as the other DGVMs. JULES and IBIS appear much closer in terms of their positive correlation between changes in EvBL and precipitation (and likewise positive correlation for DecBL/C4).

Eastern Amazonia

In eastern Amazonia (Fig. 4.5g-i), the three driest climate models, (HadGEM2-CC, CNRM-CM5 and GISS-E2-R) are associated with large decreases in EvBL (and increased DecBL) in IBIS. However, this is predominantly due to IBIS not simulating the coexistence of these PFTs very well (Fig. 4.2c,g), e.g. if a grid cell simulates decreases in EvBL, it will be a ~100% PFT shift, thus skewing the overall regional mean. Nevertheless, these climate models also elicit the largest decrease in EvBL in JULES and SDGVM, giving us confidence that this region is sensitive to precipitation decrease. For IBIS and SDGVM, the changes in EvBL (increases or decreases) are mirrored predominantly with changes in DecBL, whereas in JULES it is C4 grass that mirrors EvBL changes with very little change in DecBL.

Southern Amazonia

In southern Amazonia (Fig. 4.5j-l), all three DGVMs simulate similar decreases in EvBL in response to the driest three climate models (HadGEM2-CC, CNRM-CM5 and FGOALS-s2). There is a more mixed response across the DGVMs to the climates of IPSL-CM5A-LR, GISS-E2-R and MIROC-ESM, with decrease in EvBL cover ranging from 0-5%, despite these climate models having similar precipitation anomalies (Fig. 4.5j). As with eastern Amazonia, IBIS and SDGVM mirror the changes in EvBL with DecBL, whereas JULES shows little change in DecBL across all climate models. However, unlike eastern Amazonia, IBIS and SDGVM simulate a similar response in C4 grass as DecBL, i.e. increased C4 grass with decreased EvBL. The C4 grass response in JULES is interesting, a mix of increases and decreases across climate models with similar precipitation anomalies (e.g. IPSL-CM5A-LR, GISS-E2-R

and MIROC-ESM). Overall, the simulations in southern Amazonia appear a little noisier, perhaps attesting to the more heterogeneous nature of ecosystems in this area (Fig. 4.1a).

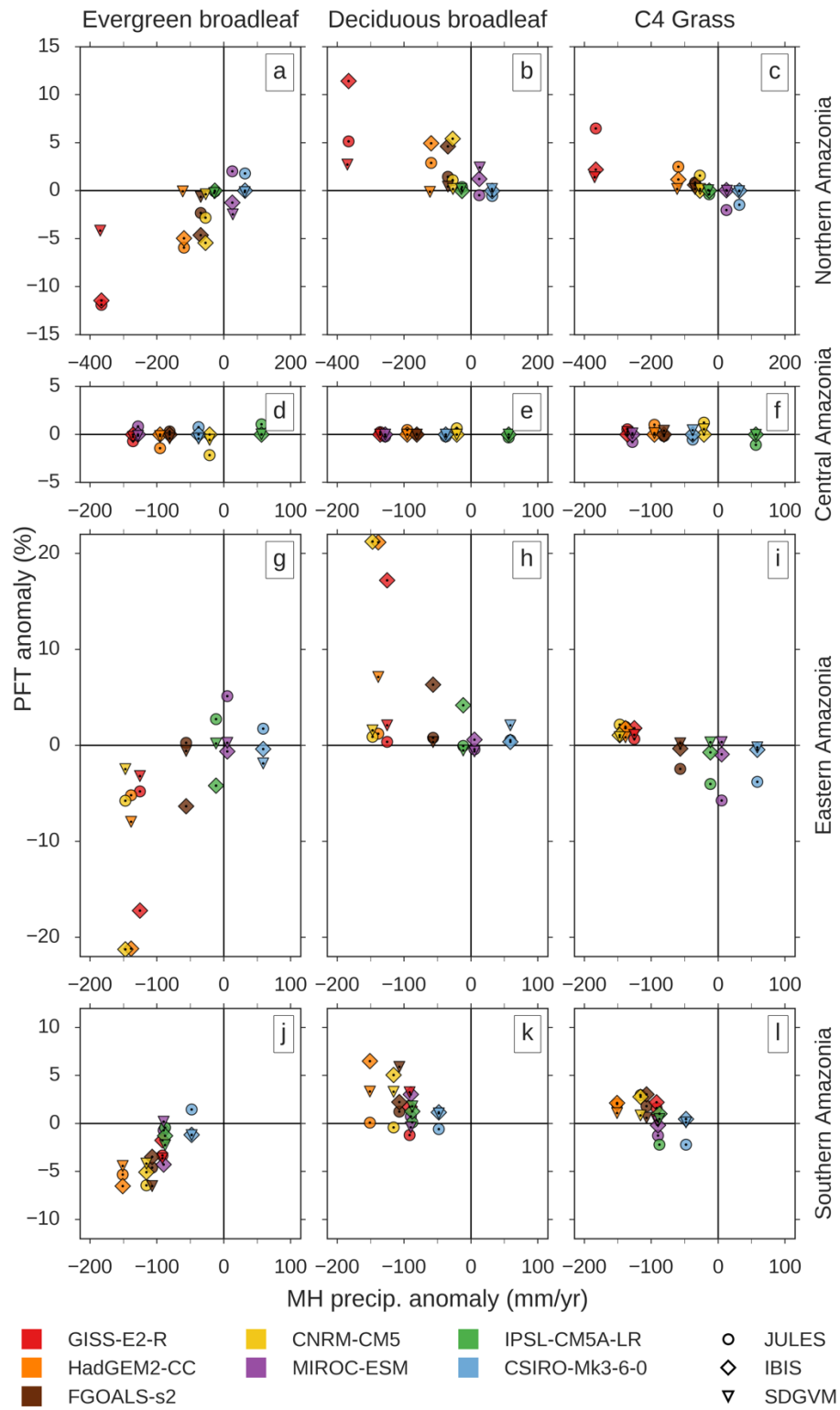


Figure 4.5 - (Caption overlaid)

Figure 4.5 - MH anomalies of the fractions for PFTs: evergreen broadleaf (a, d, g, j), Deciduous Broadleaf (b, e, h, k) and C4 grass (c, f, i, l), plotted against annual precipitation anomaly for each given climate model. Averaged for the four areas of Amazonia: northern (a-c), central (d-f), eastern (g-i) and southern (j-l) (as defined in Fig. 4.1a).

4.5.4 LDA Classification maps and comparison with palaeoecological reconstructions

Figure 4.6 presents the result of the MH LDA biome classifications for each model combination, allowing us to directly compare the MH vegetation simulations with the palaeoecological observations for Amazonia. Perhaps unsurprisingly, given the negligible PFT anomalies presented in Figure 4.5 for central Amazonia, most of the biome changes occur in northern, eastern and southern Amazonia.

Central Amazonia

Central Amazonia remains classified as HETF in all model combinations (0% of grid cells change to a MH savannah classification, Fig. 4.7b), despite the range of precipitation changes between the climate models (Fig. 4.3, Fig. 4.4b). The resilience of the central Amazonian HETF is a feature corroborated by the palaeo-data from this region (Fig. 4.6; e.g. Colinvaux *et al.* 1996; Bush *et al.* 2000; Irion *et al.* 2006; Bush *et al.* 2007a; Horbe *et al.* 2011).

Northern Amazonia

In northern Amazonia, extensive changes in biome classifications are seen in the simulations using the GISS-E2-R (Fig. 4.6d-f); across all three DGVMs, ~20-25% more of the total grid cells in this region are classified as SAV in the MH (Fig. 4.7a). Biome changes in simulations using the other climate models are much less substantial, with only a few grid cells switching classifications between MH and modern control, apparently without a strong relationship with the magnitude or direction of precipitation changes (Fig. 4.7a). Interestingly, SDGVM is the only vegetation model whose classification changes include grid cells switching to SDTF (e.g. under climates of FGOALS-s2, MIROC-ESM and CSIRO-Mk3-6-0; figs. 6l, 6r, 6x, respectively). Unfortunately, there is a lack of suitable palaeo-data records in this region for evaluation of these vegetation scenarios. Most records do not extend back to the MH (e.g. Charles-Dominique *et al.* 1998; Ledru 2001; Montoya *et al.* 2011b), some are located on isolated plateaus which reflect locally anomalous vegetation (e.g. Rull 2004; 2005), and some

areas have potentially been influenced by human activity since the early Holocene (Rull *et al.* 2015).

Eastern Amazonia

In eastern Amazonia, the available palaeoecological records show that there was some degree of MH savannah expansion in ecotonal areas, for example on the Serra Sul dos Carajás plateau (Table 4.2, id=20; Absy *et al.* 1991; Sifeddine *et al.* 2001; Hermanowski *et al.* 2012a; 2012b), at Lake Marabá (Table 4.2, id=19; Guimarães *et al.* 2013a), and at Lago do Saci (Table 4.2, id=22; Fontes *et al.* 2017). However, the spatial extent of these savannah expansions is unclear from the palaeo-records, as these sites only have local scale catchments, and in some cases (e.g. Carajás) likely reflect ecotonal shifts atop inselbergs which may be unrepresentative of the surrounding lowlands below. Nevertheless, they provide a rough guide as to where we would expect biome changes in the MH vegetation simulations.

In the JULES simulations, there is consistent savannah expansion along the eastern Amazonian ecotone in most of the climate models, despite their differences in precipitation anomalies. There is between a ~10-20% increase in the total grid cells classified as SAV in this region (Fig. 7c). Spatially, this savannah expansion appears to match well with the palaeo-records in the north-east of the area, with grid cells to the east of Carajás/Marabá consistently switching to SAV. However, in the south-west of the area, the JULES savannah expansion does not reach Lago do Saci in any of the simulations. In the IBIS simulations, there is greater variation in biome classification changes between the climate models. The climate models with a drier MH all show savannah expansion in eastern Amazonia (~5-20%; Fig. 4.7c), but the spatial distribution of this expansion varies. Under the two driest climate models, HadGEM2-CC and CNRM-CM5, grid cells switching to savannah are located all along the ecotone (Fig. 4.6h, n), both in the north-east near Carajás/Marabá, and in the south-west, almost reaching Lago do Saci. Under GISS-E2-R and FGOALS-s2 (the next two driest climates), the savannah expansions are predominantly clustered in the south-west of eastern Amazonia (Fig. 4.6e, k), in the grid cells surrounding Lago do Saci. In the SDGVM simulations, between ~10-20% grid cells change to savannah in the three driest climate models HadGEM2-CC, CNRM-CM5 and GISS-E2-R (Fig. 4.7c). These changes occur predominantly in the north-east of the area near the Carajás/Marabá palaeo-records. Further into the Amazon basin in north-east Amazonia, under the HadGEM2-CC and CNRM-CM5 climates, SDGVM shows large patches of savannah centred at ~2°0'S, 54°0'W (Fig. 4.6i, o). This does not match with the palaeo-records here, e.g. Lago Tapajós (Table 4.2, id=1; Irion *et al.* 2006) and the group

of Prainha lakes (Table 4.2, id=8; Bush *et al.* 2000; 2007b), which show persistence of the HETF biome during the MH (e.g. Irion *et al.* 2006; Bush *et al.* 2007b). In the south of the area, like in JULES, savannah expansion in the SDGVM simulations do not reach Lago do Saci in any of the simulations.

With IBIS and SDGVM, simulations using the climate models that show a zero or positive MH precipitation anomaly for eastern Amazonia (IPSL-CM5A-LR, MIROC-ESM, CSIRO-Mk-3-6-0) generally show an increase in HETF grid cells, particularly in the north of the area. This is clearly at odds with the Carajás/Marabá paleo-records, which show savannah expansion.

Southern Amazonia

There is strong evidence from the palaeoecological data that southern Amazonia experienced significant vegetation changes during the MH, compared to present. In north-eastern Bolivia, records from large lakes - Laguna Chaplin (Table 4.2, id=6) and Bella Vista (Table 4.2, id=5) - provide evidence that the southern Amazonian HETF ecotone was at least 130km further north than present (Mayle *et al.* 2000; Burbridge *et al.* 2004). To the north-west of these records, the large lake of Laguna Orícore (Table 4.2, id=4) corroborates these findings (Carson *et al.* 2014). In the north/north-west of this southern Amazonia area, the extent of northward expansion of the ecotone is somewhat constrained by results from the soil pit profiles of Jaco Sa (Table 4.2, id=34; Watling *et al.* 2017) which show persistence of rainforest during the MH.

In the JULES simulations, all climate model runs show some degree of savannah expansion in this area, with between 15-30% of grid cells switching to savannah (Fig. 4.7d). The extent of this expansion appears to be roughly related to the degree of drying in the climate models, the drier climate models having more grid cells switching to savannah. The spatial distribution of savannah expansion in JULES appears well constrained by the palaeo-records, with most climate models showing increased savannah classifications through north-east Bolivia up to Laguna Orícore. Some isolated grid cells switch to savannah further north (e.g. in HadGEM2-CC, FGOALS-s2, MIROC-ESM; Fig. 4.6g, j, p), but never as far as, for example, the Jaco Sa palaeo-records from eastern Acre. Results from the IBIS simulations are more varied than those from JULES. The drier climate models of HadGEM2-CC and FGOALS-s2 produce savannah expansion at a similar level to JULES (~20-30% grid cells switch), though the second driest climate model in this area, CNRM-CM5, appears to be a slight outlier, with only ~12% of grid cells switching to savannah (Fig. 4.7d). The remaining climate models show

<10% savannah expansion in this area, even though they all simulate a drier MH climate. IPSL-CM5A-LR and CSIRO-Mk3-6-0 even have a few grid cells that switch to HETF in north-east Bolivia near the paleo-record of Laguna Chaplin. In the SDGVM simulations, results from the driest three climate models (HadGEM2-CC, CNRM-CM5 and FGOALS-s2) match closely with those of JULES, both in terms of magnitude of grid cell changes (~25-30%; Fig. 4.7d) and the spatial distribution of these changes. Conversely, the remaining climate models show more agreement with the IBIS simulations, with much less savannah expansion across the area. These results suggest that JULES is more sensitive than IBIS and SDGVM to any amount of precipitation decrease in southern Amazonia, whereas in IBIS and SDGVM, there appears to be a threshold of ~100 mm decrease in annual precipitation needed to initiate the level of savannah expansion shown by the palaeo-records.

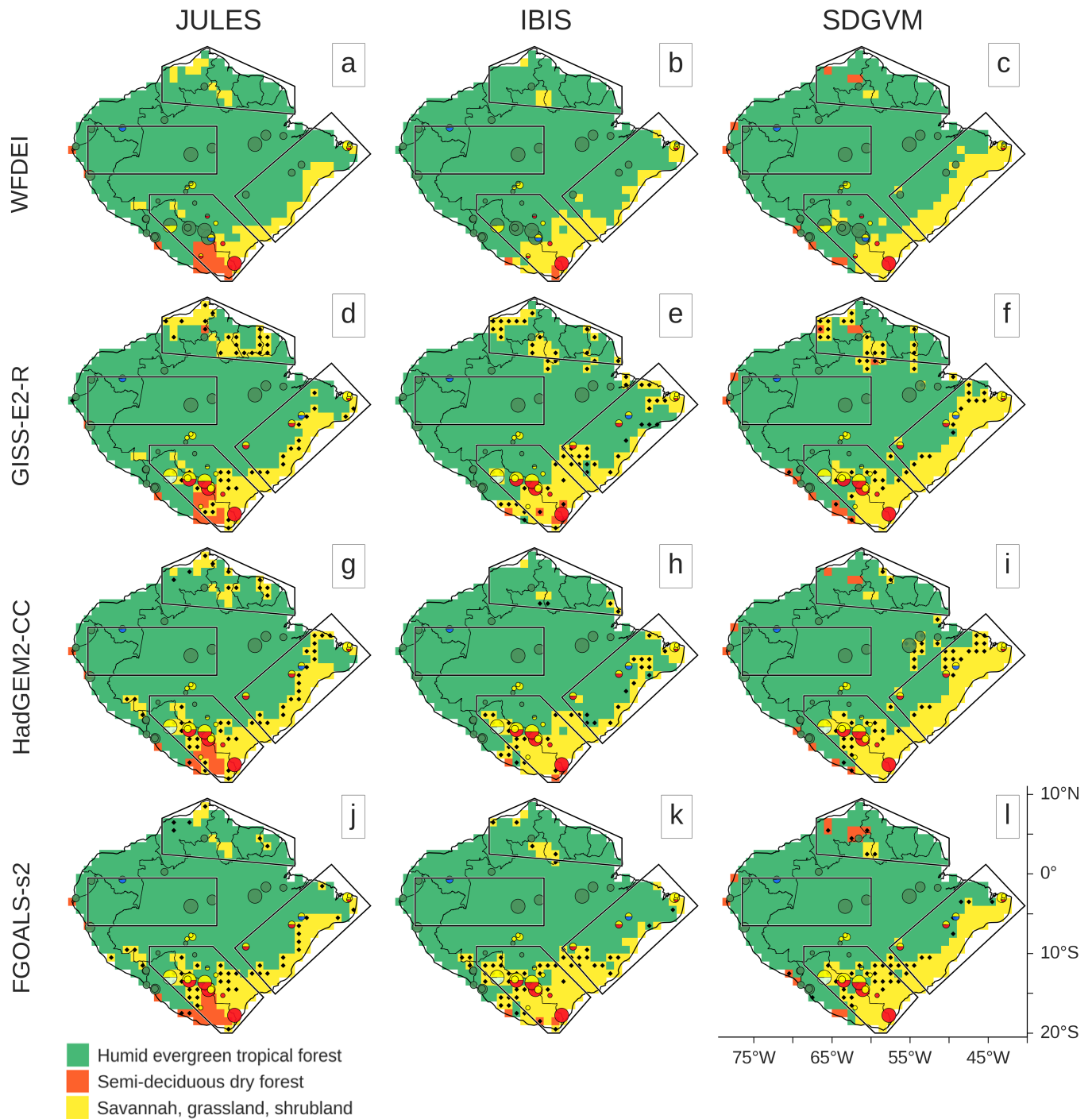


Figure 4.6 - Results of the LDA vegetation classification, overlaid with palaeoecological data reconstructions. (a-c) Modern control simulations. (d-x) MH simulations, where black dots represent grid cells where the LDA vegetation classification is different between MH and modern control. Polygons outline main areas of Amazonia, defined in Fig. 4.1a.

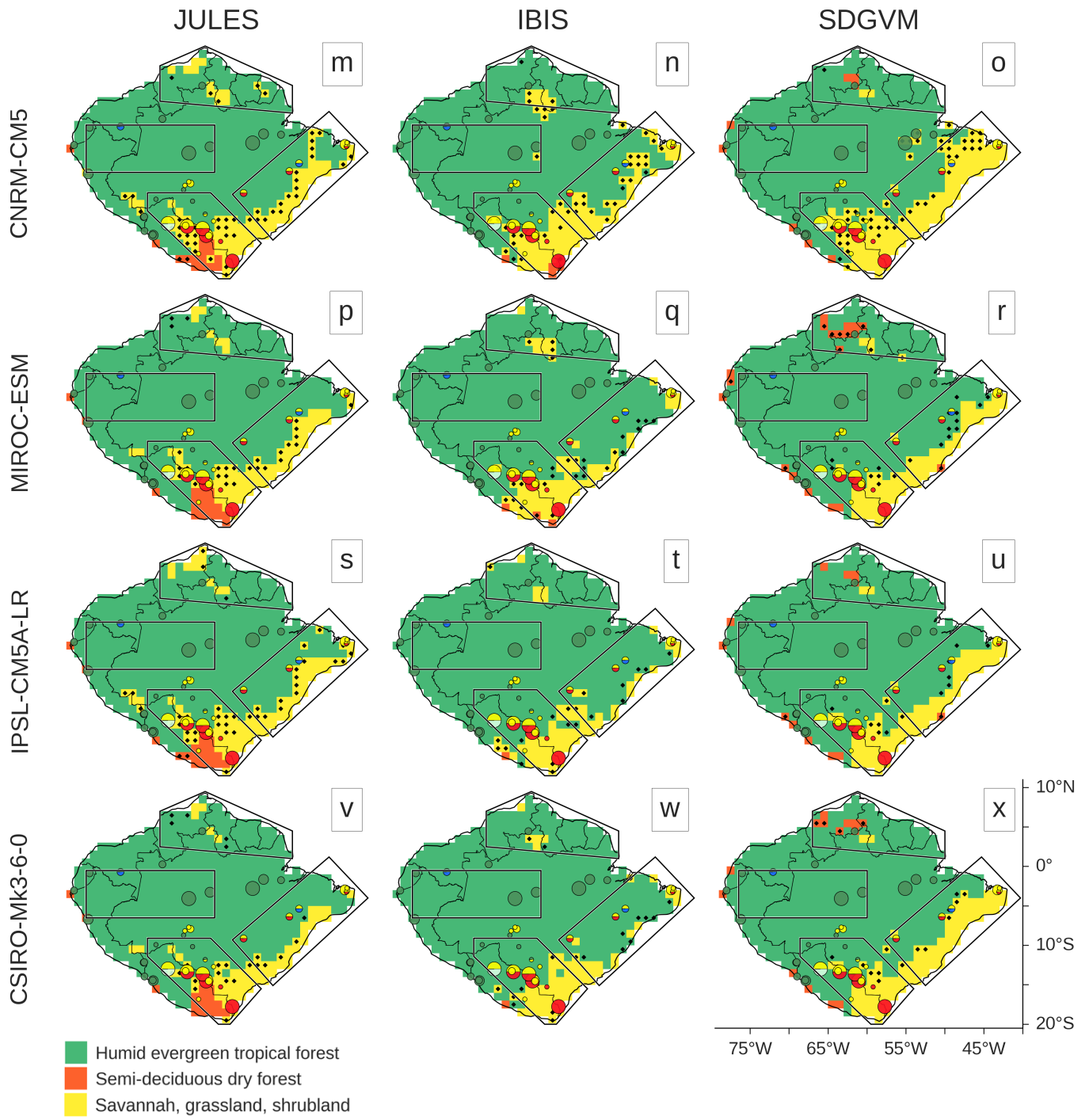


Figure 4.6 - (Continued)

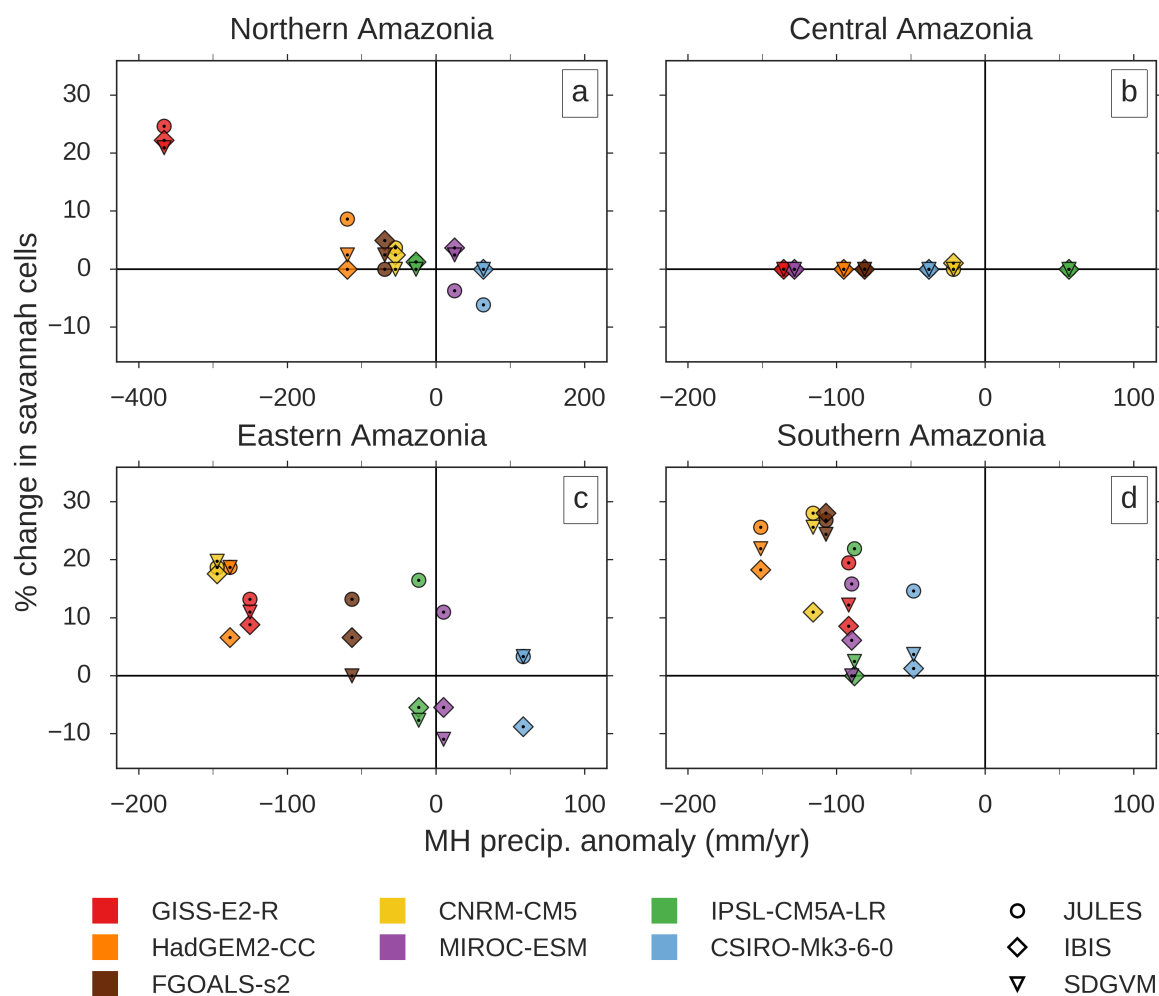


Figure 4.7 - Percentage change in the proportion of savannah cells (based on the LDA classification) relative to total cells between MH and modern control for each of the areas of Amazonia: (a) northern, (b) central, (c) eastern, and (d) southern (as defined in Fig. 4.1a).

4.6 Discussion

4.6.1 Assessment of the overall resilience of Amazonian HETF to MH precipitation changes

Central Amazonia

The central and western areas of Amazonia are presently some of the wettest parts of tropical South America (> ~2,500-3,000 mm/yr; Fig. 4.1b), with relatively consistent levels of precipitation throughout the year (Fig. 4.4b). MH speleothem records from the Peruvian Amazon (i.e. Cueva del Tigre/El Condor – Table 4.3, id=2, Shutuca Cave – Table 4.3, id=3) provide evidence that western Amazonia was moderately drier than present, though magnitude is difficult to quantify with these records alone. Generally, all climate models show some degree of MH drying in this region, but in no climate model's MH simulation does annual precipitation decrease by >300 mm in any central Amazonian grid cell (Fig. 4.3), with the average annual anomaly across the whole central Amazonian area ranging from +55 mm/yr (IPSL-CM5A-LR) to -140 mm/yr (GISS-E2-R). Therefore, given that HETF is supported in climates > ~1,600 mm/yr (Malhi & Wright 2004), we would not expect there to be any biome-scale turnover in this area based on precipitation changes alone. It is reassuring then, that our simulations show that, on a biome-scale, the core of the Amazonian humid evergreen rainforest was resilient to any scenario of MH climate change. All three DGVMs simulate negligible changes in PFT cover in central Amazonia when forced with any of the climate models (Fig. 4.5), and no biome changes are subsequently found in the LDA classifications of model outputs (Fig. 4.6, Fig. 4.7b). These simulations agree with the available palaeoecological records from this region, which show persistence of rainforest vegetation through the mid- to late Holocene (Smith & Mayle 2018). However, we note that these palaeo-records are relatively sparse in this area and, particularly in the west of this region, are predominantly from small basins (e.g. Bush & Colinvaux 1988; Behling *et al.* 1999; Bush *et al.* 2004a) that only give local-scale vegetation reconstructions. Our simulations therefore provide additional evidence that the HETF biome was resilient across the whole of central Amazonia, not just at local-scales around the small palaeoecological sites.

Northern Amazonia

In northern Amazonia, only the DGVM simulations forced with the GISS-E2-R climate predict large-scale savannah expansion (Fig. 4.6d-f). The northern Amazonian MH precipitation simulation from GISS-E2-R is a notable outlier compared with the other climate models, simulating a substantially drier MH climate across the whole area (~375 mm/yr decrease on

average). Although there are no palaeo-precipitation records from directly within this area, evidence from other palaeo-precipitation records in the northern hemisphere of tropical South America (i.e. Lake Valencia – Table 4.3, id=11, Cariaco Basin – Table 4.3, id=12) suggest this level of MH drying is unlikely. Therefore, only considering DGVM simulations forced using the other climate models, the results show overall HETF stability in this area. Some small differences are noted between these simulations, with a range of between -8 to +5% change in the number of savannah grid cells (Fig. 4.7a). These changes do not appear to be consistent between the three DGVMs even when using the same climate model (suggesting uncertainty between the DGVMs), or to have a strong relationship with the levels of precipitation changes between the climate models. Spatially, these differences occur mainly around the Gran Sabana/Roraima savannah in northern Brazil, a notoriously difficult area to understand the palaeoecological history of, given the complexity of human, edaphic, fire and climatic factors that influence the vegetation (Montoya & Rull 2011; Montoya *et al.* 2011a; Rull *et al.* 2015). Therefore, the differences in the models are likely a result of the difficulty in the DGVMs modelling this area of savannah, and/or the difficulty in the LDA algorithm to classify these grid cells.

Eastern Amazonia

In contrast to central and northern Amazonia, there is more uncertainty regarding the MH resilience of HETF in eastern Amazonia, with a range between the different model simulations in the direction, magnitude and spatial extent of any biome changes. The simulated changes in savannah extent do appear to be, at least in part, related to the different precipitation regimes in the different climate models; drier climates tend to cause more savannah expansion in all three DGVMs (Fig. 4.7c). This finding is pertinent, given the debate in the palaeo-community surrounding the MH precipitation history of eastern Amazonia. The savannah and dry forest expansion at the palaeoecological sites on the Carajás plateau (Table 4.2, id=20) and at Lago do Saci (Table 4.2, id=22) suggest drier MH conditions in eastern Amazonia, fitting with the theory of a reduction in the strength of the SASM due to a decrease in summer insolation (Absy *et al.* 1991; Sifeddine *et al.* 2001; Hermanowski *et al.* 2012a; 2012b; Fontes *et al.* 2017). The recent speleothem record from Paraíso Cave (Table 4.2, id=13) contrasts with these interpretations, instead suggesting negative $\delta^{18}\text{O}$ values suggest evidence of a wetter-than-present MH in the eastern Amazonia region (Cheng *et al.* 2013; Wang *et al.* 2017). Even though this site is not within our defined area of eastern Amazonia, it may be assumed that the precipitation record captured in the speleothem is representative of at least the northern part our defined area, given that the climate around the Paraíso Cave

is influenced predominantly by easterly winds originating from the tropical Atlantic (Wang *et al.* 2017).

Using climate models with a wetter eastern Amazonia, analogous to the Paraíso Cave interpretations, our DGVM simulations generally show HETF expansion along the eastern Amazonian ecotone. Given the palaeoecological evidence of savannah expansion, we suggest that these simulation results are unlikely and that the Paraíso Cave record may not be representative of the eastern Amazonian ecotone. Fontes *et al.* (2017) explore some potential mechanisms that explain the Paraíso Cave mis-match, such as decreased extent of Amazonian rainforest influencing the atmospheric $\delta^{18}\text{O}$ through a reduction in moisture recycling via evapotranspiration, and/or increased precipitation in north-east Brazil (e.g. Rio Grande do Norte, Fig. 4.1b, id=14; Cheng *et al.* 2013) propagating a negative $\delta^{18}\text{O}$ anomaly westward into eastern Amazonia. Nevertheless, given the paucity of palaeo-records and the uncertainty between the model simulations, it is difficult to definitively rule out any scenarios of MH precipitation/vegetation changes in eastern Amazonia; more palaeoecological and palaeoclimate records along the eastern Amazonian ecotone and into the rainforest of eastern Amazonia are going to be vital in increasing our understanding.

Southern Amazonia

The area of Southern Amazonia is where there is strongest agreement between model simulations and palaeo-data for the vulnerability of the Amazonian HETF. This area is one of the most climatically sensitive in Amazonia, with annual precipitation between ~1500-2000 mm/yr (Fig. 4.1b) and a long (5-7 month) dry season (Fig. 4.4d). This precipitation regime is on the limit of supporting HETF (Malhi & Wright 2004; Malhi *et al.* 2009). Therefore, even a relatively small decrease in precipitation may be expected to impact the extent of rainforest versus savannah/dry forest. All of the climate models simulate a drier-than-present MH, which agrees with the independent palaeoclimate records from the Bolivian/Peruvian Andes (Table 4.3, ids=4-6) and lowland south-east Bolivia (i.e. Laguna La Gaiba, Table 4.3, id=7). As a result, most of the DGVM simulations show some degree of HETF dieback (Fig. 4.5j) and expansion of savannah grid cells in the subsequent LDA classifications (Fig. 4.7d).

The relative abundance of palaeoecological records in southern Amazonia allows us to assess the skill of our simulations and LDA classifications with more confidence than in the other areas of Amazonia. The savannah/dry forest expansion along the border of north-eastern Bolivia and adjacent Brazil, as shown through the regional-scale vegetation reconstructions

from Laguna Chaplin, Bella Vista and Orícore (Table 4.2, ids=6,5,4 respectively; Mayle *et al.* 2000; Burbridge *et al.* 2004; Carson *et al.* 2014) is a relatively consistent feature amongst all three DGVMs using the climates of HadGEM2-CC, CNRM-CM5 and FGOALS-s2 (the driest three climate models in this area). However, under the climate models with less precipitation decrease (i.e. CSIRO-Mk3-6-0, IPSL-CM5A-LR and MIROC-ESM), only JULES reproduces the expected savannah expansion in eastern Bolivia, with IBIS and SDGVM showing negligible changes in biome classifications. These results suggest that JULES is more sensitive to any level of precipitation decrease in southern Amazonia, which is perhaps what we would expect given the climatically sensitive nature of this region. Whilst this may suggest that JULES is better able to simulate vegetation response to long-term precipitation changes, the 'threshold response' of the other vegetation models may also be valid, and clearly requires more experimental investigation. Overall, we have more confidence in the drier climate models to simulate MH vegetation changes in southern Amazonia, given that all DGVMs show the expected savannah expansion under these climate scenarios.

Despite southern Amazonia having more palaeoecological records than the other areas of Amazonia, there are still insufficient sites to determine the exact scale of the northward shift of the HETF ecotone. Currently, the farthest north this shift has been detected on a large-scale is at Laguna Orícore (Carson *et al.* 2014). There is some evidence for small, localised patches of savannah expansion occurring on small 'savannah islands' within the dense HETF, ~500 km north of Orícore, though the expanded savannah islands were still likely surrounded by HETF (Table 4.2, ids=31-33; de Freitas *et al.* 2001; Pessenda *et al.* 2001). In eastern Acre, the Jaco Sa soil profiles (Table 4.2, id=34) provide evidence that the bamboo forest ecosystem that exists there today was present during the MH (Watling *et al.* 2017), suggesting that the northerly shift of the HETF-savannah ecotone did not extend to this region. However, there are as yet no palaeo records to determine the extent of MH rainforest extent in the region between Orícore and Jaco Sa.

In the model simulations that show reasonable agreement with the palaeo-data (i.e. the three DGVMs using the climates of HadGEM2-CC, CNRM-CM5 and FGOALS-s2), the spatial extent of savannah expansion appears to be limited to the region around Laguna Orícore, extending into the Brazilian state of Rondônia north of Orícore by one or two grid cells (Fig. 4.6). Only in one model combination – IBIS forced with climate from FGOALS-s2 (Fig. 4.6k) – is there extensive savannah expansion across northern Bolivia, and even here the expansion does not extend further into the surrounding Brazilian rainforest. Savannah expansion is also a

feature of these simulations in the eastern part of southern Amazonia (south-west Mato Grosso state, Brazil). However, this area is mostly savannah in the present day (Fig. 4.1a), so MH savannah 'expansion' here is largely a result of the poor representation of savannah in the modern DGVM simulations and subsequent LDA classification. Overall, our model simulation results suggest that the northern Bolivian HETF was largely resilient during the MH, with the area around Laguna Orícore most likely the northernmost extent of savannah expansion.

4.6.2 Sources of simulation uncertainty

The approach taken in this study, in creating an ensemble of simulations using three different DGVMs, each driven by seven different climate models, has allowed us to demonstrate that uncertainties in the simulations of MH Amazonian vegetation are driven both by the choice of vegetation model and the choice of climate model. It is perhaps unsurprising that the different climate models will produce different vegetation simulations, given that they span quite a large range of MH climate scenarios, from a broadly drier Amazonia (e.g. NASA-GISS) to a more neutral and, in parts, wetter Amazonia (e.g. CSIRO-Mk3-6-0). Similarly, the choice of DGVM is fundamental in what vegetation predictions will be made. Each DGVM will have different ways of representing the key processes (e.g. photosynthesis, soil physics, carbon cycling, competition, mortality, etc.), leading to inevitable uncertainties in defining parameterisation schemes for these processes (Fisher *et al.* 2010; Quillet *et al.* 2010). Only using one climate and/or vegetation model in a simulation experiment precludes the ability to identify, via inter-model comparisons, the inherent uncertainties and biases within these models, only allowing one potential simulated scenario to be investigated. We advocate the use of multi-model ensembles across modelling institutions to investigate both palaeo and future climate and vegetation simulations.

4.6.3 The need for increased palaeo-data in Amazonia

As well as the uncertainties in the climate and vegetation models, this study has highlighted the problems with the incomplete palaeo-data coverage across Amazonia. Firstly, the lack of independent (i.e. not based on palaeovegetation records) palaeoclimate records from within the Amazon basin severely limits our ability to benchmark the MH climate simulations. Although the theories behind the mechanisms for MH climate changes are generally accepted (i.e. austral summer insolation changes impacting SASM intensity), the majority of direct evidence of climate change comes from speleothem records or lakes in the high Andes or across southern Brazil. This makes it difficult to assess the skill of MH climate simulations, as

it is unclear what spatial area these records represent. The recent record from Paraíso Cave is the only speleothem record from the core of the Amazon basin and challenges long held assumptions that these Andean/Brazilian records are representative of the entire Amazon basin, showing the need for more independent palaeoclimate records to be collected from across the Amazonian lowlands. Secondly, the paucity of palaeoecological data limits our ability to constrain the magnitude of HETF/savannah ecotonal shifts toward the margins of the Amazon basin. There is a clear need for transects of additional sites spanning these ecotones across southern and eastern Amazonia.

4.6.4 Implications for understanding the future resilience of Amazonian HETF

Early modelling studies predicted that future climate change could trigger large-scale Amazonian forest dieback (e.g. Cox *et al.* 2000; Betts *et al.* 2004; Cox *et al.* 2004; Huntingford *et al.* 2008). Subsequent studies have shown that these extreme dieback scenarios were largely driven by the extreme drying simulated by the driving climate model, HadCM3, and when comparable simulations were run with different climate models the extent of rainforest dieback was much reduced (e.g. Good *et al.* 2013; Huntingford *et al.* 2013). Nevertheless, it has been stressed that these newer simulations do not invalidate the extreme dieback predicted by the early HadCM3 models, given the difficulty in modelling tropical environments (Good *et al.* 2013). Varying amounts of dieback across Amazonia are still seen in simulations using different DGVMs (e.g. Sitch *et al.* 2008) and climate models (e.g. Malhi *et al.* 2009). However, the past resilience of the central Amazonian HETF biome in all of our MH model simulations, verified by the available palaeoecological data, may be a cause for optimism regarding the future of the region. Our results give support to the modelling scenarios of the core of Amazonia remaining largely forested under drier climatic conditions. However, our MH simulations add weight to evidence from other modelling and ecological studies (e.g. Fisher *et al.* 2007; Malhi *et al.* 2009; Cook *et al.* 2012; Allen *et al.* 2017) that the transitional, ecotonal forests of eastern and southern Amazonia will be especially vulnerable to future drought and may experience significant forest die-back.

Whilst the use of MH climate scenarios in this study has given important insights into the degree of resilience of tropical forests across Amazonia to changing precipitation regimes, it precludes the ability to investigate the response of vegetation to other factors that will be important over the course of this century, most notably temperature, atmospheric CO₂ concentrations and anthropogenic land-use. Increased temperatures may exacerbate dieback by enhancing evapotranspiration and reducing photosynthetic rates (Schaphoff *et al.* 2006;

Galbraith *et al.* 2010; Zhang *et al.* 2015), though some argue that tropical forests have some inherent resilience to direct effects of temperature increases (Lloyd & Farquhar 2008). The effect of rising atmospheric CO₂ levels may help mitigate against dieback through the 'CO₂ fertilisation' effect, but there is uncertainty as to how significant this process will be (Lapola *et al.* 2009; Galbraith *et al.* 2010; Rammig *et al.* 2010). Perhaps of most concern is the impact of direct anthropogenic land use (including deforestation, forest fragmentation and fire use), much of which occurs in the ecotonal areas of eastern and southern Amazonia (the "arc of deforestation"). We have shown that these regions are already sensitive to precipitation changes, with dry MH climate scenarios causing expansion of savannah at the expense of rainforest. The additional pressures of considerable land use will only serve to exacerbate any ecotonal shifts we might expect in these areas in the future. Furthermore, the resilience of central Amazonia we have demonstrated in the MH might be under pressure if the kind of land use practices seen across the arc of deforestation extend further into the Amazon basin in the coming decades.

4.7 Acknowledgements

We thank David Beerling and Lyla Taylor (University of Sheffield) for providing the SDGVM source code. JULES source code was accessed through the Met Office Science Repository Service (MOSRS). IBIS source code was accessed through the Center For Sustainability and the Global Environment, University of Wisconsin-Madison. RS was funded by a NERC 'SCENARIO' DTP PhD award (2014-18).

4.8 Supporting information

The following was provided as supporting information for the paper submitted to *Global Change Biology*.

SI Table 4-A - List of plant functional types (PFTs) used by the DGVMs in this study.

	JULES	IBIS	SDGVM
Plant functional types	9: Tropical Broadleaf Evergreen, Temperate Broadleaf Evergreen, Broadleaf Deciduous, Needleleaf Evergreen, Needleleaf Deciduous, Evergreen shrubs, Deciduous shrubs, C3 grass, C4 grass	12: Tropical Broadleaf Evergreen, Tropical Broadleaf Deciduous, Temperate Broadleaf Evergreen, Temperate Conifer Evergreen, Temperature Broadleaf Deciduous, Boreal Conifer Evergreen, Boreal Broadleaf Deciduous, Boreal Conifer Deciduous, Evergreen shrubs, Deciduous Shrubs, C3 grass, C4 grass	6: Broadleaf Evergreen, Broadleaf Deciduous, Needleleaf Evergreen, Needleleaf Deciduous, C3 grass, C4 grass

SI Table 4-B - Required climate variables and units for each DGVM. See SI Table 4-C for description of each variable

	tas	pr	clt	huss	hurs	rsds	rlds	sfcWind	ps	wetd	deltaT	trange
JULES												
<i>Frequency:</i>	3hr	3hr	-	3hr	-	3hr	3hr	3hr	3hr	-	-	-
<i>Units:</i>	K	kg m ⁻² s ⁻¹	-	kg kg ⁻¹	-	W m ⁻²	W m ⁻²	m s ⁻¹	Pa	-	-	-
IBIS												
<i>Frequency:</i>	mon	mon	mon	-	mon	-	-	mon	-	mon	mon	mon
<i>Units:</i>	°C	mm day ⁻¹	%	-	%	-	-	m s ⁻¹	-	days	°C	°C
SDGVM												
<i>Frequency:</i>	mon	mon	-	-	mon	-	-	-	-	-	-	-
<i>Units:</i>	°C	mm mon ⁻¹	-	-	%	-	-	-	-	-	-	-

SI Table 4-C - Climate variable codes and descriptions

Climate variable code	Description
tas	Surface air temperature
pr	Precipitation rate
clt	Cloud cover
huss	Specific humidity
hurs	Relative humidity
rsds	Downward shortwave radiation
rlds	Downward longwave radiation
sfcWind	Surface wind
ps	Surface air pressure
wetd	Wet days (defined here as number of days with > 1mm rainfall)
deltaT	Minimum temperature ever recorded in a location, minus average temperature of coldest month at that location
trange	Temperature range

Humidity variable conversions

The WFDEI dataset does not have a relative humidity variable. This was approximated from the following equations:

$$q = \frac{\varepsilon e}{p + (1 - \varepsilon)e}$$

$$\varepsilon = \frac{R_d}{R_v} \approx 0.622 \quad (\text{Peixoto \& Oort 1996})$$

$$\therefore q = \frac{0.622e}{p - (0.378e)}$$

$$e = \frac{qp}{0.378q + 0.622}$$

$$e_s \approx 611 \exp\left(\frac{17.67(T - T_0)}{T - 29.65}\right) \quad (\text{Bolton 1980})$$

$$RH = 100 \left(\frac{e}{e_s}\right)$$

where:

q = specific humidity
(kg/kg⁻¹)

R_d = specific gas constant
dry air = 287.05 J kg⁻¹ K⁻¹

R_v = specific gas constant
water vapor =
461.52 J kg⁻¹ K⁻¹

e = vapor pressure
(Pa)

p = surface pressure (Pa)

T_0 = reference
temperature = 273.16 K

e_s = saturation vapor
pressure (Pa)

T = surface temperature (K)

RH = relative humidity
(%)

SI Table 4-D - Required soil variables for each DGVM. See SI Table 4-E for full description of each variable

	sand	silt	clay	b	hcap	hcon	satcon	sathh	sm_crit	sm_sat	sm_wilt	ph
JULES												
<i>Units:</i>	-	-	%	n/a	J m ⁻³ K ⁻¹	W m ⁻¹ K ⁻¹	kg m ⁻² s ⁻¹	m ⁻¹	m ³ m ³	m ³ m ³	m ³ m ³	ph
IBIS												
<i>Units:</i>	%	%	%	-	-	-	-	-	-	-	-	-
SDGVM												
<i>Units:</i>	%	%	%	-	-	-	-	-	-	-	-	-

SI Table 4-E - Soil variable codes and descriptions

Soil variable code	Description
sand	Sand content of soil
silt	Silt content of soil
clay	Clay content of soil
b	Exponent in soil hydraulic characteristics. Broadly a measure of the draining characteristics of soils (Marthews <i>et al.</i> 2014)
hcap	Dry heat capacity – ability of soil to store heat
hcon	Dry thermal conductivity – ability of soil to conduct (transfer) heat
satcon	Hydraulic conductivity at saturation point – a measure of the ease of which water can move through pore spaces in the soil
sathh	1 / α (m ⁻¹), where α is a parameter of the van Genuchten model (van Genuchten 1980) and is a measure of the structure of a soil (Marthews <i>et al.</i> 2014)
sm_crit	Volumetric soil moisture content at ‘critical point’ – the volume of soil moisture below which plants begin to suffer water stress
sm_sat	Volumetric soil moisture content at ‘saturation point’ – total volume of water when all pore spaces in the soil are filled
sm_wilt	Volumetric soil moisture content at ‘wilting point’ – the volume of soil moisture when water stress completely prevents transpiration
ph	Measure of acidity of soil

Chapter 5. General discussion

The results of this thesis have been presented in journal format, focusing on specific research questions. Examined below is the contribution of this thesis to the overall understanding of the impact of long-term mid-Holocene drought upon Amazonian ecosystems. This will be categorised into three broad research themes: (1) importance of palaeo-data syntheses, (2) relationship between tropical basin characteristics and their fossil pollen archives, and (3) integration of palaeo-data and palaeo-modelling. The implications of this thesis for understanding the future of Amazonia are also discussed. Finally, the potential for extending this work in the future is discussed.

5.1 Importance of palaeo-data syntheses in tropical South America

The inclusion of chapters on palaeoclimate in both the AR4 (Jansen *et al.* 2007) and AR5 (Masson-Delmotte *et al.* 2013) IPCC reports shows the acknowledgement of how important knowledge of past environmental changes is for improving our understanding of potential future changes. Central to the premise of looking into the past is the collation and syntheses of palaeo-observational data on regional and global scales, helping to determine the spatio-temporal range of natural variability in the environment under conditions before significant anthropogenic impacts. Great efforts have gone into creating these syntheses in other areas of the world, for example several hundred mid-Holocene sites make up extensive datasets across North America (e.g. Prentice *et al.* 1993; Sawada *et al.* 2004; Viau *et al.* 2006) and Europe (e.g. Davis *et al.* 2003; Wu *et al.* 2007; Roberts *et al.* 2018). These can then feed into larger global syntheses and contribute to palaeodata-model intercomparison projects that help to develop model enhancements in those data-rich regions. However, the conspicuous absence of tropical South America from many of these projects (e.g. Kohfeld & Harrison 2000; Harrison & Prentice 2003; Braconnot *et al.* 2012) is potentially limiting our understanding and development in a region that provides crucial global biogeochemical feedbacks between the land surface and climate (e.g. through carbon sequestration, as well as vegetation feedbacks helping to drive regional and global climate patterns).

The mid- to late Holocene multi-proxy palaeo-data synthesis provided in Chapter 2 is the most up-to-date collection of palaeoecological vegetation reconstructions from across southern hemispheric tropical South America. The inclusion of non-pollen proxy reconstructions means that this synthesis includes significantly more sites than previous studies (e.g. Mayle & Power 2008; Marchant *et al.* 2009). Considering these palaeoecological records together on a sub-

continental scale alongside key palaeoclimate records provides information about how the vegetation from different regions of tropical South America responded differently (or not) to orbitally forced long-term precipitation changes through the mid-to-late Holocene. For example, the records from the central and western Amazonian region provide evidence for resilience of the humid evergreen forest biome during the middle Holocene, despite palaeoclimatological evidence that this region may have been slightly drier than present (van Breukelen *et al.* 2008; Cheng *et al.* 2013). However, eastern and southern Amazonia were much less resilient to mid-Holocene drought, with expansion of savannah and tropical dry forests at the expense of humid evergreen rainforest recorded in many of the palaeoecological records in these areas.

A key pattern revealed by this synthesis is the strong link between the palaeo-history of south-west Amazonia and southern Brazil. These regions are climatically linked through features of the South American summer monsoon, most notably strong low-level winds that are channelled southwards by the eastern Andes and the Brazilian planalto highlands that transport moisture from Amazonia into southern Brazil. A drier middle Holocene characterised both south-west Amazonia (Baker *et al.* 2001; Burbridge *et al.* 2004; Whitney *et al.* 2011) and southern Brazil (Cruz *et al.* 2005; Wang *et al.* 2007; Bernal *et al.* 2016) which caused a more northerly location of the rainforest/savannah ecotone in south-west Amazonia (north-eastern Bolivia), greater expanse of campos grassland across the south Brazilian highlands; and decreased expanse of montane forests and humid evergreen forest across the southern Atlantic forest of Brazil. Late-Holocene precipitation increases produced similar responses between these regions, with southward expansion of the humid rainforest biome in south-west Amazonia, expansion of humid evergreen forests and moist *Araucaria* forests on the southern Brazilian highlands and increase of gallery forests in the south-east Brazilian Cerrado.

As well as providing insights into the spatio-temporal dynamics of biome-scale vegetation changes across tropical South America, this synthesis also helps in identifying regions where more palaeo-data are needed. For example, in eastern Amazonia an apparent mis-match exists between the palaeoclimate speleothem record of Paraíso Cave (Wang *et al.* 2017), which suggests a wetter-than-present middle Holocene, and savannah expansion recorded in records taken from Serra Sul dos Carajás plateau. However, the spatial extent of these savannah expansions is unclear, as these sites only have local-scale catchments and may only reflect ecotonal shifts on the plateau itself rather than being representative of the surrounding lowlands. A greater number of sites across the lowlands of eastern Amazonia,

either from larger lakes (reflecting more regional-scale vegetation changes) and/or transects of smaller sites (such as swamps, bogs or soil-pit profiles) spanning the ecotone would help to improve our understanding of these clearly complex vegetation-climate interactions. In southern Amazonia, more sites could help to quantify the maximum extent of the mid-to-late Holocene savannah-rainforest ecotonal shift. North-east Brazil and the cerrado region of central Brazil are conspicuous in their paucity of palaeoecological sites, likely due to the lack of suitable lakes in these arid regions that can provide a fossil-pollen record. However, this synthesis has demonstrated the value of soil-based proxies, such as $\delta^{13}\text{C}$ isotopes and phytoliths, which could be used to great effect in these regions where lakes/bogs are scarce.

5.2 Relationship between tropical basin characteristics and their fossil pollen archive

The data synthesis presented in Chapter 2 includes records from a variety of basin sizes (e.g. small, medium, large) and basin types (e.g. lakes, bogs, swamps, soil pits). The synthesis included consideration of how the different basin sizes would affect the spatial scale of the vegetation reconstruction from a given basin, using assumptions based on research from temperate mid to high latitude North America and Europe, where thorough methodological research shows that large basins have regional-scale pollen catchment areas and are relatively insensitive to localised changes in vegetation (Sugita 1994; Sugita *et al.* 1999; Sugita 2007a), whereas small basins instead have local-scale pollen catchment areas (Davis 2000; Sugita 2007b). This general premise that large lakes and small lakes capture regional- and local-scale pollen rain, respectively, likely holds true for tropical ecosystems, even though specific quantitative estimates of temperate pollen catchment areas are not applicable to the much more complex pollination dynamics in the tropics. However, the consideration of the relationship between basin type (lake, bog, swamp etc.) and fossil pollen archives is less clear, with few methodological exercises having been carried out in tropical South America. Chapter 3 attempts to address this issue by providing a direct comparison between the fossil-pollen records of a small palm swamp (Cuatro Vientos) and a nearby large lake (Laguna Chaplin). Palm swamps are unique basins, often covered in floating mat vegetation, with palm trees dominating the basin edges whilst also growing within the basin itself. Therefore, there is often concern over their suitability for recording terrestrial vegetation history from beyond their basin, with the assumption that they may only reveal the history of vegetation growing within the basin itself.

The Cuatro Vientos record shows an evolution of basin type throughout its sedimentological history, with evidence of an open lake basin through the Last Glacial Maximum (LGM, ca. 24,000 years before present) to the early Holocene (ca. 11,000 to 7,000 years before present), with the beginnings of a swamp environment likely commencing during the middle Holocene (ca. 7,000 to 5,500 years before present). Throughout this time, the fossil pollen assemblage of Cuatro Vientos is always very similar to that of Laguna Chaplin, with both recording a savannah landscape during the LGM and a savannah/semi-deciduous forest mosaic landscape during the middle Holocene. Even during the period where it is inferred that Cuatro Vientos had developed from a lake into a swamp, during the mid- to late Holocene, the pollen assemblage reflects the wider terrestrial landscape rather than being dominated by swamp vegetation such as Cyperaceae or palms (*Mauritia/Mauritiella*). Therefore, we have shown that palm swamps may hold considerably greater value for reconstructing Amazonian Quaternary vegetation change than commonly assumed. Given the need for growing the number of palaeoecological sites across Amazonia, as shown in the synthesis of Chapter 2, palm swamps should not be dismissed as being 'sub-optimal' sites as they have the potential to record terrestrial vegetation history extending to the LGM, rather than just a history of palm swamp vegetation dynamics.

5.2.1 Implications for the rainforest refugia hypothesis

As well as corroborating the interpretation of Laguna Chaplin (Mayle *et al.* 2000; Burbridge *et al.* 2004), the smaller basin size of Cuatro Vientos enabled a closer look into local-scale vegetation dynamics during the LGM and middle Holocene. It had previously been proposed that rainforest taxa may have survived during times of drier climates in riverine/gallery forests that grow in narrow ribbons alongside rivers and streams. Then, when climate became more humid, these gallery forest 'refugia' could have initiated the expansion of rainforest into the surrounding area. The proximity of Cuatro Vientos to the Río Paraguá provided the opportunity to test this hypothesis. The results suggest that open savannah and dry forest dominated both the interfluves and the riverine areas during the drier climatic conditions of the LGM and middle Holocene, therefore challenging the gallery rainforest refugia hypothesis, at least for this area of southern Amazonia.

The findings that gallery rainforest not being as resilient as previously thought through long-term drought conditions may have implications for the future of southern Amazonia, particularly if climate model predictions of a drier climate are borne out. These gallery rainforests can host a wide variety of flora, with species diversity similar to that of dense

evergreen terra-firme rainforest (Killeen & Schulenberg 1998; Burn *et al.* 2010). Within the Brazilian cerrado, gallery and riverine forests have been shown to be the primary habitat for the majority of nonvolant mammals (Redford & da Fonseca 1986) and play a vital role for the migration, breeding and habitats of birds (Silva 1997; Silva & Bates 2002). Under a future drier climate that promises prolonged droughts, particularly in the ecotonal regions of Amazonia, the rainforest refugia hypothesis may have been cause for optimism for the resilience of floral and faunal species that could take refuge in the gallery rainforests that might exist along watercourses. However, our findings that suggest that reduced gallery forests under a drier climate could mean significantly less resilience for these species than previously thought.

5.3 Integration of palaeo-data and palaeo-modelling in Amazonia

The palaeoecological knowledge gained from Chapters 2 and 3 helps to extend our observational period to timescales suitable for investigating long-term climate-vegetation interactions, rather than the short-term annual to decadal period offered by conventional ecology. These chapters have provided a good background in understanding the vegetation history across Amazonia during the middle Holocene. Therefore, this presents the opportunity to conduct palaeo data-modelling comparisons for mid-Holocene Amazonia, helping to determine those regions of Amazonia for which we have the most/least confidence in model simulations.

The results of the multi-model vegetation model ensemble presented in Chapter 4 reveal that, on a biome scale, there is relatively good agreement between modelled and observed (palaeoecological) data. In central Amazonia, most of the mid-Holocene climate simulations show decreased precipitation, though all the vegetation simulations show that the humid evergreen rainforest was resilient to any degree of mid-Holocene drying. There are negligible changes to simulated PFT coverage, and no biome changes are found when the full suite of modelled data is run through the LDA classification algorithm. This is consistent with the story seen in the palaeoecological data, with all sites in this region showing persistence of the humid evergreen forest through the mid- to late Holocene. This therefore gives us confidence that the vegetation models are able to represent the core of the Amazon rainforest reasonably well over long timescales with climates significantly different to present.

In contrast to central Amazonia, greater divergence in simulations exists in ecotonal eastern and southern Amazonia. The primary driver of the uncertainty in these simulations is difficult to assess, with deviation in simulations occurring depending upon the choice of both

vegetation and climate models. Nevertheless, the results do show that, at least in part, all the vegetation models are sensitive to changes in precipitation in these areas, with simulated changes in savannah extent related to the 'dryness' of a given climate model; drier climates tend to cause more savannah expansion. In eastern Amazonia, this potentially provides insights into the confusion caused by the Paraíso Cave speleothem record that suggests a wetter than present middle Holocene (Wang *et al.* 2017). In vegetation simulations using climate models with a wetter eastern Amazonia at the middle Holocene, analogous to the Paraíso Cave interpretations, there is expansion of the humid evergreen rainforest into the Cerrado savannah ecoregion of Brazil. This is the opposite signal to the available evidence from the palaeoecological sites in this region, which show savannah expansion, suggesting that the Paraíso Cave record may not be representative of the eastern Amazonian ecotone. However, the available palaeo-data from this region primarily come from the Carajás plateau and, as previously stated, it is unclear how representative these records are of the surrounding lowlands. The savannah expansion in these records may be localised and occurring on scales smaller than the grid cell resolution of the models. More palaeoecological and palaeoclimate records are going to be vital in improving our understanding of mid-Holocene vegetation-climate interactions.

In southern Amazonia, all climate models simulated a drier middle Holocene and there is strongest agreement between the vegetation model simulations and palaeo-data, both showing the expansion of savannah and thus the vulnerability of the humid evergreen rainforest in this area. However, there still remains uncertainty between the models regarding the spatial position and extent of this savannah expansion. The simulated savannah expansion using the driest climate models appears to match the palaeoecological data best, with savannah expansion along the border of north-eastern Bolivia and adjacent Brazil, as shown through the regional-scale vegetation reconstructions from Laguna Chaplin, Bella Vista and Orícore (Mayle *et al.* 2000; Burbridge *et al.* 2004; Carson *et al.* 2014). With climate models that simulate a weaker mid-Holocene drying, only JULES reproduces any savannah expansion in eastern Bolivia. This suggests that JULES is sensitive to any decrease of precipitation in southern Amazonia, which is perhaps what we would expect given that this area is climatically sensitive, with the humid evergreen forest existing close to its climatic limit. Whilst this may suggest that JULES is better able to simulate vegetation response to long-term precipitation changes, the 'threshold response' of the other vegetation models (i.e. they only simulate savannah expansion once annual precipitation decreases by more than ~100 mm) may also be valid.

5.4 Implications for combining information on landscape and cultural changes

There has been a relatively recent increase in studies combining palaeoecological and archaeological data within tropical South America in an attempt to better understanding the human-environment interactions that helped shape the landscape. These include investigations into role of humans in the expansion of *Araucaria* forests in southern Brazil in the last 2,000-3,000 years (e.g. Behling *et al.* 2004; Iriarte & Behling 2007; Robinson *et al.* 2018) and the legacy of pre-Colombian cultures and their management of the landscape in south-west (e.g. Carson *et al.* 2014; 2016; Watling *et al.* 2017) and eastern (e.g. Maezumi *et al.* 2018) Amazonia. Although this project focused predominantly on the impacts of past climate change on the landscape, the results from the chapters presented may help to better inform discussions of human-environment interactions.

The qualitative vegetation reconstruction approach, used in conjunction with the findings from independent palaeoclimate data, in the data synthesis presented in Chapter 2 allowed us to more easily take into account human influence on palaeo-vegetation changes through the mid- to late-Holocene. A quantitative approach such as biomisation (Prentice *et al.* 1996) or landscape reconstruction algorithms (e.g. Sugita 2007a; 2007b; Whitney *et al.* 2018) may consider human and climate-induced vegetation changes to be equivalent, whereas our approach allowed us to take advantage of the in-depth knowledge that the author(s) will have about their site, including any archaeological findings. If the vegetation history of a given site was inconsistent with independent paleoclimate data from the area, we could consider whether human land use was the reason for a climate-vegetation mis-match.

The results from Chapter 2 have been used in a project that has helped further our understanding of the late-Holocene expansion of the Tupi-Guarani pre-Columbian culture from southern Amazonia to south-east South America (see Appendix A). The reasons for this ~4,000 km cultural expansion from ca. 3,000-2,000 years ago was hitherto uncertain. However, the concurrent late-Holocene increases in tropical forests and archaeological sites through south-east South America at this time suggests that precipitation changes facilitated the expansion of ecosystems favoured by the forest-farming culture of the Tupi-Guarani (Iriarte *et al.* 2017). The results from the pollen analysis at Cuatro Vientos from Chapter 3 may also help to provide insight into the movements of cultures such as the Tupi-Guarani. Our results suggests that open savannah and dry forest were dominant in the riverine areas of the

Bolivian southern Amazonia, challenging the assumption that gallery rainforest would have prevailed through long-term drought conditions. If this interpretation of reduced gallery rainforest was applicable to surrounding areas of southern Amazonian and Brazil, this may help to explain why the river-dwelling, agroforestry practicing (Scheel-Ybert *et al.* 2014) Tupi-Guarani culture could not take advantage of riverine gallery rainforest to expand earlier than ca. 3,000 years ago.

The modelled vegetation changes shown in Chapter 4 may also help to provide focus on the causes of observed vegetation changes. The methodology in this chapter only considered climate change as a driver of vegetation change in the DGVMs. Human land use was not included as an input for two main reasons: 1. This study, and the overall aim of this thesis, was to consider the effect of climate change in isolation to provide a 'baseline' of natural changes on top of which human impacts could be considered; and 2. Reliable data for the location and scale of human land use in this research area is lacking. The de-coupling of humans and climate in the modelled vegetation change results helps us to show where the most likely areas of large-scale climate change induced vegetation changes are. Any additional landscape changes found in palaeo-vegetation studies may show that humans had more of an influence in shaping the landscape. Although it must be acknowledged that the modelled results contain many uncertainties, comparison between models and observations may help to focus study areas to those regions with the biggest apparent mis-match.

5.5 Implications for the future of Amazonia

The rationale behind this thesis is based on the concern over what impacts future climate change, particularly projected decreases in precipitation, would have on Amazonian ecosystems. The results from the chapters presented in this thesis offer important insights into how Amazonia responded to long-term climate change in the past, which in turn provides an indication of how resilient the region may be to reduced precipitation. A cause for optimism is the resilience of the core Amazonian rainforest biome under the drier climate of the middle Holocene, as shown through the palaeoecological sites in this region (Chapter 2) and subsequent vegetation modelling results (Chapter 4). These results suggest that future simulations of extensive forest dieback across the whole of Amazonia (e.g. Cox *et al.* 2000; Betts *et al.* 2004; Cox *et al.* 2004; Huntingford *et al.* 2008) are unlikely.

Of greater concern is the degree of resilience of the humid evergreen forests in the ecotonal regions of eastern and southern Amazonia. The results from synthesis and modelling exercises add to other evidence from modelling and ecological studies (e.g. Fisher *et al.* 2007; Malhi *et al.* 2009; Cook *et al.* 2012; Allen *et al.* 2017) that suggest that the transitional, ecotonal forests of eastern and southern Amazonia will be especially vulnerable to future drought and may experience significant forest die-back. The results of the pollen analysis of Cuatro Vientos (Chapter 3) adds additional weight to these concerns over the vulnerability of southern Amazonia. The local-scale reconstruction from Cuatro Vientos shows that at no point through the LGM to the middle to late Holocene was there a pollen assemblage representative of a gallery/riverine forest. This was unexpected, given the proximity of the basin to the Río Paraguá, and the previous assumptions that gallery/riverine forests were important refugia for rainforest species in times of drier climates (Mayle *et al.* 2007). Instead, these results suggest gallery/riverine rainforests were substantially reduced during the LGM and middle Holocene compared to present. If these gallery/riverine rainforests are not likely to provide refugia for rainforest species under future drier conditions, then the resilience of ecotonal, southern Amazonian rainforest would likely be reduced.

5.6 Potential for future work

The research conducted in this thesis presents opportunities for future work to build upon our understanding of the impact of long-term mid-Holocene drought upon Amazonian ecosystems. Continuous updates to the synthesis carried out in Chapter 2 will be vital as new palaeoecological records are published from across tropical South America. Hopefully, the demonstration of the usefulness of proxies other than pollen (e.g. stable carbon isotopes, phytoliths) will encourage a greater number of new records to be taken in environments where suitable pollen-repositories (e.g. lakes, bogs) are scarce. Additionally, the pollen analysis of Cuatro Vientos has shown that palm swamps should be considered for palaeoecological analysis.

Further palaeoecological analyses from suitable sites could help to confirm the interpretation from the pollen analysis of Cuatro Vientos that gallery/riverine forests were much reduced during past drier climates of the LGM and middle Holocene. New sites would ideally be small, to capture a local- rather than regional-scale vegetation signal, and near to major rivers, to capture the dynamics of the riverine forests. Oxbow lakes could be investigated, though it is unusual for these to be old enough to record vegetation changes on the required multi-

millennial timescales. Instead, transects of soil profiles may be suitable, utilising phytolith analysis as the vegetation proxy.

With regards to the palaeo-modelling approach, further work could be done to carry out mid-Holocene vegetation simulations using different models. The next CMIP phase (CMIP6) is underway, coordinating simulations using the latest climate models from modelling centres across the world. The PMIP initiative continues to be included in the official CMIP6-endorsed model intercomparison projects, meaning there will be a new set of updated mid-Holocene climate simulations (Eyring *et al.* 2016). Additionally, new model developments are creating the next generation of vegetation models. The traditional 'big-leaf' approach of the vegetation models used in this study means that individual plants are represented as an amalgamation into one plant functional type, which is then considered one 'big-leaf' canopy for the model equations to be calculated for. This means that potentially important aspects of plant behaviour on the individual level, known to influence the likelihood of coexistence of species, are not considered. New trait- and individual- based models (e.g. ED2, SEIB, aDGVM2) allow individual plants to be simulated, with traits defining how these individuals interact and compete (Scheiter *et al.* 2013). These may more accurately simulate vegetation, particularly in heterogeneous landscapes (Restrepo-Coupe *et al.* 2017).

In summary, this thesis has shown the potential for a multi-disciplinary approach for studying palaeo-environmental change in the South American tropics. Both the palaeoecological and modelling communities can learn a lot from each other, and increased collaborations should be a priority in the coming years. Studying environmental change across thousands of years will be essential for increasing our confidence in the potential changes to come.

References

- Absy, M. L., Cleef, A. M., D'Apolito, C., & da Silva, M. F. F. (2014). Palynological differentiation of savanna types in Carajás, Brazil (southeastern Amazonia). *Palynology*, **38** (1), 78–89.
- Absy, M. L., Cleef, A., Fournier, M., et al. (1991). Mise en évidence de quatre phases d'ouverture de la forêt dense dans le Sud-Est de l'Amazonie au cours des 60 000 dernières années: première comparaison avec d'autres régions tropicales. *Comptes Rendus De L'Académie Des Sciences. Série 2, Mécanique, Physique, Chimie, Sciences De La Terre*, **312** (6), 673–678.
- Adeney, J. M., Christensen, N. L., Vicentini, A., & Cohn-Haft, M. (2016). White-sand Ecosystems in Amazonia. *Biotropica*, **48** (1), 7–23.
- Alexandre, A., Meunier, J. D., Mariotti, A., & Soubiès, F. (1999). Late Holocene phytolith and carbon-isotope record from a latosol at Salitre, south-central Brazil. *Quaternary Research*, **51** (2), 187–194.
- Allen, K., Dupuy, J. M., Gei, M. G., et al. (2017). Will seasonally dry tropical forests be sensitive or resistant to future changes in rainfall regimes? *Environmental Research Letters*, **12** (2), 023001–16.
- Andrade-Lima, D. de. (1982). Present-day forest refuges in northeastern Brazil. In *Biological Diversification in the Tropics*, New York: Columbia University Press, pp. 245–251.
- Aragão, L. E. O. C., Anderson, L. O., Fonseca, M. G., et al. (2018). 21st Century drought-related fires counteract the decline of Amazon deforestation carbon emissions. *Nature Communications*, **9** (536), 1–12.
- Aragão, L. E. O. C., Poulter, B., Barlow, J. B., et al. (2014). Environmental change and the carbon balance of Amazonian forests. *Biological Reviews*, **89** (4), 913–931.
- Baker, P. A., & Fritz, S. C. (2015). Nature and causes of Quaternary climate variation of tropical South America. *Quaternary Science Reviews*, **124**, 31–47.
- Baker, P. A., Seltzer, G. O., Fritz, S. C., et al. (2001). The history of South American tropical precipitation for the past 25,000 years. *Science*, **291** (5504), 640–643.
- Bao, Q., Lin, P., Zhou, T., et al. (2013). The flexible global ocean-atmosphere-land system model, spectral version 2: FGOALS-s2. *Advances in Atmospheric Sciences*, **30** (3), 561–576.
- Barberi, M., Salgado-Labouriau, M. L., & Suguio, K. (2000). Paleovegetation and paleoclimate of “Vereda de Águas Emendadas,” central Brazil. *Journal of South American Earth Sciences*, **13** (3), 241–254.
- Barlow, J., Gardner, T. A., Lees, A. C., Parry, L., & Peres, C. A. (2012). How pristine are tropical forests? An ecological perspective on the pre-Columbian human footprint in Amazonia and implications for contemporary conservation. *Biological Conservation*, **151** (1), 45–49.

- Bartlein, P. J., Harrison, S. P., Brewer, S., et al. (2011). Pollen-based continental climate reconstructions at 6 and 21 ka: a global synthesis. *Climate Dynamics*, **37** (3-4), 775–802.
- Batalha-Filho, H., Fjeldså, J., Fabre, P. H., & Miyaki, C. Y. (2013). Connections between the Atlantic and the Amazonian forest avifaunas represent distinct historical events. *Journal of Ornithology*, **154** (1), 41–50.
- Baudena, M., Dekker, S. C., van Bodegom, P. M., et al. (2015). Forests, savannas, and grasslands: bridging the knowledge gap between ecology and Dynamic Global Vegetation Models. *Biogeosciences*, **12** (6), 1833–1848.
- Behling, H. (1995a). A high resolution Holocene pollen record from Lago do Pires, SE Brazil: vegetation, climate and fire history. *Journal of Paleolimnology*, **14** (3), 253–268.
- Behling, H. (1995b). Investigations into the late Pleistocene and Holocene history of vegetation and climate in Santa Catarina (S Brazil). *Vegetation History and Archaeobotany*, **4** (3), 127–152.
- Behling, H. (1997a). Late Quaternary vegetation, climate and fire history from the tropical mountain region of Morro de Itapeva, SE Brazil. *Palaeogeography, Palaeoclimatology, Palaeoecology*, **129** (3-4), 407–422.
- Behling, H. (1997b). Late Quaternary vegetation, climate and fire history of the Araucaria forest and campos region from Serra Campos Gerais, Paraná State (South Brazil). *Review of Palaeobotany and Palynology*, **97** (1-2), 109–121.
- Behling, H. (1998). Late Quaternary vegetational and climatic changes in Brazil. *Review of Palaeobotany and Palynology*, **99** (2), 143–156.
- Behling, H. (2003). Late glacial and Holocene vegetation, climate and fire history inferred from Lagoa Nova in the southeastern Brazilian lowland. *Vegetation History and Archaeobotany*, **12** (4), 263–270.
- Behling, H. (2007). Late Quaternary vegetation, fire and climate dynamics of Serra do Araçatuba in the Atlantic coastal mountains of Paraná State, southern Brazil. *Vegetation History and Archaeobotany*, **16** (2-3), 77–85.
- Behling, H., & da Costa, M. L. (2000). Holocene Environmental Changes from the Rio Curuá Record in the Caxiuana Region, Eastern Amazon Basin. *Quaternary Research*, **53** (3), 369–377.
- Behling, H., & da Costa, M. L. (2001). Holocene vegetational and coastal environmental changes from the Lago Crispim record in northeastern Pará State, eastern Amazonia. *Review of Palaeobotany and Palynology*, **114** (3-4), 145–155.
- Behling, H., & Hooghiemstra, H. (1999). Environmental history of the Colombian savannas of the Llanos Orientales since the Last Glacial Maximum from lake records El Pinal and Carimagua. *Journal of Paleolimnology*, **21** (4), 461–476.

- Behling, H., & Negrelle, R. R. B. (2001). Tropical Rain Forest and Climate Dynamics of the Atlantic Lowland, Southern Brazil, during the Late Quaternary. *Quaternary Research*, **56** (3), 383–389.
- Behling, H., & Pillar, V. D. (2007). Late Quaternary vegetation, biodiversity and fire dynamics on the southern Brazilian highland and their implication for conservation and management of modern Araucaria forest and grassland ecosystems. *Philosophical Transactions of the Royal Society B: Biological Sciences*, **362** (1478), 243–251.
- Behling, H., & Safford, H. D. (2010). Late-glacial and Holocene vegetation, climate and fire dynamics in the Serra dos Órgãos, Rio de Janeiro State, southeastern Brazil. *Global Change Biology*, **16** (6), 1661–1671.
- Behling, H., Arz, H. W., Pätzold, J., & Wefer, G. (2000). Late Quaternary vegetational and climate dynamics in northeastern Brazil, inferences from marine core GeoB 3104-1. *Quaternary Science Reviews*, **19** (10), 981–994.
- Behling, H., Bauermann, S. G., & Pereira Neves, P. C. (2001a). Holocene environmental changes in the São Francisco de Paula region, southern Brazil. *Journal of South American Earth Sciences*, **14** (6), 631–639.
- Behling, H., Berrio, J. C., & Hooghiemstra, H. (1999). Late Quaternary pollen records from the middle Caquetá river basin in central Colombian Amazon. *Palaeogeography, Palaeoclimatology, Palaeoecology*, **145**, 193–213.
- Behling, H., Cohen, M. C. L., & Lara, R. J. (2001b). Studies on Holocene mangrove ecosystem dynamics of the Bragança Peninsula in north-eastern Pará, Brazil. *Palaeogeography, Palaeoclimatology, Palaeoecology*, **167** (3-4), 225–242.
- Behling, H., Dupont, L., Safford, H. D., & Wefer, G. (2007). Late Quaternary vegetation and climate dynamics in the Serra da Bocaina, southeastern Brazil. *Quaternary International*, **161** (1), 22–31.
- Behling, H., Keim, G., Irion, G., Junk, W., & Nunes de Mello, J. (2001c). Holocene environmental changes in the Central Amazon Basin inferred from Lago Calado (Brazil). *Palaeogeography, Palaeoclimatology, Palaeoecology*, **173** (1-2), 87–101.
- Behling, H., Negrelle, R. R. B., & Colinvaux, P. A. (1997). Modern pollen rain data from the tropical Atlantic rain forest, Reserva Volta Velha, South Brazil. *Review of Palaeobotany and Palynology*, **97** (3-4), 287–299.
- Behling, H., Pillar, V. D., & Bauermann, S. G. (2005). Late Quaternary grassland (Campos), gallery forest, fire and climate dynamics, studied by pollen, charcoal and multivariate analysis of the São Francisco de Assis core in western Rio Grande do Sul (southern Brazil). *Review of Palaeobotany and Palynology*, **133** (3-4), 235–248.
- Behling, H., Pillar, V. D., Orlóci, L., & Bauermann, S. G. (2004). Late Quaternary Araucaria forest, grassland (Campos), fire and climate dynamics, studied by high-resolution pollen, charcoal and multivariate analysis of the Cambará do Sul core in southern Brazil. *Palaeogeography, Palaeoclimatology, Palaeoecology*, **203** (3-4), 277–297.

- Bennett, K. D. (1996). Determination of the number of zones in a biostratigraphical sequence. *New Phytologist*, **132** (1), 155–170.
- Berger, A. (1992). Orbital Variations and Insolation Database. IGBP PAGES/World Data Center-A for Paleoclimatology Data Contribution Series #92-007. NOAA/NGDC Paleoclimatology Program, Boulder CO, USA.
- Berger, A. L. (1978). Long-Term Variations of Caloric Insolation Resulting from the Earth's Orbital Elements. *Quaternary Research*, **9** (2), 139–167.
- Berger, A., & Loutre, M. F. (1991). Insolation values for the climate of the last 10 million years. *Quaternary Science Reviews*, **10** (4), 297–317.
- Bernal, J. P., Cruz, F. W., Strikis, N. M., et al. (2016). High-resolution Holocene South American monsoon history recorded by a speleothem from Botuverá Cave, Brazil. *Earth and Planetary Science Letters*, **450**, 186–196.
- Best, M. J., Pryor, M., Clark, D. B., et al. (2011). The Joint UK Land Environment Simulator (JULES), model description – Part 1: Energy and water fluxes. *Geoscientific Model Development*, **4** (3), 677–699.
- Betts, R. A., Cox, P. M., Collins, M., Harris, P. P., Huntingford, C., & Jones, C. D. (2004). The role of ecosystem-atmosphere interactions in simulated Amazonian precipitation decrease and forest dieback under global climate warming. *Theoretical and Applied Climatology*, **78** (1-3), 157–175.
- Bitencourt, A., & Krauspenhar, P. M. (2006). Possible prehistoric anthropogenic effect on *Araucaria angustifolia* (Bert.) O. Kuntze expansion during the Late Holocene. *Revista Brasileira De Paleontologia*, **9** (1), 109–116.
- Blaauw, M., & Christen, J. A. (2011). Flexible paleoclimate age-depth models using an autoregressive gamma process. *Bayesian Analysis*, **6**, 457–474.
- Blaauw, M., Christen, J. A., Bennett, K. D., & Reimer, P. J. (2018). Double the dates and go for Bayes - Impacts of model choice, dating density and quality on chronologies. *Quaternary Science Reviews*, **188**, 58–66.
- Boisier, J. P., Ciais, P., Ducharne, A., & Guimberteau, M. (2015). Projected strengthening of Amazonian dry season by constrained climate model simulations. *Nature Climate Change*, **5** (7), 656–660.
- Bolton, D. (1980). The Computation of Equivalent Potential Temperature. *Monthly Weather Review*, **108** (7), 1046–1053.
- Boutton, T. W. (1996). Stable carbon isotopes ratios of soil organic matter and their use of indicators of vegetation and climate change. In T. W. Boutton & S. Yamasaki, *Mass Spectrometry of Soils*, New York, pp. 47–82.
- Braconnot, P., Otto-Bliesner, B., Harrison, S. P., et al. (2007). Results of PMIP2 coupled simulations of the Mid-Holocene and Last Glacial Maximum - Part 1: experiments and large-scale features. *Climate of the Past*, **3** (2), 261–277.

- Braconnot, P., Harrison, S. P., Kageyama, M., et al. (2012). Evaluation of climate models using palaeoclimatic data. *Nature Climate Change*, **2** (6), 417–424.
- Braconnot, P., Harrison, S. P., Otto-Bliesner, B., Abe-Ouchi, A., Jungclaus, J., & Peterschmitt, J. Y. (2011). The Paleoclimate Modeling Intercomparison Project contribution to CMIP5. *CLIVAR Exchanges*, **16** (2), 15–19.
- Bradbury, J. P., Leyden, B., Salgado-Labouriau, M. L., et al. (1981). Late quaternary environmental history of lake Valencia, Venezuela. *Science*, **214** (4527), 1299–1305.
- Brienen, R. J. W., Phillips, O. L., Feldpausch, T. R., et al. (2015). Long-term decline of the Amazon carbon sink. *Nature*, **519** (7543), 344–348.
- Bronk Ramsey, C. (1995). Radiocarbon Calibration and Analysis of Stratigraphy: The OxCal Program. *Radiocarbon*, **37** (2), 425–430.
- Bronk Ramsey, C. (2009). Dealing with Outliers and Offsets in Radiocarbon Dating. *Radiocarbon*, **51** (3), 1023–1045.
- Brugger, S. O., Gobet, E., van Leeuwen, J. F. N., et al. (2016). Long-term man-environment interactions in the Bolivian Amazon: 8000 years of vegetation dynamics. *Quaternary Science Reviews*, **132**, 114–128.
- Burbridge, R. E., Mayle, F. E., & Killeen, T. J. (2004). Fifty-thousand-year vegetation and climate history of Noel Kempff Mercado National Park, Bolivian Amazon. *Quaternary Research*, **61** (2), 215–230.
- Burn, M. J., & Mayle, F. E. (2008). Palynological differentiation between genera of the Moraceae family and implications for Amazonian palaeoecology. *Review of Palaeobotany and Palynology*, **149** (3-4), 187–201.
- Burn, M. J., Mayle, F. E., & Killeen, T. J. (2010). Pollen-based differentiation of Amazonian rainforest communities and implications for lowland palaeoecology in tropical South America. *Palaeogeography, Palaeoclimatology, Palaeoecology*, **295** (1-2), 1–18.
- Bush, M. B., & Colinvaux, P. A. (1988). A 7000-Year Pollen Record from the Amazon Lowlands, Ecuador. *Vegetatio*, **76** (3), 141–154.
- Bush, M. B., & Rivera, R. (2001). Reproductive ecology and pollen representation among neotropical trees. *Global Ecology and Biogeography*, **10** (4), 359–367.
- Bush, M. B., & Weng, C. (2007). Introducing a new (freeware) tool for palynology. *Journal of Biogeography*, **34** (3), 377–380.
- Bush, M. B., Correa-Metrio, A., McMichael, C. N. H., et al. (2016). A 6900-year history of landscape modification by humans in lowland Amazonia. *Quaternary Science Reviews*, **141**, 52–64.
- Bush, M. B., De Oliveira, P. E., Colinvaux, P. A., Miller, M. C., & Moreno, J. E. (2004a). Amazonian paleoecological histories: one hill, three watersheds. *Palaeogeography, Palaeoclimatology, Palaeoecology*, **214** (4), 359–393.

- Bush, M. B., Miller, M. C., De Oliveira, P. E., & Colinvaux, P. A. (2000). Two histories of environmental change and human disturbance in eastern lowland Amazonia. *The Holocene*, **10** (5), 543–553.
- Bush, M. B., Silman, M. R., & Listopad, C. M. C. S. (2007a). A regional study of Holocene climate change and human occupation in Peruvian Amazonia. *Journal of Biogeography*, **34** (8), 1342–1356.
- Bush, M. B., Silman, M. R., & Urrego, D. H. (2004b). 48,000 years of climate and forest change in a biodiversity hot spot. *Science*, **303** (5659), 827–829.
- Bush, M. B., Silman, M. R., De Toledo, M. B., et al. (2007b). Holocene fire and occupation in Amazonia: records from two lake districts. *Philosophical Transactions of the Royal Society B: Biological Sciences*, **362** (1478), 209–218.
- Bustamante, M. G., Cruz, F. W., Vuille, M., et al. (2016). Holocene changes in monsoon precipitation in the Andes of NE Peru based on $\delta^{18}\text{O}$ speleothem records. *Quaternary Science Reviews*, **146**, 274–287.
- Calegari, M. R., Madella, M., Vidal-Torrado, P., Pessenda, L. C. R., & Marques, F. A. (2013). Combining phytoliths and $\delta^{13}\text{C}$ matter in Holocene palaeoenvironmental studies of tropical soils: An example of an Oxisol in Brazil. *Quaternary International*, **287**, 47–55.
- Carson, J. F., Mayle, F. E., Whitney, B. S., Iriarte, J., & Soto, J. D. (2016). Pre-Columbian ring ditch construction and land use on a “chocolate forest island” in the Bolivian Amazon. *Journal of Quaternary Science*, **31** (4), 337–347.
- Carson, J. F., Watling, J., Mayle, F. E., et al. (2015). Pre-Columbian land use in the ring-ditch region of the Bolivian Amazon. *The Holocene*, **25** (8), 1285–1300.
- Carson, J. F., Whitney, B. S., Mayle, F. E., et al. (2014). Environmental impact of geometric earthwork construction in pre-Columbian Amazonia. *Proceedings of the National Academy of Sciences*, **111** (29), 10497–10502.
- Carvalho, L., Jones, C., & Liebmann, B. (2004). The South Atlantic convergence zone: Intensity, form, persistence, and relationships with intraseasonal to interannual activity and extreme rainfall. *Journal of Climate*, **17** (1), 88–108.
- Cassino, R. F., & Meyer, K. E. B. (2013). Reconstituição paleoambiental do Chapadão dos Gerais (Quaternário tardio) a partir da análise palinológica da Vereda Laçador, Minas Gerais, Brasil. *Revista Brasileira De Paleontologia*, **16** (1), 127–146.
- Castanho, A. D. A., Coe, M. T., Costa, M. H., Malhi, Y., Galbraith, D. R., & Quesada, C. A. (2013). Improving simulated Amazon forest biomass and productivity by including spatial variation in biophysical parameters. *Biogeosciences*, **10** (4), 2255–2272.
- Cavaleri, M. A., Coble, A. P., Ryan, M. G., Bauerle, W. L., Loescher, H. W., & Oberbauer, S. F. (2017). Tropical rainforest carbon sink declines during El Niño as a result of reduced photosynthesis and increased respiration rates. *New Phytologist*, **216** (1), 136–149.

- Charles-Dominique, P., Blanc, P., Larpin, D., et al. (1998). Forest perturbations and biodiversity during the last ten thousand years in French Guiana. *Acta Oecologica*, **19** (3), 295–302.
- Chen, T.-C., Weng, S.-P., & Schubert, S. (1999). Maintenance of Austral Summertime Upper-Tropospheric Circulation over Tropical South America: The Bolivian High–Nordeste Low System. *Journal of the Atmospheric Sciences*, **56** (13), 2081–2100.
- Cheng, H., Sinha, A., Cruz, F. W., et al. (2013). Climate change patterns in Amazonia and biodiversity. *Nature Communications*, **4** (1411), 1–6.
- Christensen, J. H., Hewitson, B., Busuioc, A., et al. (2007). Regional climate projections. In *Climate Change 2007: The Physical Science Basis. Contribution of Working Group I to the Fourth Assessment Report of the Intergovernmental Panel on Climate Change*, Cambridge, United Kingdom and New York, NY, USA: Cambridge University Press.
- Clark, D. B., Mercado, L. M., Sitch, S., et al. (2011). The Joint UK Land Environment Simulator (JULES), model description – Part 2: Carbon fluxes and vegetation dynamics. *Geoscientific Model Development*, **4** (3), 701–722.
- Cohen, M. C. L., França, M. C., Rossetti, D. de F., et al. (2014a). Landscape evolution during the late Quaternary at the Doce River mouth, Espírito Santo State, Southeastern Brazil. *Palaeogeography, Palaeoclimatology, Palaeoecology*, **415**, 48–58.
- Cohen, M. C. L., Rossetti, D. de F., Pessenda, L. C. R., Friaes, Y. S., & Oliveira, P. E. (2014b). Late Pleistocene glacial forest of Humaitá—Western Amazonia. *Palaeogeography, Palaeoclimatology, Palaeoecology*, **415**, 37–47.
- Colinvaux, P. A., De Oliveira, P. E., & Moreno Patiño, J. E. (1999). Amazon pollen manual and atlas/Manual e atlas palinológico da Amazônia, Amsterdam: Harwood Academic Publishers.
- Colinvaux, P. A., De Oliveira, P. E., Moreno, J. E., & Miller, M. C. (1996). A long pollen record from lowland Amazonia: forest and cooling in glacial times. *Science*, **274** (5284), 85–88.
- Colinvaux, P. A., Miller, M. C., Liu, K. B., SteinitzKannan, M., & Frost, I. (1985). Discovery of Permanent Amazon Lakes and Hydraulic Disturbance in the Upper Amazon Basin. *Nature*, **313** (5997), 42–45.
- Collins, M., Knutti, R., Arblaster, J., et al. (2013). Long-term Climate Change: Projections, Commitments and Irreversibility. In *Climate Change 2013: The Physical Science Basis. Contribution of Working Group I to the Fifth Assessment Report of the Intergovernmental Panel on Climate Change*, Cambridge, United Kingdom and New York, NY, USA: Cambridge University Press.
- Collins, W. J., Bellouin, N., Doutriaux-Boucher, M., et al. (2011). Development and evaluation of an Earth-System model - HadGEM2. *Geoscientific Model Development*, **4** (4), 1051–1075.

- Condit, R., Aguilar, S., Hernandez, A., et al. (2004). Tropical forest dynamics across a rainfall gradient and the impact of an El Niño dry season. *Journal of Tropical Ecology*, **20** (1), 51–72.
- Cook, B., Zeng, N., & Yoon, J.-H. (2012). Will Amazonia Dry Out? Magnitude and Causes of Change from IPCC Climate Model Projections. *Earth Interactions*, **16** (3), 1–27.
- Cordeiro, R. C., Turcq, B., Suguio, K., Oliveira da Silva, A., Sifeddine, A., & Volkmer-Ribeiro, C. (2008). Holocene fires in East Amazonia (Carajás), new evidences, chronology and relation with paleoclimate. *Global and Planetary Change*, **61** (1-2), 49–62.
- Costa, L. P. (2003). The historical bridge between the Amazon and the Atlantic Forest of Brazil: a study of molecular phylogeography with small mammals. *Journal of Biogeography*, **30** (1), 71–86.
- Costa, M. H., & Foley, J. A. (2000). Combined Effects of Deforestation and Doubled Atmospheric CO₂ Concentrations on the Climate of Amazonia. *Journal of Climate*, **13** (1), 18–34.
- Cowling, S. A., & Shin, Y. (2006). Simulated ecosystem threshold responses to co-varying temperature, precipitation and atmospheric CO₂ within a region of Amazonia. *Global Ecology and Biogeography*, **15**, 553–566.
- Cox, P. M., Betts, R. A., Collins, M., Harris, P. P., Huntingford, C., & Jones, C. D. (2004). Amazonian forest dieback under climate-carbon cycle projections for the 21st century. *Theoretical and Applied Climatology*, **78**, 137–156.
- Cox, P. M., Betts, R. A., Jones, C. D., Spall, S. A., & Totterdell, I. J. (2000). Acceleration of global warming due to carbon-cycle feedbacks in a coupled climate model. *Nature*, **408** (9), 184–187.
- Cross, S. L., Baker, P. A., Seltzer, G. O., Fritz, S. C., & Dunbar, R. B. (2000). A new estimate of the Holocene lowstand level of Lake Titicaca, central Andes, and implications for tropical palaeohydrology. *The Holocene*, **10** (1), 21–32.
- Cruz, F. W., Burns, S. J., Karmann, I., et al. (2005). Insolation-driven changes in atmospheric circulation over the past 116,000 years in subtropical Brazil. *Nature*, **434** (7029), 63–66.
- Cruz, F. W., Burns, S. J., Karmann, I., Sharp, W. D., & Vuille, M. (2006a). Reconstruction of regional atmospheric circulation features during the late Pleistocene in subtropical Brazil from oxygen isotope composition of speleothems. *Earth and Planetary Science Letters*, **248** (1-2), 495–507.
- Cruz, F. W., Burns, S. J., Karmann, I., Sharp, W. D., Vuille, M., & Ferrari, J. A. (2006b). A stalagmite record of changes in atmospheric circulation and soil processes in the Brazilian subtropics during the Late Pleistocene. *Quaternary Science Reviews*, **25** (21-22), 2749–2761.
- Cruz, F. W., Vuille, M., Burns, S. J., et al. (2009). Orbitally driven east-west antiphasing of South American precipitation. *Nature Geoscience*, **2** (3), 210–214.

- Cubasch, U., Wuebbles, D., Chen, D., et al. (2013). Introduction. In *Climate Change 2013: The Physical Science Basis. Contribution of Working Group I to the Fifth Assessment Report of the Intergovernmental Panel on Climate Change*, Cambridge, United Kingdom and New York, NY, USA: Cambridge University Press.
- Curtis, J. H., Brenner, M., & Hodell, D. A. (1999). Climate change in the Lake Valencia Basin, Venezuela, ~12600 yr BP to present. *The Holocene*, **9** (5), 609–619.
- Cutler, D. R., Edwards, T. C., Beard, K. H., et al. (2007). Random forests for classification in ecology. *Ecology*, **88** (11), 2783–2792.
- Davis, B. A. S., Brewer, S., Stevenson, A. C., & Guiot, J. (2003). The temperature of Europe during the Holocene reconstructed from pollen data. *Quaternary Science Reviews*, **22** (15-17), 1701–1716.
- Davis, M. B. (2000). Palynology after Y2K - Understanding the source area of pollen in sediments. *Annual Review of Earth and Planetary Sciences*, **28**, 1–18.
- de Freitas, H. A., Pessenda, L. C. R., Aravena, R., Gouveia, S. E. M., de Souza Ribeiro, A., & Boulet, R. (2001). Late Quaternary Vegetation Dynamics in the Southern Amazon Basin Inferred from Carbon Isotopes in Soil Organic Matter. *Quaternary Research*, **55** (1), 39–46.
- De Oliveira, P. E., Barreto, A. M. F., & Suguio, K. (1999). Late Pleistocene/Holocene climatic and vegetational history of the Brazilian caatinga: the fossil dunes of the middle São Francisco River. *Palaeogeography, Palaeoclimatology, Palaeoecology*, **152** (3-4), 319–337.
- Dean, W. E. (1974). Determination of carbonate and organic matter in calcareous sediments and sedimentary rocks by loss on ignition; comparison with other methods. *Journal of Sedimentary Research*, **44** (1), 242–248.
- Dickau, R. E., Whitney, B. S., Iriarte, J., et al. (2013). Differentiation of neotropical ecosystems by modern soil phytolith assemblages and its implications for palaeoenvironmental and archaeological reconstructions. *Review of Palaeobotany and Palynology*, **193**, 1–23.
- Dirzo, R., & Raven, P. H. (2003). Global state of biodiversity and loss. *Annual Review of Environment and Resources*, **28**, 137–167.
- Doughty, C. E., Metcalfe, D. B., Girardin, C. A. J., et al. (2015). Drought impact on forest carbon dynamics and fluxes in Amazonia. *Nature*, **519** (7541), 78–82.
- Duffy, P. B., Brando, P. M., Asner, G. P., & Field, C. B. (2015). Projections of future meteorological drought and wet periods in the Amazon. *Proceedings of the National Academy of Sciences*, **112** (43), 13172–13177.
- Dümic, A., Schad, P., Rumpel, C., Dignac, M.-F., & Kögel-Knabner, I. (2008). Araucaria forest expansion on grassland in the southern Brazilian highlands as revealed by ¹⁴C and ^δ13C studies. *Geoderma*, **145** (1-2), 143–157.

- Eltahir, E., & Bras, R. L. (1994). Precipitation recycling in the Amazon basin. *Quaternary Journal of the Royal Meteorological Society*, **120**, 861–880.
- Enters, D., Behling, H., Mayr, C., Dupont, L., & Zolitschka, B. (2010). Holocene environmental dynamics of south-eastern Brazil recorded in laminated sediments of Lago Aleixo. *Journal of Paleolimnology*, **44** (1), 265–277.
- Eva, H. D., Huber, O., Achard, F., et al. (2005). A proposal for defining the geographical boundaries of Amazonia: Synthesis of the results from an Expert Consultation Workshop organized by the European Commission in collaboration with the Amazon Cooperation Treaty Organization - JRC Ispra, 7-8 June 2005, Luxembourg: Luxembourg: Office for Official Publications of the European Communities.
- Eyring, V., Bony, S., Meehl, G. A., et al. (2016). Overview of the Coupled Model Intercomparison Project Phase 6 (CMIP6) experimental design and organization. *Geoscientific Model Development*, **9** (5), 1937–1958.
- Faegri, K., & Iversen, J. (1989). Textbook of pollen analysis, Chichester: Wiley.
- Feldpausch, T. R., Phillips, O. L., Brienen, R. J. W., et al. (2016). Amazon forest response to repeated droughts. *Biogeosciences*, **30** (7), 964–982.
- Fisher, R. A., McDowell, N., Purves, D., et al. (2010). Assessing uncertainties in a second-generation dynamic vegetation model caused by ecological scale limitations. *New Phytologist*, **187** (3), 666–681.
- Fisher, R. A., Williams, M., Lola da Costa, A., et al. (2007). The response of an Eastern Amazonian rain forest to drought stress: results and modelling analyses from a throughfall exclusion experiment. *Global Change Biology*, **13** (11), 2361–2378.
- Flantua, S. G. A., Hooghiemstra, H., Grimm, E. C., et al. (2015). Updated site compilation of the Latin American Pollen Database. *Review of Palaeobotany and Palynology*, **223**, 104–115.
- Flantua, S. G. A., Hooghiemstra, H., Vuille, M., et al. (2016). Climate variability and human impact in South America during the last 2000 years: synthesis and perspectives from pollen records. *Climate of the Past*, **12** (2), 483–523.
- Flato, G. M. (2011). Earth system models: an overview. *Wiley Interdisciplinary Reviews: Climate Change*, **2** (6), 783–800.
- Flato, G. M., Marotzke, J., Abiodun, B., et al. (2013). Evaluation of Climate Models. In *Climate Change 2013: The Physical Science Basis. Contribution of Working Group I to the Fifth Assessment Report of the Intergovernmental Panel on Climate Change*.
- Foley, J. A., Prentice, I. C., Ramankutty, N., et al. (1996). An integrated biosphere model of land surface processes, terrestrial carbon balance, and vegetation dynamics. *Global Biogeochemical Cycles*, **10** (4), 603–628.
- Fontes, D., Cordeiro, R. C., Martins, G. S., et al. (2017). Paleoenvironmental dynamics in South Amazonia, Brazil, during the last 35,000 years inferred from pollen and geochemical records of Lago do Saci. *Quaternary Science Reviews*, **173**, 161–180.

- Gajewski, K. (2008). The Global Pollen Database in biogeographical and palaeoclimatic studies. *Progress in Physical Geography*, **32** (4), 379–402.
- Galbraith, D. R., Levy, P. E., Sitch, S., et al. (2010). Multiple mechanisms of Amazonian forest biomass losses in three dynamic global vegetation models under climate change. *New Phytologist*, **187** (3), 647–665.
- Gallimore, R., Jacob, R., & Kutzbach, J. (2005). Coupled atmosphere-ocean-vegetation simulations for modern and mid-Holocene climates: role of extratropical vegetation cover feedbacks. *Climate Dynamics*, **25** (7-8), 755–776.
- Garreaud, R. D., Vuille, M., Compagnucci, R., & Marengo, J. A. (2009). Present-day South American climate. *Palaeogeography, Palaeoclimatology, Palaeoecology*, **281** (3-4), 180–195.
- Gash, J. H. C., Huntingford, C., Marengo, J. A., et al. (2004). Amazonian climate: results and future research. *Theoretical and Applied Climatology*, **78** (1-3), 1–7.
- Gatti, L. V., Gloor, M., Miller, J. B., et al. (2014). Drought sensitivity of Amazonian carbon balance revealed by atmospheric measurements. *Nature*, **506** (7486), 76–80.
- Gentry, A. H. (1995). Diversity and floristic composition of neotropical dry forests. In S. H. Bullock, H. A. Mooney, & E. Medina, *Seasonally Dry Tropical Forests*, Cambridge, United Kingdom: Cambridge University Press, pp. 146–194.
- Giorgi, F., & Francisco, R. (2000). Evaluating uncertainties in the prediction of regional climate change. *Geophysical Research Letters*, **27** (9), 1295–1298.
- Glaser, B., & Woods, W. I. (2004). Amazonian dark earths: explorations in space and time, New York: Springer-Verlag.
- Gond, V. R., Freycon, V., Molino, J.-F., et al. (2011). Broad-scale spatial pattern of forest landscape types in the Guiana Shield. *International Journal of Applied Earth Observations and Geoinformation*, **13** (3), 357–367.
- Good, P., Jones, C., Lowe, J., Betts, R. A., & Gedney, N. (2013). Comparing Tropical Forest Projections from Two Generations of Hadley Centre Earth System Models, HadGEM2-ES and HadCM3LC. *Journal of Climate*, **26** (2), 495–511.
- Gordon, H. B., O'Farrell, S. P., Collier, M. A., et al. (2010). *The CSIRO Mk3.5 Climate Model*, Aspendale, Victoria, Australia: The Centre for Australian Weather and Climate Research Technical Report No. 21.
- Gordon, H. B., Rotstayn, L. D., McGregor, J. L., et al. (2002). *The CSIRO Mk3 Climate System Model*, Aspendale, Victoria, Australia: CSIRO Atmospheric Research Technical Paper No. 60.
- Gosling, W. D., Mayle, F. E., Tate, N. J., & Killeen, T. J. (2005). Modern pollen-rain characteristics of tall terra firme moist evergreen forest, southern Amazonia. *Quaternary Research*, **64** (3), 284–297.

- Gosling, W. D., Mayle, F. E., Tate, N. J., & Killeen, T. J. (2009). Differentiation between Neotropical rainforest, dry forest, and savannah ecosystems by their modern pollen spectra and implications for the fossil pollen record. *Review of Palaeobotany and Palynology*, **153** (1-2), 70–85.
- Gouveia, S. E. M., Pessenda, L. C. R., Aravena, R., et al. (2002). Carbon isotopes in charcoal and soils in studies of paleovegetation and climate changes during the late Pleistocene and the Holocene in the southeast and centerwest regions of Brazil. *Global and Planetary Change*, **33** (1-2), 95–106.
- Graham, E. A., Mulkey, S. S., Kitajima, K., Phillips, N. G., & Wright, S. J. (2003). Cloud cover limits net CO₂ uptake and growth of a rainforest tree during tropical rainy seasons. *Proceedings of the National Academy of Sciences*, **100** (2), 572–576.
- Grimm, E. C. (1987). CONISS: a FORTRAN 77 program for stratigraphically constrained cluster analysis by the method of incremental sum of squares. *Computers & Geosciences*, **13** (1), 13–35.
- Guimarães, J. T. F., Cohen, M. C. L., França, M. C., et al. (2013a). An integrated approach to relate Holocene climatic, hydrological, morphological and vegetation changes in the southeastern Amazon region. *Vegetation History and Archaeobotany*, **22** (3), 185–198.
- Guimarães, J. T. F., Cohen, M. C. L., França, M. C., Pessenda, L. C. R., & Behling, H. (2013b). Morphological and vegetation changes on tidal flats of the Amazon Coast during the last 5000 cal. yr BP. *The Holocene*, **23** (4), 528–543.
- Guimarães, J. T. F., Cohen, M. C. L., Pessenda, L. C. R., França, M. C., Smith, C. B., & Nogueira, A. C. R. (2012). Mid- and late-Holocene sedimentary process and palaeovegetation changes near the mouth of the Amazon River. *The Holocene*, **22** (3), 359–370.
- Guimarães, J. T. F., Souza-Filho, P. W. M., Alves, R., et al. (2014). Source and distribution of pollen and spores in surface sediments of a plateau lake in southeastern Amazonia. *Quaternary International*, **352**, 181–196.
- Harper, A. B., Baker, I. T., Denning, A. S., Randall, D. A., Dazlich, D., & Branson, M. (2014). Impact of Evapotranspiration on Dry Season Climate in the Amazon Forest. *Journal of Climate*, **27** (2), 574–591.
- Harris, I. C., & Jones, P. D. (2017). University of East Anglia Climatic Research Unit. CRU TS4.01: Climatic Research Unit (CRU) Time-Series (TS) version 4.01 of high-resolution gridded data of month-by-month variation in climate (Jan. 1901- Dec. 2016). Centre for Environmental Data Analysis.
- Harris, I. C., Jones, P. D., Osborn, T. J., & Lister, D. H. (2014). Updated high-resolution grids of monthly climatic observations - the CRU TS3.10 Dataset. *International Journal of Climatology*, **34** (3), 623–642.
- Harrison, S. P., & Prentice, I. C. (2003). Climate and CO₂ controls on global vegetation distribution at the last glacial maximum: analysis based on palaeovegetation data, biome modelling and palaeoclimate simulations. *Global Change Biology*, **9** (7), 983–1004.

- Harrison, S. P., Jolly, D., Laarif, F., et al. (1998). Intercomparison of simulated global vegetation distribution in response to 6 kyr BP orbital forcing. *Journal of Climate*, **11** (11), 2721–2742.
- Harrison, S. P., Bartlein, P. J., Izumi, K., et al. (2015). Evaluation of CMIP5 palaeo-simulations to improve climate projections. *Nature Climate Change*, **5** (8), 735–743.
- Harrison, S. P., Braconnot, P., Joussaume, S., Hewitt, C., & Stouffer, R. J. (2002). Fourth International Workshop of the Palaeoclimate Modelling Intercomparison Project (PMIP): Launching PMIP2 Phase II. *Eos*, **83** (40), 447.
- Haug, G. H., Hughen, K. A., Sigman, D. M., Peterson, L. C., & Röhl, U. (2001). Southward migration of the intertropical convergence zone through the Holocene. *Science*, **293** (5533), 1304–1308.
- Heckenberger, M., & Neves, E. G. (2009). Amazonian Archaeology. *Annual Review of Anthropology*, **38** (1), 251–266.
- Heiri, O., Lotter, A. F., & Lemcke, G. (2001). Loss on ignition as a method for estimating organic and carbonate content in sediments: reproducibility and comparability of results. *Journal of Paleolimnology*, **25** (1), 101–110.
- Hermanowski, B., da Costa, M. L., & Behling, H. (2012a). Environmental changes in southeastern Amazonia during the last 25,000yr revealed from a paleoecological record. *Quaternary Research*, **77** (1), 138–148.
- Hermanowski, B., da Costa, M. L., & Behling, H. (2014). Possible linkages of palaeofires in southeast Amazonia to a changing climate since the Last Glacial Maximum. *Vegetation History and Archaeobotany*, **24** (2), 279–292.
- Hermanowski, B., da Costa, M. L., Carvalho, A. T., & Behling, H. (2012b). Palaeoenvironmental dynamics and underlying climatic changes in southeast Amazonia (Serra Sul dos Carajás, Brazil) during the late Pleistocene and Holocene. *Palaeogeography, Palaeoclimatology, Palaeoecology*, **365-366**, 227–246.
- Heyer, J. P., Power, M. J., Field, R. D., & van Marle, M. J. E. (2018). The impacts of recent drought on fire, forest loss, and regional smoke emissions in lowland Bolivia. *Biogeosciences*, **15** (14), 4317–4331.
- Hodnett, M. G., & Tomasella, J. (2002). Marked differences between van Genuchten soil water-retention parameters for temperate and tropical soils: a new water-retention pedo-transfer functions developed for tropical soils. *Geoderma*, **108** (3-4), 155–180.
- Hogg, A. G., Hua, Q., Blackwell, P. G., Niu, M., & Buck, C. E. (2013). SHCal13 Southern Hemisphere calibration, 0–50,000 years cal BP. *Radiocarbon*, **55** (4), 1889–1903.
- Horák, I., Vidal-Torrado, P., Silva, A. C., & Pessenda, L. C. R. (2011). Pedological and isotopic relations of a highland tropical peatland, Mountain Range of the Espinhaço Meridional (Brazil). *Revista Brasileira De Ciência Do Solo*, **35** (1), 41–52.
- Horbe, A. M. C., Behling, H., Nogueira, A. C. R., & Mapes, R. (2011). Environmental changes in the western Amazônia: morphological framework, geochemistry, palynology

- and radiocarbon dating data. *Annals of the Brazilian Academy of Sciences*, **83** (3), 863–874.
- Hueck, K. (1953). Distribuição e habitat natural do Pinheiro do Paraná (*Araucaria angustifolia*). *Boletim Da Faculdade De Filosofia, Ciências E Letras, Universidade De São Paulo. Botânica*, **10**, 1–24.
- Huete, A. R., Didan, K., Shimabukuro, Y. E., et al. (2006). Amazon rainforests green-up with sunlight in dry season. *Geophysical Research Letters*, **33** (6), 981–4.
- Huffman, G. J., Bolvin, D. T., Nelkin, E. J., et al. (2007). The TRMM Multisatellite Precipitation Analysis (TMPA): Quasi-Global, Multiyear, Combined-Sensor Precipitation Estimates at Fine Scales. *Journal of Hydrometeorology*, **8** (1), 38–55.
- Huntingford, C., Fisher, R. A., Mercado, L. M., et al. (2008). Towards quantifying uncertainty in predictions of Amazon “dieback.” *Philosophical Transactions of the Royal Society B: Biological Sciences*, **363** (1498), 1857–1864.
- Huntingford, C., Harris, P. P., Gedney, N., et al. (2004). Using a GCM analogue model to investigate the potential for Amazonian forest dieback. *Theoretical and Applied Climatology*, **78**, 177–185.
- Huntingford, C., Zelazowski, P., Galbraith, D. R., et al. (2013). Simulated resilience of tropical rainforests to CO₂-induced climate change. *Nature Geoscience*, **6** (4), 268–273.
- Indermühle, A., Stocker, T. F., Joos, F., et al. (1999). Holocene carbon-cycle dynamics based on CO₂ trapped in ice at Taylor Dome, Antarctica. *Nature*, **398** (6723), 121–126.
- Iriarte, J., & Behling, H. (2007). The expansion of *Araucaria* forest in the southern Brazilian highlands during the last 4000 years and its implications for the development of the Taquara/Itararé tradition. *Environmental Archaeology*, **12** (2), 115–127.
- Iriarte, J., DeBlasis, P., Souza, J. G., & Corteletti, R. (2017). Emergent Complexity, Changing Landscapes, and Spheres of Interaction in Southeastern South America During the Middle and Late Holocene. *Journal of Archaeological Research*, **25** (3), 251–313.
- Iriarte, J., Smith, R. J., Gregorio de Souza, J., et al. (2017). Out of Amazonia: Late-Holocene climate change and the Tupi–Guarani trans-continental expansion. *The Holocene*, **27** (7), 967–975.
- Irion, G., Bush, M. B., Nunes de Mello, J. A., et al. (2006). A multiproxy palaeoecological record of Holocene lake sediments from the Rio Tapajós, eastern Amazonia. *Palaeogeography, Palaeoclimatology, Palaeoecology*, **240** (3-4), 523–535.
- Jacobson, G. L., & Bradshaw, R. H. W. (1981). The Selection of Sites for Paleovegetational Studies. *Quaternary Research*, **16** (1), 80–96.
- Jansen, E., Overpeck, J., Briffa, K. R., et al. (2007). Palaeoclimate. In *Climate Change 2007: The Physical Science Basis. Contribution of Working Group I to the Fourth Assessment Report of the Intergovernmental Panel on Climate Change*, Cambridge, United Kingdom and New York, NY, USA: Cambridge University Press.

- Jeffrey, S. J., Rotstayn, L. D., & Collier, M. A. (2013). Australia's CMIP5 submission using the CSIRO Mk3. 6 model. *Australian Meteorological and Oceanographic Journal*, **63**, 1–13.
- Jeske-Pieruschka, V., & Behling, H. (2011). Palaeoenvironmental history of the São Francisco de Paula region in southern Brazil during the late Quaternary inferred from the Rincão das Cabritas core. *The Holocene*, **22** (11), 1251–1262.
- Jeske-Pieruschka, V., Fidelis, A., Bergamin, R. S., Vélez, E., & Behling, H. (2010). Araucaria forest dynamics in relation to fire frequency in southern Brazil based on fossil and modern pollen data. *Review of Palaeobotany and Palynology*, **160** (1-2), 53–65.
- Jeske-Pieruschka, V., Pillar, V. D., De Oliveira, M. A. T., & Behling, H. (2012). New insights into vegetation, climate and fire history of southern Brazil revealed by a 40,000 year environmental record from the State Park Serra do Tabuleiro. *Vegetation History and Archaeobotany*, **22** (4), 299–314.
- Joetzjer, E., Douville, H., Delire, C., & Ciais, P. (2013). Present-day and future Amazonian precipitation in global climate models: CMIP5 versus CMIP3. *Climate Dynamics*, **41** (11-12), 2921–2936.
- Jones, H. T., Mayle, F. E., Pennington, R. T., & Killeen, T. J. (2011). Characterisation of Bolivian savanna ecosystems by their modern pollen rain and implications for fossil pollen records. *Review of Palaeobotany and Palynology*, **164** (3-4), 223–237.
- Joussaume, S., & Taylor, K. E. (1995). Status of the Paleoclimate Modeling Intercomparison Project (PMIP). In *Proceedings of the First International AMIP Scientific Conference, WCRP-92 Report*, pp. 425–430.
- Juggins, S. (2017). rioja: analysis of quaternary science data. R package version 0.9-15.1. Retrieved from <http://cran.r-project.org/package=rioja>
- Kageyama, M., Braconnot, P., Bopp, L., et al. (2013a). Mid-Holocene and last glacial maximum climate simulations with the IPSL model: part II: model-data comparisons. *Climate Dynamics*, **40** (9-10), 2469–2495.
- Kageyama, M., Braconnot, P., Bopp, L., et al. (2013b). Mid-Holocene and Last Glacial Maximum climate simulations with the IPSL model—part I: comparing IPSL_CM5A to IPSL_CM4. *Climate Dynamics*, **40** (9-10), 2447–2468.
- Kanner, L. C., Burns, S. J., Cheng, H., Edwards, R. L., & Vuille, M. (2013). High-resolution variability of the South American summer monsoon over the last seven millennia: insights from a speleothem record from the central Peruvian Andes. *Quaternary Science Reviews*, **75**, 1–10.
- Kelley, D. I., Prentice, I. C., Harrison, S. P., et al. (2013). A comprehensive benchmarking system for evaluating global vegetation models. *Biogeosciences*, **10** (5), 3313–3340.
- Killeen, T. J., & Schulenberg, T. S. (Eds.). (1998). A biological assessment of Parque Nacional Noel Kempff Mercado, Bolivia. Rapid Assessment Program Working Papers 10, Washington, D.C., USA: Conservation International.

- Killeen, T. J., Douglas, M., Consiglio, T., Jørgensen, P. M., & Mejia, J. (2007). Dry spots and wet spots in the Andean hotspot. *Journal of Biogeography*, **34** (8), 1357–1373.
- Killeen, T. J., Jardim, A., Mamani, F., & Rojas, N. (1998). Diversity, composition and structure of a tropical semideciduous forest in the Chiquitanía region of Santa Cruz, Bolivia. *Journal of Tropical Ecology*, **14** (6), 803–827.
- Killeen, T. J., Siles, T. M., Grimwood, T., et al. (2003). Habitat heterogeneity on a forest-savanna ecotone in Noel Kempff Mercado National Park (Santa Cruz, Bolivia): implications for the long-term conservation of biodiversity in a changing climate. In *How Landscapes Change. Ecological Studies (Analysis and Synthesis)*, Springer, pp. 285–312.
- Kipnis, R., Caldarelli, S. B., & de Oliveira, W. C. (2005). Contribuição para a cronologia da colonização amazônica e suas implicações teóricas. *Revista De Arqueologia*, **18**, 81–93.
- Kohfeld, K. E., & Harrison, S. P. (2000). How well can we simulate past climates? Evaluating the models using global palaeoenvironmental datasets. *Quaternary Science Reviews*, **19** (1-5), 321–346.
- Koutavas, A., & Joannides, S. (2012). El Niño-Southern Oscillation extrema in the Holocene and Last Glacial Maximum. *Paleoceanography*, **27** (4), 1–15.
- Kucharik, C. J., Foley, J. A., Delire, C., et al. (2000). Testing the performance of a dynamic global ecosystem model: water balance, carbon balance, and vegetation structure. *Global Biogeochemical Cycles*, **14** (3), 795–825.
- Lachniet, M. S. (2009). Climatic and environmental controls on speleothem oxygen-isotope values. *Quaternary Science Reviews*, **28** (5-6), 412–432.
- Langan, L., Higgins, S. I., & Scheiter, S. (2017). Climate-biomes, pedo-biomes or pyro-biomes: which world view explains the tropical forest-savanna boundary in South America? *Journal of Biogeography*, **44** (10), 2319–2330.
- Lapola, D. M., Oyama, M. D., & Nobre, C. A. (2009). Exploring the range of climate biome projections for tropical South America: The role of CO₂ fertilization and seasonality. *Biogeosciences*, **23** (3), 1–16.
- Latrubesse, E. M. (2012). Amazon Lakes. In *Encyclopedia of Lakes and Reservoirs*, Springer, pp. 13–26.
- Laurance, W. F., Delamônica, P., Laurance, S. G. W., Vasconcelos, H. L., & Lovejoy, T. E. (2000). Rainforest fragmentation kills big trees. *Nature*, **404** (6780), 836–836.
- Leal, M. G., & Lorscheitter, M. L. (2007). Plant succession in a forest on the Lower Northeast Slope of Serra Geral, Rio Grande do Sul, and Holocene palaeoenvironments, Southern Brazil. *Acta Botanica Brasilica*, **21** (1), 1–10.
- Ledru, M.-P. (1993). Late Quaternary Environmental and Climatic Changes in Central Brazil. *Quaternary Research*, **39** (1), 90–98.

- Ledru, M.-P. (2001). Late Holocene rainforest disturbance in French Guiana. *Review of Palaeobotany and Palynology*, **115** (3-4), 161–176.
- Ledru, M.-P., Bertaux, J., Sifeddine, A., & Suguio, K. (1998). Absence of Last Glacial Maximum Records in Lowland Tropical Forests. *Quaternary Research*, **49** (2), 233–237.
- Ledru, M.-P., Ceccantini, G., Gouveia, S. E. M., López-Sáez, J. A., Pessenda, L. C. R., & Ribeiro, A. S. (2006). Millennial-scale climatic and vegetation changes in a northern Cerrado (Northeast, Brazil) since the Last Glacial Maximum. *Quaternary Science Reviews*, **25** (9-10), 1110–1126.
- Ledru, M.-P., Mourguiart, P., & Riccomini, C. (2009). Related changes in biodiversity, insolation and climate in the Atlantic rainforest since the last interglacial. *Palaeogeography, Palaeoclimatology, Palaeoecology*, **271** (1-2), 140–152.
- Ledru, M.-P., Rousseau, D. D., Cruz, F. W., Riccomini, C., Karmann, I., & Martin, L. (2005). Paleoclimate changes during the last 100,000 yr from a record in the Brazilian Atlantic rainforest region and interhemispheric comparison. *Quaternary Research*, **64** (3), 444–450.
- Leonhardt, A., & Lorscheitter, M. L. (2010). The last 25,000 years in the Eastern Plateau of Southern Brazil according to Alpes de São Francisco record. *Journal of South American Earth Sciences*, **29** (2), 454–463.
- Levine, N. M., Zhang, K., Longo, M., et al. (2016). Ecosystem heterogeneity determines the ecological resilience of the Amazon to climate change. *Proceedings of the National Academy of Sciences*, **113** (3), 793–797.
- Li, W., Fu, R., & Dickinson, R. E. (2006). Rainfall and its seasonality over the Amazon in the 21st century as assessed by the coupled models for the IPCC AR4. *Journal of Geophysical Research*, **111** (D2), D02111.
- Liu, K.-B., & Colinvaux, P. A. (1988). A 5200-Year History of Amazon Rain Forest. *Journal of Biogeography*, **15** (2), 231–248.
- Llopart, M., Coppola, E., Giorgi, F., da Rocha, R. P., & Cuadra, S. V. (2014). Climate change impact on precipitation for the Amazon and La Plata basins. *Climatic Change*, **125** (1), 111–125.
- Lloyd, J., & Farquhar, G. D. (2008). Effects of rising temperatures and [CO₂] on the physiology of tropical forest trees. *Philosophical Transactions of the Royal Society B: Biological Sciences*, **363** (1498), 1811–1817.
- Lorente, F. L., Buso Junior, A. A., De Oliveira, P. E., & Pessenda, L. C. R. (2017). Atlas Palinológico. Laboratório C14 - CENA/USP, Piracicaba: Fundação de Estudos Agrários Luiz de Queiroz (FEALQ).
- Lorente, F. L., Pessenda, L. C. R., Oboh-Ikuenobe, F., et al. (2014). Palynofacies and stable C and N isotopes of Holocene sediments from Lake Macuco (Linhares, Espírito Santo, southeastern Brazil): Depositional settings and palaeoenvironmental evolution. *Palaeogeography, Palaeoclimatology, Palaeoecology*, **415**, 69–82.

- Macedo, R. B., Souza, P. A., Bauermann, S. G., & Bordignon, S. A. L. (2010). Palynological analysis of a late Holocene core from Santo Antônio da Patrulha, Rio Grande do Sul, Southern Brazil. *82* (3), 731–745.
- Maezumi, S. Y., Alves, D., Robinson, M., et al. (2018a). The legacy of 4,500 years of polyculture agroforestry in the eastern Amazon. *Nature Plants*, *4* (8), 540–547.
- Maezumi, S. Y., Power, M. J., Mayle, F. E., McLauchlan, K. K., & Iriarte, J. (2015). Effects of past climate variability on fire and vegetation in the cerrádo savanna of the Huanchaca Mesetta, NE Bolivia. *Climate of the Past*, *11* (6), 835–853.
- Maezumi, S. Y., Whitney, B. S., Mayle, F. E., de Souza, J. G., & Iriarte, J. (2018b). Reassessing climate and pre-Columbian drivers of paleofire activity in the Bolivian Amazon. *Quaternary International*, *488*, 81–94.
- Malhi, Y., & Wright, J. (2004). Spatial patterns and recent trends in the climate of tropical rainforest regions. *Philosophical Transactions of the Royal Society B: Biological Sciences*, *359* (1443), 311–329.
- Malhi, Y., Aragão, L. E. O. C., Galbraith, D. R., et al. (2009). Exploring the likelihood and mechanism of a climate-change-induced dieback of the Amazon rainforest. *Proceedings of the National Academy of Sciences*, *106* (49), 20610–20615.
- Malhi, Y., Phillips, O. L., Lloyd, J., et al. (2002). An international network to monitor the structure, composition and dynamics of Amazonian forests (RAINFOR). *Journal of Vegetation Science*, *13* (3), 439–450.
- Malhi, Y., Roberts, J. T., Betts, R. A., Killeen, T. J., Li, W., & Nobre, C. A. (2008). Climate change, deforestation, and the fate of the Amazon. *Science*, *319* (5860), 169–172.
- Marchant, R., Cleef, A., Harrison, S. P., et al. (2009). Pollen-based biome reconstructions for Latin America at 0, 6000 and 18 000 radiocarbon years ago. *Climate of the Past*, *5* (1), 725–767.
- Marengo, J. A., Douglas, M. W., & Dias, P. L. S. (2002). The South American low-level jet east of the Andes during the 1999 LBA-TRMM and LBA-WET AMC campaign. *Journal of Geophysical Research*, *107* (D20), 8079.
- Marthews, T. R., Quesada, C. A., Galbraith, D. R., et al. (2014). High-resolution hydraulic parameter maps for surface soils in tropical South America. *Geoscientific Model Development*, *7* (3), 711–723.
- Marti, O., Braconnot, P., Dufresne, J. L., et al. (2010). Key features of the IPSL ocean atmosphere model and its sensitivity to atmospheric resolution. *Climate Dynamics*, *34* (1), 1–26.
- Martin, G. M., Bellouin, N., Collins, W. J., et al. (2011). The HadGEM2 family of Met Office Unified Model climate configurations. *Geoscientific Model Development*, *4* (3), 723–757.
- Masson-Delmotte, V., Schulz, M., Abe-Ouchi, A., et al. (2013). Information from Paleoclimate Archives. In *Climate Change 2013: The Physical Science Basis*.

- Contribution of Working Group I to the Fifth Assessment Report of the Intergovernmental Panel on Climate Change*, Cambridge, United Kingdom and New York, NY, USA: Cambridge University Press.
- May, P. H., Soares-Filho, B. S., & Strand, J. (2013). *How Much is the Amazon Worth? The State of Knowledge concerning the Value of Preserving Amazon Rainforests*, The World Bank.
- Mayle, F. E., & Power, M. J. (2008). Impact of a drier Early-Mid-Holocene climate upon Amazonian forests. *Philosophical Transactions of the Royal Society B: Biological Sciences*, **363** (1498), 1829–1838.
- Mayle, F. E., Burbidge, R. E., & Killeen, T. J. (2000). Millennial-scale dynamics of southern Amazonian rain forests. *Science*, **290** (5500), 2291–2294.
- Mayle, F. E., Langstroth, R. P., Fisher, R. A., & Meir, P. (2007). Long-term forest-savannah dynamics in the Bolivian Amazon: implications for conservation. *Philosophical Transactions of the Royal Society B: Biological Sciences*, **362** (1478), 291–307.
- McCormac, F. G., Hogg, A. G., Blackwell, P. G., & Buck, C. E. (2004). SHCal04 Southern Hemisphere calibration, 0–11.0 cal kyr BP. *Radiocarbon*, **46** (3), 1087–1092.
- McMichael, C. N. H., Bush, M. B., Piperno, D. R., Silman, M. R., Zimmerman, A. R., & Anderson, C. (2012). Spatial and temporal scales of pre-Columbian disturbance associated with western Amazonian lakes. *The Holocene*, **22** (2), 131–141.
- Meave, J., & Kellman, M. (1994). Maintenance of Rain-Forest Diversity in Riparian Forests of Tropical Savannas - Implications for Species Conservation During Pleistocene Drought. *Journal of Biogeography*, **21** (2), 121–135.
- Meave, J., Kellman, M., MacDougall, A., & Rosales, J. (1991). Riparian Habitats as Tropical Forest Refugia. *Global Ecology and Biogeography Letters*, **1** (3), 69–76.
- Meehl, G. A., Stocker, T. F., Collins, W. D., et al. (2007). Global climate projections. In *Climate Change 2007: The Physical Science Basis. Contribution of Working Group I to the Fourth Assessment Report of the Intergovernmental Panel on Climate Change*, Cambridge, United Kingdom and New York, NY, USA: Cambridge University Press.
- Meggers, B. J. (1954). Environmental Limitation on the Development of Culture. *American Anthropologist*, **56** (5), 801–824.
- Meggers, B. J. (1992). Prehistoric Population Density in the Amazon Basin. In J. W. Verano & D. H. Uberlaker, *Disease and Demography in the Americas*, Washington D.C.: Smithsonian Institution Press, pp. 197–205.
- Meggers, B. J. (2003). Revisiting Amazonia Circa 1492. *Science*, **302** (5653), 2067.
- Meinshausen, M., Smith, S. J., Calvin, K., et al. (2011). The RCP greenhouse gas concentrations and their extensions from 1765 to 2300. *Climatic Change*, **109** (1-2), 213–241.

- Meir, P., & Woodward, F. I. (2010). Amazonian rain forests and drought: response and vulnerability. *New Phytologist*, **187** (3), 553–557.
- Meneses, M. E. N. S., Costsa, M. L., Enters, D., & Behling, H. (2015). Environmental changes during the last millennium based on multi-proxy palaeoecological records in a savanna-forest mosaic from the northernmost Brazilian Amazon region. *Anais Da Academia Brasileira De Ciências*, **87** (3), 1623–1651.
- Metcalf, S. E., Whitney, B. S., Fitzpatrick, K. A., et al. (2014). Hydrology and climatology at Laguna La Gaiba, lowland Bolivia: complex responses to climatic forcings over the last 25 000 years. *Journal of Quaternary Science*, **29** (3), 289–300.
- Meyers, P. A. (1994). Preservation of elemental and isotopic source identification of sedimentary organic matter. *Chemical Geology*, **114** (3-4), 289–302.
- Monnin, E., Indermühle, A., Dällenbach, A., et al. (2001). Atmospheric CO₂ concentrations over the last glacial termination. *Science*, **291** (5501), 112–114.
- Montade, V., Ledru, M.-P., Burte, J., et al. (2014). Stability of a Neotropical microrefugium during climatic instability. *Journal of Biogeography*, **41** (6), 1215–1226.
- Montoya, E., & Rull, V. (2011). Gran Sabana fires (SE Venezuela): a paleoecological perspective. *Quaternary Science Reviews*, **30** (23-24), 3430–3444.
- Montoya, E., Rull, V., & Nogué, S. (2011a). Early human occupation and land use changes near the boundary of the Orinoco and the Amazon basins (SE Venezuela): Palynological evidence from El Paují record. *Palaeogeography, Palaeoclimatology, Palaeoecology*, **310** (3-4), 413–426.
- Montoya, E., Rull, V., Stansell, N. D., et al. (2011b). Forest–savanna–morichal dynamics in relation to fire and human occupation in the southern Gran Sabana (SE Venezuela) during the last millennia. *Quaternary Research*, **76** (3), 335–344.
- Morrás, H., Moretti, L., Píccolo, G., & Zech, W. (2009). Genesis of subtropical soils with stony horizons in NE Argentina: Autochthony and polygenesis. *Quaternary International*, **196** (1-2), 137–159.
- Moy, C. M., Seltzer, G. O., Rodbell, D. T., & Anderson, D. M. (2002). Variability of El Niño/Southern Oscillation activity at millennial timescales during the Holocene epoch. *Nature*, **420** (6912), 162–165.
- Murphy, B. P., & Bowman, D. M. J. S. (2012). What controls the distribution of tropical forest and savanna? *Ecology Letters*, **15** (7), 748–758.
- Nakicenovic, N., & Swart, R. (2000). *IPCC Special Report: Emissions Scenarios*, Cambridge, UK: Cambridge University Press.
- Ni, J., Yu, G., Harrison, S. P., & Prentice, I. C. (2010). Palaeovegetation in China during the late Quaternary: Biome reconstructions based on a global scheme of plant functional types. *Palaeogeography, Palaeoclimatology, Palaeoecology*, **289** (1-4), 44–61.

- Nogueira, E. M., Yanai, A. M., Vasconcelos, S. S., Graça, P. M. L. A., & Fearnside, P. M. (2018). Carbon stocks and losses to deforestation in protected areas in Brazilian Amazonia, *18*, 261–270.
- Nolte, C., Agrawal, A., Silvius, K. M., & Soares-Filho, B. S. (2013). Governance regime and location influence avoided deforestation success of protected areas in the Brazilian Amazon. *Proceedings of the National Academy of Sciences*, *110* (13), 4956.
- Nuno Veríssimo, P., Safford, H. D., & Behling, H. (2012). Holocene vegetation and fire history of the Serra do Caparao, SE Brazil. *The Holocene*, *22* (11), 1243–1250.
- Oksanen, J., Blanchet, F. G., Kindt, R., et al. (2018). vegan: Community Ecology Package. R package version 2.4-6. Retrieved from <https://CRAN.R-project.org/package=vegan>
- Olson, D. M., Dinerstein, E., Wikramanayake, E. D., et al. (2001). Terrestrial Ecoregions of the World: A New Map of Life on Earth A new global map of terrestrial ecoregions provides an innovative tool for conserving biodiversity. *BioScience*, *51* (11), 933–938.
- Pan, Y., Birdsey, R. A., Fang, J., et al. (2011). A large and persistent carbon sink in the world's forests. *Science*, *333* (6045), 988–993.
- Parizzi, M. G., Salgado-Labouriau, M. L., & Kohler, H. C. (1998). Genesis and environmental history of Lagoa Santa, southeastern Brazil. *The Holocene*, *8* (3), 311–321.
- Pärssinen, M., Schaan, D., & Ranzi, A. (2009). Pre-Columbian geometric earthworks in the upper Purús: a complex society in western Amazonia. *Antiquity*, *83* (322), 1084–1095.
- Peixoto, J. P., & Oort, A. H. (1996). The Climatology of Relative Humidity in the Atmosphere. *Journal of Climate*, *9* (12), 3443–3463.
- Pennington, R. T., Prado, D. E., & Pendry, C. A. (2000). Neotropical seasonally dry forests and Quaternary vegetation changes. *Journal of Biogeography*, *27* (2), 261–273.
- Pessenda, L. C. R. (2004). Holocene fire and vegetation changes in southeastern Brazil as deduced from fossil charcoal and soil carbon isotopes. *Quaternary International*, *114* (1), 35–43.
- Pessenda, L. C. R., Boulet, R., Aravena, R., et al. (2001). Origin and dynamics of soil organic matter and vegetation changes during the Holocene in a forest-savanna transition zone, Brazilian Amazon region. *The Holocene*, *11* (2), 250–254.
- Pessenda, L. C. R., De Oliveira, P. E., Mofatto, M., et al. (2009). The evolution of a tropical rainforest/grassland mosaic in southeastern Brazil since 28,000 14C yr BP based on carbon isotopes and pollen records. *Quaternary Research*, *71* (3), 437–452.
- Pessenda, L. C. R., Gomes, B. M., Aravena, R., Ribeiro, A. S., Boulet, R., & Gouveia, S. E. M. (1998). The carbon isotope record in soils along a forest-cerrado ecosystem transect: implications for vegetation changes in the Rondonia state, southwestern Brazilian Amazon region. *The Holocene*, *8* (5), 599–603.
- Pessenda, L. C. R., Gouveia, S. E. M., Ribeiro, A. de S., De Oliveira, P. E., & Aravena, R. (2010). Late Pleistocene and Holocene vegetation changes in northeastern Brazil

- determined from carbon isotopes and charcoal records in soils. *Palaeogeography, Palaeoclimatology, Palaeoecology*, **297** (3-4), 597–608.
- Pessenda, L. C. R., Ledru, M.-P., Gouveia, S. E. M., et al. (2005). Holocene palaeoenvironmental reconstruction in northeastern Brazil inferred from pollen, charcoal and carbon isotope records. *The Holocene*, **15** (6), 812–820.
- Pessenda, L. C. R., Ribeiro, A. de S., Gouveia, S. E. M., Aravena, R., Boulet, R., & Bendassolli, J. A. (2004). Vegetation dynamics during the late Pleistocene in the Barreirinhas region, Maranhão State, northeastern Brazil, based on carbon isotopes in soil organic matter. *Quaternary Research*, **62** (2), 183–193.
- Phillips, O. L., Aragão, L. E. O. C., Lewis, S. L., et al. (2009). Drought Sensitivity of the Amazon Rainforest. *Science*, **323** (5919), 1344–1347.
- Piperno, D. R. (2006). *Phytoliths: A Comprehensive Guide for Archaeologists and Paleoecologists*, Lanham, MD: Altamira Press.
- Pires, G. L. P., Meyer, K. E. B., & Gomes, M. O. S. (2016). Palinologia da Vereda Juquinha/Cuba, Parque Estadual da Serra do Cabral, Minas Gerais, Brasil. *Revista Brasileira De Paleontologia*, **19** (1), 95–110.
- Potapov, P., Hansen, M. C., Laestadius, L., et al. (2017). The last frontiers of wilderness: Tracking loss of intact forest landscapes from 2000 to 2013. *Science Advances*, **3** (1), 1–13.
- Power, M. J., Marlon, J., Ortiz, N., et al. (2008). Changes in fire regimes since the Last Glacial Maximum: an assessment based on a global synthesis and analysis of charcoal data. *Climate Dynamics*, **30** (7-8), 887–907.
- Prado, D. E., & Gibbs, P. E. (1993). Patterns of Species Distributions in the Dry Seasonal Forests of South America. *Annals of the Missouri Botanical Garden*, **80** (4), 902–28.
- Prado, L. F., Wainer, I., & Chiessi, C. M. (2013a). Mid-Holocene PMIP3/CMIP5 model results: Intercomparison for the South American Monsoon System. *The Holocene*, **23** (12), 1915–1920.
- Prado, L. F., Wainer, I., Chiessi, C. M., Ledru, M.-P., & Turcq, B. (2013b). A mid-Holocene climate reconstruction for eastern South America, **9** (5), 2117–2133.
- Prentice, I. C. (1985). Pollen representation, source area, and basin size: toward a unified theory of pollen analysis. *Quaternary Research*, **23** (1), 76–86.
- Prentice, I. C., & Webb, T., III. (1998). BIOME 6000: reconstructing global mid-Holocene vegetation patterns from palaeoecological records. *Journal of Biogeography*, **25** (6), 997–1005.
- Prentice, I. C., Bartlein, P. J., & Webb, T. (1993). Vegetation and Climate Change in Eastern North America Since the Last Glacial Maximum. *Ecology*, **74** (4), 998–998.

- Prentice, I. C., Guiot, J., Huntley, B., Jolly, D., & Cheddadi, R. (1996). Reconstructing biomes from palaeoecological data: a general method and its application to European pollen data at 0 and 6 ka. *Climate Dynamics*, **12** (3), 185–194.
- Quillet, A., Peng, C., & Garneau, M. (2010). Toward dynamic global vegetation models for simulating vegetation–climate interactions and feedbacks: recent developments, limitations, and future challenges. *Environmental Reviews*, **18**, 333–353.
- Raczka, M. F., De Oliveira, P. E., Bush, M. B., & McMichael, C. N. H. (2013). Two paleoecological histories spanning the period of human settlement in southeastern Brazil. *Journal of Quaternary Science*, **28** (2), 144–151.
- Raia, A., & Cavalcanti, I. F. A. (2008). The Life Cycle of the South American Monsoon System. *Journal of Climate*, **21** (23), 6227–6246.
- Rammig, A., Jupp, T., Thonicke, K., et al. (2010). Estimating the risk of Amazonian forest dieback. *New Phytologist*, **187** (3), 694–706.
- Randall, D. A., Wood, R. A., Bony, S., et al. (2007). Climate models and their evaluation. In *Climate Change 2007: The Physical Science Basis. Contribution of Working Group I to the Fourth Assessment Report of the Intergovernmental Panel on Climate Change*, Cambridge University Press.
- Redford, K. H., & da Fonseca, G. A. B. (1986). The Role of Gallery Forests in the Zoogeography of the Cerrado's Non-volant Mammalian Fauna. *Biotropica*, **18** (2), 126–135.
- Reimer, P. J., Bard, E., Bayliss, A., et al. (2013). IntCal13 and Marine13 Radiocarbon Age Calibration Curves 0–50,000 Years cal BP. *Radiocarbon*, **55** (4), 1869–1887.
- Rein, B., Lückge, A., Reinhardt, L., Sirocko, F., Wolf, A., & Dullo, W.-C. (2005). El Niño variability off Peru during the last 20,000 years. *Paleoceanography*, **20** (4), 1–17.
- Reis, L. S., Guimarães, J. T. F., Souza-Filho, P. W. M., et al. (2017). Environmental and vegetation changes in southeastern Amazonia during the late Pleistocene and Holocene. *Quaternary International*, **449**, 83–105.
- Restrepo-Coupe, N., Levine, N. M., Christoffersen, B. O., et al. (2017). Do dynamic global vegetation models capture the seasonality of carbon fluxes in the Amazon basin? A data-model intercomparison. *Global Change Biology*, **23** (1), 191–208.
- Roberts, N., Fyfe, R. M., Woodbridge, J., et al. (2018). Europe's lost forests: a pollen-based synthesis for the last 11,000 years. *Scientific Reports*, **8** (716), 1–8.
- Robinson, M., de Souza, J. G., Maezumi, S. Y., et al. (2018). Uncoupling human and climate drivers of late Holocene vegetation change in southern Brazil. *Scientific Reports*, **8** (7800), 1–10.
- Rodrigues-Filho, S., Behling, H., Irion, G., & Müller, G. (2002). Evidence for Lake Formation as a Response to an Inferred Holocene Climatic Transition in Brazil. *Quaternary Research*, **57** (1), 131–137.

- Rodríguez-Zorro, P. A. (2017). Mid-Holocene vegetation dynamics with an early expansion of *Mauritia flexuosa* palm trees inferred from the Serra do Tepequém in the savannas of Roraima State in Amazonia, northwestern Brazil. *Vegetation History and Archaeobotany*, **26** (5), 455–468.
- Rodríguez-Zorro, P. A., Enters, D., Hermanowski, B., da Costa, M. L., & Behling, H. (2015). Vegetation changes and human impact inferred from an oxbow lake in southwestern Amazonia, Brazil since the 19th century. *Journal of South American Earth Sciences*, **62**, 186–194.
- Roubik, D. W., & Moreno Patiño, J. E. (1991). Pollen and spores of Barro Colorado Island, Vol. 36, St Louis, MO: Monographs in Systematic Botany, v. 36. Missouri Botanical Garden.
- Roucoux, K. H., Lawson, I. T., Jones, T. D., et al. (2013). Vegetation development in an Amazonian peatland. *Palaeogeography, Palaeoclimatology, Palaeoecology*, **374**, 242–255.
- Rowe, H. D., Dunbar, R. B., Mucciarone, D. A., Seltzer, G. O., Baker, P. A., & Fritz, S. C. (2002). Insolation, moisture balance and climate change on the South American Altiplano since the last glacial maximum. *Climatic Change*, **52** (1-2), 175–199.
- Rowland, L., da Costa, A. C. L., Galbraith, D. R., et al. (2015). Death from drought in tropical forests is triggered by hydraulics not carbon starvation. *Nature*, **528** (7580), 119–122.
- Rull, V. (2004). An evaluation of the Lost World and Vertical Displacement hypotheses in the Chimanta Massif, Venezuelan Guayana. *Global Ecology and Biogeography Letters*, **13** (2), 141–148.
- Rull, V. (2005). Palaeovegetational and palaeoenvironmental trends in the summit of the Guaiquinima massif (Venezuelan Guayana) during the Holocene. *Journal of Quaternary Science*, **20** (2), 135–145.
- Rull, V., Montoya, E., Vegas-Vilarrúbia, T., & Ballesteros, T. (2015). New insights on palaeofires and savannisation in northern South America. *Quaternary Science Reviews*, **122**, 158–165.
- Saha, S., Moorthi, S., Pan, H.-L., et al. (2010a). NCEP Climate Forecast System Reanalysis (CFSR) Monthly Products, January 1979 to December 2010, Boulder, CO: Research Data Archive at the National Center for Atmospheric Research, Computational and Information Systems Laboratory.
- Saha, S., Moorthi, S., Pan, H.-L., et al. (2010b). The NCEP Climate Forecast System Reanalysis. *Bulletin of the American Meteorological Society*, **91** (8), 1015–1057.
- Saia, S. E. M. G., Pessenda, L. C. R., Gouveia, S. E. M., Aravena, R., & Bendassolli, J. A. (2008). Last glacial maximum (LGM) vegetation changes in the Atlantic Forest, southeastern Brazil. *Quaternary International*, **184** (1), 195–201.
- Saleska, S. R., Didan, K., Huete, A. R., & da Rocha, H. R. (2007). Amazon Forests Green-Up During 2005 Drought. *Science*, **318** (5850), 612–612.

- Sampaio, E. V. S. B. (1995). Overview of the Brazilian caatinga. In S. H. Bullock, H. A. Mooney, & E. Medina, *Seasonally Dry Tropical Forests*, Cambridge, United Kingdom: Cambridge University Press, pp. 35–63.
- Sawada, M. C., Viau, A. E., Vettoretti, G., Peltier, W. R., & Gajewski, K. (2004). Comparison of North-American pollen-based temperature and global lake-status with CCCma AGCM2 output at 6ka. *Quaternary Science Reviews*, **23** (3-4), 225–244.
- Schaphoff, S., Lucht, W., Gerten, D., Sitch, S., Cramer, W., & Prentice, I. C. (2006). Terrestrial biosphere carbon storage under alternative climate projections. *Climatic Change*, **74** (1-3), 97–122.
- Scheel-Ybert, R., Beauclair, M., & Buarque, A. (2014). The forest people: landscape and firewood use in the Araruama region, southeastern Brazil, during the late Holocene. *Vegetation History and Archaeobotany*, **23** (2), 97–111.
- Scheiter, S., Langan, L., & Higgins, S. I. (2013). Next-generation dynamic global vegetation models: learning from community ecology. *New Phytologist*, **198** (3), 957–969.
- Schmidt, G. A. (2010). Enhancing the relevance of palaeoclimate model/data comparisons for assessments of future climate change. *Journal of Quaternary Science*, **25** (1), 79–87.
- Schmidt, G. A., Annan, J. D., Bartlein, P. J., et al. (2014a). Using palaeo-climate comparisons to constrain future projections in CMIP5, **10** (1), 221–250.
- Schmidt, G. A., Kelley, M., Nazarenko, L., et al. (2014b). Configuration and assessment of the GISS ModelE2 contributions to the CMIP5 archive. *Journal of Advances in Modeling Earth Systems*, **6** (1), 141–184.
- Seltzer, G. O., Rodbell, D. T., Baker, P. A., et al. (2002). Early warming of tropical South America at the last glacial-interglacial transition. *Science*, **296** (5573), 1685–1686.
- Seltzer, G. O., Rodbell, D., & Burns, S. J. (2000). Isotopic evidence for late Quaternary climatic change in tropical South America. *Geology*, **28** (1), 35–38.
- Seth, A., Rojas, M., & Rauscher, S. A. (2010). CMIP3 projected changes in the annual cycle of the South American Monsoon. *Climatic Change*, **98** (3-4), 331–357.
- Shangguan, W., Dai, Y., Duan, Q., Liu, B., & Yuan, H. (2014). A global soil data set for earth system modeling. *Journal of Advances in Modeling Earth Systems*, **6** (1), 249–263.
- Sifeddine, A., Albuquerque, A. L. S., & Ledru, M.-P. (2003). A 21 000 cal years paleoclimatic record from Caçó Lake, northern Brazil: evidence from sedimentary and pollen analyses. *Palaeogeography, Palaeoclimatology, Palaeoecology*, **189** (1-2), 25–34.
- Sifeddine, A., Bertrand, P., & Fournier, M. (1994). La sédimentation organique lacustre en milieu tropical humide (Carajás, Amazonie orientale, Brésil): relation avec les changements climatiques au cours des 60 000 dernières années. *Bulletin De La Societe Geologique De France*, **165** (6), 613–621.

- Sifeddine, A., Martin, L., Turcq, B., et al. (2001). Variations of the Amazonian rainforest environment: a sedimentological record covering 30,000 years. *Palaeogeography, Palaeoclimatology, Palaeoecology*, **168** (3-4), 221–235.
- Sifeddine, A., Wirrmann, D., Albuquerque, A. L. S., et al. (2004). Bulk composition of sedimentary organic matter used in palaeoenvironmental reconstructions: examples from the tropical belt of South America and Africa. *Palaeogeography, Palaeoclimatology, Palaeoecology*, **214** (1-2), 41–53.
- Silva, J. M. C. D. (1997). Endemic bird species and conservation in the Cerrado Region, South America. *Biodiversity and Conservation*, **6** (3), 435–450.
- Silva, J. M. C. D., & Bates, J. M. (2002). Biogeographic Patterns and Conservation in the South American Cerrado: A Tropical Savanna Hotspot. *BioScience*, **52** (3), 225–233.
- Silva, L., Sternberg, L., & Haridasan, M. (2008). Expansion of gallery forests into central Brazilian savannas. *Global Change Biology*, **14** (9), 2108–2118.
- Silva, V. B. S., & Kousky, V. E. (2012). The South American Monsoon System: Climatology and Variability. In S. Wang & R. R. Gillies, *Modern Climatology*, pp. 123–152.
- Singarayer, J. S., Valdes, P. J., & Roberts, W. H. G. (2017). Ocean dominated expansion and contraction of the late Quaternary tropical rainbelt. *Scientific Reports*, **7** (9283), 1–9.
- Sitch, S., Huntingford, C., Gedney, N., et al. (2008). Evaluation of the terrestrial carbon cycle, future plant geography and climate-carbon cycle feedbacks using five Dynamic Global Vegetation Models (DGVMs). *Global Change Biology*, **14** (9), 2015–2039.
- Skole, D., & Tucker, C. (1993). Tropical Deforestation and Habitat Fragmentation in the Amazon - Satellite Data From 1978 to 1988. *Science*, **260** (5116), 1905–1910.
- Smith, R. J., & Mayle, F. E. (2018). Impact of mid- to late Holocene precipitation changes on vegetation across lowland tropical South America: a paleo-data synthesis. *Quaternary Research*, **89** (1), 134–155.
- Soares-Filho, B. S., Nepstad, D. C., & Curran, L. M. (2006). Modelling conservation in the Amazon basin. *Nature*, **440**, 550–523.
- Soares-Filho, B., Moutinho, P., Nepstad, D., et al. (2010). Role of Brazilian Amazon protected areas in climate change mitigation. *Proceedings of the National Academy of Sciences*, **107** (24), 10821–10826.
- Spracklen, D. V., Arnold, S. R., & Taylor, C. M. (2012). Observations of increased tropical rainfall preceded by air passage over forests. *Nature*, **489** (7415), 282–285.
- Stocker, T. F., Qin, D., Plattner, G. K., et al. (2013). *Climate Change 2013: The Physical Science Basis. Contribution of Working Group I to the Fifth Assessment Report of the Intergovernmental Panel on Climate Change*, Cambridge, United Kingdom and New York, NY, USA: Cambridge University Press.
- Stockmarr, J. (1971). Tablets with Spores used in Absolute Pollen Analysis. *Pollen Et Spores*, **13**, 615–621.

- Stríkis, N. M., Cruz, F. W., Cheng, H., et al. (2011). Abrupt variations in South American monsoon rainfall during the Holocene based on a speleothem record from central-eastern Brazil. *Geology*, **39** (11), 1075–1078.
- Stute, M., Forster, M., Frischkorn, H., et al. (1995). Cooling of Tropical Brazil (5°C) During the Last Glacial Maximum. *Science*, **269** (5222), 379–383.
- Sueyoshi, T., Ohgaito, R., Yamamoto, A., et al. (2013). Set-up of the PMIP3 paleoclimate experiments conducted using an Earth system model, MIROC-ESM. *Geoscientific Model Development*, **6** (3), 819–836.
- Sugita, S. (1993). A model of pollen source area for an entire lake surface. *Quaternary Research*, **39** (2), 239–244.
- Sugita, S. (1994). Pollen Representation of Vegetation in Quaternary Sediments - Theory and Method in Patchy Vegetation. *Journal of Ecology*, **82** (4), 881–897.
- Sugita, S. (2007a). Theory of quantitative reconstruction of vegetation I: pollen from large sites REVEALS regional vegetation composition. *The Holocene*, **17** (2), 229–241.
- Sugita, S. (2007b). Theory of quantitative reconstruction of vegetation II: all you need is LOVE. *The Holocene*, **17** (2), 243–257.
- Sugita, S., Gaillard, M. J., & Broström, A. (1999). Landscape openness and pollen records: a simulation approach. *The Holocene*, **9** (4), 409–421.
- Taylor, K. E., Stouffer, R. J., & Meehl, G. A. (2012). An Overview of CMIP5 and the Experiment Design. *Bulletin of the American Meteorological Society*, **93** (4), 485–498.
- Taylor, Z. P., Horn, S. P., Mora, C. I., Orvis, K. H., & Cooper, L. W. (2010). A multi-proxy palaeoecological record of late-Holocene forest expansion in lowland Bolivia. *Palaeogeography, Palaeoclimatology, Palaeoecology*, **293** (1-2), 98–107.
- Thompson, L. G., Davis, M., Mosley-Thompson, E., et al. (1998). A 25,000-year tropical climate history from Bolivian ice cores. *Science*, **282** (5395), 1858–1864.
- Tian, F., Cao, X., Dallmeyer, A., Zhao, Y., Ni, J., & Herzschuh, U. (2017). Pollen-climate relationships in time (9 ka, 6 ka, 0 ka) and space (upland vs. lowland) in eastern continental Asia. *Quaternary Science Reviews*, **156**, 1–11.
- Toivonen, T., Mäki, S., & Kalliola, R. (2007). The riverscape of Western Amazonia - a quantitative approach to the fluvial biogeography of the region. *Journal of Biogeography*, **34** (8), 1374–1387.
- Tollefson, J. (2012). Brazil set to cut forest protection. *Nature*, **485** (7396), 19.
- Tomasella, J., & Hodnett, M. G. (2004). Pedotransfer functions for tropical soils. In *Development of Pedotransfer Functions in Soil Hydrology*, Vol. 30, Elsevier, pp. 415–429.

- Turcq, B., Albuquerque, A. L. S., Cordeiro, R. C., et al. (2002). Accumulation of organic carbon in five Brazilian lakes during the Holocene. *Sedimentary Geology*, **148** (1-2), 319–342.
- Twiddle, C. L., & Bunting, M. J. (2010). Experimental investigations into the preservation of pollen grains: A pilot study of four pollen types. *Review of Palaeobotany and Palynology*, **162** (4), 621–630.
- Urrego, D. H., Bush, M. B., Silman, M. R., et al. (2013). Holocene fires, forest stability and human occupation in south-western Amazonia. *Journal of Biogeography*, **40** (3), 521–533.
- van Breukelen, M. R., Vonhof, H. B., Hellstrom, J. C., Wester, W. C. G., & Kroon, D. (2008). Fossil dripwater in stalagmites reveals Holocene temperature and rainfall variation in Amazonia. *Earth and Planetary Science Letters*, **275** (1-2), 54–60.
- van Genuchten, M. T. (1980). A Closed-form Equation for Predicting the Hydraulic Conductivity of Unsaturated Soils. *Soil Science Society of America Journal*, **44**, 892–898.
- van Vuuren, D. P., Edmonds, J., Kainuma, M., et al. (2011). The representative concentration pathways: an overview. *Climatic Change*, **109** (1-2), 5–31.
- Vera, C., Silvestri, G., Liebmann, B., & González, P. (2006). Climate change scenarios for seasonal precipitation in South America from IPCC-AR4 models. *Geophysical Research Letters*, **33** (13), L13707.
- Viau, A. E., Gajewski, K., Sawada, M. C., & Fines, P. (2006). Millennial-scale temperature variations in North America during the Holocene. *Journal of Geophysical Research*, **111** (D9), 483–12.
- Voltaire, A., Sanchez-Gomez, E., & Méliá, D. Y. (2013). The CNRM-CM5. 1 global climate model: description and basic evaluation. *Climate Dynamics*, **40** (9), 2091–2121.
- Vuille, M., Burns, S. J., Taylor, B. L., et al. (2012). A review of the South American monsoon history as recorded in stable isotopic proxies over the past two millennia. *Climate of the Past*, **8** (4), 1309–1321.
- Walker, J. H. (2013). Pre-Columbian Ring Ditches along the Yacuma and Rapulo Rivers, Beni, Bolivia: A Preliminary Review. *Journal of Field Archaeology*, **33** (4), 413–427.
- Wang, X., Auler, A. S., Edwards, R. L., et al. (2007). Millennial-scale precipitation changes in southern Brazil over the past 90,000 years. *Geophysical Research Letters*, **34** (23), L23701.
- Wang, X., Edwards, R. L., Auler, A. S., et al. (2017). Hydroclimate changes across the Amazon lowlands over the past 45,000 years. *Nature*, **541** (7636), 204–207.
- Watanabe, S., Hajima, T., Sudo, K., et al. (2011). MIROC-ESM 2010: model description and basic results of CMIP5-20c3m experiments. *Geoscientific Model Development*, **4** (4), 845–872.

- Watling, J., Iriarte, J., Mayle, F. E., et al. (2017). Impact of pre-Columbian “geoglyph” builders on Amazonian forests. *Proceedings of the National Academy of Sciences*, **114** (8), 1868–1873.
- Watling, J., Iriarte, J., Whitney, B. S., et al. (2016). Differentiation of neotropical ecosystems by modern soil phytolith assemblages and its implications for palaeoenvironmental and archaeological reconstructions II: Southwestern Amazonian forests. *Review of Palaeobotany and Palynology*, **226** (C), 30–43.
- Watson, J. E. M., Evans, T., Venter, O., et al. (2018). The exceptional value of intact forest ecosystems. *Nature Ecology & Evolution*, 1–12.
- Weedon, G. P., Balsamo, G., Bellouin, N., Gomes, S., Best, M. J., & Viterbo, P. (2014). The WFDEI meteorological forcing data set: WATCH Forcing Data methodology applied to ERA-Interim reanalysis data. *Water Resources Research*, **50** (9), 7505–7514.
- Weng, C., Bush, M. B., & Athens, J. S. (2002). Holocene climate change and hydrarch succession in lowland Amazonian Ecuador. *Review of Palaeobotany and Palynology*, **120** (1-2), 73–90.
- Werneck, F. P. (2011). The diversification of eastern South American open vegetation biomes: Historical biogeography and perspectives. *Quaternary Science Reviews*, **30** (13-14), 1630–1648.
- Werth, D., & Avissar, R. (2002). The local and global effects of Amazon deforestation. *Journal of Geophysical Research*, **107** (D20), 1–8.
- Whitney, B. S., & Mayle, F. E. (2012). *Pediastrum* species as potential indicators of lake-level change in tropical South America. *Journal of Paleolimnology*, **47** (4), 601–615.
- Whitney, B. S., Mayle, F. E., Punyasena, S. W., et al. (2011). A 45kyr palaeoclimate record from the lowland interior of tropical South America. *Palaeogeography, Palaeoclimatology, Palaeoecology*, **307** (1-4), 177–192.
- Whitney, B. S., Smallman, T. L., Mitchard, E. T., Carson, J. F., Mayle, F. E., & Bunting, M. J. (2018). Constraining pollen-based estimates of forest cover in the Amazon: A simulation approach. *The Holocene*, **29** (2), 262-270.
- Woodward, F. I., & Lomas, M. R. (2004). Vegetation dynamics - simulating responses to climatic change. *Biological Reviews of the Cambridge Philosophical Society*, **79** (3), 643–670.
- Woodward, F. I., Smith, T. M., & Emanuel, W. R. (1995). A global land primary productivity and phytogeography model. *Global Biogeochemical Cycles*, **9** (4), 471–490.
- Wright, H. E. (1967). A square-rod piston sampler for lake sediments. *Journal of Sedimentary Research*, **37** (3), 975–976.
- Wu, H., Guiot, J., Brewer, S., & Guo, Z. (2007). Climatic changes in Eurasia and Africa at the last glacial maximum and mid-Holocene: reconstruction from pollen data using inverse vegetation modelling. *Climate Dynamics*, **29** (2-3), 211–229.

- Ybert, J.-P., Turcq, B., Albuquerque, A. L., & Cocquit, C. (2000). Evolution paléoécologique et paléoclimatique holocène dans la région moyenne du Rio Doce (Minas Gerais, Brésil) déduite de l'analyse palynologique de deux carottes du lac Dom Helvécio. In *Dynamique à long terme des écosystèmes forestiers intertropicaux*, pp. 413–421.
- Yin, L., Fu, R., Shevliakova, E., & Dickinson, R. E. (2013). How well can CMIP5 simulate precipitation and its controlling processes over tropical South America? *Climate Dynamics*, **41**, 3127–3143.
- Zech, M., Zech, R., Morrás, H., Moretti, L., Glaser, B., & Zech, W. (2009). Late Quaternary environmental changes in Misiones, subtropical NE Argentina, deduced from multi-proxy geochemical analyses in a palaeosol-sediment sequence. *Quaternary International*, **196** (1-2), 121–136.
- Zhang, K., Castanho, A. D. A., Galbraith, D. R., et al. (2015). The fate of Amazonian ecosystems over the coming century arising from changes in climate, atmospheric CO₂, and land use. *Global Change Biology*, **21** (7), 2569–2587.
- Zhou, J., & Lau, K. M. (1998). Does a monsoon climate exist over South America? *Journal of Climate*, **11**, 1020–1040.
- Zizka, A., Govender, N., & Higgins, S. I. (2014). How to tell a shrub from a tree: A life-history perspective from a South African savanna. *Austral Ecology*, **39** (7), 767–778.

Appendix A. Out of Amazonia: Late-Holocene climate change and the Tupi–Guarani trans-continental expansion

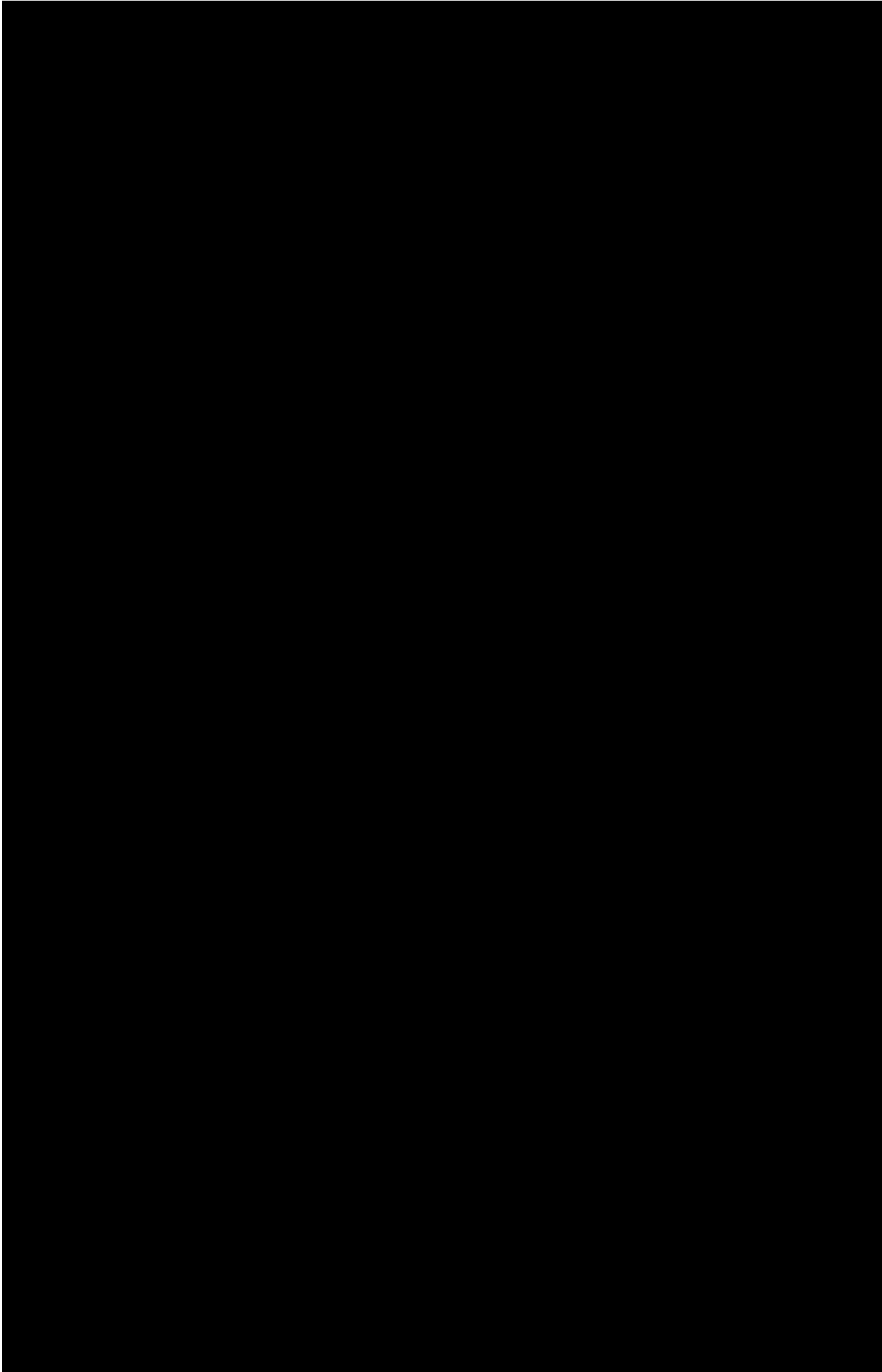
Authors: José Iriarte, **Richard J. Smith**, Jonas Gregorio de Souza, Francis E. Mayle, Bronwen S. Whitney, Macarena Lucia Cárdenas, Joy S. Singarayer, John F. Carson, Shovonlal Roy and Paul Valdes

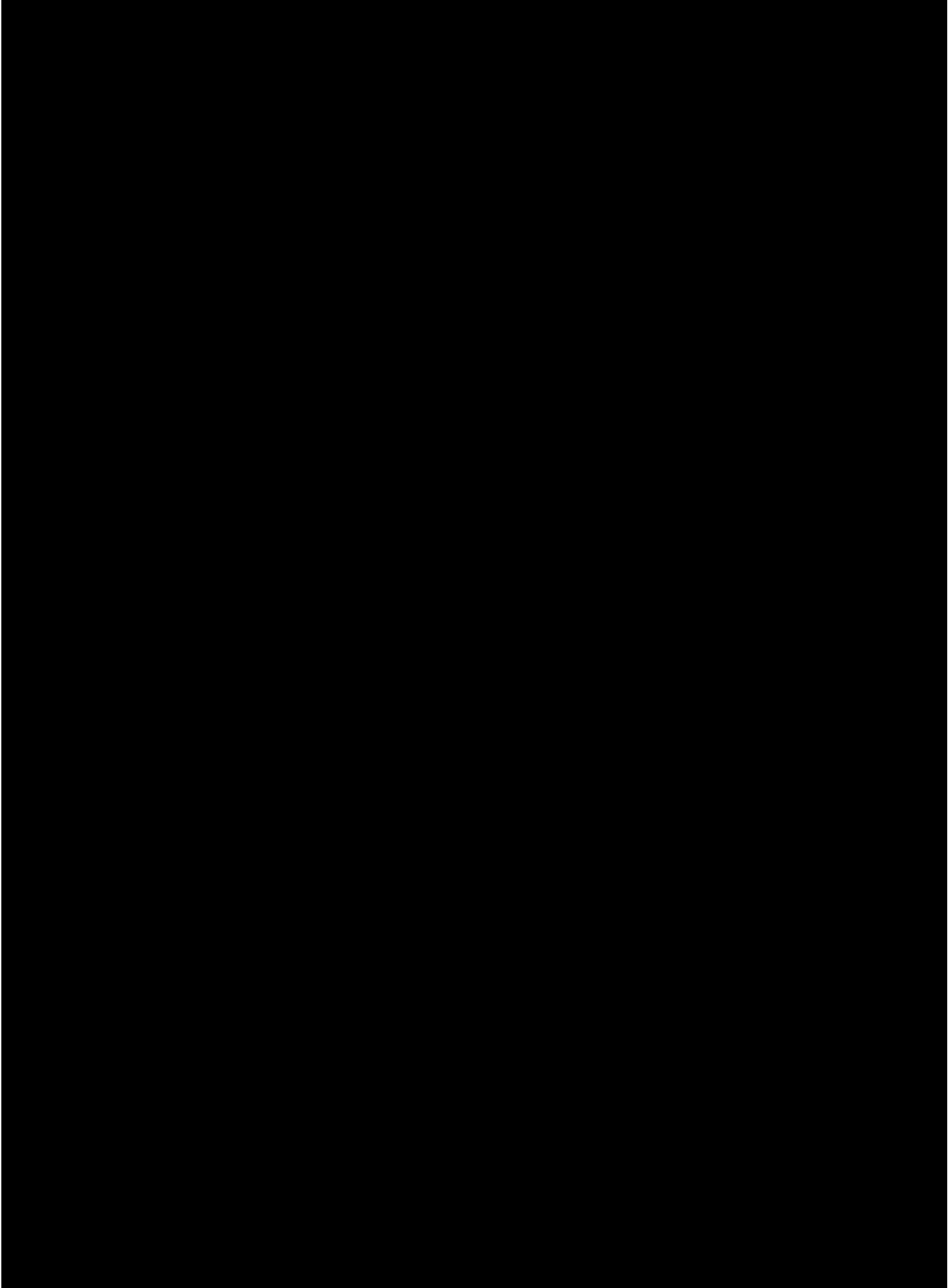
Preface

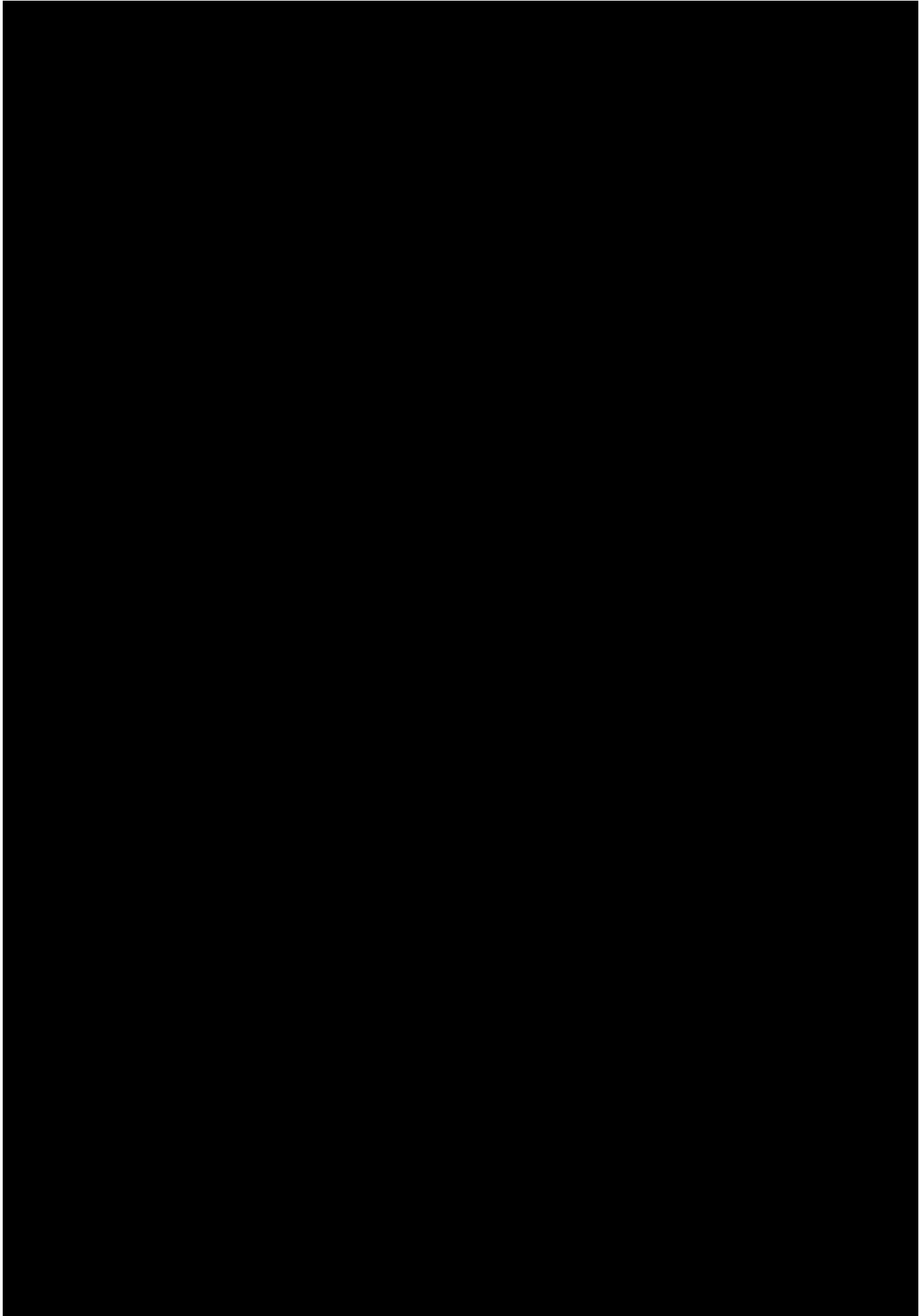
The following is the paper using the palaeoecological synthesis data from Chapter 2, examining the relationship between expansion of the Tupi-Guarani pre-Columbian culture, climate change, and vegetation change (Iriarte *et al.* 2017).

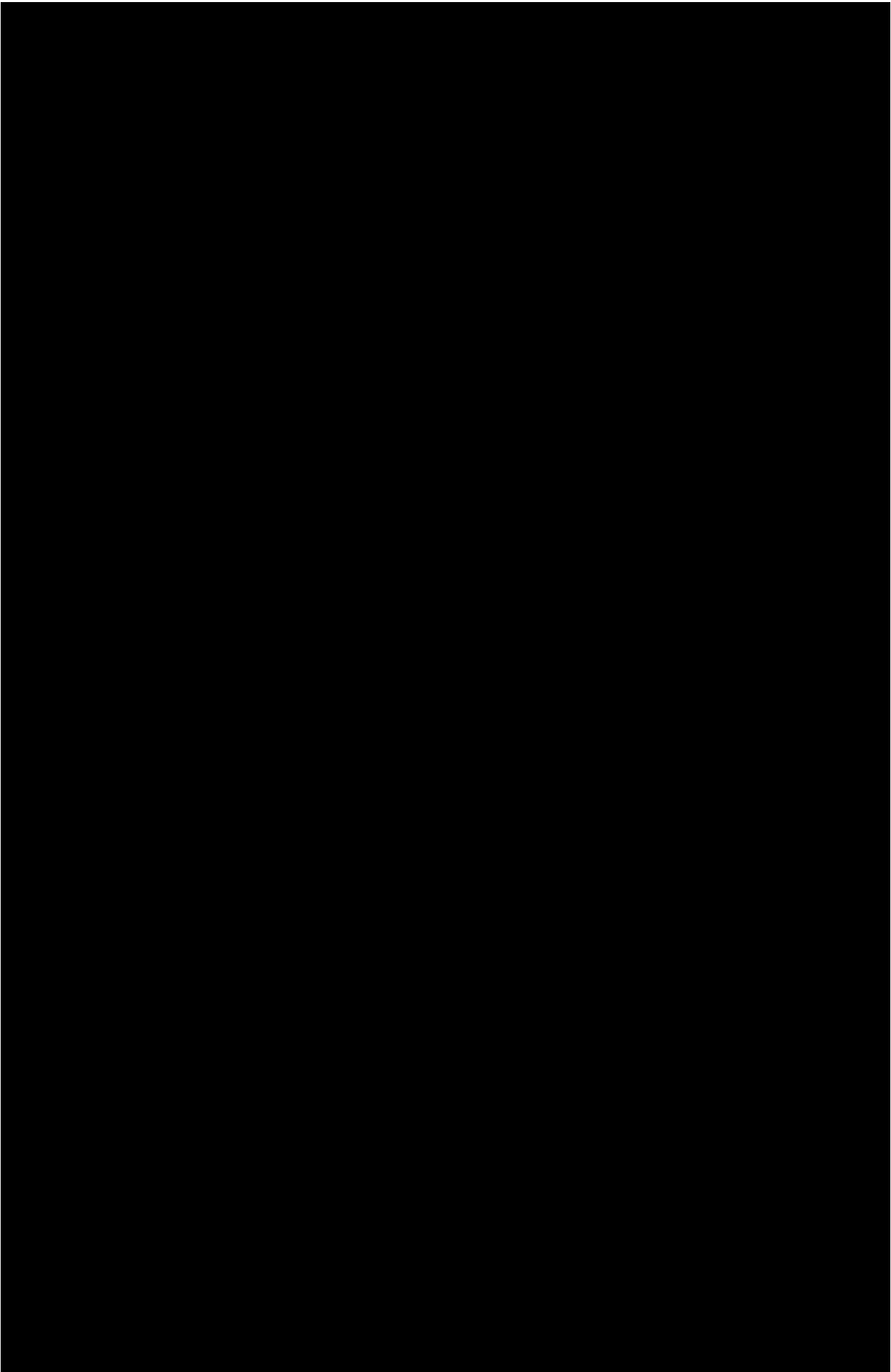
Reference

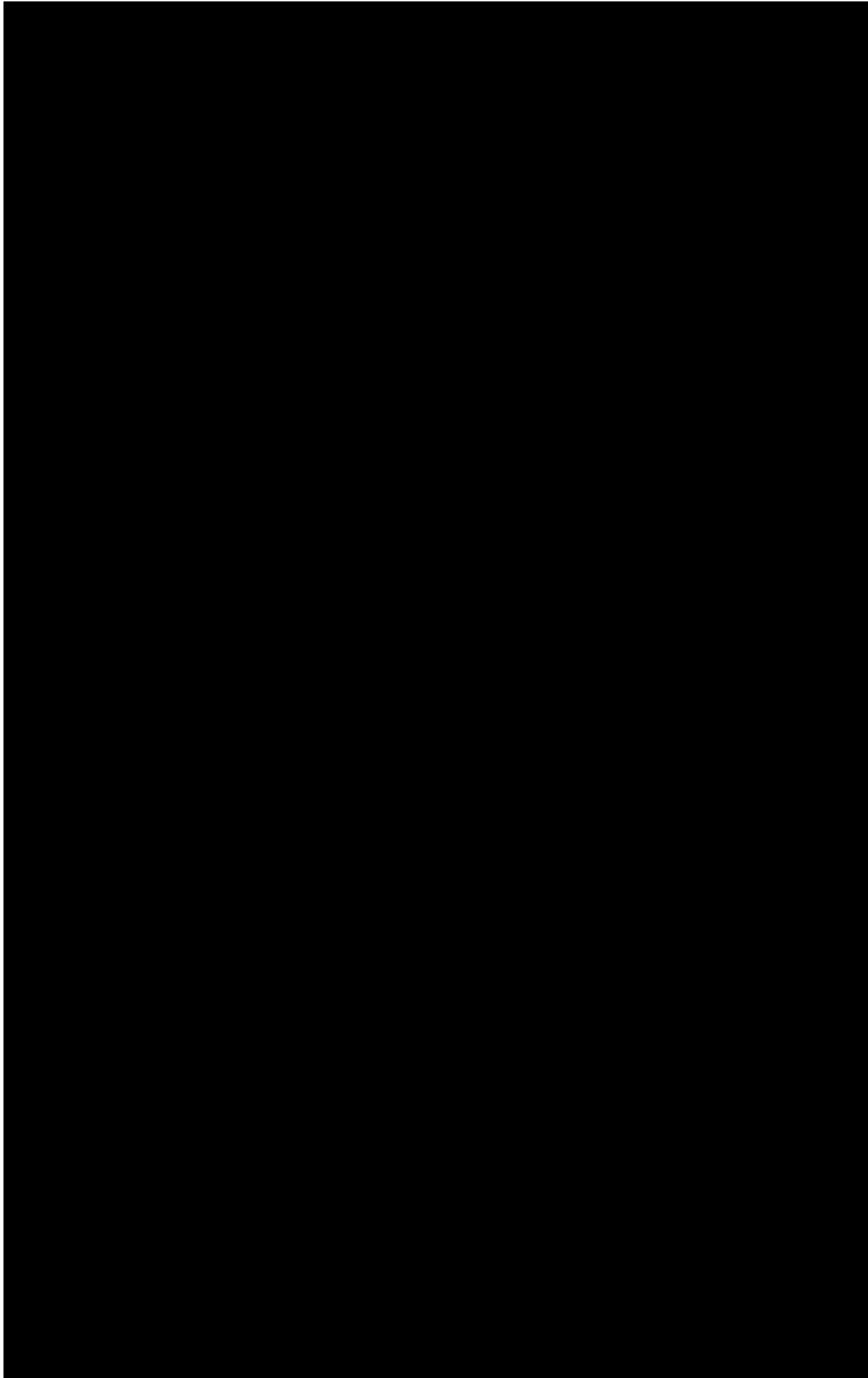
Iriarte, J., Smith, R.J., Gregorio de Souza, J., Mayle, F.E., Whitney, B.S., Cárdenas, M.L., Singarayer, J.S., Carson, J.F., Roy, S., Valdes, P., 2017. Out of Amazonia: Late-Holocene climate change and the Tupi–Guarani trans-continental expansion. *The Holocene* 27, 967–975. DOI: 10.1177/0959683616678461

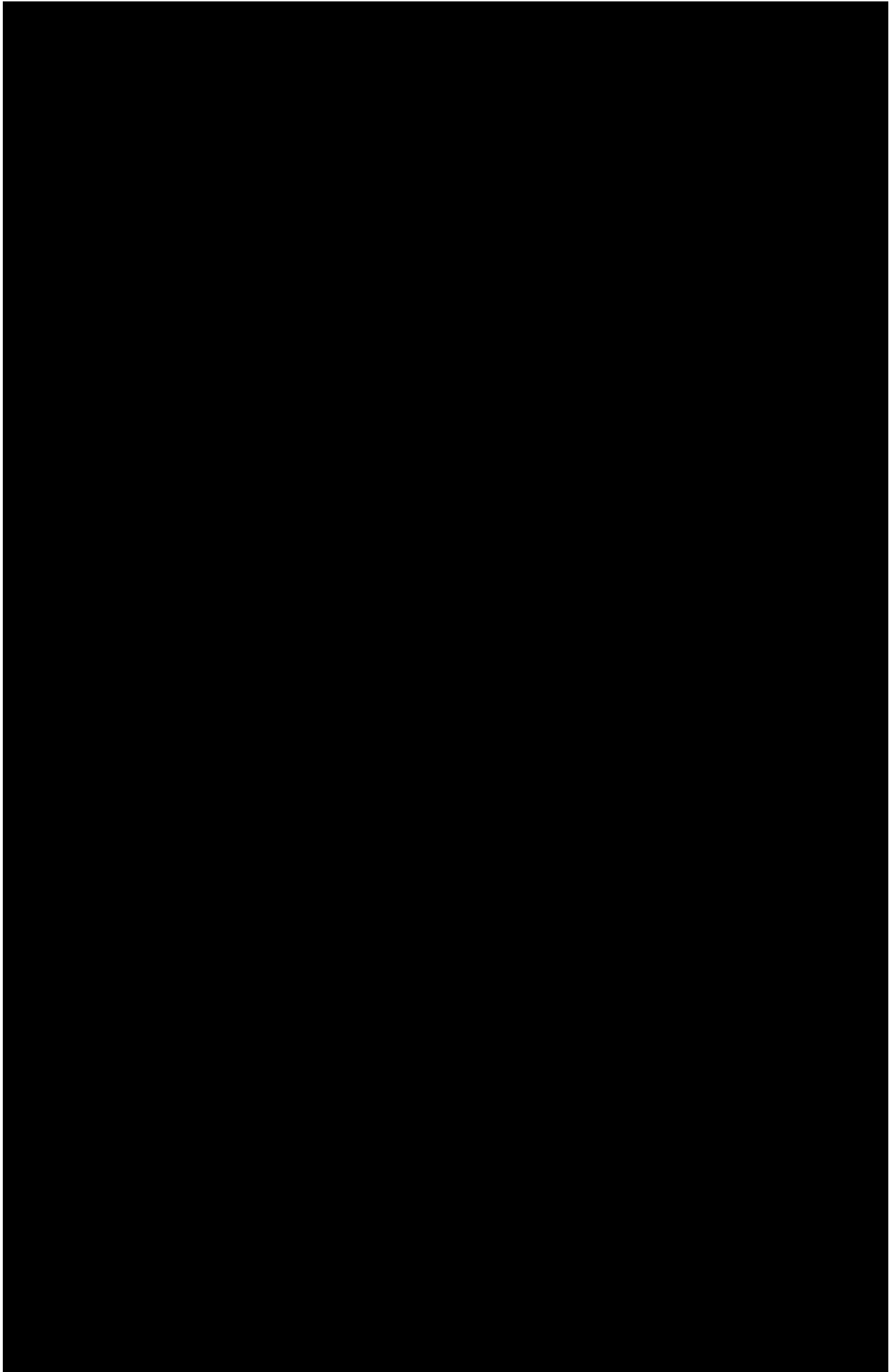


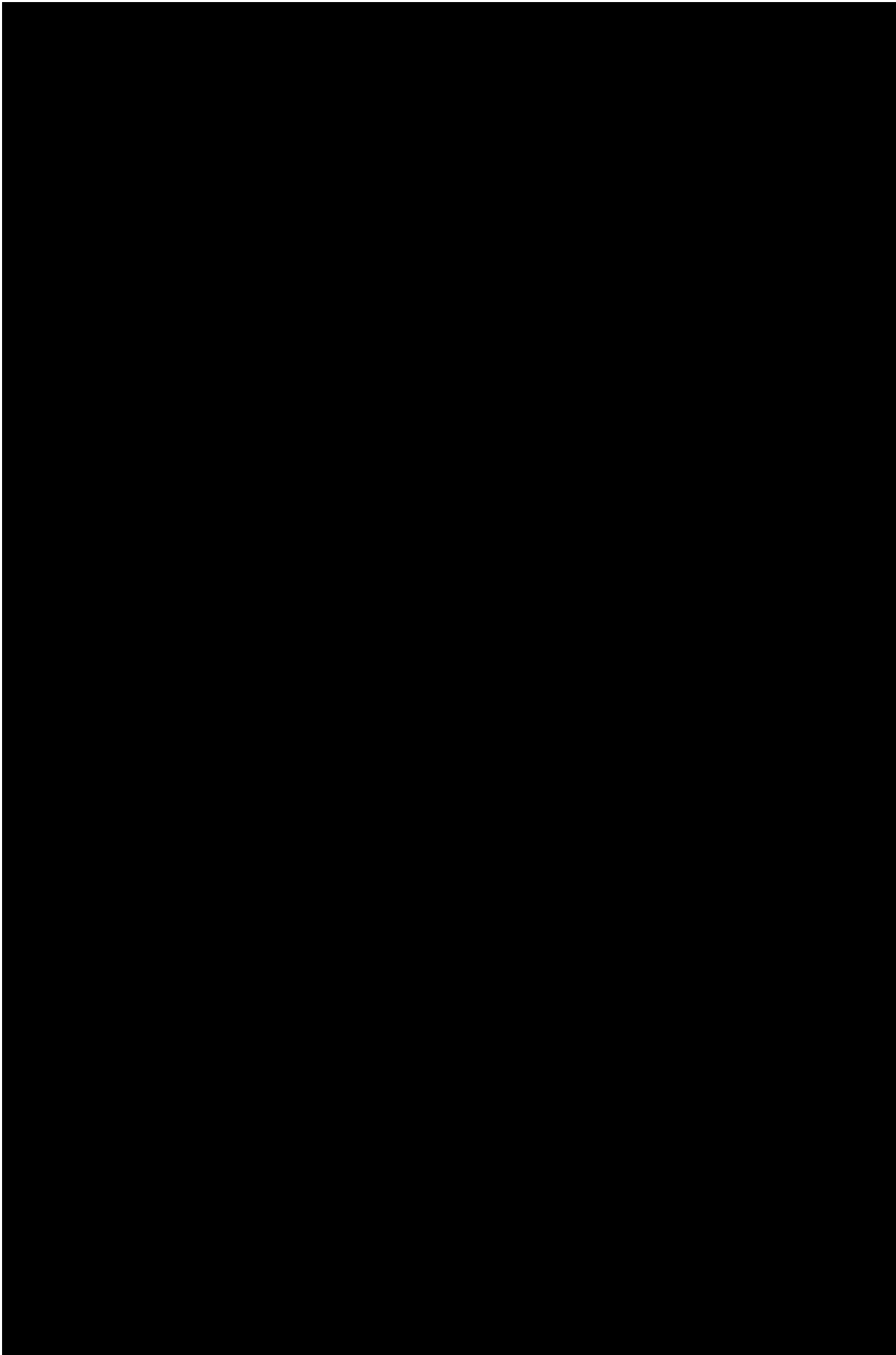


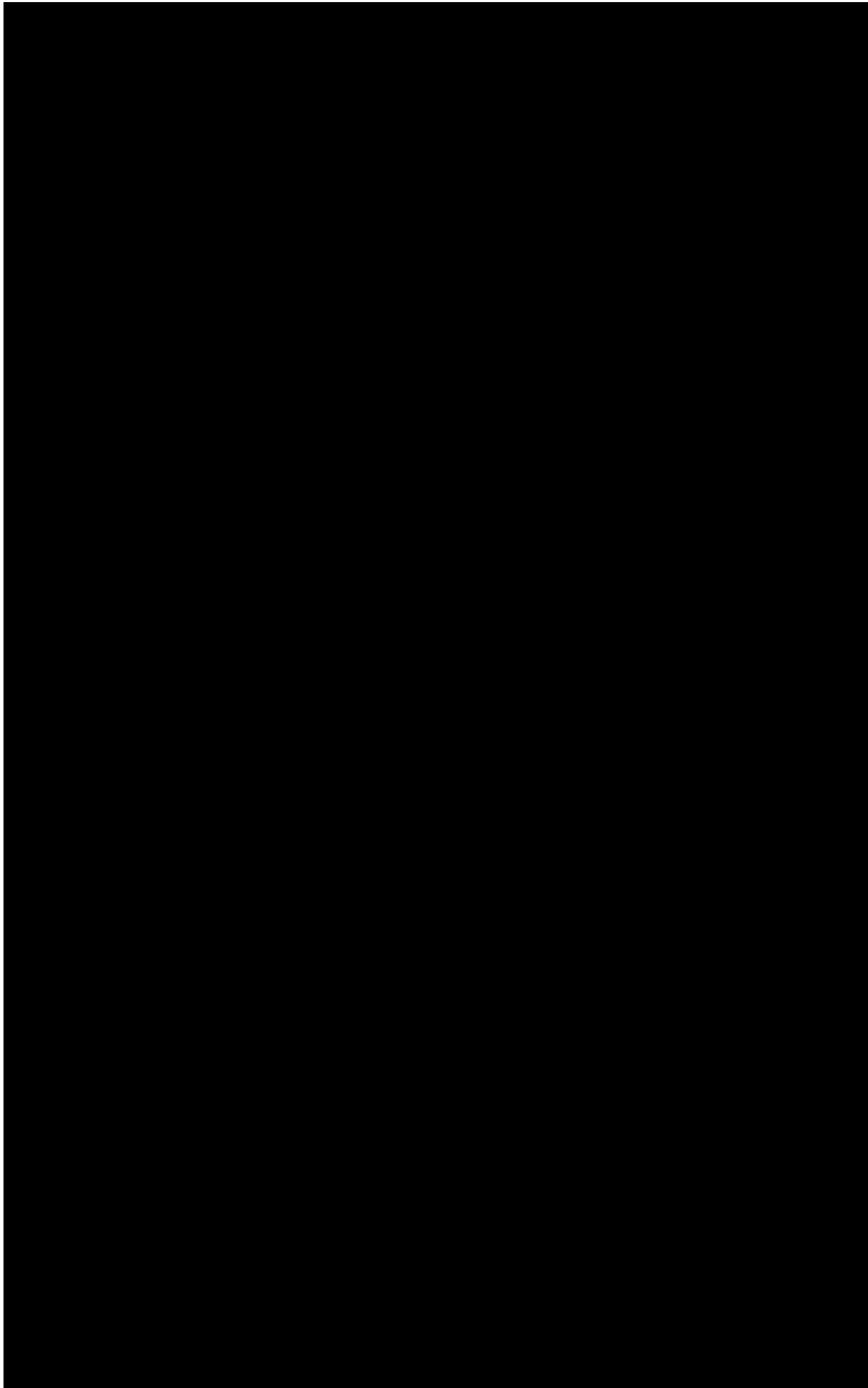


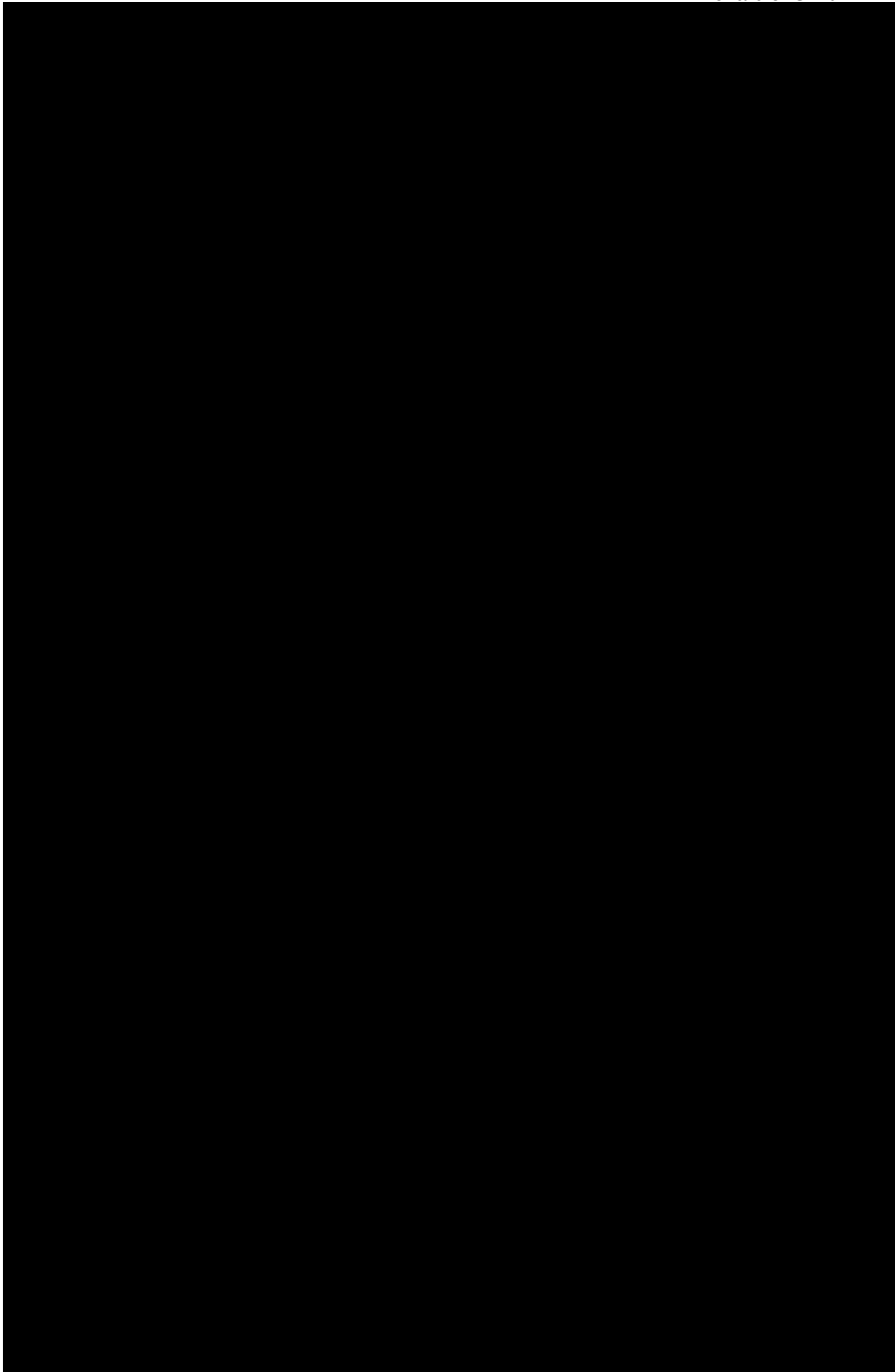










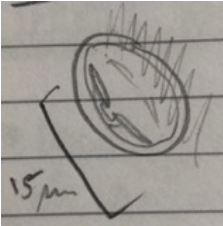
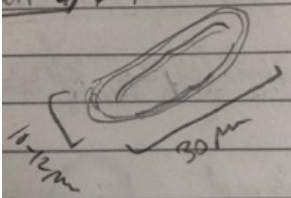
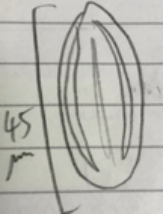
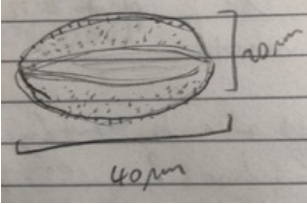


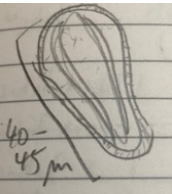
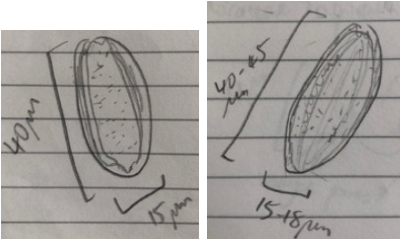
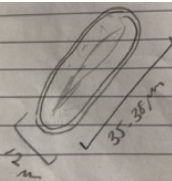
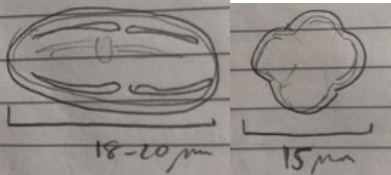
Appendix B. Unknown pollen grains of Cuatro Vientos

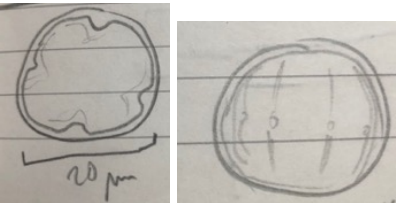
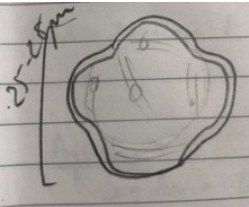
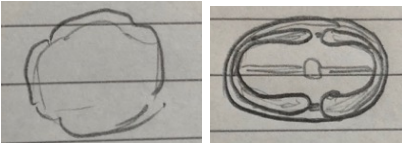
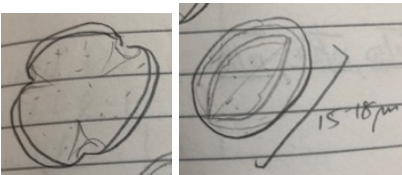
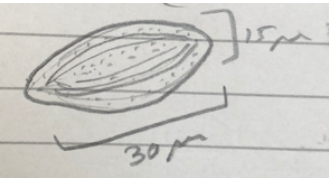
Authors: **Richard J. Smith**

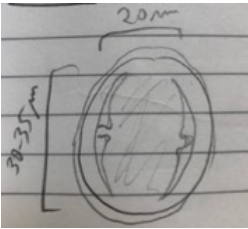
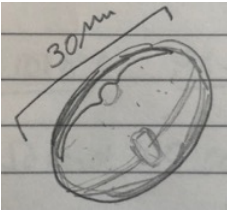
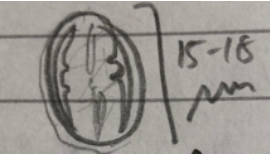
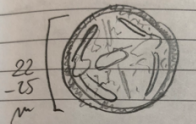
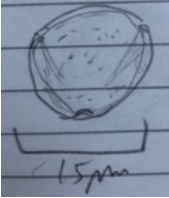
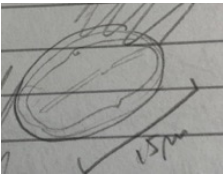
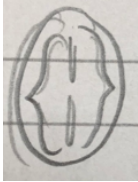
Preface

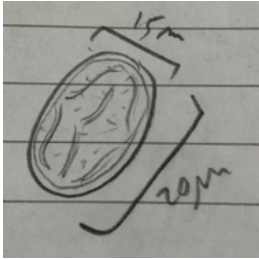
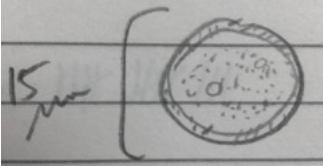
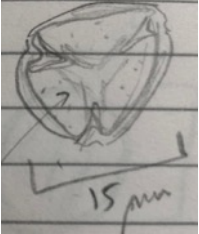
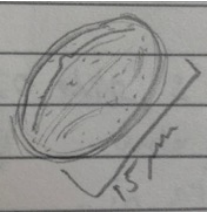
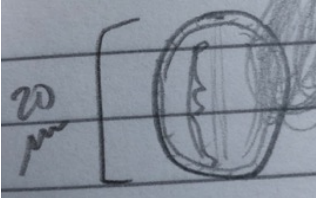
The following Appendix presents photos and drawings of unknown pollen grains from the examination of the fossil pollen record of Cuatro Vientos (see Chapter 3). The unknown pollen grains are presented with a brief description of the features and the microscope slide where an example of the grain can be found. Coordinates of specific pollen grain examples can be found in the pollen count notebooks for Cuatro Vientos. These location coordinates were made using the DME2 microscope in the Reading University Tropical Palaeoecology laboratory. The 'undif' labels refer to the name used for the pollen grain in the pollen count notebooks.

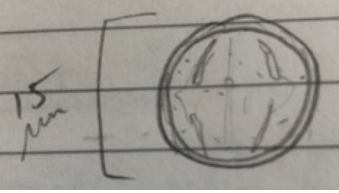
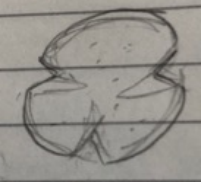
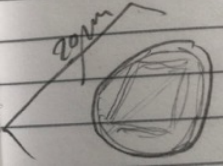
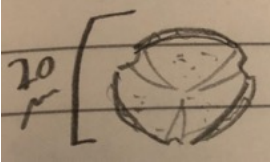
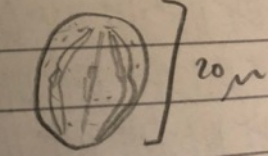
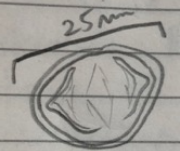
Type	Description	Slides and 'undif' no.	Photos/Drawings
Type 1	Tricolporate Psilate Slightly prolate ~15um	CVC1D1 03 slide 1 undif 1 CVC1D2 134 slide 3 undif 1	
Type 2	Tricolporate Psilate/very fine scabrate? Very prolate ~30 x 12 um	CVC1D1 03 slide 1 undif 5 CVC1D1 35 slide 3 undif 1 CVC1D1 51 slide 1 undif 3 CVC1D1 75 slide 3 undif 7 CVC1D1 91, slide 4 undif 3 CVC1D2 186 slide 1 undif 4	  
Type 2b	Tricolporate? Psilate, finely scabrate? Prolate, ~45 x 15um	CVC1D2 146 slide 2 undif 3	
Type 3	Monocolpate? Seems to be one big opening in centre of grain Reticulate? ~40 x 20 um	CVC1D1 03 slide 1 undif 18 CVC1D1 43 slide 1 undif 8 CVC1D1 75 slide 2 undif 5 CVC1D2 194 slide 1 undif 2	  

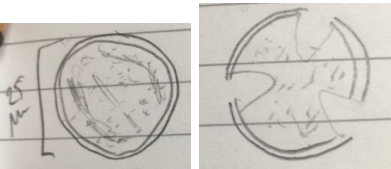
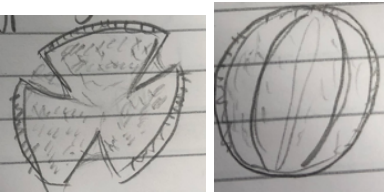
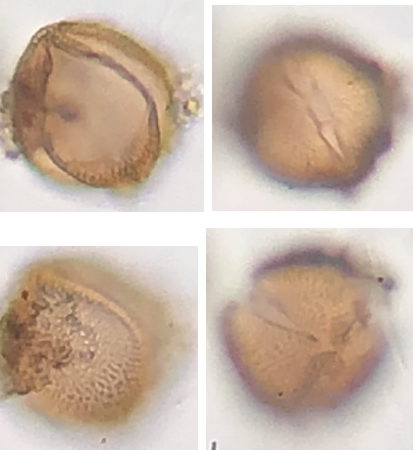
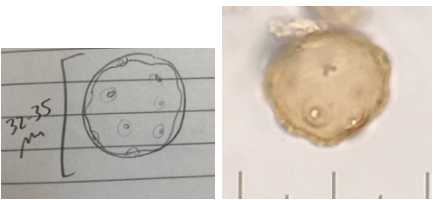
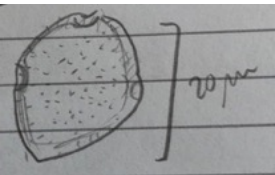
Type 3b	Dicolpate? Reticulate Long colpi Prolate, 45 x 20 um	CVC1D1 83 slide 2 undif 5 CVC1D1 83 slide 4 undif 13	
Type 3c	A couple of colpi, maybe just 2? Colpi as long as grain Scabrate, prolate, ~40 x 15 um	CVC1D1 19 slide 2 undif 4 CVC1D1 75 slide 1 undif 4 CVC1D1 83 slide 1 undif 3 CVC1D2 132 slide 3 undif 7	
Type 4	Monocolpate? One big colpi/opening in centre? Psilate/Finely scabrate Thin walls ~ 35 x 12 um	CVC1D1 03 slide 1 undif 21 CVC1D1 43 slide 2 undif 3 CVC1D1 59 slide 2 undif 1 CVC1D1 67 slide 3 undif 1 CVC1D2 202 slide 2 undif 9	 
Type 4b	Monocolpate? Scabrate, colpi thin, big grain, ~50um	CVC1D1 51 slide 2 undif 15	
Type 5	4 – colporate Sub-prolate, fairly big pores, ~ 20 x 15 um	CVC1D1 27 slide 1 undif 6 CVC1D1 67 slide 1 undif 4 CVC1D2 234 slide 1 undif 8	

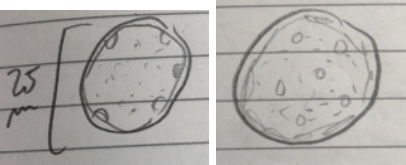
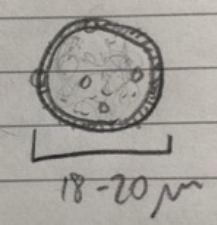
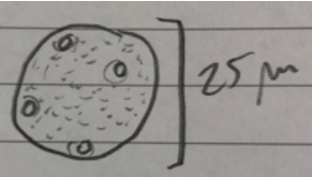
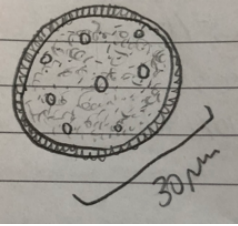
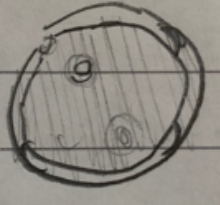
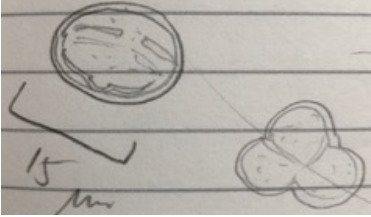
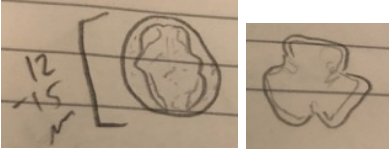
Type 5b	4 – colporate spherical, slightly oblate, ~ 20x25 um psilate, small pores but clear on equatorial view	CVC1D1 35 slide 2 undif 7	
Type 5c	Pericolporate, initially looks like 4 but other colpori seem to be present in grain. Psilate, fairly spherical, ~ 28um	CVC1D1 67 slide 2 undif 5	
Type 5d	Perhaps 4 colporate Thick colpi on equatorial view, centre pore clear Psilate, Prolate	CVC1D1 115 slide 2	
Type 6	Tricolporate Scabrate Clear colpi shape with indents for pores Sub prolate/spheroidal ~ 25 x 20 um	CVC1D1 27 slide 1 undif 16 CVC1D1 27 slide 3 undif 10	
Type 6b	Tricolporate Scabrate, simple colpi, joined top and bottom Spherical, ~18 um	CVC1D1 75 slide 2 undif 6	
Type 6c	Tricolporate, coarse scabrate. Long thick colpi, joined top and bottom, quite clustered in centre of grain, prolate, 30 x 15um	CVC1D2 250 slide 3 undif 3 CVC1D2 234 slide 1 –undif 4	

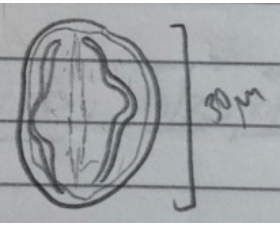
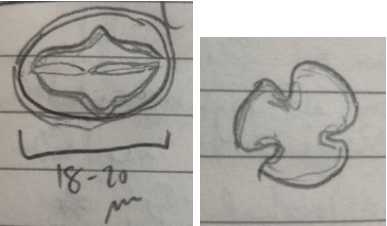
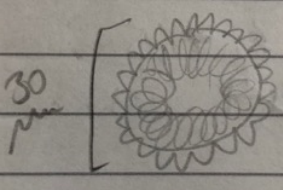
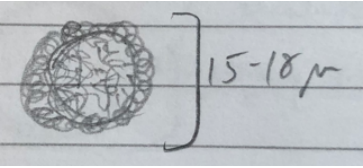
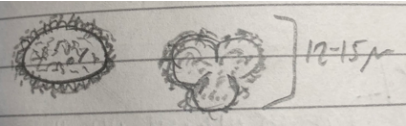
Type 7	Tricolporate Psilate, clear colpi with 'cuts' for pores. Quite thin colpi. Slightly prolate. ~35 x 20 um	CVC1D1 27 slide 2 undif 1		
				
Type 7b	Tricolporate, Psilate, Clear colpi with cuts for pore, quite big clear pores. ~30um, prolate	CVC1D1 83 slide 2 undif 3		
Type 7c	Tricolporate, Psilate, clear colpi shape, slightly bulbous middle Prolate ~18 x 12um	CVC1D2 194 slide 1 undif 9		
Type 8e	Tricolporate Reticulate Wide, big, oval pores Big, rounded lobes on colpi on polar view Spherical, ~25um	CVC1D2 138 slide 3 undif 7		
Type 9	Tricolporate Scabrate Not particularly distinct ~ 15 um	CVC1D1 75 slide 1 undif 1		
Type 10	Tricolporate Psilate. Feint colpi, 'curly bracket' type. Prolate	CVC1D1 51 slide 2 undif 9		
		CVC1D2 234 slide 1 undif 9		

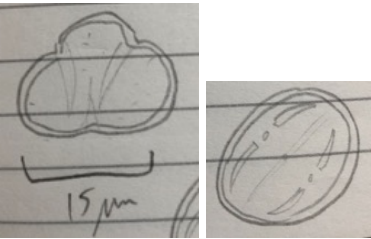
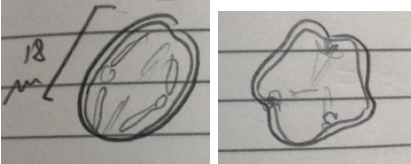
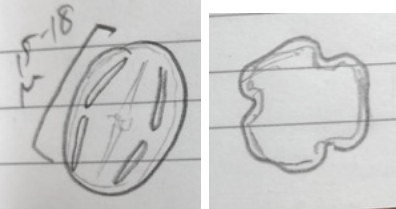
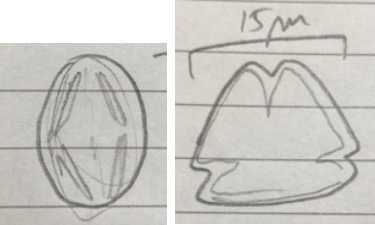
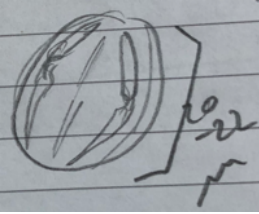
Type 10b	Tricolporate Scabrate. Curly bracket type colpi, slight gap in middle for pore. Colpi joined top and bottom. Prolate, ~20x15um	CVC1D2 169, slide 1 undif 5	
Type 12	Diporate Coarse scabrate/reticulate Spherical, ~ 15 um	CVC1D1 75 slide 1 undif 6 CVC1D2 226 slide 1 undif 14	
Type 14	6 colporate (peri) clear pores, quite rectangular. Scabrate or finely reticulate. 'Flower' shape on polar ~ 25 um on polar	CVC1D1 83 slide 1 undif 1 CVC1D1 99 slide 2 undif 2	  
Type 15	Tricolporate. Scabrate. Fairly thick pores/colpi on polar view. Colpi seem to join in middle Pores not obvious on equatorial view. Slightly prolate, ~ 15 um	CVC1D1 83 slide 1 undif 5	 
Type 16	Tricolporate Looks to have columella on walls. Scabrate. Clear cut for pore on colpi.	CVC1D1 83 slide 1 undif 10	

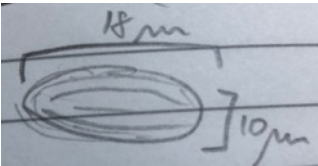
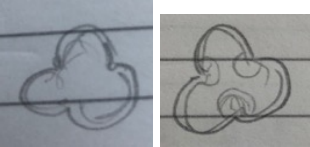
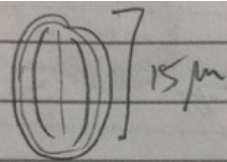
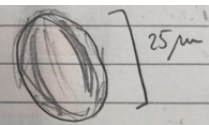
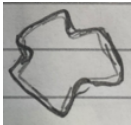
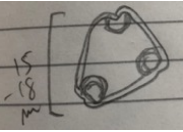
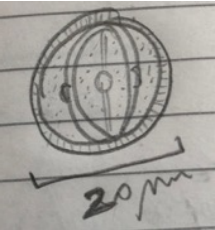
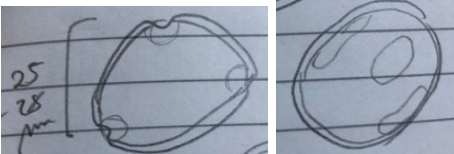
Type 17	Tricolporate. Finely scabrate. Fairly big 'cuts' on polar view for pore/colpi opening Spherical, ~ 15 um	CVC1D1 91 slide 1 undif 2 CVC1D1 51 slide 3 undif 4 CVC1D1 27 slide 3 undif 12	 
Type 17b	Tricolporate Psilate/finely scabrate Big triangle cuts on polar ~ 20 um	CVC1D1 99 slide 2 undif 1 CVC1D2 132 slide 3 undif 6	 
Type 17c	Tricolporate, Scabrate Biggish triangle colpi on polar view. Lolongate pores on equatorial view. Slightly prolate.	CVC1D1 75 slide 3 undif 13	 
Type 17d	Tricolporate. Psilate. Big triangle cuts on polar Fairly big, thick colpi on equatorial view. Slightly oblate, ~20x25um	CVC1D1 99 slide 3 undif 6 CVC1D1 115 slide 3 undif 4 CVC1D2 178 slide 1 undif 2 CVC1D2 132 slide 2 undif 9	     

Type 17e	Tricolporate Scabrate/finely reticulate Big triangle cuts on polar view for pore/colpi Spherical, ~ 25 um	CVC1D1 115 slide 2	
Type 17f	Tricolporate. Scabrate Big triangle cuts for colpi on polar, ~ 22um	CVC1D2 169 slide 3 - undif 9	
Type 17g	Tricolporate. Reticulate, columella present. Big cuts for colpi on polar view. Long straight colpi on equatorial view, no obvious cuts for pores – joined top and bottom Spherical, ~25um	CVC1D1 03 slide 2 undif 5	 
Type 18	Periporate, perhaps 12-14 annulated pores. Psilate. Spherical, ~35 um	CVC1D1 91 slide 1 undif 5	 
Type 19	Triporate Reticulate Fairly spherical ~ 20 um	CVC1D1 91 slide 2 undif 2	

Type 19b	Periporate, perhaps 5 pores. Coarse scabrate Spherical, ~25um	CVC1D1 83 slide 3 undif 6 CVC1D2 190 slide 1 undif 9	
Type 19c	Periporate, perhaps 6-8 Reticulate Spherical, ~ 20um	CVC1D1 67 slide 2 undif 6 CVC1D2 226 slide 2 undif 1	
Type 19d	4 porate, slightly annulated pores. Coarse scabrate. Spherical, ~ 25 um	CVC1D2 169 slide 3 -undif 10	
Type 19e	Periporate, perhaps 10-12. Reticulate. Spherical, ~30um	CVC1D2 132, slide 2 undif 4	
Type 19f	Periporate, perhaps 5 or 6 annulated pores. Thick wall. Spherical		
Type 20	Tricolporate Generic grain Psilate / finely Scabrate, no columella on walls Slightly prolate, ~ 15 um	CVC1D1 123 slide 1 undif 5	
Type 20b	Tricolporate Psilate / finely scabrate Curly bracket type colpi, joined top and bottom Small, 12-15um	CVC1D1 75 slide 3 undif 12 CVC1D1 83 slide 3 undif 8	

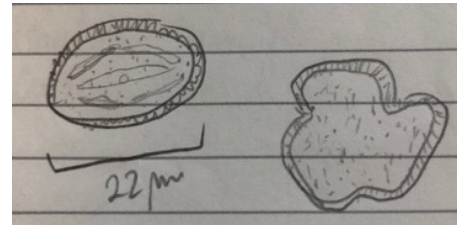
Type 20c	Tricolporate. Scabrate. Curly bracket colpi type - 'bulge' in centre of colpi Quite a big grain, slightly prolate, 30 x 25um	CVC1D1 67 slide 1 undif 7 CVC1D2 146 slide 3 undif 3 CVC1D2 226 slide 2 undif 5 CVC1D2 218 slide 3 undif 4	
Type 20d	Tricolporate. Psilate. 'Curly bracket' colpi type centre colpi apparently in half around pore. Quite big dips for pores/colpi on polar view Slightly prolate ~20 x 15um	CVC1D1 35 slide 1 undif 6 CVC1D1 107 slide 2 undif 4 CVC1D2 146 slide 3 undif 1 CVC1D2 226 slide 1 undif 1	
Type 21	Clavate structure. No other recognisable features. Spherical, ~30um	CVC1D2 134 slide 1 undif 6 CVC1D2 226 slide 1 undif 6	
Type 21b	Clavate structure. Spherical, ~18um	CVC1D2 210 slide 3 undif 9 CVC1D2 242 slide 2 undif 16 CVC1D2 218 slide 1 undif 2	
Type 21c	Clavate. Has distinct polar and equatorial views. Polar view with the standard 3 'sections' ~15um	CVC1D2 250 slide 4 undif 7	

Type 22	Tricolporate. Finely scabrate. Clear separation between colpi and pores on equatorial view. Fairly spherical, ~15um	CVC1D2 134 slide 1 undif 10 CVC1D1 35 slide 1 undif 9	
Type 22b	Tricolporate. Psilate. Clear separation between colpi and pores – colpi apparently in half around pore. Slightly prolate ~18x15um	CVC1D1 83 slide 4 undif 10 CVC1D1 115 slide 2 undif 1	
Type 22c	Tricolporate. Psilate. Colpi apparently in half. Side pores not clear. Slightly prolate ~18 x 15um	CVC1D1 43 slide 2 undif 2 CVC1D1 115 slide 1 undif 7 CVC1D2 146 slide 2 undif 6	
Type 22d	Tricolporate. Psilate. Colpi apparently in half. Pores not clear on equatorial view. Triangular polar view. Slightly prolate, 20x15um	CVC1D1 67 slide 3 undif 2 CVC1D2 234 slide 1 undif 5 CVC1D2 202 slide 1 undif 7	
22e	Tricolporate. Psilate. Colpi nearly in half around pore, slightly bulbous near pore ~22um	CVC1D2 150 slide 2 undif 3	

Type 24	Tricolporate, Psilate, Long thin grain, colpi long and thin Prolate, ~18-22 x 10um	CVC1D1 27 slide 2 undif 2 CVC1D1 115 slide 1 undif 8 CVC1D1 210 slide 1 undif 12 CVC1D2 250 slide 1 undif 8 CVC1D2 194 slide 1 -undif 7	  
Type 24b	Tricolporate Psilate / Finely scabrate Long colpi, no clear cuts for pores. Prolate, 25x 15um. Quite 'square' sections on polar view	CVC1D2 226, slide 1 undif 2 CVC1D2 178 slide 1 undif 7	 
Type 25	Triplicate. Annulated, big pores. Psilate. Triangular ~18um	CVC1D1 27 slide 3 undif 1 CVC1D1 91 slide 1 undif 8	
Type 26	Tricolporate. Reticulate. Clear pores on equatorial view, quite small circular pores on colpi. Long colpi, joined top and bottom Spherical, ~20um	CVC1D1 27 slide 3 undif 4 CVC1D1 51 slide 2 undif 11	
Type 27	Triplicate. Psilate. Really big, oval pores Spherical, ~25 um	CVC1D1 27 slide 3 undif 5	

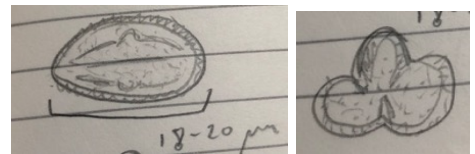
Type 28 Tricolporate Reticulate. Simple colpi, centre quite thick. Slightly prolate ~22um x 15um

CVC1D1 19 slide 2 undif 7
 CVC1D2 134 slide 2 undif 12
 CVC1D1 115 slide 3 undif 5
 CVC1D2 210 slide 2 undif 6



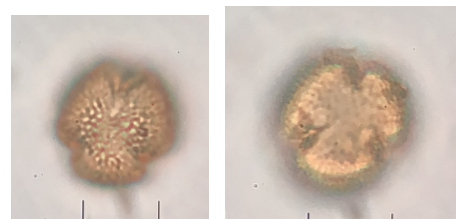
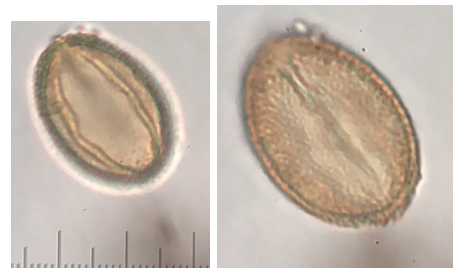
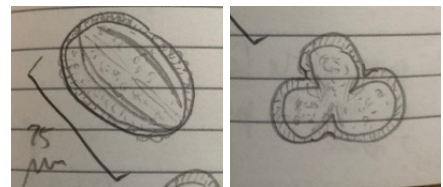
Type 28b Tricolporate. Reticulate. Simple colpi, slight bulge for pore. Prolate, ~20 x 15um

CVC1D1 83 slide 2 undif 2



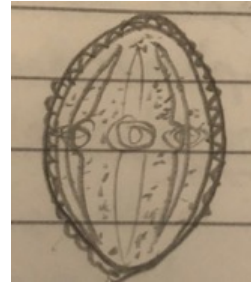
Type 28c Tricolporate. Reticulate. Simple colpi, straight, no clear openings for pores, perhaps slight indent in middle of colpi. Prolate, ~25 x 18um. Similar to type 63.

CVC1D1 51 slide 2 undif 13
 CVC1D1 91 slide 3 undif 2
 CVC1D1 99, slide 3 undif 3
 CVC1D1 210 slide 2 undif 3



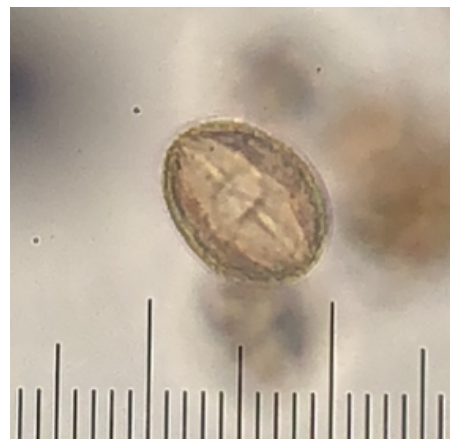
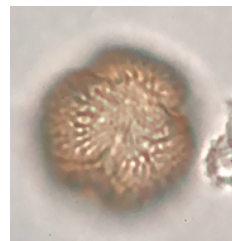
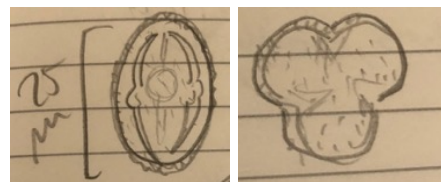
Type 28d Tricolporate. Reticulate Simple colpi, slight cut for pores. Centre colpi clearly defined. Prolate

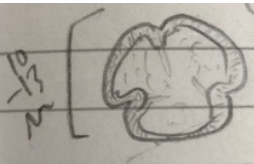
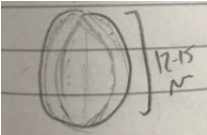
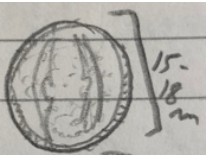
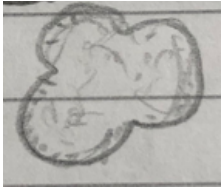
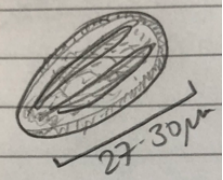
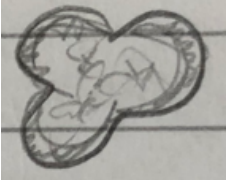
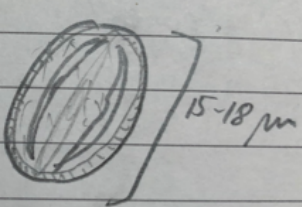
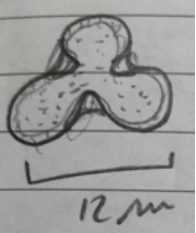
CVC1D1 27 slide 3 undif 4
 CVC1D1 27 slide 3 undif 9
 CVC1D1 75 slide 2 undif 2
 CVC1D1 91 slide 4 undif 7 (previously 8d)

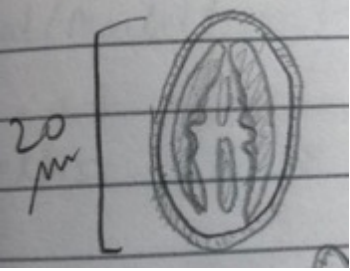
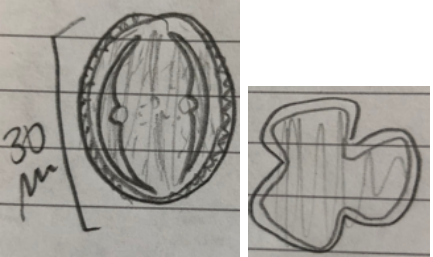
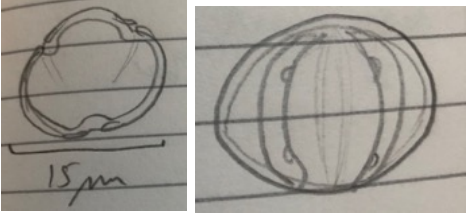
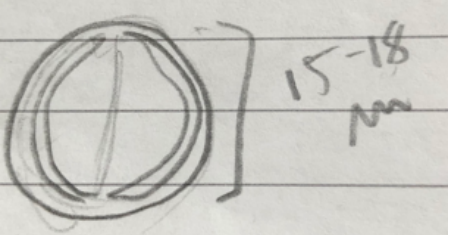
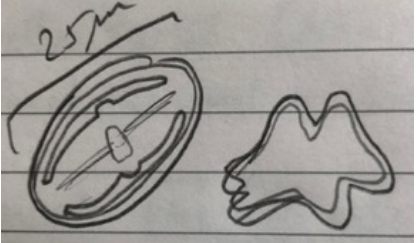


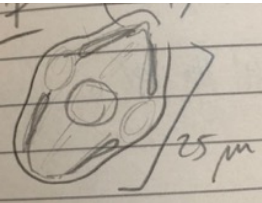
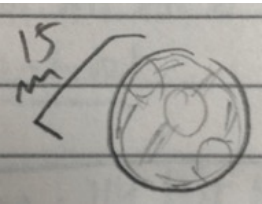
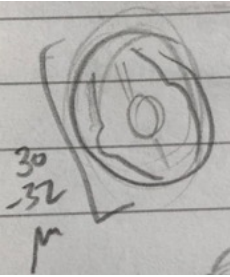
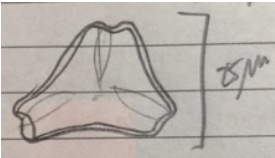
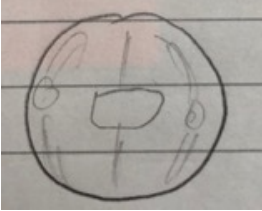
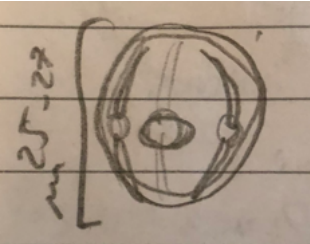
Type 28e Tricolporate Reticulate. Simple colpi, cut/bulge for pores Big pore in centre, circular. Prolate ~25 x 18um

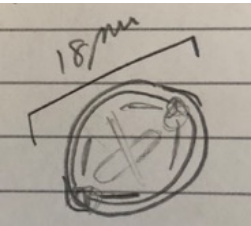
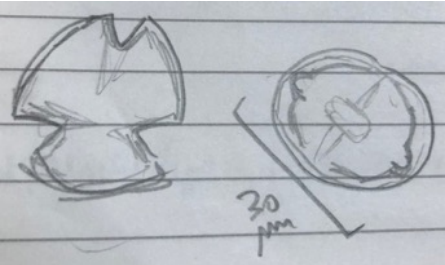
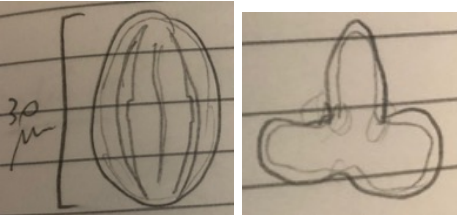
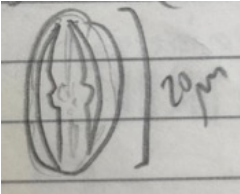
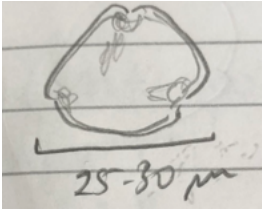
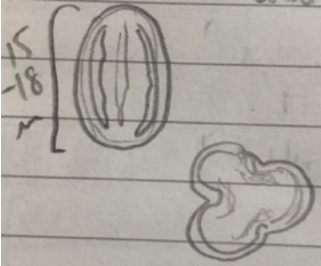
CVC1D1 43 slide 2 undif 4
 CVC1D1 75, slide 3 undif 7
 CVC1D1 91 slide 4 undif 9
 CVC1D1 99, slide 3 undif 9

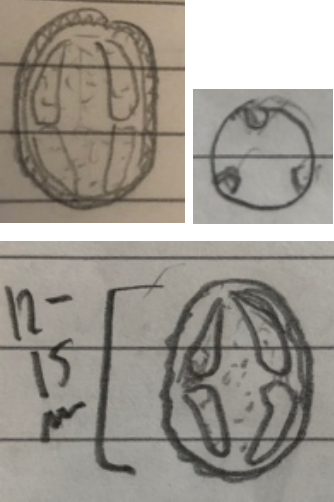
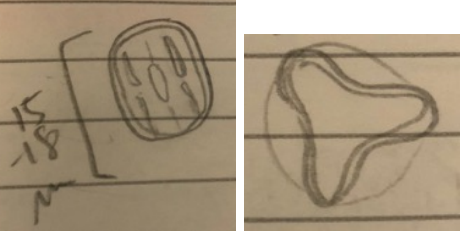
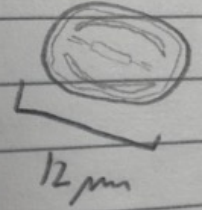
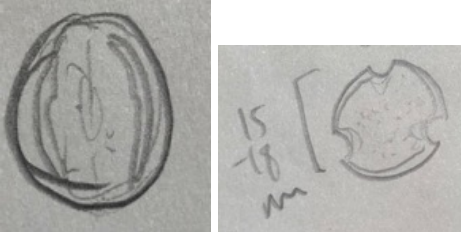
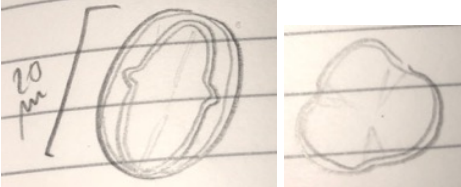


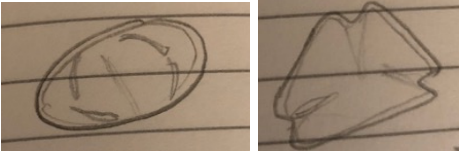
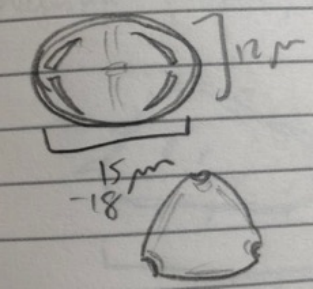
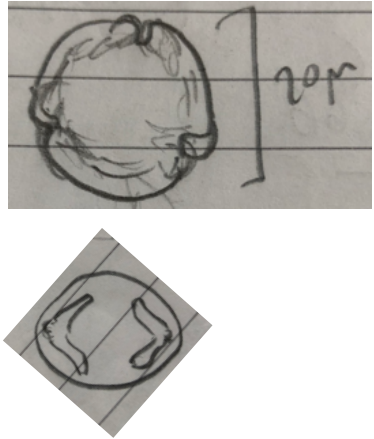
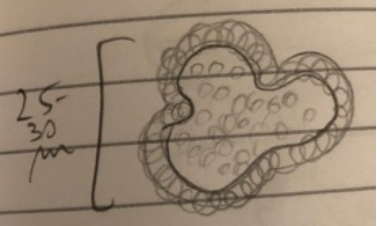
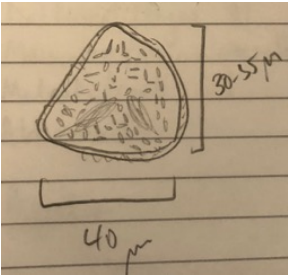
Type 28f	Tricolporate. Reticulate. Simple colpi, pores not that clear on equatorial view – perhaps lolongate. Smaller grain than other ‘type 28’s’	CVC1D1 210 slide 2 undif 1	 
Type 28g	Tricolporate. Reticulate. Colpi well defined, clear shape. Spherical, ~18um	CVC1D2 234 slide 1 - undif 7 CVC1D2 142 slide 3 undif 4	 
Type 28h	Tricolporate. Reticulate. Colpi clear, quite thick, rounded. No cuts for pores. Prolate, ~30 x 15-20um	CVC1D2 202 slide 2 undif 8 CVC1D2 142 slide 1 undif 2 CVC1D2 142 slide 3 undif 3 CVC1D2 150 slide 3 undif 1	 
Type 28i	Tricolporate. Reticulate. Clear colpi, long, slight cut for pores. Centre colpi has feint lolongate pore. Distinct polar view, 3 clear lobate sections, thickening where colpi/pores are. Prolate, ~18 x 12 um	CVC1D2 132 slide 1 undif 3	 

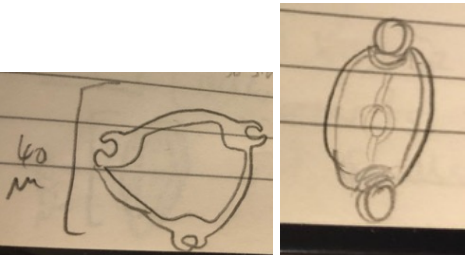
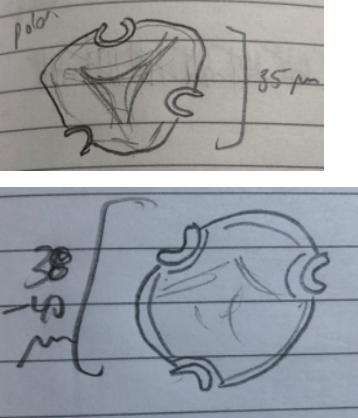
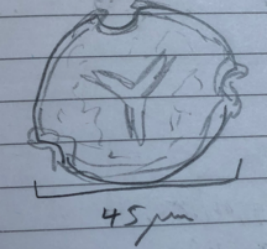
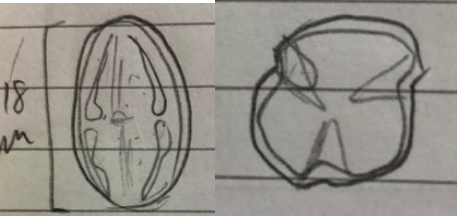
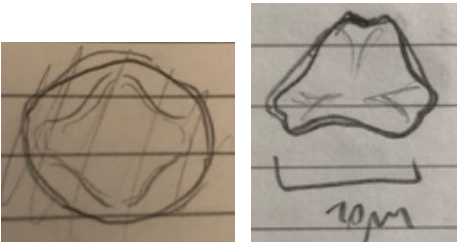
Type 29	Tricolporate. Reticulate. Thick colpi. Prolate, 20x 15um	CVC1D1 75 slide 2 undif 1 CVC1D1 99 slide 3 undif 8 CVC1D1 67 slide 2 undif 2 CVC1D2 142 slide 4 undif 4	
Type 29b	Tricolporate. Reticulate Thickish, dark colpi – indent for pore. Squarish polar sections Prolate 30x25um	CVC1D2 132 slide 1 undif 7	
Type 30	Tricolporate. Psilate Slightly annulated pores Very thick colpi on equatorial view. Oblate, ~15 x 20um	CVC1D1 91 slide 3 count undif 1	
Type 30b	Tricolporate. Psilate Colpi long, curved around side of grain Spherical to slightly oblate ~15x18um	CVC1D2 142 slide 3 undif 5	
Type 31c	Tricolporate. Psilate Fairly big rectangular centre pore. Long colpi, cuts for pores. Distinct polar view. Prolate ~25 x 18um	CVC1D1 59 slide 2 undif 2	

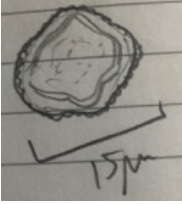
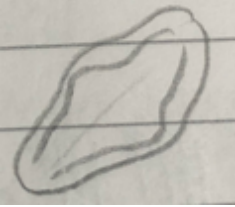
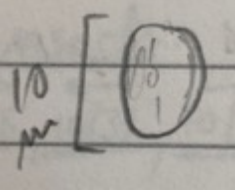
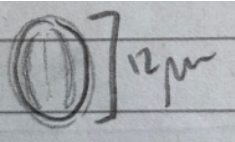
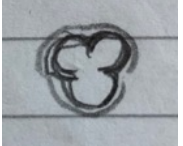
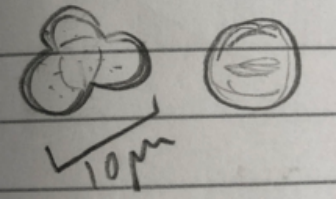
Type 32	Tricolporate. Psilate Very big circular pores, bulge out side of grain Shortish colpi, seemingly in half either side of pores Similar to type 50b	CVC1D1 91 slide 3 count undif 7 CVC1D1 91 slide 4 count undif 4 CVC1D2 242 slide 2 undif 10 CVC1D2 138 slide 3 undif 3	
Type 32b	Tricolporate Psilate Very big circular pores Spherical grain, ~ 15um	CVC1D1 83 slide 3 undif 4	
Type 32c	Tricolporate. Psilate Very big circular centre pore. Colpi long with bulges for pores Slightly prolate, ~30x 25 um	CVC1D1 67, slide 1 undif 8	
Type 32d	Tricolporate. Psilate Big, squarish centre pore. Colpi big on polar view. Fairly triangular polar. Spherical, ~ 25um	CVC1D1 115 slide 1 undif 1	 
Type 32e	Tricolporate. Psilate Large pores, circular pores. ~27um	CVC1D1 35 slide 1 undif 8	

Type 33	Tricolporate. Psilate. Wide centre pore on eq. view. Oblate, ~12 x 18um. Side pores slightly bulge	CVC1D1 91 slide 4 undif 3 CVC1D2 146 slide 1 undif 6	
Type 33b	Tricolporate. Wide centre pore on eq. view. Colpi quite long, look to join at top and bottom. Psilate/finely scabrate. Oblate, ~22x30um Big cuts on polar view for pores/colpi	CVC1D1 99 slide 4 undif 13	
Type 34	Tricolporate. Long colpi, Prolate, ~30x20um	CVC1D2 134 slide 2 undif 1 CVC1D2 146 slide 1 undif 2	
Type 34b	Tricolporate. Long colpi, Prolate, ~20 x 15um	CVC1D1 03 slide 1 undif 1 CVC1D1 19 slide 2 undif 1 CVC1D1 91 slide 4 undif 5 CVC1D 142 slide 3 undif 1	 
Type 34c	Tricolporate. Quite long colpi, fairly thick. Psilate. Prolate ~18x12 um	CVC1D1 35 slide 3 undif 2 CVC1D1 107 slide 5 undif 2 CVC1D2 210, slide 2 – undif 1	

Type 35	Tricolporate. Reticulate Really thick colpi Slightly prolate	CVC1D2 134 slide 2 undif 5 CVC1D2 138 slide 2 undif 5	
Type 36	Tricolporate – perhaps more though, up to 5. Elongated centre pore on equatorial view (lolongate). Slightly rectangular grain. Straight colpi. ~ 18um	CVC1D2 134 slide 2 undif 6	
Type 36b	Tricolporate Long thin colpi Elongated centre pore (lolongate) ~ 12 um	CVC1D1 91 slide 4 undif 6	
Type 36c	Tricolporate. Scabrate. Lolongate centre pore Quite big cuts on polar view for pore/colpi	CVC1D2 134 slide 4 undif 7	
Type 37	Tricolporate. Long thin colpi, joined top and bottom. Clear bulge for pores. Psilate Slightly prolate, ~20x18um (maybe as type 20d)	CVC1D2 134 slide 2 undif 9 CVC1D1 91 slide 1 undif 4	

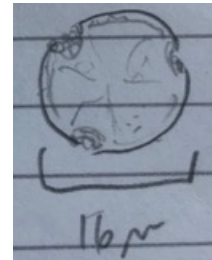
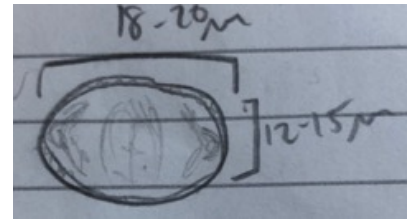
Type 38	Tricolporate. Psilate Simple colpi, no clear pores on equatorial view Slightly triangular polar view. Oblate	CVC1D2 134 slide 2 undif 10	
Type 38b	Tricolporate. Psilate Colpi triangular, apparently cut in half for pore. Triangular polar view. Oblate, ~12x18um	CVC1D1 99, slide 3 undif 2 CVC1D2 242 slide 1 undif 5	
Type 38c	Tricolporate. Psilate to finely scabratae. Annulated pores – protrude slightly (“2 knuckle’ shape) on polar. Short, thick colpi on equatorial view. Oblate, ~ 15x18um	CVC1D1 51 slide 2 undif 5 CVC1D1 91 slide 2 - undif 3 CVC1D2 169 slide 1 undif 6	
Type 39	Tricolporate ‘Curly’ verrucate structure, ~30um	CVC1D1 03 slide 2 undif 1	
Type 40	Interesting surface – perhaps fossulate. Fairly big, circular to triangluer ~ 40 x 35 um	CVC1D1 03 slide 2 undif 5	

Type 41	Triporate. Very big, distinctly annulated pores – ‘claw’ on polar Elongated equatorial view. ~40um	CVC1D1 27 slide 3 undif 2	
Type 41b	Triporate. Big distinctly annulated pores – ‘claw’ Equatorial view diamond shaped. Psilate, ~35 um	CVC1D2 186 slide 2 undif 6 CVC1D2 186 slide 4/5 undif 8	
Type 41c	Triporate. Big, annulated pores – ‘claw’. Trilete shape in centre. Scabrate. Spherical, ~45um	CVC1D2 182 slide 1 undif 7	
Type 42	Tricolporate. Psilate Centre pore quite rectangular. Clear colpi shape – cut in half with bulbous ends. Slightly prolate, ~18 x 15 um	CVC1D1 27 slide 3 undif 3 CVC1D1 75 slide 2 undif 3 CVC1D1 115 slide 2 undif 3 CVC1D2 146 slide 2 undif 13	
Type 44	Tricolporate. Psilate Distinct colpi, curly bracket with biggish bulge. Spherical to slightly oblate	CVC1D1 51 slide 3 undif 5 CVC1D1 59 slide 1 undif 1 CVC1D2 250 slide 1 undif 14	

Type 44b	Tricolporate or Dicolporate. Micro reticulate. Fairly spherical, ~15um	CVC1D1 19 slide 3 undif 5	
Type 44c	Tricolporate. Psilate. Colpi, curly bracket type, bulges grain in middle. Prolate	CVC1D2 226 slide 2 undif 10 CVC1D2 150 slide 3 undif 8	
Type 45	Small, tricolporate Psilate. Non-descript 10-12um	CVC1D1 83 slide 3 undif 3	
Type 45b	Tiny tricolporate Psilate. Non-descript, simple grain. Colpi just straight lines, pores not clear. Slightly prolate 10-12 x 6-8 um	CVC1D1 210 slide 2 undif 4 CVC1D2 250 slide 1 -undif 1 CVC1D2 250 slide 3 undif 1 CVC1D2 146 slide 2 undif 1	    
Type 45c	Tricolporate. Scabrate. Spherical grain, ~ 10um Colpi as long as grain.	CVC1D2 226 side 1 undif 11	

Type 46 Tricolporate. Scabrate, shortish colpi, centre colpi apparently quite thick. Oblate, ~20 x 12um

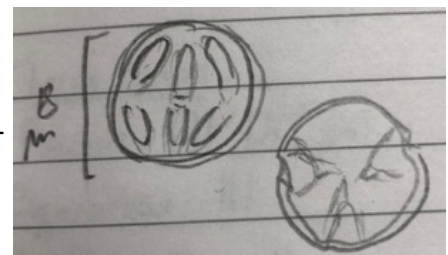
CVC1D1 83 slide 3 undif 5



Type 46b Tricolporate. Psilate. Very thick colpi Spherical, ~18um

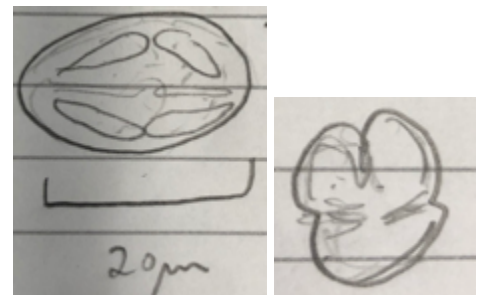
CVC1D1 67 slide 1 undif 6

CVC1D1 67 slide 4 – undif 3



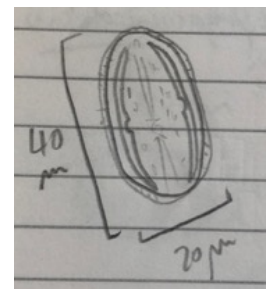
Type 46c Tricolporate. Scabrate Thick colpi – apparently in half. Slightly prolate, ~20x15um

CVC1D2 146 slide 2 undif 4

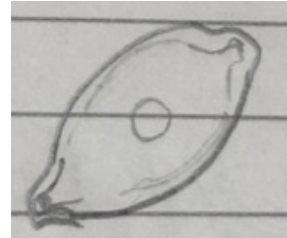
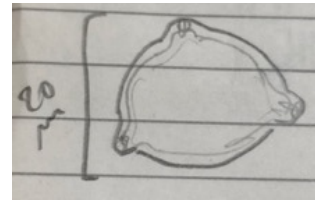


Type 47 Tricolporate. Reticulate – striate. Long thin colpi, small cuts for pores. Big grain. Prolate, ~ 40 x 20um

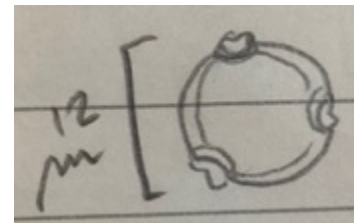
CVC1D1 83 slide 4 undif 14



Type 48 Triporate. 3 annulated pores, protruding from grain. Psilate. Circular on polar view, elongated on equatorial view. ~20um

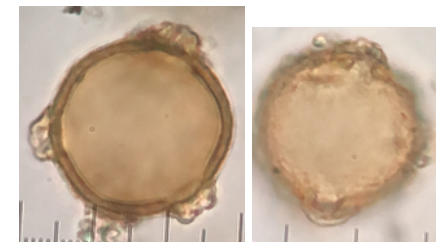


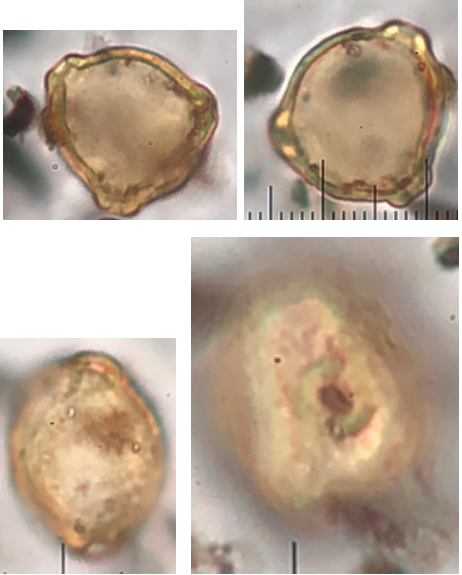
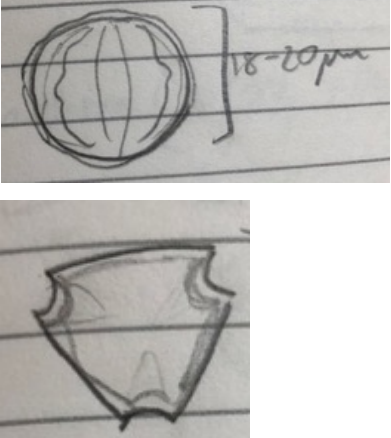
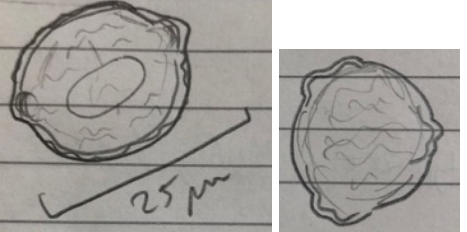
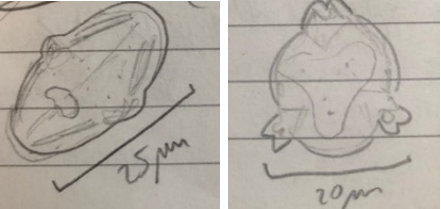
Type 48b Triporate. 3 annulated pores, slightly protruding from grain. Psilate. Spherical, ~ 12um

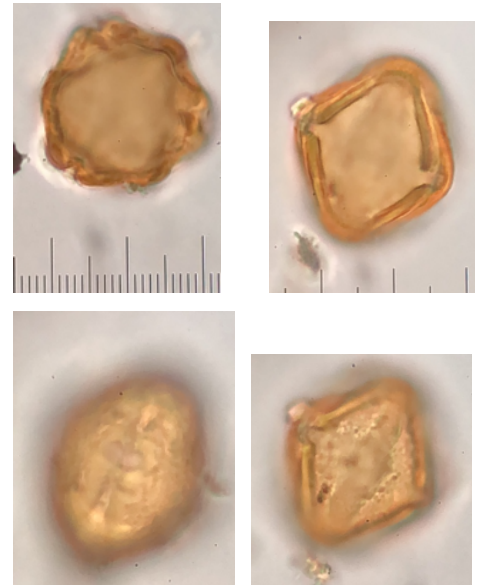


Type 48c Triporate. Annulated pores, very big, protrude from grain. Psilate to finely Scabrate. Spherical ~ 25 um

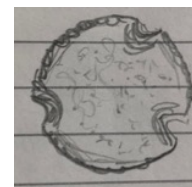
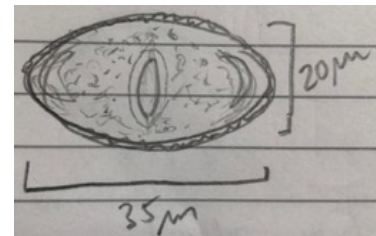
CVC1D1 59 slide 2 undif 4
CVC1D2 202 slide 3 undif 12



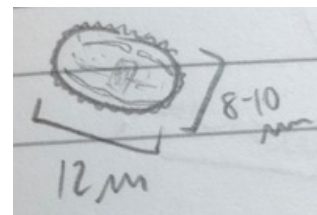
Type 48d	Triporate. Annulated grains protrude from grain. Psilate to finely Scabrate. Spherical polar view, ~15-20um, elongated equatorial view	CVC1D2 146 slide 4	
Type 49	Tricolporate. Thick colpi Psilate. Slight cut for pores on equatorial view Spherical, ~20um	CVC1D1 99 slide 3 undif 1	
Type 50	Tricolporate. Huge oval pores that bulge out sides on equatorial view. Annulated on polar view Regulate surface. Slightly oblate, 20x25um	CVC1D1 99 slide 4 undif 11	
Type 50b	Tricolporate. Big pores. Lalongate (oval) – bulge out sides on equatorial view. Annulated pores, sticking out on polar view Psilate to finely Scabrate. Prolate, ~25x20um	CVC1D1 19 slide 1 undif 2 CVC1D1 35 slide 2 undif 11	



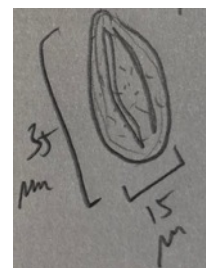
- Type 51 Tricolporate. Reticulate Short colpi, lolongate elongated pores – quite big and annulated Circular polar view Oblate, ~20x35um
- CVC1D1 99 slide 4 undif 12

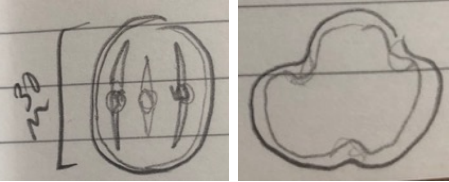
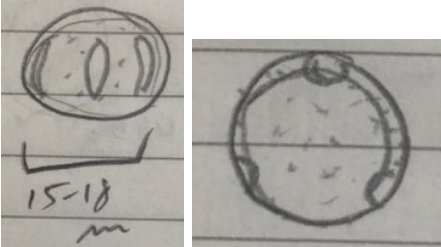
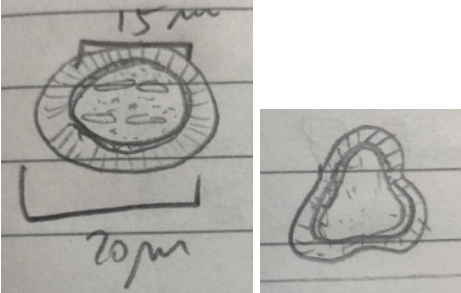
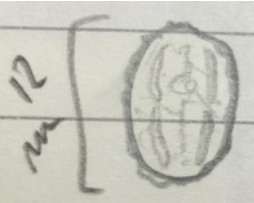
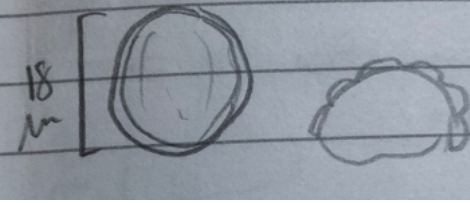
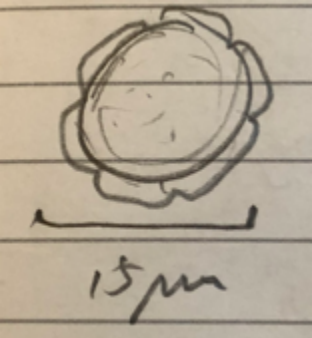


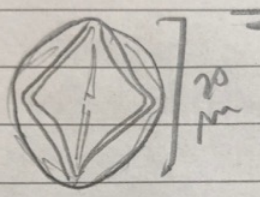
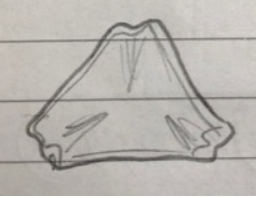
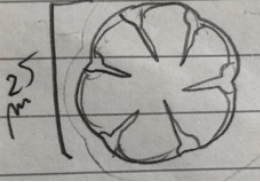
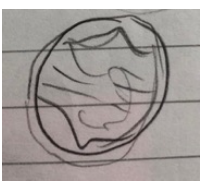
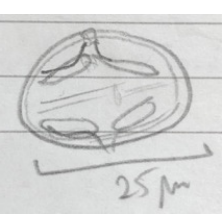
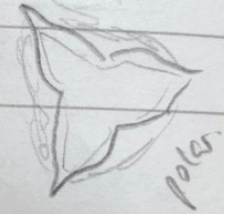
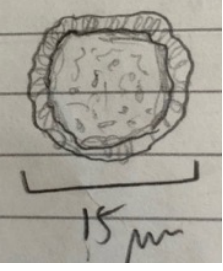
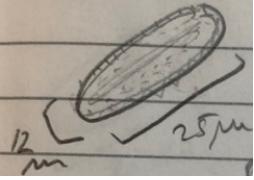
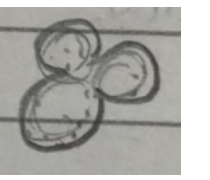
- Type 52 Tricolporate. Reticulate Very small grain, slightly prolate 12x8um.
- CVC1D1 123 slide 3 undif 2



- Type 53 Tricolporate. Finely Scabrate. Long, thin colpi. Very prolate, 35x15um
- CVC1D2 134 slide 3/4 undif 4
CVC1D2 150 slide 4 undif 5

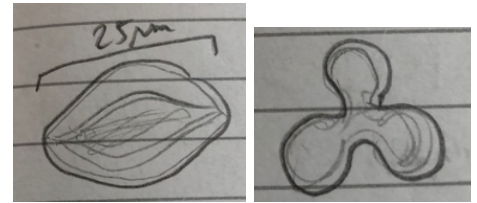


Type 54	Tricolporate. Psilate Straight colpi, quite short Fairly big, circular pores on colpi. Slightly prolate, ~30x25um	CVC1D1 19 slide 3 undif 7	
Type 55	Tricolporate? Either big, lolongate pores, or short thick colpi. Scabrata. Oblate ~ 18 x 12um	CVC1D1 19 slide 3 undif 8	
Type 56	Tricolporate. Reticulate Very thick 'outer' wall (~5um). Short colpi, apparently in half 'inner' grain ~15um, with outer wall ~20um	CVC1D1 35 slide 1 undif 4	
Type 57	Tricolporate. Small grain ~12um. Reticulate Short, straight colpi, apparently in half Centre pore fairly clear	CVC1D1 35 slide 3 undif 4	
Type 58b	Square/rectangular 'sections' on wall Psilate Spherical, ~ 18um	CVC1D2 250 slide 1 undif 7	
Type 58c	Square/rectangular 'sections' on wall – perhaps 6 colpi Psilate to finely scabrata Spherical, ~15um	CVC1D2 202 slide 2 undif 5	

Type 59	Tricolporate. Psilate Long colpi, joined top and bottom, bulge out in middle. Triangle polar view, annulated pores. Fairly spherical, ~ 20um	CVC1D1 59, slide 3 undif 3	 
Type 60	6 colporate, but not the 'traditional' flower shape. Distinct colpi shape on polar view. Psilate. Spherical, ~25um	CVC1D1 67, slide 3 undif 2	 
Type 61	Tricolporate. Psilate Fairly thick colpi, bulge out in middle. Distinct polar view – like 3 petals Slightly prolate, 25x20um	CVC1D1 107, slide 2 undif 3	 
Type 62	Reticulate / Clavate? Very thick walls Any apertures hidden under surface structure Spherical, ~15um	CVC1D1 210 slide 1 undif 4	
Type 63	Tricolporate. Reticulate Long thin colpi. Very prolate, ~ 25 x 12um Very circular sections on polar view.	CVC1D1 210 slide 1 undif 6 CVC1D2 226 slide 1 undif 3 CVC1D2 234 slide 2 undif 5 CVC1D2 186 slide 1 undif 2 + undif 9	 

Type 65 Tricolporate. Psilate, finely Scabrate. Colpi long clustered in centre, joined top and bottom. Slight bulge in grain in middle. Distinct, separate circular sections on polar Prolate, ~25 x 18um

CVC1D2 210 slide 2 undif 6



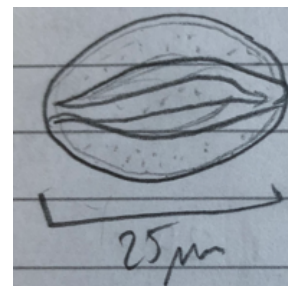
Type 65b Tricolporate? Scabrate Colpi long, quite thick, joined top and bottom Colpi apparently clustered in centre of grain Distinct sections on polar view Slightly Prolate, ~25 x 20um

CVC1D2 250 slide 3 undif 7

CVC1D2 218 slide 2 undif 5

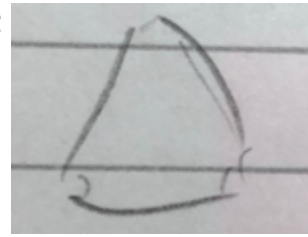
CVC1D2 242 slide 1 undif 12

CVC1D2 174 slide 1 undif 7



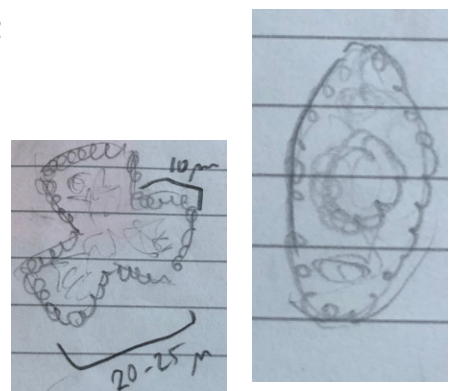
Type 66 Triporate. Psilate
Often damaged – grain
is flat. Triangular shape,
~15um

CVC1D2 210, slide 2
undif 5
CVC1D2 226 slide 1
undif 7
CVC1D2 226 slide 2
undif 6
CVC1D2 194 slide 2
undif 3
CVC1D2 194 slide 3,
undif 4



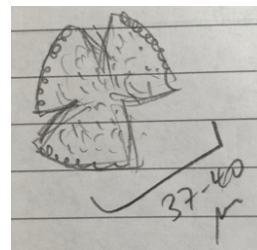
Type 67 Tricolporate. 3 big
sections on polar view
big pore on equatorial
view. Gemmate or
verrucate surface.
Oblate, 10 x 25um

CVC1D2 250, slide 2
undif 3



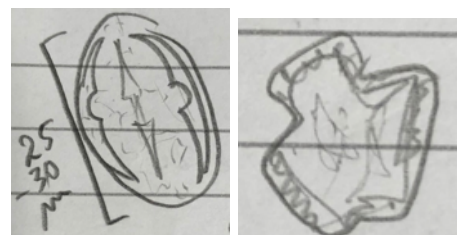
Type 67b 3 big sections on polar.
'curly' surface, perhaps
heavily reticulate ~40um

CVC1D2 174 slide 1
undif 4

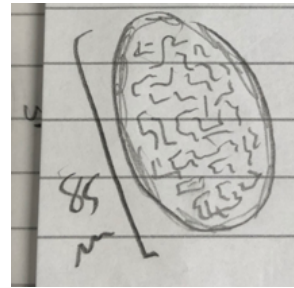


Type 68 Tricolporate. Light
reticulate. Big colpi,
centre colpi quite
triangular. Prolate,
~30um x 20um

CVC1D1 146 slide 1
undif 9

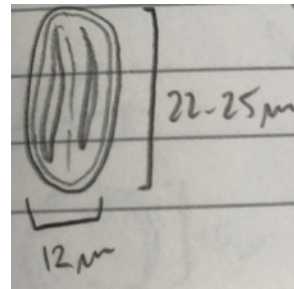


Type 69 Very big grain ~85um
Interesting surface
pattern – short channels
Can't see any apertures
– possible hidden by
surface structure



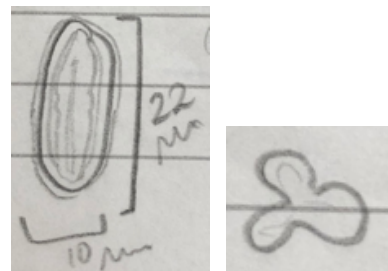
Type 70 Tricolporate. Long
straight colpi. Psilate
Quite a rectangular
shaped equatorial view,
prolate, 22 x 12 um

CVC1D2 226 slide 1
undif 4
CVC1D2 234 slide 1
undif 10
CVC1D2 186 slide 2
undif 4



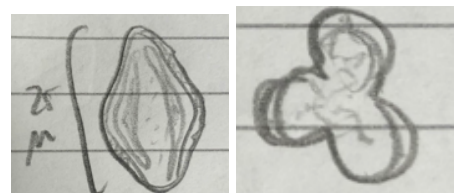
Type 70b Tricolporate. Long colpi,
apparently joined top
and bottom. Slight cuts
for pores. Prolate 22 x
10um

CVC1D2 178 slide 1
undif 4
CVC1D2 234 slide 1
- undif 6
CVC1D2 242 slide 1
undif 10



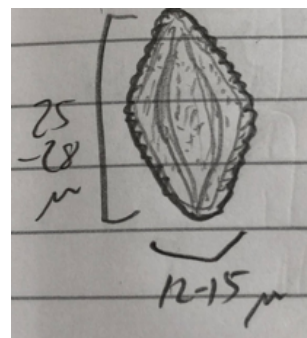
Type 71 Tricolporate. Reticulate
Thick colpi, bulge the
sides of the grain out in
middle. Elongated
diamond shape
(rhombic). Prolate, ~ 25
x 15 um

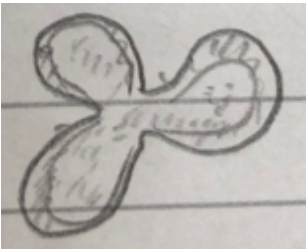
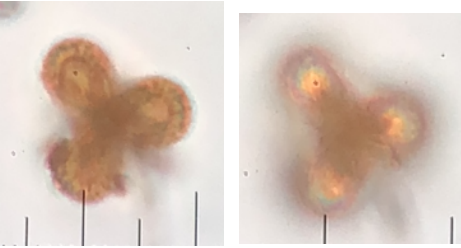
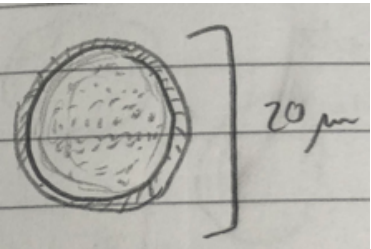
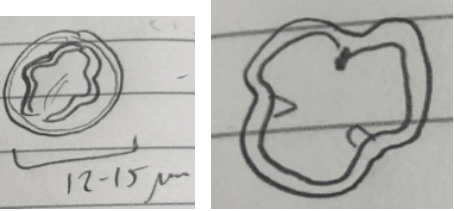
CVC1D2 226 slide 1
undif 15
CVC1D2 226 slide 1
undif 5

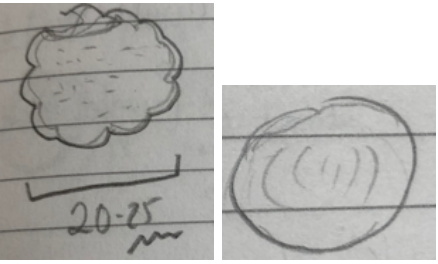
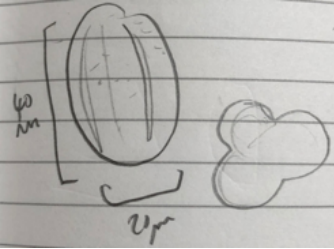
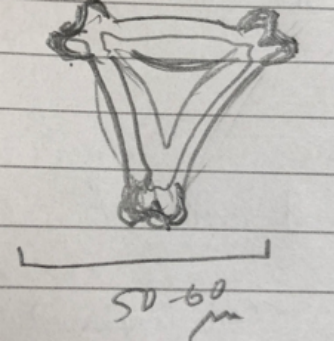
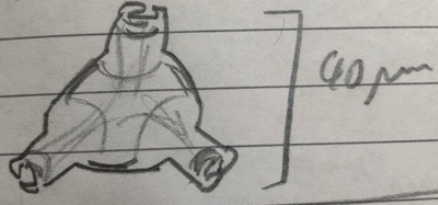
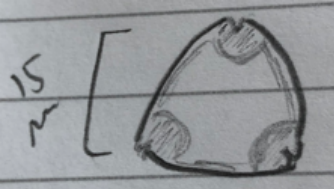


Type 71b Tricolporate. Heavily
reticulate. Colpi
apparently clustered in
centre of grain, joined at
ends. Elongated
diamond shape

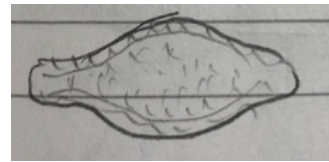
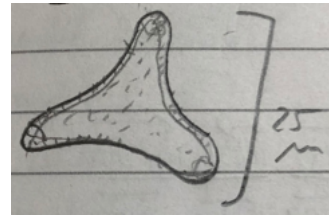
CVC1D2 194 slide 4
undif 6
CVC1D2 234 slide 1
undif 6
CVC1D2 186 slide 4
–undif 7



	(rhombic), bulge in centre of grain Prolate, ~28x15um		
Type 71c	Tricolporate. Reticulate Long colpi, joined at ends. Polar view, 3 distinct sections Prolate, ~30 x 12 um	CVC1D2 234 slide 2 undif 3 CVC1D2 186 slide 3 undif 3 CVC1D2 218 slide 3 undif 5 CVC1D2 242 slide 1 undif 13	
			
			
Type 72	Reticulate, apparently inaperturate. Thick walls, almost a double wall. Spherical, ~20um	CVC1D2 226 slide 1 undif 4 CVC1D2 250 slide 1 count undif 12 CVC1D2 178 slide 2 -undif 4 CVC1D2 186 slide 1 undif 1	
Type 73	Tricolporate. Psilate Curly bracket colpi type – bulges in middle for pores. Small, spherical grain ~12-15um	CVC1D2 226 slide 2, 3 rd 10 –undif 7	

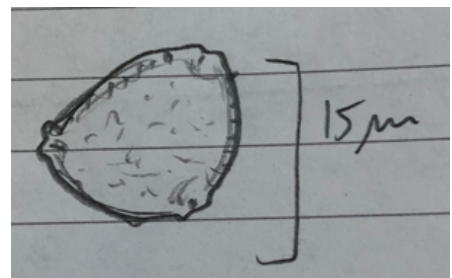
Type 74	Pericolporate, approximately 12. Scabrate / reticulate. Distinct flower shape on polar, 12 sections Short colpi on eq. view ~25 um	CVC1D2 194 slide 1 undif 6	
Type 75	Tricolporate. Fine Scabrate. Prolate, ~40x20um. Long, straight colpi, no clear cuts for pores	CVC1D2 194 slide 4 undif 7 CVC1D2 186 slide 1 undif 5	
Type 76	Triporate. Big annulated pores ('claws') on a triangle grain. ~60um	CVC1D2 194 slide 4 undif 8	
Type 76b	Triporate. Big annulated 'claw' pores. The 3 sections for the pores make it triangular. Concave triangle shape in centre of grain ~40um	CVC1D2 190 slide 1 undif 10	
Type 77	Triporate. Annulated pores. Rounded triangular polar Psilate. ~15um	CVC1D2 178 slide 3 undif 1	

Type 78 Trilete sort, 3 lobes on equatorial view in a sort of concave triangle shape. Scabrate to finely reticulate. ~25um



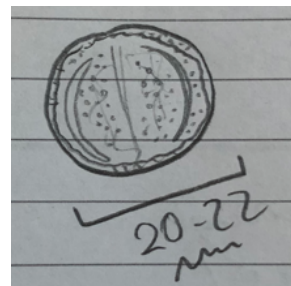
Type 79 Triporate. Scabrate to reticulate. With columella. Slightly annulated pores, like 2 knuckles. Rounded triangle polar, ~ 15um

CVC1D2 186 slide 4 undif 4
CVC1D2 190 slide 1 undif 3
CVC1D2 242 slide 1 undif 6



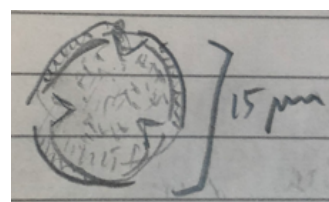
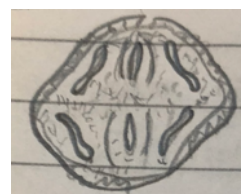
Type 80 Tricolporate. Reticulate – distinct giraffe pattern. Thin colpi, curved round grain, no cuts for pores ~20x22um

CVC1D2 186 slide 4 undif 5



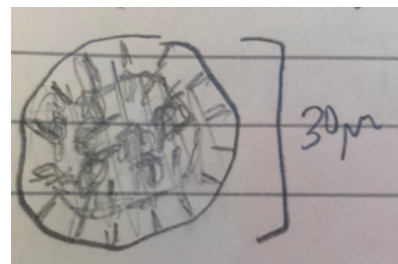
Type 81 Tricolporate. Reticulate Short colpi, apparently in half – each half kind of S shaped. ~15 x20um Circular polar, small triangle cuts for colpi

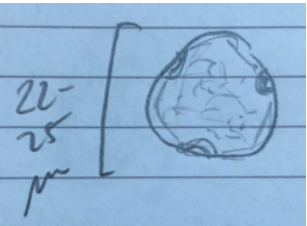
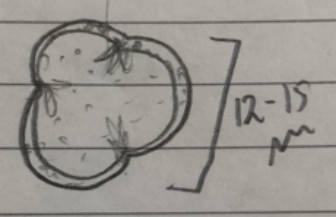
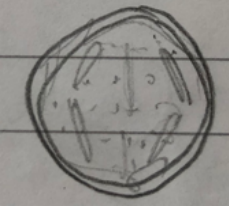
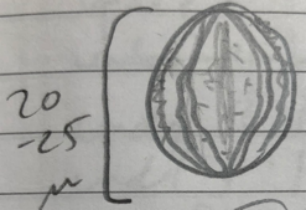
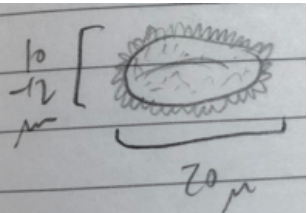
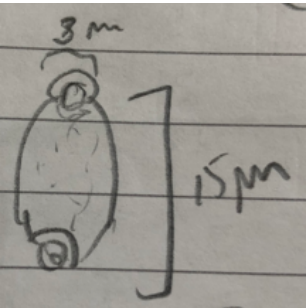
CVC1D2 202 slide 2 undif 2



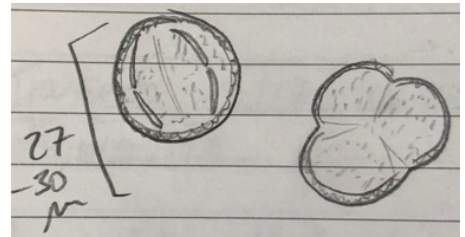
Type 82 Interesting surface pattern. Apertures not clear. Spherical ~30um

CVC1D2 202 slide 4 –undif 4



83	Type Triporate. Slightly annulated pores. Scabrate to reticulate. Pores in centre of walls Very slightly rounded triangular, ~ 25um	CVC1D2 182 slide 1 undif 11	
84	Type Tricolporate Looks almost periporate on surface, perhaps Gemnate structure. Spherical, ~ 15-18um	CVC1D2 174 slide 1 undif 5	 
85	Type Tricolporate. Reticulate Long colpi, joined top and bottom. No obvious cuts for pores on colpi Spherical ~ 25um	CVC1D2 142 slide 1 undif 4	
86	Type Clavate or Baculate structure. 20 x 12 um no apertures obvious	CVC1D2 169 slide 1 undif 2	
87	Type Diporate – 2 big annulated pores. Scabrate. Prolate ~15x10um	CVC1D2 190 slide 1 undif 5	

Type 88 Tricolporate. Reticulate
Thin, straight colpi, undif 2
apparently in half around
pore. Acute (triangulate)
colpi apex on polar view



Type 89 Tricolporate. Thick colpi, CVC1D2 138 slide 1
apparently in half. undif 3
Bulbous ends to each
half. Reticulate

